Transgenerational Stress Memory in Response to Low Temperatures in *Arabidopsis thaliana*

By

Korawit Opassathian

A thesis submitted in partial fulfilment of the requirements for the degree of

Doctor of Philosophy in Life Sciences

The University of Warwick, School of Life Sciences

September 2022

Abstract

Low temperature is one of the environmental stimuli that affect multiple aspects of plant growth and development. Plants, as sessile organisms, have developed defined cold-responsive pathways that are coordinated by a discrete number of transcription factors. This gene network is thought to be modulated by INDUCER of CBF EXPRESSION 1 (ICE1), which activates the transcription of C-REPEAT BINDING FACTORs (CBFs) and ultimately of COLD-REGULATED GENES (CORs), resulting in short-term adaptive responses to cold stress. However, recent reports have proposed an ICE-1-independent regulation of CBFs in response to cold. In this study, we have used existing ICE1 genetic lesions and newly generated artificial microRNAs (amiR-ice1) lines to define the precise function of ICE1 using a genome-wide transcriptomic analysis. Our results show that *CBFs'* cold-activated transcription is independent of ICE1, but ICE1 plays a modulatory role of multiple *COR* genes. Our data indicate that in Arabidopsis CBFs and ICE1 act independently to activate the cold-responsive pathway. Our study has also revealed that ICE1 function is regulated epigenetically by the deposition of chromatin marks on the promoter regions of direct targets.

Plants also show long-term adaptive responses to cold stress, supporting the existence of 'transgenerational stress memory' (TSM) responses. It has been proposed that the integration of this stress memory is limited in meristematic stem cells and their transmission to offspring restricted during gametogenesis and fertilisation. However, the precise molecular mechanisms implicated are not fully known. In this study, we have tested the possibility of enhancing TSM through cloning of somatic cells exposed to cold. Our data shows that clonal plants primed with cold accumulate stable transcriptional and epigenetic imprints at COR genes and that the transcriptional activity of CBF genes is necessary for a cold-mediated TSM.

Collectively, our analyses have revealed some of the mechanisms underpinning cold-mediated short-term and long-term memory response in plants.

Table of Content

List of Figures

List of Tables

Acknowledgements

I would like to thank my scholarship, **the Development and Promotion for Science and Technology talents project (DPST)** for funding my research and my postgraduate studies. I would like to express my gratitude to my supervisor, **Prof Jose Gutierrez-Marcos**, for all the effort, guidance and encouragement throughout my studies. During this challenging journey, there were a lot of times when I doubted myself and my motivation seemed to have fainted away. He always gives me his support. Without his support, I cannot achieve what I have done in this research.

I would like to express my appreciation to all former members of the JGM group. Dr Jonathan Price, Dr Robert Maple, Dr Julia Engelhorn, Dr Julius Durr, Dr Nosheen Hassain, who have helped me in experimental works during my early years.

My special thanks to all the lovely people around me during all these years. J Antunez-Sanchez, Ryan Merritt, Dr Yang Seok Lee, Dr Jing Yuan, Dr Claudia Payacán Ortiz, Lorenzo Pellegrini, Stefano Amantia, Dr Sho Ono, and Dr Cathal Meehan for all of your support and for being amazing group of friends. No word can describe the importance of all of you to me. I would like to thank Gary Grant for all of his support in plants work in phytobiology facility, and also a great conversation about all things.

I am grateful for all support from far away, all of the support from my girlfriend for being there for me and your support when I'm down, and all of my friends back in Thailand. To my family members: my dad, mom, my sisters and my brother, who always support me in many ways, I am really grateful to be a part in this wonderful family and thank you for believing in me at all times.

Declarations

This thesis is submitted to the University of Warwick in support of my application for the degree of Doctor of Philosophy. The work composed in this thesis is original and has not been published or presented for any other degree. The experiments and analyses described in this thesis have been carried out by myself under the supervision of Prof. Jose Gutierrez-Marcos, with the exceptions described below:

Dr Hadi Lanang Putra (Department of Plant Sciences, University of Cambridge, United Kingdom)

Providing transcriptome data and methylome data used in the analysis in Chapter 4 (sections 4.2.1 and 4.2.2)

Ryan Merritt (School of Life Sciences, University of Warwick, United Kingdom)

Assisting differentially methylated regions from methylome data in Chapter 4 (section 4.2.2)

Abbreviations

ABA	Abscisic Acid
amiR	Artificial microRNAs
ATP	Adenosine Triphospate
BABA	ß-aminobutyric acid
bHLH	basic helix-loop-helix
bp	base pair
bZIP	basic leucine zipper
CBF	C-Repeat Binding Factor
cm	Centimeter
COR	Cold-Regulated Gene
DEG	Differentially Expressed Genes
DEX	Dexamethasone
DMGs	Differentially Methylated Genes
DMRs	Differentially Methylated Regions
DMSO	Dimethylsulfoxide
DNA	Deoxyribonucleic Acid
dNTP	Deoxynucleotide
dsRNA	Double-Stranded RNA
Est	estradiol
FDR	FALSE Discovery Rate
GO	Gene Ontology
h	Hour
HAT	Histone Acetyltransferase
HDAC	Histone Deacetylase
ICE1	Inducer of CBFs Expression 1
JA	Jasmonic Acid
lncRNA	Long Non-Coding RNA
LO	Leaf Origin
log2FC	Log2 Fold Change
MAPK	Mitogen Activated Protein Kinase
mg	milligram
min	Minute

mL	Milliliter
mM	Milimolar
mRNA	Messenger RNA
MS	Murashige and Skoog
nt	Nucleotide
PCA	Principal Component Analysis
PCR	Polymerase Chain Reaction
PTGS	Post Transcriptional Gene Silencing
RdDM	RNA Directed DNA Methylation
RNA	Ribonucleic Acid
RO	Root Origin
ROS	Reactive Oxygen Species
rpm	Rotation per Minute
SA	Salicylic Acid
SC	Sperm Cell
SE	Somatic embryogenesis
sec	Second
siRNA	Small Interfering RNA
ssRNA	Single Stranded RNA
TE	Transposable Element
TF	Transcription Factor
TSM	Transgenerational Stress Memory
U	Unit
VN	Vegetative Nucleus
µL	Micro Litre
µM	Micro Molar

Chapter 1 Introduction

1.1 Effects of Low Temperature on Plant Growth and Productivity

One of the most noticeable differences between plants and other multicellular organisms is that plants are sessile. Plants grow vertically above and below ground to receive light energy and absorb soil nutrients. Because of the immobility, plants are also affected by unpredictable environmental changes originating from biotic and abiotic factors. Under unfavourable conditions, plants maintain growth and fertility by activating stress-responsive pathways resulting in expression changes of stress-related genes that lead to physiological adjustments. Most plant species also can survive the lethal level of stress exposure after being pre-treated with a mild level of similar stressors, this process is known as stress acclimation or hardening.

Low temperature (LT) has various effects on plant development depending on the degree of temperature: chilling stress from the temperature around 0°C – 15°C and freezing stress from the temperature below freezing point (0°C). The severity of low-temperature exposure also depends on the types of plants. For instance, tropical and subtropical crop species like rice (*Oryza sativa* L.) or maize (*Zea mays*) are not capable of surviving under chilling temperatures due to the absence of the cold acclimation process (Ritonga and Chen 2020; Zhang et al. 2014; Zhou et al. 2022). Temperate species such as wheat (*Triticum aestivum*), barley (*Hordeum vulgare*), and *Arabidopsis thaliana* acclimate to cold during autumn resulting in freezing-tolerance in winter (Hassan et al. 2021; Visioni et al. 2013; Wanner and Junttila 1999). Moreover, some woody plant species, such as white birch (*Betula pubescens*), can survive at -40°C after a cold-hardening (Rinne et al. 1998).

The chilling temperature generally reduces cellular metabolism starting from the limitation of cell membrane fluidity leading to dysfunctional membrane proteins (Örvar et al. 2000; Takahashi et al. 2013). Inside plant cells, cold stress causes an imbalance between light energy harvesting, resulting in photoinhibition and the accumulation of reactive oxygen species (ROS) (Miura and Furumoto 2013; O'Kane et al. 1996). Cold affects protein stability and alters the folding formation of some proteins or protein complexes (Ding et al. 2019; Kang et al. 2016). Similarly, plants enhance the activity of RNA chaperone proteins like COLD-SHOCK DOMAIN proteins (CSDs) to maintain correctness in the RNA folding (Kang et al. 2016; Karlson

et al. 2002). While chilling stress reduces cellular metabolism and affects plant growth, the temperature below freezing point turns water into frost. It then damages plants more with dehydration problems (Knight and Knight 2012b).

In conclusion, sessility, a unique characteristic of organisms in the plant kingdom, has been considered the main evolutionary force driving adaptive mechanisms to adapt to fluctuating environments. Low temperature is an important environmental stress that affects plant growth and development. Cold stress causes various abnormalities in metabolic and cellular processes, which are thought to be driven by transcriptional changes. Some plant species cannot tolerate cold stress, while some species can survive under freezing conditions after a period of acclimation.

1.2 Cold-Stress Sensory Pathways

To comprehensively understand cold-responsive pathways in plants, the essential question is – how cold is perceived in higher plant species. Several studies suggest that cold-stress sensory pathways are complex due to the existence of multiple temperature sensors (Ding et al. 2019).

The most well-accepted concept is the membrane fluidity hypothesis. Changes in the physical properties of cell membranes correlate with changes in expression levels of genes in cold-responsive pathways. Induction of cell membrane rigidification by chemicals such as DMSO enhances COLD-ACCLIMATION SPECIFIC 30 (*CAS30*) expression in alfalfa (*Medicago sativa*) protoplasts in ambient growth condition (Örvar et al. 2000). On the contrary, an increase of membrane fluidity during cold treatment inhibits BRASSICA NAPUS 115 (*BN115*) in *Brassica napus* (Sangwan et al. 2001). Chemical changes in the cytosol are also connected to low-temperature sensing. The influx of calcium ion/Ca^{2+} wave into the cytosol after cold shock suggests the crucial role of Ca^{2+} in the cold-signal transduction (Knight et al. 1996; Knight et al. 1991). Interestingly, physical changes in membrane fluidity are associated with Ca^{2+} influx through an adjustment of cytoskeleton structure beneath the cell membrane (Örvar et al. 2000; Sangwan et al. 2001). Further study in rice has found membrane protein complex consisting of CHILLING TOLERANCE DIVERGENCE1 (COLD1) and RICE G-PROTEIN α SUBUNIT1 (RGA1), and cold temperature activates the interaction between COLD1-RGA1 and Ca^{2+} channels leading to Ca^{2+} influx following by expression of several cold-responsive genes (*CORs*) (Ma et al. 2015). However, specific Ca^{2+} channels or mediator proteins related

to low-temperature perception have not been found in *Arabidopsis*. Hence, the complete mechanism of cold-stress sensing is still unclear. A recent study also proposes the possibility of plants using PHYTOCHROME B (phyB, a photoreceptor protein) as a cold sensor (Jung et al. 2016).

1.3 Cold-Stress Responsive Pathway

Even though cold-sensing mechanisms need to be confirmed, the cold-responsive pathway has been studied for over two decades. Low temperature induces complex transcriptional cascades to control expression levels of cold-responsive genes (*CORs*). Cold-responsive pathways can be categorised into (i) the ABA-dependent pathway and (ii) the *ICE1-CBFs-CORs* pathway.

1.3.1 Abscisic Acid (ABA)-Dependent Pathways

ABA is known as a plant hormone responsible for seed germination, senescence, and drought stress, but it also regulates specific pathways in the cold response (Shi and Yang 2014). *Arabidopsis* accumulates ABA under LT, and exogenous application on plants results in cold acclimation leading to increased freezing tolerance (Mantyla et al. 1995). The ABA-INSENSITIVE mutant *abi-5* and ABA deficient mutant *freezing sensitive 1* (*frs1*) show impaired freezing tolerance with the reduced expression level of several known *CORs,* suggesting the involvement of ABA in the cold response (Llorente et al. 2000; Mantyla et al. 1995). Exposure to low temperature also induces the expression of ABA-RESPONSIVE ELEMENTS BINDING FACTOR 1 and 4 (*ABF1* and *ABF4*), which transcribe basic leucine zipper (bZIP) transcription factors binding specific ABA-responsive elements (ABREs) motif in ABA-responsive pathway (Llorente et al. 2000; Mantyla et al. 1995). Further transcriptome and promoter sequence analysis has revealed enrichment for ABREs motifs in genes activated by cold (Maruyama et al. 2012). Especially, some *CORs* such as RESPONSIVE TO ABA 18 (*RAB18*), RESPONSE TO DESSICATION 29B (*RD29B*), and COLD-RESPONSIVE 8.6 (*COR8.5*) contain multiple ABREs motifs within 500 base-pair (bp) upstream to the transcription start site (TSS) (Hannah et al. 2005).

1.3.2 ICE1-CBFs-CORs Pathways

A family of CBF/DREB1 proteins (C-REPEAT BINDING FACTORS/ DROUGHT-RESPONSIVE ELEMENT BINDING 1 PROTEINS) has been identified as one of the key transcription factors that control the expression of around 7 - 20% of cold-responsive genes by binding to the consensus sequence "A/GCCGAC" motifs in the promoter regions (Jia et al. 2016; Liu et al. 2019; Park et al. 2015). In *Arabidopsis*, the *CBFs/DREB1s* gene family consists of four genes: *CBF1, CBF2, CBF3,* and *CBF4* (*DREB1B*, *DREB1C*, *DREB1A*, and *DREB1D* respectively). *CBF1 - 3* locate tandemly on chromosome 4 and share around 85% similarity (Gilmour et al. 2004; Gilmour et al. 1998; Liu et al. 2019; Novillo et al. 2007). *CBF4* is the latest family member located in chromosome 5, and its function is related more to drought stress than the low temperature stress (Haake et al. 2002). An individual *CBF* seems to have a partial overlap function in cold response, albeit sharing consensus sequences. Null mutant *cbf2* shows enhanced freezing tolerance with increased expression levels of *CBF1, CBF3,* and downstream genes, but RNAi hairpins targeting *CBF1* and *CBF3* show the opposite results with no effect on *CBF2* expression level, suggesting that *CBF2* might be the negative regulator of *CBF1* and *CBF3* (Novillo et al. 2004; Novillo et al. 2007). Overexpressing *CBFs* in *Arabidopsis* results in an induction of several downstream genes in a non-cold condition (Gilmour et al. 2000; Park et al. 2015).

Because *CBFs* are rapidly induced by cold treatment, it was proposed that upstream transcription factors also regulate CBFs' expression levels. Chinnusamy et al. (2003), using a luciferase reporter fused with the promoter of *CBF3,* showed that a mutation in INDUCER OF CBF EXPRESSION 1 *(ICE1*), known as *ice1-1*, cannot induce *CBF3* expression during cold stress. ICE1 is a basic helix-loop-helix (bHLH) transcription factor that binds the E-box consensus sequence (CANNTG; N is any nucleotide). The promoter analysis found that *CBFs* contain a few E-box binding motifs, especially *CBF3,* which has five copies in the promoter region (Chinnusamy et al. 2003). In the normal growth temperature, ICE1 (also known as *SCREAM 1* (SCRM1)) is constitutively expressed to control the development of stomata in leaves (Kanaoka et al. 2008). But upon cold exposure, ICE1 has been implicated in the *ICE1-CBFs-CORs* responsive pathway. Moreover, ICE1 protein undergoes multiple post-translational modifications induced by cold (figure 1.1, (Knight and Knight 2012a; Miura and Furumoto 2013)). Phosphorylation by OPEN STOMATA 1 (OST1) during

the cold temperature stabilises and activates the binding activity of ICE1 (Ding et al. 2015). ICE1 is also stabilised by conjugation with SUMOs (small ubiquitin-like modifiers) by SIZ1 (SUMO-protein ligase) (Miura et al. 2007). In contrast, in *Arabidopsis* phosphorylation by MPK3/6 (MITOGEN-activated PROTEIN KINASE 3 and 6) and ubiquitination by HOS1 (HIGH EXPRESSION OF OSMOTICALLY RESPONSIVE GENE 1) activates a ubiquitin E3 ligase that results in the degradation of ICE1 and increased cold sensitivity (Miura et al. 2007; Zhao et al. 2017). Microarray expression analysis of *ice1-1* has shown that around 40% of *CORs* are misregulated during cold treatment, which has led to the view that ICE1 plays a major role in the cold-responsive pathway (Lee et al. 2005).

ICE1 is not the only factor controlling *CBFs* expression under low temperatures. There is a connection between Ca^{2+} and *CBFs-CORs* pathways through CALMODULIN-BINDING TRANSCRIPTION ACTIVATOR1-6 (CAMTA1-6). Some members of the CAMTA family show both specific and overlap regulations upon *CBFs*. For instance, *camta3/5* double mutant plants show impaired induction of only *CBF1* and *CBF2* under a rapid cold treatment (Kidokoro et al. 2017). The promoter region of *CBF2* binds specifically to CAMTA3 (Doherty et al. 2009). Double mutant *camta1/3* and *camta2/3* but not *camta1/2* exhibit reduced expression levels of all *CBF1, CBF2,* and *CBF3*, suggesting the dominant role of CAMTA3 in the pathway (Kim et al. 2013). CAMTA1, CAMTA4, and CAMTA6 are less important in cold due to the instabilities (Kidokoro et al. 2017).

Circadian rhythm-related proteins also regulate expression levels of *CBF1-3*. PSEUDO RESPONSE REGULATORS (PRRs), one of the circadian clock components, act as negative regulators of *CBF1-3* during day-time cold exposure (Nakamichi et al. 2009). Antagonistic components of PRRs such as CIRCADIAN CLOCK-ASSOCIATED 1 (CCA1) and LATE ELONGATED HYPOCOTYL (LHY) also positively regulate *CBF1-3* expression (Dong et al. 2011).

In conclusion, to physiologically adjust to low-temperature stress, plants regulate the activities of cold-responsive genes through ABD-required pathways or transcriptional cascades consisting of *CBF1-3* as central members. Genes in *CBFs* are the targets of several transcription factors related to Ca^{2+}, circadian cycle, and other aspects of biological pathways. Recent work has shown that there are cold-responsive pathways that act independent of either CBFs or ABA and are controlled by three

transcription factors (HSFC1, ZAT12, and CZF1). However, this pathway is not as well-studied as the CBF-dependent pathway (Liu et al. 2019).

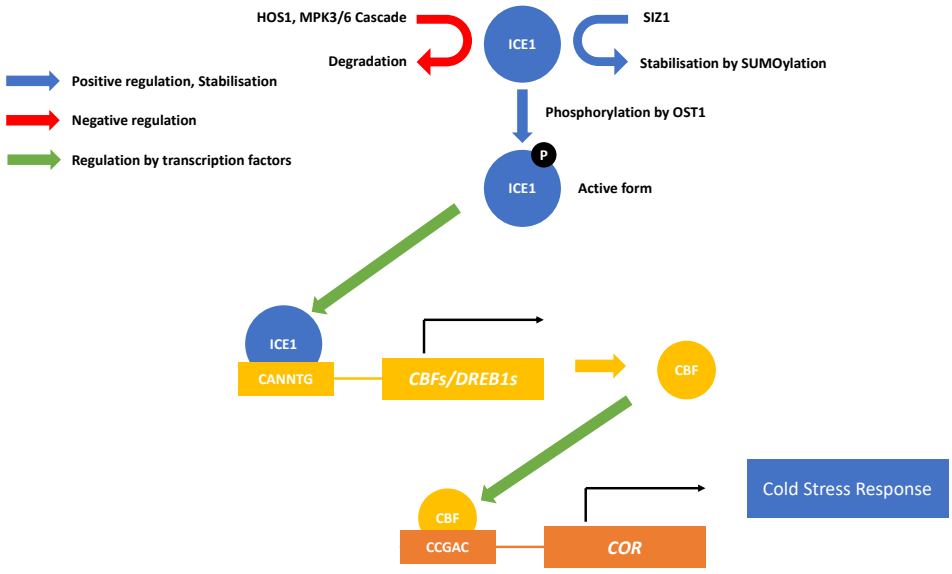

Figure 1.1 Cold-responsive pathway mediated by ICE1 and CBFs transcription factors in *Arabidopsis thaliana*. During cold stress, phosphorylation and ubiquitination of ICE1 is carried out by the MPK3/6 cascade and HOS1 resulting in protein degradation, whilst SIZ1 stabilises ICE1 by SUMOylation. OST1 phosphorylates and enhances the binding activity of ICE1 (blue arrow). ICE1 binds the promoter and activates the expression of *CBF/DREB1* genes. CBFs regulate downstream cold-regulated genes (*COR*), leading to cold tolerance. ICE1, an inducer of CBF expression1, MPK3/6, mitogen-activated protein kinase 3/6, HOS1, high expression of osmotically responsive genes 1, SIZ1, SUMO-protein ligase, CBFs/DREB1s, C-repeat binding factors/ drought-responsive element binding proteins, *COR,* cold-regulated genes. (Modified from Miura and Furumoto 2013)

1.4 Epigenetic Regulation of Gene Expression in Plants

In eukaryotic genomes, a DNA molecule is packed inside the nucleosome structure consisting of a core histone protein complex surrounded by approximately 147 base pairs of double-strand DNA (Luger et al. 1997). The function of nucleosomes is not limited only to storing DNA molecules inside the nucleus. Nucleosome occupancy also plays a crucial role in controlling gene expression (Lauria and Rossi 2011). An *in vitro* study using mammalian transcription machinery revealed the unsuccessful transcription initiation in the promoter of the gene, which contacts with the nucleosome structure (Lorch et al. 1987). In contrast, the depletion of a single histone subunit leading to incomplete nucleosome structure increases the global gene expression in yeast (Han and Grunstein 1988). In higher plants such as *Arabidopsis* and rice (*Oryza sativa*), there is a negative correlation between the nucleosome occupancy in the promoter region with the expression level of the gene (Zhang et al. 2015). Results from *in vitro* and *in vivo* studies suggest that nucleosomes function as barriers to gene expression in eukaryotic cells. Thus, to gain the accessibility of DNA sequence for transcription machinery, eukaryotes (including plants) use three systems to alter chromatin structure: DNA methylation, histone modifications, and chromatin remodelling protein complexes (Bell et al. 2011; Lauria and Rossi 2011). These methods are considered epigenetic marks due to their ability to regulate gene expression without any alteration in DNA sequence.

1.4.1 DNA Methylation

DNA methylation results from the transfer of a methyl group from the donor, S-adenosylmethionine, to the cytosine (C) residue by different methyltransferases (Moore et al. 2013). In plants, there are three patterns of DNA methylation and can be categorised within two groups: symmetric CG and CHG methylation (where H is A, C, or T) and asymmetric CHH methylation and there are two processes of DNA methylation in plants: (1) *de novo* DNA methylation (the establishment of DNA methylation) and (2) the maintenance of DNA methylation patterns (He et al. 2011).

To establish newly DNA methylation patterns in the plant genome, plants use RNA-directed DNA methylation (RdDM). The RdDM pathway consists of several steps: Firstly, the production of double strands 24-nt small interfering RNAs (siRNAs) that is carried out by RNA polymerase IV (Pol IV), RNA-DEPENDENT RNA POLYMERASE 2 (RDR2), and DICER-LIKE 3 (DCL3). Then, ARGONAUTE 4

(AGO4) involves in the process by carrying only one strand of siRNA and form the protein complex with RNA polymerase V (Pol V). Finally, the protein complex of AGO4 and Pol V directs DOMAIN REARRANGED METHYLTRANSFERRASE 2 (DRM2, the methyl transferase enzyme) to transfer the methyl group to specific DNA sequences (figure 1.2A). Apart from establishing all methylation patterns, each methylation pattern is maintained by a different process. For example, in CG methylation, plants use DNA methyltransferase 1 (MET1) together with VARIANT IN METHLATION1 (VIM1) to methylate the newly synthesised DNA during DNA replication (figure 1.2B, Hauser et al. 2011; Kawashima and Berger 2014; Law and Jacobsen 2010). The mechanisms of CG maintenance during DNA replication begin with VIM1, as a reader protein binding to the hemi-methylated CG in the parental strand. Then, VIM1 recruits MET1 to methylate the CG sites in the complement strand (Grimanelli and Ingouff 2020). To maintain CHG methylation, DNA methyltransferase specific to the plant named CHROMOMETHYLASE 3 (CMT3) is used together with the histone methyltransferase SU(VAR)3-9 HOMOLOG4/KRYPTONITE (SUVH4/KYP). SUVH4 transfers two methyl groups to the ninth lysine residue in the histone 3 (H3) subunit generating H3K9me2, which is required for the function of CMT3 (figure 1.2C, (Hauser et al. 2011; Kawashima and Berger 2014; Stroud et al. 2014). Because plant cells cannot copy asymmetrical methylation patterns directly to the new strand DNA during the cell division, the maintenance of CHH methylation is carried out by re-establishment. CHH can be re-established by the RdDM pathway using 24nt siRNAs mediated by SAWADEE HOMEODOMAIN HOMOLOGUE 1 (SHH1) binding with H3K9me2 or by RdDM pathway using 21-22nt siRNAs produced from RNA polymerase II (Pol II), RNA-DEPENDENT RNA POLYMERASE 6 (RDR 6), and ARGONAUTE 2 (AGO2) (figure 1.2D) (Kawashima and Berger 2014; Matzke and Mosher 2014).

In contrast to the maintenance, the methyl group(s) of methylated cytosine are removed by either a loss of maintenance during DNA replication or from the activity of the DNA glycosylase (Law and Jacobsen 2010). In plants, demethylation is carried out by DNA glycosylases: DEMETER (DME) or REPRESSOR OF SILENCING 1 (ROS1) (Choi et al. 2002; Gong et al. 2002). A report from Baute and Depicker (2008) proposed that base excision repair is the possible mechanism to demethylate the methyl group due to the functions of DME and ROS1 that can remove nitrogenous base (i.e., methylated cytosine) and break the backbone of DNA. Although DME and

ROS1 have the same function in DNA demethylation, the activities of DME and ROS1 are different in plant developmental stages. While ROS1 acts in the vegetative stage, DME can demethylate DNA during the gametogenesis (Law and Jacobsen 2010).

All methylation contexts are mainly found in transposable elements and repetitive DNA sequences in *Arabidopsis* genomes (Zhang et al. 2006; Zilberman et al. 2007). Only 5% of DNA methylation in *Arabidopsis* is found in gene promoters, and the methylation in promoter regions shows a higher effect on the expression than the methylation in transcribed regions (Zhang et al. 2006).

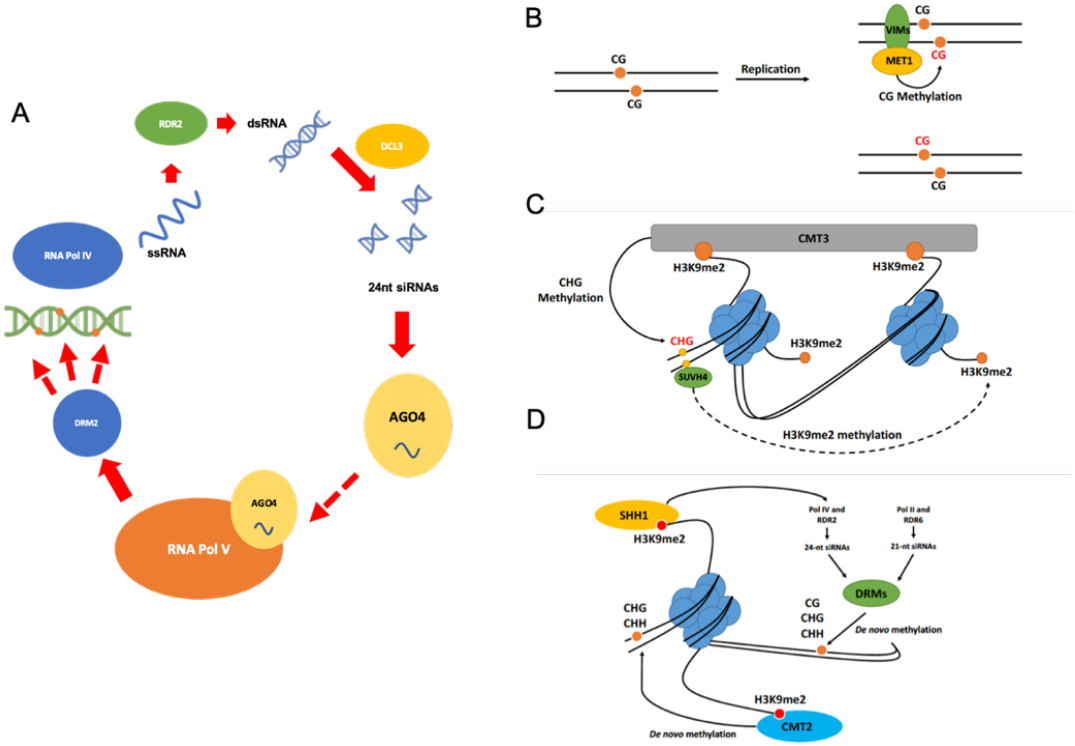

Figure 1.2 A model for the establishment and maintenance of DNA methylation in plants. (A) RNA-directed DNA methylation (RdDM) is the de novo DNA methylation model in all DNA methylation contexts. Single-strand RNA transcripts (ssRNA) are produced by RNA polymerase IV (RNA Pol IV) and converted to double-strand RNA (dsRNA) by RNA-dependent RNA polymerase 2 (RDR2). Then ssRNA is cleaved by dicer-like protein 3 (DCL3), generating 24-nucleotide small interference RNA molecules (siRNAs), which bind to ARGONAUTE protein (AGO4). AGO4 also co-localises with RNA polymerase V (RNA Pol V). The AGO4-Pol V complex, in association with domain, rearranged methyltransferase 2 (DRM2) directs methylation at specific cytosine residues. (Modified from Law and Jacobsen 2010). (B) Model of DNA methylation maintenance at CG context in plants. CG methylation is recognised by a variant in methylation 1 (VIM1), and VIM1 recruits DNA methyltransferase 1 (MET1) to maintain CG methylation in DNA replication. (C) The maintenance of CHG methylation by chromomethylase 3 (CMT3) requires the binding of CMT3 with H3K9me2. Methylated CHG recruits SU(VAR)3-9 HOMOLOG4/KRYPTONITE (SUVH4/KYP) to establish the histone methylation and H3K9 residues. (D) The re-establishment of CHG methylation by RdDM pathways. In canonical pathways, SAWADEE HOMODOMAIN HOMOLOGUE 1 (SHH1) binds to H3K9me2 and recruits RNA Pol IV. RNA pol IV, RDR2, and other components in the RdDM

pathway generate 24-nt siRNAs, which bind to AGO4 to activate DRM proteins (DRMs) to establish DNA methylation in all contexts. Non-canonical RdDM includes activities of RNA polymerase II and RDR6 to generate 21-nt siRNAs to activate DRMs. (Modified from Kawashima and Berger (2014)).

1.4.2 Histone Modifications

The histone core that forms the nucleosome consists of 8 subunits (two of each H2A, H2B, H3, and H4). Each histone has the extension of amino acid residues at the N-terminal which are essential in the alteration of chromatin structure (Albert et al., 2002). In plants, four types of post-translational modification of histone are observed to affect gene transcription: ubiquitination on lysine residues, methylation on lysine and/or arginine residues, acetylation on lysine residues, and phosphorylation on serine and/or threonine residues (Pfluger and Wagner 2007). The former two modifications can have positive and negative effects on gene expressions, while the latter two only cause gene activation (Pfluger and Wagner 2007). The other mechanisms include SUMOylation and ADP ribosylation (Lauria and Rossi 2011). Histone acetylation and methylation are the most well-studied mechanisms among all histone modifications, especially at N-terminal tails of histone H3 and H4 subunits that are understood to affect gene regulation (Hauser et al. 2011).

Histone acetylation and deacetylation are carried out by two enzymes: histone acetyltransferase (HAT) and histone deacetylase (HDAC), respectively. The acetylation on lysine residues decreases positive charges of histone subunits leading to a less compacted nucleosome structure that can open the DNA region and activate gene transcription. Thus, histone acetylation is the positive mark of transcription, while histone deacetylation by HDAC gives the opposite results (Shahbazian and Grunstein 2007). Many histone acetylation marks and their effects are observed in *Arabidopsis*: acetylation at the 5^{th}, 8^{th}, 12^{th}, and 16^{th} of N-terminal lysine residues of histone H4 together with H3K18Ac (acetylation at 18^{th} lysine of H3 subunit) are involved in changes of chromosome structure during the cell cycle. Notably, acetylation at H3K9 is involved with highly transcribed genes at euchromatin regions (Boycheva et al. 2014).

Histone methylation is carried out by histone lysine methyltransferase (HMKT), functioning as a writer protein. Unlike histone acetylation, which always causes transcriptional activation, histone methylation establishes variant effects

depending on the location and degree of methylation (mono-, di-, or tri-methylation) (Hauser et al. 2011; Liu et al. 2010). Histone methylation in lysine residue is also reversible by two different erasure enzymes: LYSINE-SPECIFIC DEMETHYLASE I (LSD1), removing methyl group only from mono- and di-methylated lysine and Jumonji C (JmjC), which can demethylate from all degrees (Hauser et al. 2011). The examples of histone methylation in *Arabidopsis* include the heterochromatin marks (causing inactivation of transcription) such as H3K9me1 (mono-methylation at lysine 9 of H3 subunit), H3K9me2 (di-methylation at lysine 9 of H3 subunit), and H3K27me1 (Liu et al. 2010). H3K9me2 is also involved in the maintenance of CHG methylation in the DNA (Hauser et al. 2011; Kawashima and Berger 2014; Stroud et al. 2014). H3K27me3, another repressive histone mark, is found in more than 25% of protein-coding genes in the *Arabidopsis* genome with dynamic activity during plant growth and development (Lafos et al. 2011). H3K27me3 is deposited by POLYCOMB REPRESSIVE COMPLEX 2 (PRC2) in all mono-, di-, trimethylation (Laugesen et al. 2019). Five JMJ demethylases catalyse the removal of H3K27me3 in *Arabidopsis*, RELATIVE OF EARLY FLOWERING 6 (REF6), EARLY FLOWERING 6 (ELF6), JMJ13, JMJ30, and JMJ32 (Gan et al. 2014; Lu et al. 2011). It is assumed that many H3K27me3 demethylases have overlapping functions in euchromatin regions (Yan et al. 2018). A recent study has reported the distinct functions between REF6 and ELF6 in *Arabidopsis* (Antunez-Sanchez et al. 2020). Interestingly, REF6 is found the regulate the homeostasis of H3K27me1 in euchromatin regions in *Arabidopsis*, resulting in basal expression of genes (Antunez-Sanchez et al. 2020). The regulation of H3K27me3 is also found as an epigenetic modification regulating gene expression in response to environmental stimuli (Kwon et al. 2009; Shen et al. 2021; Yamaguchi et al. 2021).

1.4.3 ATP-Dependent Chromatin Remodelling Complexes

While DNA methylation and histone modification focus on adding or removing functional groups at DNA or histone molecules, the modulation by chromatin remodelling complexes (CRCs) alters the interaction between DNA and histone without changing the chemical components, this process is done by using protein complexes such as SWITCHING DEFECTIVE2/SUCROSE NONFERMENTING2 (SWI2/SNF2) family (Clapier and Cairns 2009; Peterson et al. 1994). In eukaryotes, the SWI2/SNF2 family can be classified into four groups due to

the protein sequence: SWI/SNF subfamily, Imitation Switch (ISWI) subfamily, Chromodomain Helicase DNA-Binding (CHD) subfamily, and Inositol requiring 80 (INO) subfamilies (Clapier and Cairns 2009; Ojolo et al. 2018). Each of them takes a crucial role in different biological aspects of eukaryotic cells. However, chromatin remodellers contain ATPase/helicase domains to utilise energy from ATP hydrolysis for modulating the interaction between DNA and histone (Clapier and Cairns 2009; Ojolo et al. 2018). The activity of CRCs results in nucleosome repositioning, ejection, unwrapping, or composition altering by histone variants leading to accessible (open) DNA regions that can interact with DNA-binding domains of proteins involved in transcription replication, or DNA repair (Clapier and Cairns 2009). In plants, CRCs are involved in all stages in the life cycle of each plant, including the maintenance of shoot and root apical meristem (SAM and RAM), cell differentiation, organ differentiation, and the development of reproductive organs (Ojolo et al. 2018). Moreover, one of the CRCs named BRAHMA (BRM) shows its physical interaction with the essential components in the abscisic acid (ABA) pathway, the phytohormone used in stress response in plants (Peirats-Llobet et al. 2016).

In conclusion, DNA methylation, histone modification, and chromatin remodelling are the mechanisms used by plants and other eukaryotes for controlling the interaction between histones and adjacent DNA. Enzymatic processes or protein complexes carry out these mechanisms and all of them are reversible, which allows the plant to use them in time-specific or cell type-specific manners in development.

1.5 Epigenetic Regulation in Response to Cold Stress in Plants

1.5.1 Epigenetic Regulation in Long-Term Cold Stress (Vernalisation)

Vernalisation, which promotes flowering after a long period of cold, is one of the most well-studied effects of environmental changes on specific gene expression mediated by epigenetic modifications. A key mechanism in vernalisation includes the epigenetic silencing of *FLOWERING LOCUS C* (*FLC*), a flowering repressor gene (Song et al. 2012; Sung and Amasino 2004). The silencing starts with the binding of PRC2 to the *FLC* before the cold exposure (De Lucia et al. 2008). Then, during the cold, PRC2 associates with two plant homeodomain (PHD) proteins: VERNALISATION INSENSITIVE3 (VIN3) and VERNALISATION5 (VRN5 or VIL1), resulting in the accumulation of H3K27me3 at the *FLC* locus (De Lucia et al.

2008; Sung and Amasino 2004). Interestingly, the silencing of *FLC* by the PHD-PRC2 complex continues to exist even after the cold exposure terminates, suggesting the stable epigenetic regulation under stress in plants (De Lucia et al. 2008).

1.5.2 Epigenetic Regulation of Short-Term Cold Responses

Various types of epigenetic regulation also exhibit crucial roles in short-term cold exposure. Kwon et al. (2009) showed the removal of repressive H3K27me3 at cold-responsive gene loci *COR15A* and *AtGolS3* during cold treatment. Histone acetylation associated with open chromatin is also involved in gene expression during cold treatment. HOS15, a WD40-repeat protein, acts as a facilitator of CULLIN4 (CUL4, one of CULLIN RING E3 ligases) to ligate ubiquitin to HISTONE DEACETYLASE 2C (HD2C), leading to the degradation of HD2C. The removal of HD2C at promoters of *COR15A, COR47,* and *RD29* results in opened promoter for binding with an upstream transcription factor, CBF proteins in this case (Park et al. 2018). A recent study has revealed the involvement of POWERDRESS (PWR) in the formation of the PWR-HOS15-CUL4 complex to remove HD2C and to act as a co-activator of CBF3 (Lim et al. 2020). Similarly, PICKLE (PKL), a CHD3-type chromatin remodelling factor, also regulates the expression of *CBF3* and a few downstream genes. A null mutant *pkl-1* shows an impaired expression of *CBF3* and *RD29A* (Yang et al. 2019). Interestingly, PKL is reported to be involved in the establishment of the H3K27me3 and the RdDM pathway (Yang et al. 2019).

The integration of DNA methylation with the cold stress response is still poorly understood (Kim et al. 2015). However, a few reports show the connection between prolonged cold treatment and DNA methylation levels in cold-responsive genes. In one cultivar of rubber tree (*Hevea brasiliensis* Reyan 7-33-97), a long period of chilling temperature induces hypomethylation of *HbICE1* and *HbCBF2* in association with increased transcriptional activities (Tang et al. 2018). In sugar beet (*Beta vulgaris*), hypermethylation in the *BvFLC* locus is crucial to promote vernalisation (Trap-Gentil et al. 2011). In *Arabidopsis*, *rdm4,* a null mutant of RNA-DIRECTED DNA METHYLATION 4 (RDM4), shows impaired *CBF2-3* and CBF regulon expression levels together with visible freezing sensitive phenotypes. However, the same effect is not found in *nrpe1,* a mutant in the large subunit of PolIV, suggesting that RDM4 regulate the cold-responsive pathway independently of RdDM. It is possible that RDM4 guides PolII to the promoter of *CBFs* to rapidly enhance the

expression under a cold stress (Chan et al. 2016). The observation of four *Arabidopsis* accessions (Per-0, Gy-0, Ms-0, and Wa-1) shows the negative correlation between methylation levels of *AtICE1* and the expression levels of *CBFs*. The inhibition of DNA methylation by 5-azacytidine increases freezing tolerance, suggesting the connection between DNA methylation and the cold-responsive pathway (Xie et al. 2018).

Apart from epigenetic regulation modulating nucleosome structures, long non-coding RNA (lncRNA) can indirectly regulate genes in the cold-responsive pathways. For instance, *SVALKA,* a lncRNA that overlaps in antisense orientation with *CBF1* transcripts (*asCBF1*), down-regulates *CBF1* expression in response to cold (Kindgren et al. 2018).

Recently, several studies have investigated how multiple epigenetic mechanisms act on cold-responsive pathways. These studies have concluded that histone modifications play crucial roles in modulating the expression of several *CORs*, establishing a close connection between environmental changes, epigenetics and transcription.

1.6 Stress Memory in Plants

Like human immunity, plants are thought to have an adaptive stress memory that allows them to survive under recurrent environmental stress conditions (Crisp et al. 2016). This stress memory is thought to be underpinned by epigenetic changes that accumulate during stress exposure and that are mitotically, and sometimes meiotically stable (Chinnusamy and Zhu 2009). Moreover, stress memory can help plants withstand harmful stress exposures when pre-exposed to the same or related stress before, a phenomenon known as priming (Crisp et al. 2016). There are two levels of stress memory in plants: (1) the somatic stress memory - the stress memory that is established and maintained through the life cycle of an individual plant and (2) the heritable stress memory (or transgenerational stress memory) - the memory that can be passed on to the next generation after sexual reproduction.

Based on the gene expression patterns, Baurle and Trindade (2020) defined three types of memory genes: (1) type I memory genes showing the induced/repressed expression levels after the first stress exposure and are maintained in the recovery stage (normal growth condition), (2) type II memory genes showing an induction/repression during the first exposure (priming stress), but the expression level

is back to normal in the recovery period. However, these genes will exhibit hyper-induction/hyper-repression during subsequent stress exposures (triggering stress), and (3) non-memory genes, which are used for the genes that cannot be categorised by the previous types (figure 1.3). Following this rule, vernalisation is a great example of a type I memory gene due to the maintenance of repressive H3K27me3 at the *FLC* locus after the endpoint of prolonged winter. However, examples of type II memory genes in cold response are hardly found. It has been reported that the survival rates in freezing temperature of plants pre-treated with 4oC are higher than in plants with non-acclimation, suggesting that a group of type II memory genes are hyper-induced. However, there is no comparison between expression levels of cold-responsive genes in both samples (Park et al. 2018). At the molecular level, Kwon et al. (2009) found no evidence for changes in H3K27me3 at *COR15* and *AtGOLS3* loci after the first cold treatment that could result in hyper-induction of expression after subsequent exposures.

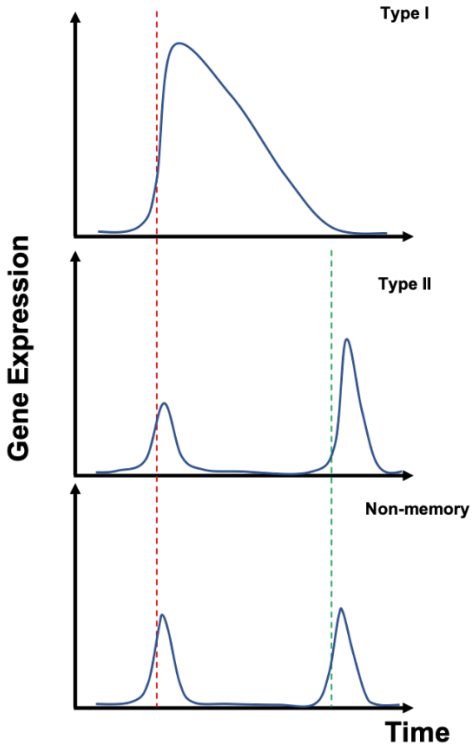

Figure 1.3 Three types of stress memory genes in plants. Type I stress memory genes peak after the stress exposure (red dash line), and the expression level is detectable even in the recovery stage. Type II memory genes show an induction by the first stress treatment (red dashed line). The expression level is back to normal in the recovery stage. The hyper-induction of expression level is caused by subsequent exposure (green dashed line). Non-memory genes show equal expression levels in all stress exposure with no expression during recovery (modified from Baurle and Trindade (2020)).

Heritable stress memory in plants contains two sub-classes depending on the stability of memory through plant reproduction: intergenerational stress memory and transgenerational stress memory. Intergenerational stress memory in the plant is defined as the stress memory that comes from the stressed generation (G_0) that can be inherited only by the first stress-free generation (G_1), while detectable memory from more than two non-stress generations (G_2) is classified as transgenerational stress memory or adaptive transgenerational plasticity (Lamke and Baurle 2017). Various biotic and abiotic stresses have been shown to establish stable memory in plants mediated by epigenetic modifications (Crisp et al. 2016; Hauser et al. 2011; Lamke and Baurle 2017). Boyko et al. (2007) used the first progeny of tobacco plant

(*Nicotiana tabacum*) infected by tobacco mosaic virus (TMV) to show genome-wide hypermethylation and specific hypomethylation patterns in the leucine-rich repeat (LRR) region of viral resistance genes. In *Arabidopsis*, the first stress-free generation from plants primed with a mild level of sodium chloride exhibited changes in methylation pattern associated with expression level compared with control samples (Bilichak et al. 2012). Boyko et al. (2010) used *Arabidopsis* plants exposed to five different types of abiotic stress (salinity, heat, cold, flood, and ultraviolet light). Only the first stress-free progeny from salt-treated plants shows enhanced adaptation. Genomic methylome data from better-adapted samples show hypermethylation in the promoter region/ gene body of several genes associated with signalling, protein metabolism, histone modification, stress and pathogen response. Moreover, intergenerational stress memory in response to iron deficiency has been reported to associate with increased Somatic Homologous Recombinant (SHR) (Murgia et al. 2015). One non-stress generation is not enough to claim the effect of transgenerational stress memory because of the influence of that particular stress during gamete production or fertilisation (Lamke and Baurle 2017). However, some evidence supports the possibility of stable transgenerational stress memory mediated by chromatin marks. Hypomethylation is found in genes involved in some signalling pathways and DNA repair. Priming *Arabidopsis* in G_0 generation with avirulent pathogen *Pseudomonas syringae* pv *tomato* DC3000 (*Pst*DC3000) results in increased resistance to lethal oomycetes *Hyaloperonospora arabidopsidis* in non-stress G_2 generation, indicating transgenerational stress memory in response to biotic stress (Luna et al. 2012). However, changes in methylation were only investigated in the resistant G_1 generation.

Studies on inter- and trans-generational stress memory in plants indicate that DNA methylation plays an important role in maintaining the memory created during the initial exposure to stress and in the inheritance to offspring. This is possible because DNA methylation is mitotically and meiotically stable (Crisp et al. 2016; Hauser et al. 2011). So, when the first stress exposure induces changes in DNA methylation at the genomic scale, the changes are carried out from vegetative to reproductive development until fertilisation. It has been shown that *Arabidopsis* DICER-LIKE2 and DICER-LIKE3 mutants, *dcl2* and *dcl3*, which are impaired in the RdDM pathway, lack transgenerational salt stress memory (Boyko et al. 2010).

Even though many studies support the possibility of stress memory in plants, there are also reports of memory resetting or forgetfulness mechanisms taking place during the recovery stage (Crisp et al. 2016). Transgenerational stress memory requires long-term stability of stress-induced epigenetic changes, therefore bypassing three key development processes: (1) the transition from vegetative growth to reproductive growth, (2) the generation of male and female gametes and (3) double fertilisation and seed development. During the transition from vegetative to reproductive development, lateral margins of shoot apical meristem (SAM) form the floral meristem and give rise to the inflorescence (Sharma and Fletcher 2002). So, stress-induced changes in epigenetic levels are supposed to originate in these meristems for stable transmission. However, in a recent study Gutzat et al. (2018) monitored DNA methylation and expression level of transposable elements (TEs) and found stage-specific epigenetic reprogramming in the shoot apical meristem during the vegetative stage and reproductive growth. These results suggest that a yet unknown mechanism protects meristem cells from the accumulation of epigenetic changes, which could be considered a barrier to transgenerational stress memory. In addition, male and female gametogenesis undergo multiple epigenetic resetting mechanisms. For example, CHH methylation is lost due to the downregulation of a gene encoding DRM2 during the production of sperm cells (Calarco et al. 2012). The expression of genes encoding MET1 and CMT3 is barely detected in egg cells suggesting the loss of CG and CHG methylation maintenance during the female gametogenesis (Kawashima and Berger 2014). Moreover, loss of CG methylation mediated by the activity of DME glycosylase in male germlines is necessary for the transmission of salt stress memory in the *Arabidopsis* (Wibowo et al. 2016).

In summary, multiple reports have proposed the idea that plants have a form of stress memory that can be maintained within and across multiple generations. However, the precise mechanisms underpinning this memory is limited and the phenotypic consequences are unclear. DNA methylation has been implicated in the establishment and maintenance of stress memory, but previous studies have been hampered by the complexity of multiple resetting/reprogramming mechanisms taking place during vegetative growth and sexual reproduction.

1.7 Transgenerational memory in clonal plants

A major barrier to the transmission of transgenerational stress memory may be caused by the epigenetic reprogramming taking place in meristematic cells and during gametogenesis and sexual reproduction. In nature, most plant species can propagate asexually from meristematic structures formed in vegetative tissues (roots, stems, leaves, and storage organs such as rhizomes and tubers) (Silvertown 2008). Asexual propagation also includes apomixis, resulting from the asexual formation of embryos in developing ovules (Bicknell and Koltunow 2004; Silvertown 2008). Moreover, clonal plants can be generated by the exogenous application of phytohormones in tissue culture leading to the development of new organs (organogenesis) or by inducing the formation of embryo-like structures (somatic embryogenesis) (Zimmerman 1993).

In *Arabidopsis*, somatic embryogenesis (SE) can be induced by overexpression of several zygotic transcription factors (Stone et al. 2008; Waki et al. 2011). The RWP-RK DOMAIN-CONTAINING PROTEIN (RKD) gene family is of particular interest because its member genes are widely conserved in a range of plant species (Koi et al. 2016). Ectopic expression of RWP-RK DOMAIN-CONTAINING 4 (RKD4) enables the production of clonal plants from multiple tissues and organs (Wibowo et al. 2018). This strategy allows the generation of independent progenies from roots and leaves, termed root-origin (RO) and leaf-origin (LO) regenerants, which can be used to investigate the basis of cellular memory (figure 1.4). DNA methylation analysis of clonal plants has revealed that the DNA methylation accumulating in clonal plants is underpinned by the tissue of origin and DNA methylation imprints found in clonal plants are meiotically heritable after several cycles of sexual reproduction. Moreover, these epigenetic imprints have profound phenotypic consequences as plant clones from different organs displayed differences in growth and their relationship with beneficial and pathogenic microbial organisms.

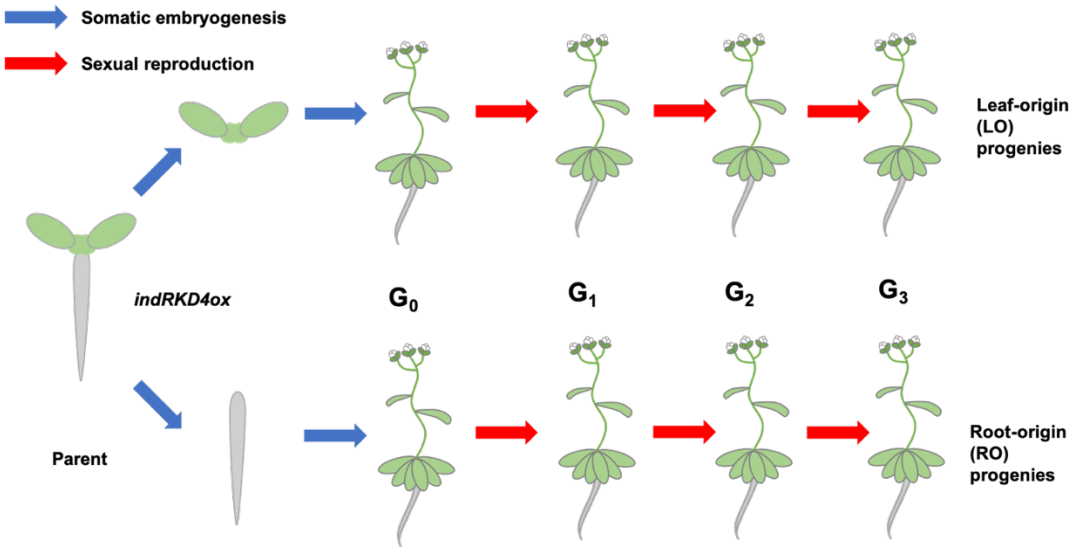

Figure 1.4 The induction of somatic embryogenesis upon ectopic overexpression of RKD4. The overexpression of the RKD4 transcription factor (indRKD4) results in the induction of somatic embryos in primordial leaves and developing roots. Leaf-origin and root-origin plants in the G_0 generation are grown in normal growth conditions, and G_0 seeds are used to propagate G_1 – G_3 generations. LO, leaf-origin plants, RO, root-origin plants. (Modified from Wibowo et al. 2018)

Since the DNA methylation imprints found in progenies of LO and RO plants are partially stable, Putra et al. (2018) hypothesised that this could enable the transmission of stress-induced epigenetic marks and bypass the resetting mechanisms operating in meristematic cells. To test this hypothesis, plants were exposed to abiotic and biotic stress during cloning, and independent progenies were created by sexual reproduction under normal growth conditions (figure 1.5). Heritable adaptive phenotypes were assessed in clones from G2 and G3 progenies, which revealed higher adaptability of clonal lineages to both abiotic and biotic stress.

In conclusion, clonal lines from different tissues using zygotic transcription factors enables the dissection of the molecular mechanisms underpinning the establishment and maintenance of stress memory responses in plants.

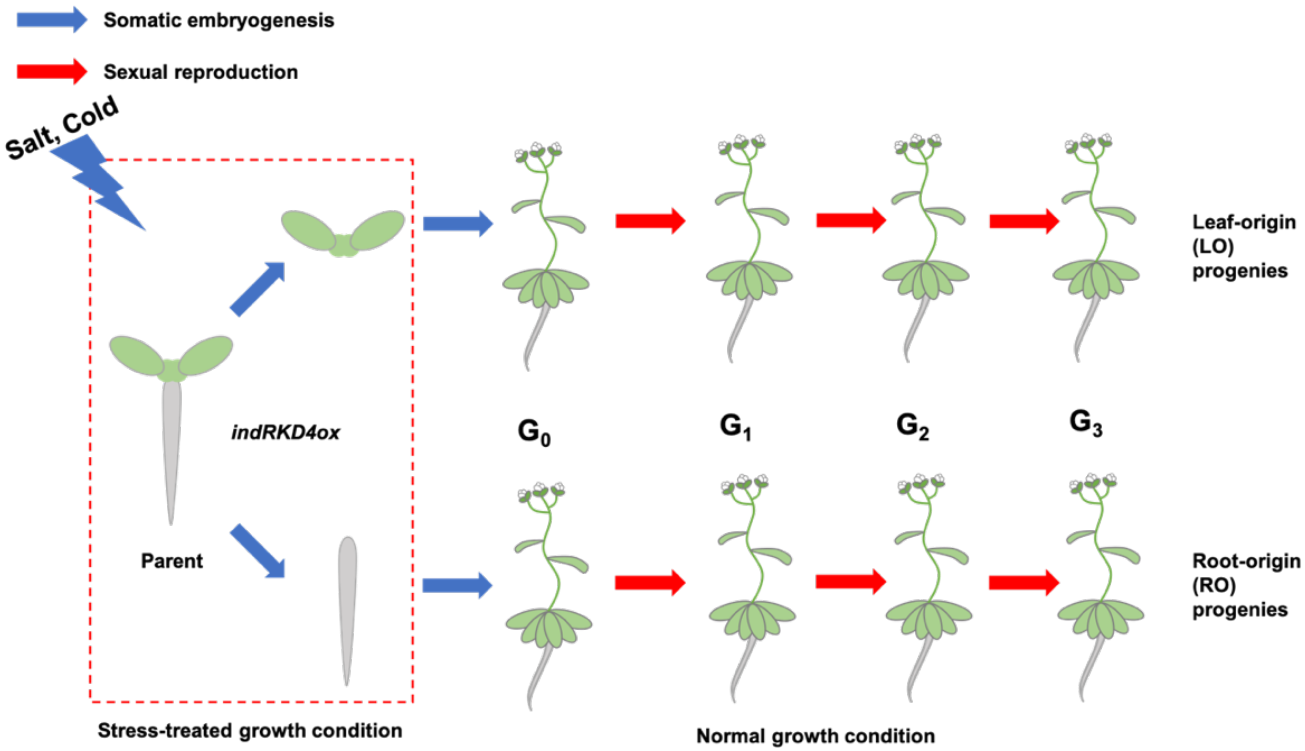

Figure 1.5 Enhanced transgenerational stress memory in *A. thaliana* regenerated by indRKD4 system. (A) During the induction of somatic embryogenesis, parent plants were exposed to salinity (75 mM NaCl) or cold (4°C). Leaf-origin and root-origin plants in the G_0 generation were grown in normal growth condition, and G_0 seeds were used to propagate G_1 – G_3 generations. LO, leaf-origin plants, RO, root-origin plants.

1.8 A hypothetical model for enhanced transgenerational stress memory in plants

Previous work has revealed that cloning from specific tissues could result in stable adaptive stress responses. However, the molecular mechanisms implicated in the establishment and maintenance of epigenetic changes through multiple generations are still unclear. In this study, I hypothesised that the transcriptional cascade activated in response to stress underpins the formation of epigenetic imprints in somatic cells and that these marks can be propagated after cloning through sexual reproduction (figure 1.6). These epigenetic imprints could ultimately modulate transcriptional changes and enhance the tolerance to stress of clonal lineages.

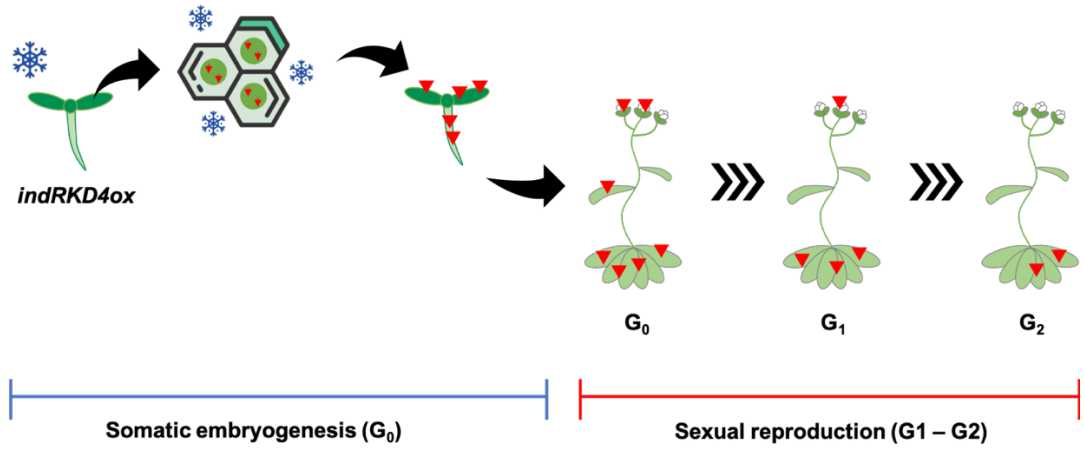

Figure 1.6 The schematic diagram representing the hypothesis of the study. Epigenetic modifications mediated by stress priming during somatic embryogenesis (red arrows) are carried to the progenies as a memory. Plants propagated from somatic embryos are expected to maintain high stress-mediated epigenetic changes due to no barrier to sexual reproduction. Then, plants in G_1 and G_2 are propagated by seeds and will gradually lose some changes in the genome. However, it is still possible to observe some epigenetic changes, which can refer to transgenerational stress memory.

1.9 Project Aims and Objectives

The main aim of this thesis is to dissect the molecular mechanisms implicated in the establishment and maintenance of induced stress memory in plants, using Arabidopsis and low temperature conditions as model systems. To this aim, I have defined two different objectives:

(1) Define the role of ICE1 in the cold signalling pathway. Recent reports have questioned the role of this transcription factor in the transcriptional network modulated by low temperature. To address this unresolved issue, I will use genetic lesions and artificial microRNA targeting to determine if ICE1 is necessary for cold-mediated transcriptional responses. In addition, I will determine how the interaction between ICE1, and its direct targets is regulated.

(2) Define the molecular mechanisms underpinning transgenerational stress memory responses observed upon asexual propagation. First, I will monitor the molecular and phenotypic changes present in clonal lineages generated from different tissue exposed to low temperatures. Secondly, I will manipulate during cloning the expression of *CBF* transcription factors, integral components of the transcriptional network modulated by cold. Using a genome-wide approach I will determine if activation of the CBF transcriptional network is necessary and sufficient to mediate transgenerational stress memory responses in clonal plants.

Chapter 2 Materials and Methodology

2.1 Plant Materials and Growth Conditions

Arabidopsis thaliana (Col-0) was used as wildtype plants and *A. thaliana* plants (Col-0) containing the dexamethasone-inducible construct of synthetic RWP-RKD4 (AT5G53040) gene (so-called indRKD4) were used as the background plants in this study. Constructs of all transgenes were transformed to wildtype and/or background plants by agrobacterium transformation except for *ice1-2* mutant seeds stock (SALK_003155), which was provided by Dr Chien-Chih Yang (National Taiwan University).

Seeds of *A. thaliana* were sterilised using the gas sterilisation method: a bleach solution (50 mL) mixed with concentrated HCl (3mL) was used to sterilise seeds for 4 hours. Then, sterilised seeds were kept in 0.1% agarose and stratified at 4^{o}C for 2-3 days to break seed dormancy. Seeds were sowed into MS (Murashige and Skoog) media (Sigma Aldrich) containing 8 g/L of phytoagar (Duchefa Biochemie) (pH 5.7-5.8 with 1M KOH). The media plates were kept in a short-day growth cabinet (12 h/12 h; day/night-time) at 22^{o}C. In the case of growing plants in soil, plants in the seedling stage were transferred to soil and kept in long day conditions (16 h (22^{o}C)/8 h (18^{o}C); day/night-time).

2.2 General Cloning Methods

2.2.1 Generation of amiRNA Transgenic Lines

To downregulate gene expression of selected genes we constructed artificial microRNAs (amiRNA) (Schwab et al. 2006). The selection of amiRNA to target *ICE1* or *CBFs (CBF1*, *CBF2,* and *CBF3*) was carried out following standard procedures described in http://wmd3.weigelworld.org/. The selection process of the best candidate was based on the criteria suggested by (Schwab et al. 2006). The best candidate for amiRNA construct must meet the following selection criteria.

(i) No mismatch between nucleotides at positions 2 to 12 in all targets.
(ii) Similar mismatches in all intended targets
(iii) Absolute Hybridization energy between -35 and -38 kcal/mole
(iv) (optional) One or two mismatches at the positions 18 – 20
(v) (optional) Target site position towards the 3’ end of all targets

The best two candidates from all selection criteria were chosen to minimise the risk of not having an efficient transgenic line. After candidate selection, the amiRNA construct was engineered into miR319a precursor by site-directed mutagenesis. The lists of primers used in amiRNA construction process were automatically generated from web-based oligos design (http://wmd3.weigelworld.org/). pRS300 containing miR319a precursor was used as a template to amplify the amiRNA fragments. The DNA primers used in constructing amiRNA targeting *ICE1* and *CBFs* were listed in table 2.1. The PCR conditions used to amplify DNA fragments were shown in http://wmd3.weigelworld.org/. Each amiRNA construct has four specific primers (P1 – P4) to amplify amiRNA fragments, and two generic primers, amiRNA_A and amiRNA_B, used in the final PCR step. The amiRNA construct from site-directed mutagenesis in the pRS300 vector was then fused with attB1 and attB2 adapters and was applied using PCR with primers attB1_amiRNA_A and attB2_amiRNA_B. Then, the amplified DNA fragments were cloned in pDONR207 using Gateway recombination and sequenced to confirm their integrity. These clones were integrated into the pMDC7:OLE1-pCsVMV binary vector using Gateway recombination and fully sequenced to confirm their integrity.

2.2.2 Generation of Over-expression Lines

To generate ICE1 and CBF3 over-expression construct, we generated chemically synthesised gBlocks (IDT). These constructs were designed to contain the full Open Reading Frame flanked attB1 and attB2 Gateway recombination sites. The Gibson assembly method was carried out following the manufacturer's instruction (New England Biolab®). Two fragments of ICE1 or CBF3 in minimum concentration (0.02 pmole) were mixed with Gibson Assembly® master mix and incubated at 50^{o}C for 1 hour. Synthetic gBlocks were subcloned in pDONR207 using Gateway recombination and sequenced to confirm their integrity. These clones were subcloned in pMDC7:OLE1 binary vectors using Gateway recombination and fully sequenced to confirm their integrity.

Table 2.1 List of DNA primers used in cloning and genotyping

Primer names	Sequence (5' – 3')	Description
amiRNA_A	CTGCAAGGCGATTAAGTTGGGTAAC	amiRNA construct
amiRNA_B	GCGGATAACAATTTCACACAGGAAACAG	amiRNA construct
amiRNA-ice1_1_P1	GATCAGACTCATAGTTCAACCGATCTCTCTTTTGTATTCC	amiRNA-ice1 candidate #1
amiRNA-ice1_1_P2	GATCGGTTGAACTATGAGTCTGATCAAAGAGAATCAATGA	amiRNA-ice1 candidate #1
amiRNA-ice1_1_P3	GATCAGTTGAACTATCAGTCTGTTCACAGGTCGTGATATG	amiRNA-ice1 candidate #1
amiRNA-ice1_1_P4	GAACAGACTGATAGTTCAACTGATCTACATATATATTCCT	amiRNA-ice1 candidate #1
amiRNA-ice1_2_P1	GATTTTAAAGGGACTTAGTTCTGTCTCTCTTTTGTATTCC	amiRNA-ice1 candidate #2
amiRNA-ice1_2_P2	GACAGAACTAAGTCCCTTTAAAATCAAAGAGAATCAATGA	amiRNA-ice1 candidate #2
amiRNA-ice1_2_P3	GACAAAACTAAGTCCGTTTAAATTCACAGGTCGTGATATG	amiRNA-ice1 candidate #2
amiRNA-ice1_2_P4	GAATTTAAACGGACTTAGTTTTGTCTACATATATATTCCT	amiRNA-ice1 candidate #2
amiRNA-cbfs_1_P1	GATACGAAACTTCTTACGAGCCGTCTCTCTTTTGTATTCC	amiRNA-cbfs candidate #1
amiRNA-cbfs_1_P2	GACGGCTCGTAAGAAGTTTCGTATCAAAGAGAATCAATGA	amiRNA-cbfs candidate #1
amiRNA-cbfs_1_P3	GACGACTCGTAAGAACTTTCGTTTCACAGGTCGTGATATG	amiRNA-cbfs candidate #1
amiRNA-cbfs_1_P4	GAAACGAAAGTTCTTACGAGTCGTCTACATATATATTCCT	amiRNA-cbfs candidate #1
amiRNA-cbfs_4_P1	GATTTGGGTGACGAGTCTCACGCTCTCTCTTTTGTATTCC	amiRNA-cbfs candidate #4
amiRNA-cbfs_4_P2	GAGCGTGAGACTCGTCACCCAAATCAAAGAGAATCAATGA	amiRNA-cbfs candidate #4
amiRNA-cbfs_4_P3	GAGCATGAGACTCGTGACCCAATTCACAGGTCGTGATATG	amiRNA-cbfs candidate #4
amiRNA-cbfs_4_P4	GAATTGGGTCACGAGTCTCATGCTCTACATATATATTCCT	amiRNA-cbfs candidate #4

Primer names	Sequence (5’ – 3’)	Description
attB1_amiRNA_A	GGGGACAAGTTTGTACAAAAAAGCAGGCTCT-GCAAGGCGATTAAGTTGGGTAAC	attB1 adapter of amiRNA constructs
attB2_amiRNA_B	GGGGACCACTTTGTACAAGAAAGCTGGGTGC-GGATAACAATTTCACACAGGAAACAG	attB2 adapter of amiRNA constructs
ICE1_F_J.Durr	TGTGGTGGTTTCACAGCTCC	Genotyping ICE1
ICE1_R_J.Durr	TGATGCTCTATCCATTTTGCTGA	Genotyping ICE1
ICE1_CDS_F	AAGCGGCTGAGAGTGTTCAGAT	Genotyping ICE1
ICE1_CDS_R	GAGTTTGCGGTGTAGGTGTCAA	Genotyping ICE1
ice1-2_F	AATCTGATGGCTGAGAGGAGAA	Genotyping ice1-2 T-DNA
ice1-2 R	TTCATGGTAGCGAGCAACAGAC	Genotyping ice1-2 T-DNA
M13_F	ACTGGCCGTCGTTTTAC	Colony PCR in pMDC7:OLE1

2.2.3 Gateway Recombination

Gateway cloning was carried out following standard procedures as per the manufacturer's instructions (Invitrogen). The BP reaction mixture contained the cloning vector (pDONOR207) and BP enzyme mix and was incubated at room temperature overnight. The reaction was transformed into *E. coli* competent cells (Top10 F^1) via heat shock method.

2.2.4 Plasmid Transformation and Propagation in *Escherichia coli.*

For the transformation of plasmids, 50 µl of competent cells (*E. coli* Top10 F^1) was mixed with DNA fragments. The mixture was incubated in ice for 30 minutes. Then, the heat shock process was done by incubating the mixture at 42ºC for 45 seconds and immediately placed in ice for 3 minutes. Finally, the chemically competent cells containing DNA product were incubated in 1ml of LB media at 37ºC for 1 hr and grown overnight at 37ºC on media plates containing antibiotics for the screening.

2.2.5 Plasmid Transformation and Propagation in *Agrobacterium tumefaciens*.

The electrocompetent Agrobacterium tumefaciens GV3101 was thawed on ice. A binary vector was directly added to the cells and mixed gently. The cells were transferred into an electrophoresis cuvette, put into MicroPulserTM Electroporator (Bio-Rad, UK) and pulse applied using the Agr setting (2.20 kV). LB low salt (1 mL) was added to the cells and the resulting mixture was incubated in a 28°C shaking incubator (220 rpm) for 1 hour. The cells were spread onto an LBA plate supplemented with rifampicin (10 mg·L-1), spectinomycin (50 mg·L-1), streptomycin (50 mg·L-1) and gentamycin (10 mg·L-1) grown for 48 hours 28°C and positive transformants were confirmed by colony PCR.

2.2.6 Plasmid Miniprep Isolation

Bacterial colonies were picked and inoculated into 5ml of LB overnight at 37°C in suitable antibiotic selection. The bacterial cells were centrifuged at 5000g for 5 minutes and plasmid DNA extraction was carried out using Qiaprep Spin Miniprep Kit (Qiagen) following the manufacturer's manual. The plasmid DNA was stored at -20°C for subsequent use.

2.2.7 DNA Sanger Sequencing

Bacterial cultures were inoculated with positive colonies selected on antibiotic media and grown overnight at 37°C. Plasmid isolation was carried out with overnight cultures using Plasmid mini kit (Qiagen). The isolated plasmid (500ng) was combined with sequencing primers or internal oligos and sequenced using Sanger sequencing (Eurofins-GATC).

2.2.8 Stable Transformation of Arabidopsis Plants by Floral Dip

A single Agrobacterium colony carrying a binary vector was inoculated in 5ml of low salt LB containing appropriate antibiotics. The overnight culture was used to inoculate 500ml low-salt liquid culture with appropriate antibiotics and grown overnight at 28^{o}C. Agrobacterium cell cultures were spun down at 4000g for 15 minutes and the cell pellet was resuspended in 500 mL of 5% sucrose. Arabidopsis plants were transformed using the floral dip method described previously (Zhang et al. 2006).

2.3 General Molecular Methods

2.3.1 Genomic DNA Extraction

For genotyping of transgenic plants, high throughput DNA extraction was performed. Leaf samples of approximately 1cm^2 were collected in 96-well block with a 2 mm diameter metal bead in each well. Samples were flash frozen and were ground for 18 revolutions per second for 1 minute. Then the block was centrifuged to allow the tissue to sit on the well's bottom. 300 µl of DNA extraction buffer (100 mM Tris-Cl, pH 8.0; 50 mM EDTA, pH 8.0; 500 mM NaCl; 10 mM β-Mercaptoethanol) was added to each well using a multi-channel pipette, after adding 40 µl of 10% SDS samples were mixed by vortexing and incubated at 65^{o}C for 20 minutes. Later, samples were incubated on ice for 5 minutes before adding 100ul of 5M potassium acetate. Samples were further incubated for at least 20 minutes on ice. Samples were centrifuged at maximum speed for 20 minutes, and 125 µl of supernatant was transferred into a fresh 96-well block. After adding 200 µl of isopropanol, samples were incubated at -20^{o}C for at least 30 minutes. Samples were centrifuged at max speed for 15 minutes; isopropanol was removed, and the pellet was washed with 70%

ethanol. DNA pellet was dried after removing 70% ethanol. Samples were resuspended in 100 µl of TE buffer (10 mM Tris-HCL, 1 mM EDTA, pH 8.0 with 20 µg/µl RNase (Invitrogen, UK)).

2.3.2 PCR Genotyping

For genotyping of transgenic plants, all PCR reactions were carried out in an MJ Research, PTC-225 Peltier thermal cycler. Extracted gDNA was used as a template. A master mix was prepared for a 20 µl PCR mixture. PCR reaction mixture contained 0.5 µl gene-specific primers (0.2 µM), 0.5 µl dNTPs (10mM), 2 µl 10X KAPA Taq Buffer A (KAPA Biosystems), 0.1 µl KAPA Taq DNA Polymerase (5 units·µl^{-1}; KAPA Biosystems), H2O (13.7 µl). 17 µl of master mix was combined with 3 µl of template DNA. The programme was set at 95^{o}C for 2 minutes initially for denaturation, followed by 30 cycles at 95^{o}C for 30 seconds, 58^{o}C for 30 seconds and 72^{o}C with varied extension times depending on the length of the target sequence (1kb = 1minute), followed by a final extension at 72^{o}C for 5 minutes. The amplified fragments were checked via gel electrophoresis.

2.3.3 Colony PCR

A master mix was prepared for a 20 µl PCR mixture. PCR reaction mixture contained 0.5 µl gene-specific primers (0.2 µM), 0.5 µl dNTPs (10mM), 2 µl 10X KAPA Taq Buffer A (KAPA Biosystems), 0.1 µl KAPA Taq DNA Polymerase (5 units·µl^{-1}; KAPA Biosystems), H2O (16.7 µl). Overnight colonies were picked, resuspended in water and added directly to the PCR reaction. The amplified fragments were checked via gel electrophoresis.

2.3.4 RNA Extraction

Around 100 mg of the whole plant tissue was collected in a 1.5 ml Eppendorf tube, frozen in liquid nitrogen and stored in a -80^{o}C freezer. Tissue samples were ground using TissueLyser II (Qiagen) with sterile RNAse-free glass beads. RNA samples were extracted using the RNeasy plant mini kit (Qiagen). RNA quantity was measured by NanoDrop (Thermo Fisher Scientific). Genomic DNA in RNA samples was removed by a TURBO DNA-free kit (Thermo Fisher Scientific).

2.3.5 cDNA Synthesis and Reverse Transcription Polymerase Chain Reaction (RT-PCR)

Approximately 250 ng of DNA-free RNA was used to synthesise first-strand cDNA using the RevertAid First Strand cDNA synthesis kit (Thermo Fisher Scientific). 1 µl of cDNA suspension was used as a template in PCR using the KAPA Taq PCR kit (Sigma-Aldrich) with primers listed in table 2.2 with the following condition: 2.5 µl of 10X PCR buffer, 0.5 µl of 10 mM dNTP, 0.5 µl of forward and reverse primers, 0.1 µl of Taq polymerase, and 18 µl of ddH_2O. The following PCR program was used: 95 ºC for 2 minutes followed by 25 cycles of 95ºC for 30 seconds, annealing temperature (depending on a pair of primers) for 30 seconds, 72ºC for 2 minutes, and 72ºC for 10 minutes to finish PCR.

PCR products were mixed with 6X loading dye and performed gel electrophoresis in 1% agarose gel. The results were visualised under UV light to check the level of expression of specific genes by the intensity of DNA bands. *GAPDH* was used as a control to check the integrity of the cDNA template.

2.3.6 Quantitative RT-PCR (qRT-PCR)

Approximately 500 ng of DNA-free RNA was used as a template to synthesise first-strand cDNA using the RevertAid First Strand cDNA synthesis kit (Thermo Fisher Scientific). The qRT-PCR mixture contained 5 µl of 1:10 diluted cDNA template, 0.2 µM of each primer (forward and reverse), and 12.5 µl of SYBR® Green master mix (Thermo Fisher Scientific). The following cycling profile was used: 95 ºC for 10 min, followed by 40 cycles of 95 ºC for 10 s, 60 ºC for 15 s, and 72 ºC for 15 s. The melting curve was determined in the range of 60–95 ºC, with a temperature increment of 0.01 ºC/sec. Three technical replicates were run per sample. Ct data were obtained and used to calculate the relative expression level by the ΔΔCt method using GADPH (AT1G13440) in normalisation (Schmittgen and Livak 2008). The primers for qRT-PCR were listed in table 2.2.

Table 2.2 List of DNA primers used in RT-PCR and qRT-PCR

Primer names	Sequence (5' – 3')	Experiment
RT_ICE1_F	TCAACTCCTCCTGGATCTTTGC	RT-PCR
RT_ICE1_R	TCTAACCTCAACTCTAGCTTGCTG	RT-PCR
RT_CBF3_F	GAAACTCCGGTAAGTGGGTTTG	RT-PCR
RT_CBF3_R	TTGGATGTCCTTAGCGCAAGTT	RT-PCR
RT_COR15A_F	TCTCTCATGGCGATGTCTTTCT	RT-PCR
RT_COR15A_R	AGCTTTCTTTGTGGCCTCGTT	RT-PCR
GAPDH_F	TTGGTGACAACAGGTCCAAGCA	RT-PCR
GAPDH_R	AAACTTGTCGCTCAATGCAATC	RT-PCR
DREB1A_qRTf	CGCTGACTCGGCTTGGA	qRT-PCR
DREB1A_qRTr	GCATCACACATCTCATCCTGAAAC	qRT-PCR
DREB1B_qRTf	AGTCAACATGCGCCAAGGAT	qRT-PCR
DREB1B_qRTr	ATGTCCAGGCCATGATTCG	qRT-PCR
DREB1C_qRTf	TGACGTGTCCTTATGGAGCTA	qRT-PCR
DREB1C_qRTr	CTGCACTCAAAAACATTTGCA	qRT-PCR
COR15A_qRTf	GTCAGAGTCGGCCAGAAAACTC	qRT-PCR
COR15A_qRTr	AACAACGTAGTCTTTCGCTTTCTCA	qRT-PCR
RD29A_qRTf	CTTGATGGTCAACGGAAGGT	qRT-PCR
RD29A_qRTr	CAATCTCCGGTACTCCTCCA	qRT-PCR
AT5G41740_qRTf	ACAACGATCAGTGTCCAGGT	qRT-PCR
AT5G41740_qRTr	TCGTAGCTCTCAACTGGCAA	qRT-PCR

2.4 Selection for Homozygous Transgenic Lines

Binary vectors used for plant transformation carry the pOLE1:OLE1-RFP reporter. Seeds from Agrobacterium-transformed plants (T_0 seeds) were collected and screened under a fluorescent dissecting microscope. Then seeds with RFP were grown to propagate plants in the T_1 generation. Seeds from individual T_1 plants (so-called T_1 seeds) were collected and screened for RFP. The excellent candidate of T_1 seeds must have a ratio of RFP and non-RFP seeds around 3 to 1, indicating that only one copy of T-DNA was inserted. The T_1 candidates were continually grown in soil to propagate T_2 seeds, and the T_2 seeds will be used to screen for homozygous transgenic plants.

2.5 Induction of Somatic Embryogenesis

Seeds of indRKD4 plants carrying different transgene constructs were sterilised and stratified for 48 hours at 4°C with no light. Seeds were sowed in ½ MS media plates for 36 – 48 hours before being transferred to full MS media + 1% sucrose and 30 µM dexamethasone (Sigma Aldrich) for 7 days before moving to specific growth conditions when callus-like structures are visible in root and leaves. If transgene induction with a different chemical inducer is required, plants were transferred to media with β-estradiol or a mock solution. MS media plates contained 1% sucrose, 20 µM dexamethasone, and 30 µM β-estradiol or 30 µM DMSO. Plants were grown in long day condition (16 h (22°C)/8 h (18°C); day/night-time). If the cold treatment is required, plants were incubated in the cold cabinet for seven days with two days at 4°C and one day at 22°C and continued the cycle until it reached seven days. Then, plants in all growth conditions were transferred to MS media with 1% Sucrose and continued growing until somatic embryos could be extracted (figure 2.1). Somatic embryos were kept under short-day conditions for 14-21 days before transferring to the soil as plants in the G_0 generation. Seed stocks from G_0 plants were labelled as G_1 seeds and used for sexual propagation until the G_2 generation of plants, as illustrated in figure 2.2. All generated clonal lines and the method for sexual propagation are summarised in table 2.3.

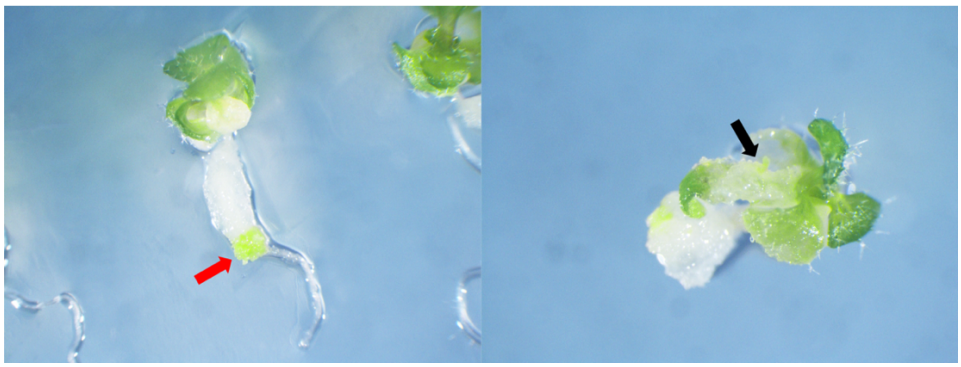

Figure 2.1 Clonal propagation in *Arabidopsis* using indRKD4. After growth in media with dexamethasone, plants are transferred to MS media + 1% sucrose to induce the somatic embryos from root meristem (red arrow) and leaf primordial (black arrow).

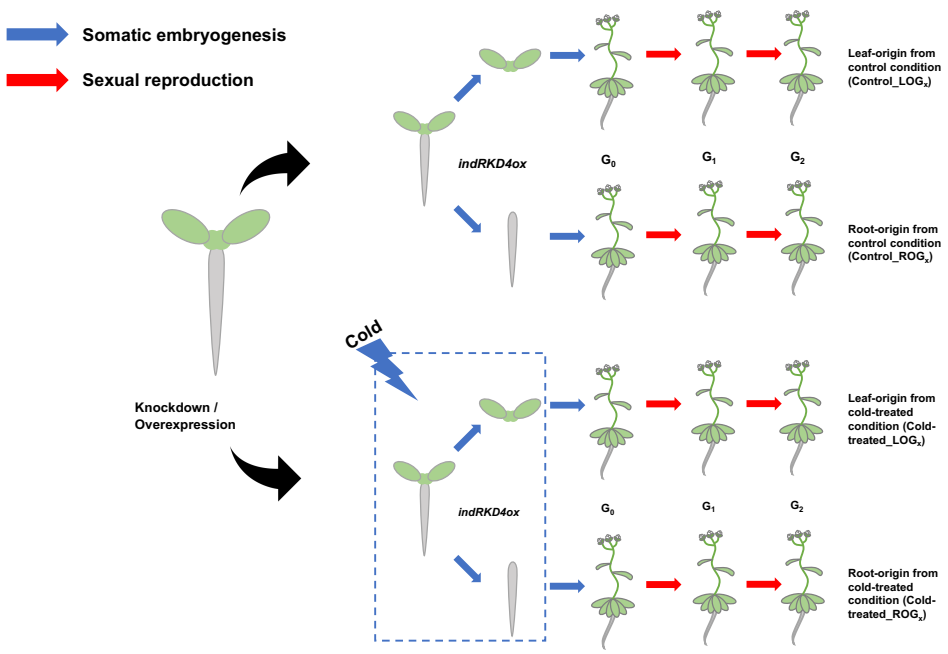

Figure 2.2 Experimental approach employed to determine the mechanisms underpinning cold stress memory in clonal plants. The indRKD4 (Col-0) line was used to transform amiRNA and overexpression constructs (indCBF3) of key transcription factors implicated in transcriptional responses mediated by cold. Somatic embryos are induced under different conditions to generate independent progenies named G_0 generation. Propagation of these lines was carried out by pooling seeds from three randomly chosen G_0 regenerants to create a clonal line that was propagated by pooling seeds for five plants for each generation. Plants in generation G_2 were used for molecular and phenotypic analysis.

Table 2.3 List of Regenerated Clonal Plant Lines used in this study

Plant lines	Symbols in RNA-seq analysis	Number of Lines	Treatment during somatic embryogenesis	Seed Origin	
				G_1	G_2
indRKD Control LO	WT-22/LO	3	Control (22ºC)	Each line comes from pool of 3 G_0 plants	Each line comes from pool of 5 G_1 plants
indRKD Control RO	-	3	Control (22ºC)	Each line comes from pool of 3 G_0 plants	Each line comes from pool of 5 G_1 plants
indRKD Cold LO	WT-4/LO	3	Cold (4ºC)	Each line comes from pool of 3 G_0 plants	Each line comes from pool of 5 G_1 plants
indRKD Cold RO	-	3	Cold (4ºC)	Each line comes from pool of 3 G_0 plants	Each line comes from pool of 5 G_1 plants
amiRNA-cbfs Control LO	WT*-22*/LO	3	Control (22ºC)	Each line comes from pool of 3 G_0 plants	Each line comes from pool of 5 G_1 plants
amiRNA-cbfs Control RO	-	3	Control (22ºC)	Each line comes from pool of 3 G_0 plants	Each line comes from pool of 5 G_1 plants
amiRNA-cbfs Cold LO	WT*-4*/LO	3	Cold (4ºC)	Each line comes from pool of 3 G_0 plants	Each line comes from pool of 5 G_1 plants
amiRNA-cbfs Cold RO	-	3	Cold (4ºC)	Each line comes from pool of 3 G_0 plants	Each line comes from pool of 5 G_1 plants

Plant lines	Symbols in RNA-seq analysis	Number of Lines	Treatment during somatic embryogenesis	Seed Origin	
				G_1	G_2
indCBF3 Control Mock LO	22LOM	3	Control (22ºC) with mock treatment	Each line comes from pool of 3 G_0 plants	Each line comes from pool of 5 G_1 plants
indCBF3 Control Mock RO	-	3	Control (22ºC) with mock treatment	Each line comes from pool of 3 G_0 plants	Each line comes from pool of 5 G_1 plants
indCBF3 Cold Mock LO	4LOM	3	Cold (4ºC) with mock treatment	Each line comes from pool of 3 G_0 plants	Each line comes from pool of 5 G_1 plants
indCBF3 Cold Mock RO	-	3	Cold (4ºC) with mock treatment	Each line comes from pool of 3 G_0 plants	Each line comes from pool of 5 G_1 plants
indCBF3 Control Est LO	22LOE	3	Control (22ºC) with 30 μM β-estradiol	Each line comes from pool of 3 G_0 plants	Each line comes from pool of 5 G_1 plants
indCBF3 Control Est RO	-	3	Control (22ºC) with 30 μM β-estradiol	Each line comes from pool of 3 G_0 plants	Each line comes from pool of 5 G_1 plants
indCBF3 Cold Est LO	-	3	Cold (4ºC) with 30 μM β-estradiol	Each line comes from pool of 3 G_0 plants	Each line comes from pool of 5 G_1 plants
indCBF3 Cold Est RO	-	3	Cold (4ºC) with 30 μM β-estradiol	Each line comes from pool of 3 G_0 plants	Each line comes from pool of 5 G_1 plants

2.6 RNA Sequencing (RNA-seq)

2.6.1 Sample Collection for RNA Sequencing

Due to the diverse experimental design, each experiment required specific sample preparation for RNA sequencing. 14-day-old *Arabidopsis* seedlings of WT (Col-0), amiRNA-ice1, and *ice1-2* were collected at 2-hour after the light-on growth cycle and used as untreated samples. Then, the seedlings treated with cold (4 ºC), or ambient (22 ºC) temperature for 3 hours were used as cold-treated samples and control samples, respectively. Each replicate has 10 seedlings, and 2 technical replicates were used to extract RNA for RNA sequencing (figure 2.3A). In the overexpression of the ICE1 experiment, 14-day-old seedlings from WT (Col-0), indICE1ox, and indICE1^{S278D} were collected at 2-hour after the light-on growth cycle and used as untreated samples. Then, plants were treated with 30 μM of β-estradiol or an equivalent amount of DMSO for 12 hours as β-estradiol-treated samples and mock-treated samples, respectively. Each replicate has 10 seedlings, and 2 technical replicates were used to extract RNA for RNA sequencing (figure 2.3B).

Clonal plants from cold-treated and control-treated parents in G_2 generation obtained from Putra et al. (2018) were grown in soil for 4 weeks. Plants were treated with cold (4 ºC) or ambient (22 ºC) temperature for 1 hour before collecting mature leaves. To generate biological and technical replicates for this experiment, a mature leaf from 3 different plants was collected in the same 1.5 Eppendorf tubes as 1 technical replicate. Three technical replicates from each clonal line were collected and mixed before RNA extraction and used as a biological replicate. RNA samples from three biological replicates per treatment were sent to RNA sequencing (figure 2.3C).

Seeds in G2 generation from background plants (indRKD4) and CBFs transgenic lines (amiRNA-cbfs and indCBF3) were grown in soil for 4 weeks. A mature leaf from 3 different plants was collected in the same 1.5 Eppendorf tubes, and three tubes per plant line were used in further steps. To make a biological replicate per treatment, ground tissue samples from three different plant lines in the same treatment were mixed and used for RNA extraction. Finally, RNA samples from three biological replicates per treatment were sent to RNA sequencing (figure 2.3D).

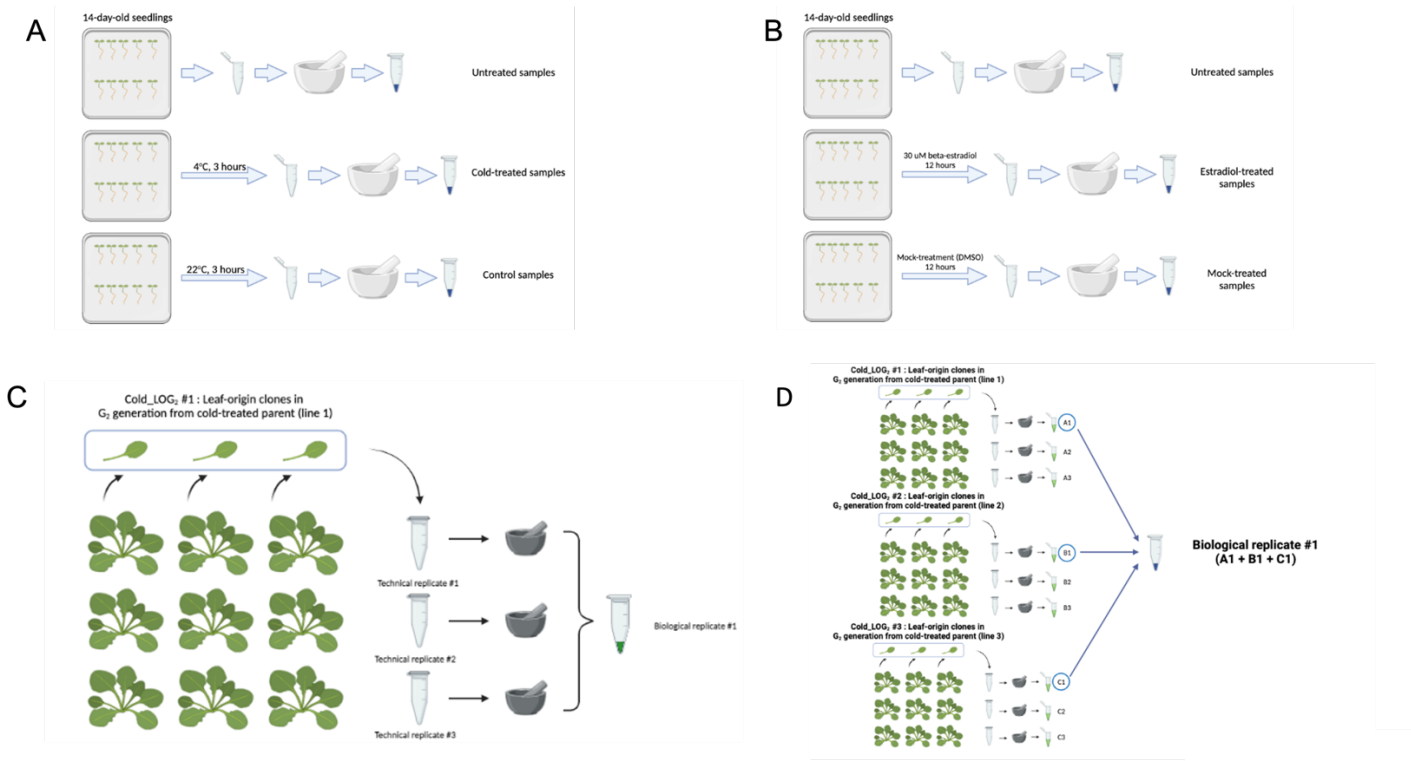

Figure 2.3 Sample collection and processing for RNA Sequencing Experiments. (A) Sample preparation for untreated-, cold-treated, and ambient-treated seedling samples of WT (Col-0), amiRNA-ice1, and *ice1-2*. (B) Sample preparation for untreated-, β-estradiol-treated and mock-treated samples of WT (Col-0), indICE1, and indICE1^{S278D}. (C) Sample collection for a biological replicate of cold-treated (4°C) and control experiment of clonal plants in G_2 generation from Putra et al., (2018). (D) Sample collection for a biological replicate of clonal plants in G_2 generation from CBF transgenic lines

2.6.2 RNA-seq Analysis

All RNA samples were submitted to Novogene Co., Ltd. to perform RNA sequencing by the Illumina HiSeq2000 instrument. The RNA libraries were prepared by the company and sequenced as 150 bp paired end. The quality of RNA-seq results was checked using MultiQC (Ewels et al. 2016). The process of trimming low-quality reads and removing adapters was done by fastp (Chen et al. 2018). Trimmed reads with good quality were aligned and mapped to the latest version of *Arabidopsis* reference genome, Araport 11, using STAR aligner (Dobin et al. 2013). Raw count files were also generated by STAR (parameter: --runThreadN 10 --readFilesCommand zcat --outSAMtype BAM SortedByCoordinate --quantMode GeneCounts).

Raw count files were used to analyse differentially expressed genes (DEGs) by R package DESeq2 version 3.0 (Love et al. 2014). Lists of DEGs from different pair-wised comparisons were obtained with false discovery rate < 0.05 and various log2 foldchange (log2fc) thresholds depending on experiments.

2.6.3 Heatmap

Lists of genes of interest with normalised log-transformed values were submitted to ComplexHeatmap (Gu et al. 2018). Each row in the heatmap represents gene values across treatments (column). Hierarchical clustering was applied to rows with dendrogram.

2.6.4 Gene Ontology Analysis

Enriched gene ontology terms (GO terms) were analysed using the R package gprofiler2 (Kolberg et al. 2020). A list of gene identifiers (gene id) was used as an input. The gprofiler2 provides an option to find the enriched GO terms in *Arabidopsis* annotated GO database.

2.6.5 K-Means Clustering Analysis

Scaled normalised counts (z-score) for each gene of interest were used as an input to categorise genes into clusters. The clustering method was adapted from R package pheatmap (Kolde and Kolde 2018). The optimal numbers of the cluster were selected based on the elbow-plot.

2.6.6 GeneOverlap Analysis

Two lists of genes were submitted to the GeneOverlap package to calculate the statistical significance of number of genes in overlapped area (Shen 2014). To calculate the statistical significance by Fisher's exact test, the number of gene in two overlapping lists are required along with the number of genes in universe, a superset of genes. In this study, the number of universe gene set is 37,362, including protein-coding sequences, pseudogenes, non-coding genes, and transposable elements annotated in Araport 11 (https://www.arabidopsis.org/). GeneOverlap also provides the odd's ratio representing the association degree between two lists of genes.

2.7 Chromatin Immunoprecipitation Sequencing (ChIP-seq) Data Analysis

2.7.1 ChIP-seq Data Processing

Public data from (Xi et al. 2020) and (Tang et al. 2020) was obtained from https://www.ncbi.nlm.nih.gov/sra/ using GEO accession numbers, GSE145258 and GSE130291, respectively. The quality of sequencing data was checked using FastQC. Trimming step was performed with fastp with parameters --cut_right --cut_window_size 4 --cut_mean_quality 20 --length_required 40 --overrepresentation_analysis (Chen et al. 2018). Trimmed sequences were mapped with indexed genome by chromap, producing .bed files as input for MACS2 peak-calling process (Zhang et al. 2008). Finally, BAMscale was used to generate scaled Bigwigs (.bw) files for further analysis. The locations of peaks from ChIP-seq data were annotated to the closest genes within three kilobases range from transcription start sites (TSS).

2.7.2 Metaplot and Enrichedheatmap

EnrichedHeatmap was used to illustrate the ChIP-seq signal between two gene lists or between genes of interest and random genes (Gu et al. 2018). Scaled ChIP-seq signal (.bw) files were used together with lists of genes to generate matrix data consisting of normalised signals of each gene in a determined range, i.e., a gene with 3 kilobases extension in both upstream and downstream directions. Normalised signals were used to generate heatmap and metaplot using adjusted enriched heatmap function.

2.7.3 Boxplot from ChIP-seq Signal

The average of ChIP-seq signals generated in 2.7.2 was used to represent signal over the determined range of each gene. Boxplots were generated from values from lists of genes and were compared statistically by ANOVA, following by post-hoc comparisons.

2.8 DNA Methylation Analysis

Raw bisulfite sequencing data (Bi-seq) was obtained from Putra et al. (2018). According to the sequencing procedure, lines 1, 2, and 3 of control LO, control RO, cold LO, and cold RO clonal lineages were used separately as replicates in library preparation. Each library was prepared from leaf samples from 10 individual plants. The bisulfite sequencing libraries were prepared using the Illumina TruSeq Nano kit (Illumina, CA, U.S.A). The DNA was segregated to the size of 350 bp, and the adapter was ligated to DNA fragments using Epitect Plus DNA Bisulfite Conversion Kit (Qiagen, Hilden, Germany). Finally, the bisulphite sequencing was performed by an Illumina HiSeq2000. The SHORE pipeline v0.9.0 was used in trimming and filtering bad-quality reads. The processed reads were mapped to Araport 11 *Arabidopsis* reference genome.

2.8.1 Quality Assessment

In this study, DMRcaller, a R/bioconductor package, was used to perform the methylation profile together with methylation coverage in all samples (Catoni et al. 2018). Then, we selected only samples with similar and acceptable methylation coverage. Only one replicate from bisulfite sequencing data of each regenerated plant line was chosen to process in further analysis.

2.8.2 Identification of Differentially Methylated Regions

DMRcaller was used in computing differentially methylated regions (DMRs) between reference samples, control LO and control RO regenerated lines, and treatment samples, cold LO and cold RO regenerated lines, respectively. The changes in methylation were calculated in different methylation contexts, CG, CHG, and CHH. Gain and loss of CG and CHG in the comparisons were calculated by the noise-filtering method (DMRcaller-NF), while the changes in CHH methylation were

computed by the bins method (DMRcaller-B). Both methods require the input length of DNA (window size, bin size) and the threshold for calling DMRs between reference samples and treatment samples (Minimum Proportion Difference). DRMcaller also applies statistical analysis using Fisher's exact test and the Score test in the DMRs calculation. For CG contexts, the DMRs computed in the range of 100 bp window size with a Minimum Proportion Difference equal to 0.6. For CHG contexts, the DMRs calculated in the range of 100 bp window size with a Minimum Proportion Difference equal to 0.4. For CHH contexts, the DMRs computed in the range of 100 bp bins size with a Minimum Proportion Difference equal to 0.3.

2.9 Phenotypic Assays

2.9.1 Freezing Tolerance Assay

The protocol was adapted from (Shi et al. 2012). Seeds were sterilised and stratified for at least 48 hours at 4^{o}C as described in 2.1. After five days in MS media plates (4.5 g/L MS basal media (Sigma Aldrich), 8 g/L Phyto agar (Duchefa Biochemie), 10 g/L sucrose (Sigma Aldrich), pH 5.7 – 5.8) at 22^{o}C, seedlings with normal germination from each genotype/ plant lines were transferred to another MS media plates in equal amounts, around 50 seedlings. Plants were grown in the long-day condition in a growth chamber until the age of two weeks. Then, plates were placed in the freezing chamber (LMS Ltd) with opened lids. The temperature was set to 0^{o}C for 1 hour before decreasing at the rate of 1^{o}C per hour until it reached the desired temperature. Then, plants were kept at 4^{o}C for 12 hours in the dark, followed by the recovery stage for 48 hours in long-day growth conditions. The survivors were counted by seedlings which showed healthy green leaves.

2.9.2 Seed Dormancy Assay

Seeds were sterilised and stratified at different time points (0, 3, 5, and 7 days) in 0.1% agarose at 4^{o}C in the dark. Around 50 stratified seeds were sown in water-phyto agar plates (0.9% w/v, Duchefa Biochemie) without basal nutrients. The number of germinations was scored by the emerging radicles after seven days under short-day growth conditions.

2.9.3 Stomata Development Visualisation

The stomata tape-peel method was modified from (Lawrence II et al. 2018). Leaves from 4-week-old plants were collected and stored in 15 mL tubes containing 2 mL deionised H_2O. Each leaf was attached to a glass slide by using two-sided tape adhering to an adaxial (upper epidermis) side of the leaf. Then, a thin layer of polyvinylpyrrolidone (PVP) glue was applied to the abaxial side of the leaf for 5 minutes to imprint the lower epidermis. A leaf-size piece of clear tape was attached to the coated leaf, gently peeled off, and re-attached to a new glass slide. The imprinted slide was used to observe the stomata shape under a microscope. The stomatal density was calculated by counting the number of stomata in the observation field divided by the size of the area.

2.10 Statistical Analysis

One-way Analysis of variance (ANOVA) with Tukey's honestly significant difference (HSD) post hoc test using the statistical package in R, rstatix, to compare the means of two or more samples.

Chapter 3 The Alternative Roles of ICE1 in the Cold-Responsive Pathway

3.1 Introduction

3.1.1 Role of ICE1 in Growth and Development of *Arabidopsis thaliana*

ICE1, also known as SCRM (Kanaoka et al. 2008), has a significant impact throughout the life cycle of *Arabidopsis*. Some of the developmental defects observed in ICE1 mutants are also observed in ZHOUPI, an endosperm-specific bHLH transcription factor (Denay et al. 2014). Mutations in *ice1-2* and *zou* mutants result in endosperm persistence with underdeveloped embryos in mature seeds (Denay et al. 2014). It has been shown that ICE1 and ZOU form a heterodimer protein complex which is required to regulate downstream genes in the endosperm breakdown process (Denay et al. (2014). ICE1 also acts as a negative regulator of ABA INSENSITIVE 3 (*ABI3)* – a B3 transcription factor controlling seed dormancy. As such, *ABI3* expression is significantly induced in *ice1-2,* resulting in an accumulation of ABA content, lower germination frequency, and higher sensitivity to ABA in the early seedling stage (Liang and Yang 2015; MacGregor et al. 2019). ICE1 is also involved in the sequential differentiation process of leaf epidermal cells to form stomata. Three major bHLH-type transcription factors regulate stomata development, including SPEECHLESS (SPCH), MUTE, and FAMA (Pillitteri et al. 2007). ICE1 or ICE2 (SCRM2) mutants resemble the stomatal defects found in *fama*, *mute*, or *spch* mutants, while gain-of-function mutant *scrm*-D results in an excessive number of stomata (Kanaoka et al. 2008). Yeast two-hybrid assays have shown the heterodimerisation between ICE1 and ICE2 proteins with SPCH, MUTE, and FAMA, suggesting that ICE1 and ICE2 act as partner proteins to regulate the stomatal differentiation process (Kanaoka et al. 2008). Additional studies have found the ACT-like (ACTL) domain at the C-terminal of ICE1. This domain is responsible for heterodimerisation with MUTE and with a lower affinity to SPCH and FAMA (Seo et al. 2012). SPCH, MUTE, and FAMA are all type Ia bHLH transcription factors and in the same phylogenetic clade as ZOU, suggesting that ICE1 forms heterodimers with multiple bHLH transcription factors (Seo et al. 2012). ICE1 also functions in male fertility during reproductive development. *ice1-2* exhibit severe silique development due to non-

viable pollen and defective anther dehydration. However, the molecular mechanisms implicated are less well understood (Wei et al. 2018).

3.1.2 ICE1 acts as a Transcription Factor in the Unique Cold-Responsive Pathway

C-REPEAT BINDING FACTORs **(***CBFs*) are the core transcription factors regulating around 20% of cold-responsive genes (*CORs*) (Jia et al. 2016). The expression of *CBFs* is induced by low temperature with a peak at 3 h after initial exposure (Kidokoro et al. 2022; Zarka et al. 2003; Zhou et al. 2017a). Almost all *CBFs* are involved, at least indirectly, with the regulation of biological processes after cold stress. For instance, the connection between the cold-sensing pathway and induction of *CBFs* is linked to the activity of CAMTAs through Ca^{2+} signalling (Doherty et al. 2009). LHY and CCA1 are positive regulators of *CBFs,* integrating circadian rhythms into the cold signalling pathway (Dong et al. 2011). Intriguingly, ICE1 is not misregulated by environment signals (Chinnusamy et al. 2003; Miura et al. 2007), however, low temperature induces post-translational modifications that affect ICE1 stability and DNA-binding affinity (Ding et al. 2015; Dong et al. 2006; Li et al. 2017; Miura et al. 2007). HOS1 marks ICE1 for ubiquitination resulting in protein degradation, a process that occurs within 1 hour after cold treatment (Dong et al. 2006). The substitution of a serine residue with alanine at position 403 ($ICE1^{S403A}$) reduces the polyubiquitination (Miura et al. 2011). By contrast, phosphorylation at serine 278 by OST1 increases the stability of ICE1 and enhances its binding affinity to the *CBF3* promoter (Ding et al. 2015). Interestingly, overexpression of both *ICE1* and *OST1* show slightly higher binding efficiency to *CBF3* promoter, suggesting possible ICE1 function as a *CBF3* regulator in ambient temperature (Ding et al. 2015). On the other hand, phosphorylation of serine/threonine residues by MPK3/6 reduces ICE1 stability in the cold (Li et al. 2017). As such, *mpk3* and *mpk6* mutants are more sensitive to freezing stress. There are six serine/threonine phosphorylation sites (S94, S203, T366, T382, T384, and S403) targeted by MPK3/6. By mutating all six residues to alanine ($ICE1^{6A}$), the stability of ICE1 increases even after 12 hours of cold treatment (Li et al. 2017). In addition to phosphorylation, SIZ1 conjugates ICE1 with SUMOs (small ubiquitin-like modifiers) at lysine 393 to stabilise ICE1 protein under

a cold stress (Miura et al. 2007). Figure 3.1 illustrates all known modifications and the modifiers implicated in ICE posttranscriptional regulation.

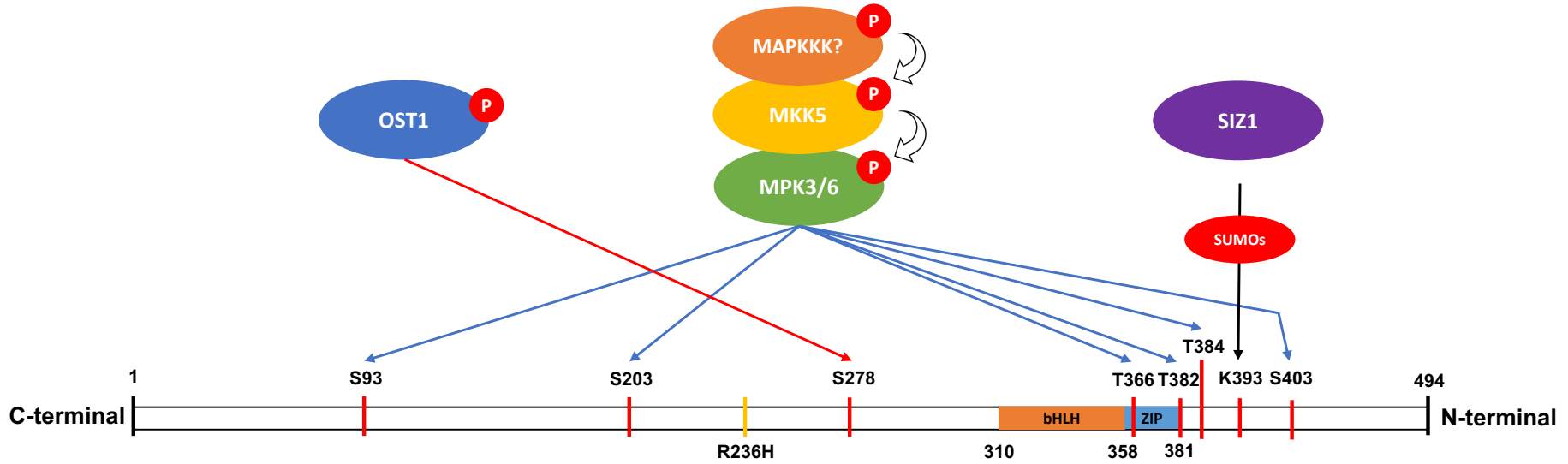

Figure 3.1 Post-translational modifications of ICE1 under low temperature. Under cold treatment, ICE1 undergoes various post-translational modifications. The phosphorylation of ICE1 at serine 278 (S278) by OST1 stabilises the ICE1 protein. Phosphorylated MPK3/6 have six possible phosphorylation sites, which facilitate the degradation of ICE1. SIZ1 ligate SUMOs at lysine 393 (K393) that prevent the degradation of ICE1 from polyubiquitination. R236H indicates the point mutation in the *ice1-1* mutant. The red arrow indicates stabilising phosphorylation. Blue arrows indicate destabilising phosphorylation. The black arrow indicates SUMOylation. The orange box shows the basic helix-loop-helix domain. The blue box indicates the leucine zipper domain. Modified from Chinnusamy et al. (2003), Ding et al. (2015), Li et al. (2017), and Miura et al. (2007)

3.1.3 The role of ICE1 in Different Plant Species

Since the proposed hypothesis of the *ICE1-CBFs-CORs* transcriptional cascade in *Arabidopsis* cold-responsive pathway by Chinnusamy et al. (2003), several genetic approaches have been carried out in different plant species to investigate ICE1 function. Constitutive overexpression of *Arabidopsis ICE1* (*AtICE1*) into cucumber (*Cucumis sativus* L.), indica rice (*Oryza sativa* subsp. *indica*), and Korean lawn grass (*Zoysia japonica*) improves cold tolerance and enhances expression levels of endogenous *CBFs/DREB1* (Liu et al. 2010; Verma et al. 2020; Zuo et al. 2019). Similarly, *ICE1* genes isolated from the rubber tree (*Hevea brasiliensis*) have been overexpressed in *Arabidopsis,* resulting in higher tolerance to freezing stress with increased expression levels of several *CORs* (Li et al. 2022; Yuan et al. 2017). The results from previous reports suggest that the ICE1 protein is conserved in terms of sequence similarity and its function across plant species.

3.1.4 The role of ICE1 in Cold-Response Requires a Comprehensive Re-evaluation

Until now, a considerable number of publications are based on the *ICE1-CBFs-CORs* transcriptional cascade and support the roles of ICE1 in cold responses. However, a recent study has challenged the idea that ICE1 functions as a critical regulator of cold responses (Kidokoro et al. 2020). This study shows that repression of *CBF3* expression in the original *ice1-1* (*ICE1*^{R238H}) mutant appears to be caused by a reporter transgene containing the *CBF3* promoter fused with luciferase (*pCBF3-LUC*). Multiple insertions of *pCBF3-LUC* have been found inside the *ice1-1* original mutant (figure 3.2). One insertion was found at chromosome 5 inside the 3' untranslated region (3' UTR) of AT5G45760 with 204-bp deletion. The other insertion was found inside a transposable element (AT1TE25865) and shows an inverted repeat pattern. DNA hypermethylation has been found in the promoter region of endogenous *CBF3,* suggesting a correlation between the repression of endogenous *CBF3* and hypermethylation caused by the transgene via the small RNA-directed RdDM pathway. Moreover, *scrm-D* mutants containing ICE1^{R238H} without *pCBF3-LUC* transgene show no repression of *CBF3* under cold treatment suggesting no relationship between *ICE1* mutation and the expression level of *CBF3* under cold response. Thus, the concept of the *ICE1-CBFs-CORs* pathway should be carefully revisited.

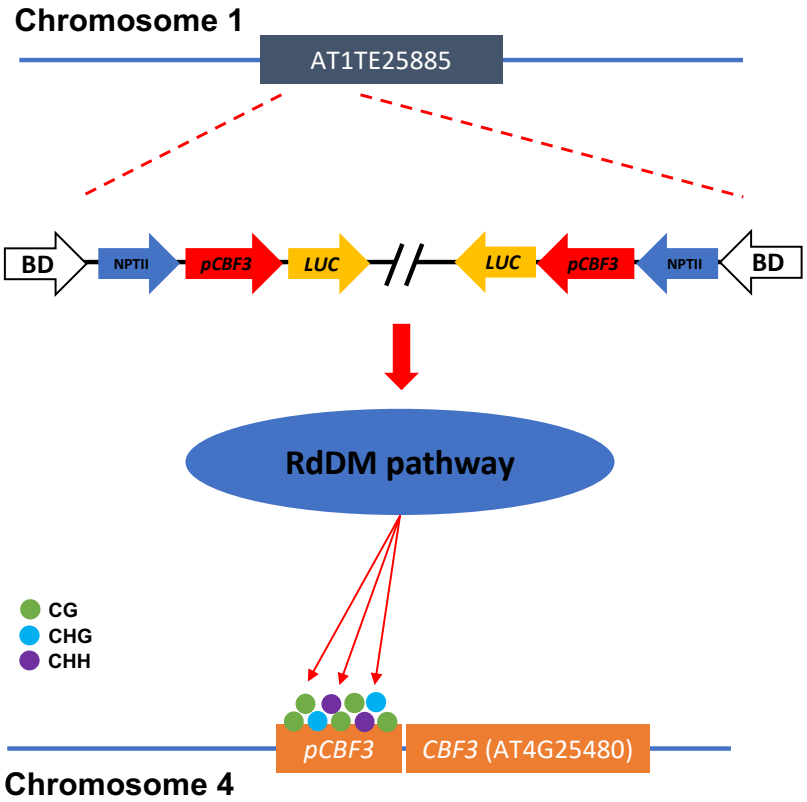

Figure 3.2 Insertion of reporter transgene (*pCBF3-LUC*) is potentially associated with the repression of endogenous *CBF3* by small RNA silencing and DNA methylation. The inverted repeat of *pCBF3-LUC is* inside a transposable element (AT1E25865) in chromosome 1 and it is associated with hypermethylation at the promoter region of endogenous *CBF3* (AT4G25480), possibly through small RNAs and the RdDM pathway. Modified from Kidokoro et al. (2020).

3.1.5 Chapter Aims

Due to the debatable functions of ICE1 in a cold-responsive regulatory network, this chapter aims to clarify the roles of ICE1 under short-term cold treatment. Here, we developed a new strategy to investigate the function of ICE1 in cold acclimation. I generated knock-down mutants using an artificial microRNAs method (amiR-ice1). Genome-wide transcriptomic analysis was used to compare gene expression between wild-type, amiR-ice1, and *ice1-2* under different temperature growth conditions.

3.2 Results

3.2.1 Downregulation of *ICE1* with amiRNA partially phenocopies *ice1-2* genetic lesions.

ICE1 regulates seed germination in two different layers. Firstly, ICE forms a heterodimer protein complex with ZOU regulating endosperm breakdown in the embryo development (Denay et al. 2014). Secondly, ICE1 negatively regulates the ABA pathway (MacGregor et al. 2019). *ice1-2* mutant is reported to have an abnormal seed shape and low germination rate. To define ICE1 functions, I generated two independent amiR-ice1 lines and selected one for further analysis after confirmation of strong downregulation of ICE1 expression and apparent defects on stomata development (data not shown). I performed seed dormancy assays and found that compared to wild-type seeds, the germination rate of *ice1-2* and amiR-ice1 was significantly reduced. However, the seed germination defects found in *ice1-2* were much stronger than in amiR-ice1 (figure 3.3). Moreover, microscopy analysis did not reveal differences between the seed shape of WT and amiR-ice1, while *ice1-2* mutants displayed a shrunken seed phenotype (appendix figure 7.1). Freshly harvested seed stocks were used to test germination frequency in agar-water plates under different stratification time points. The germination rates increased in conjunction with more stratification time in all genotypes. At all-time points, WT exhibited the highest germination rate, followed by amiR-ice1 and *ice1-2*, respectively. Very highly significant differences ($p < 0.001$ or lower) were found in the comparison between WT and *ice1-2* in all time points, but the significance of the difference in germination rate between WT and amiR-ice1 decreased over stratification time. These results suggest the different effects of amiR-ice1 and *ice1-2* on seed germination.

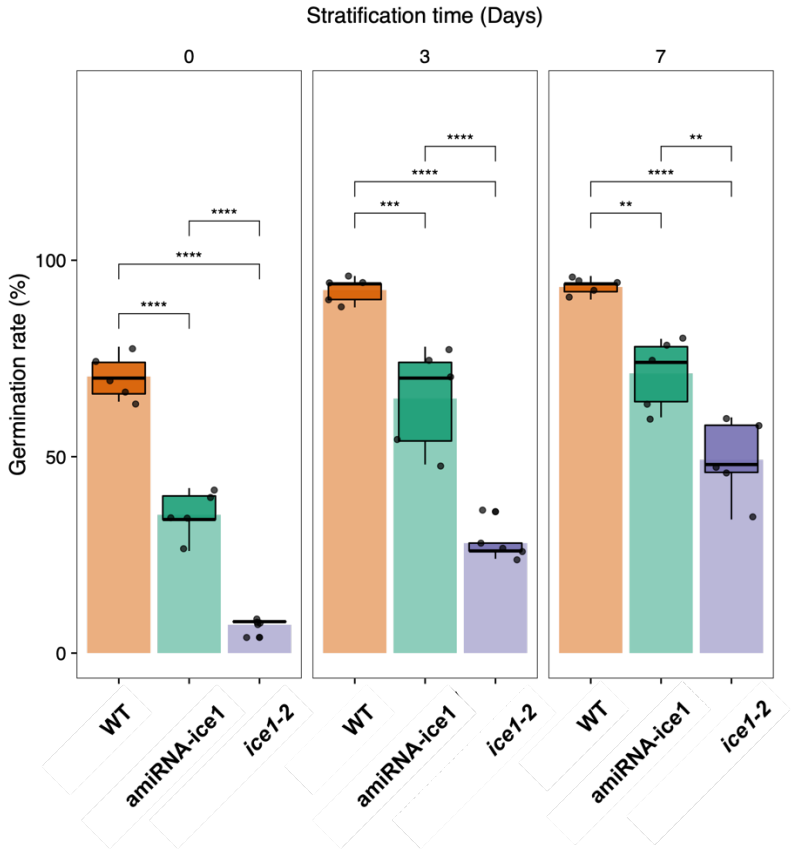

Figure 3.3 Seed dormancy assay between WT, amiR-ice1, and *ice1-2* under different stratification time points. Fifty seeds were sown on a 10% agar plate without nutrients. The germinating seeds were counted for visible radicles at 7 d after sowing. Five replicates were used in each genotype per time point. Asterisk indicates the significant different between comparisons (Tukey's HSD test, **** $p < 0.0001$, *** $p < 0.001$, ** $p < 0.01$, and * $p < 0.05$)

I next investigated the role of ICE on stomata development. Stomata guard cells are formed from specific protodermal cells named meristemoid mother cells (MMCs). They undergo sequential cell divisions and differentiation. MMCs divide asymmetrically to generate meristemoids. Meristemoids undergo asymmetric cell division and differentiation resulting in guard mother cells (GMCs) surrounded by stomatal lineage ground cells (SLGCs). Finally, a pair of guard cells are formed by a symmetrical division of GMC (Nadeau and Sack 2002). SPCH, MUTE, and FAMA regulate the sequential stomata development in different steps. SPCH controls the division from MMCs to meristemoids. MUTE regulates the formation of GMCs. FAMA is required in the final division to form guard cells (Pillitteri et al. 2007). The

heterodimerisation of ICE1/ICE2 with SPCH, MUTE, and FAMA determines the smooth stomatal development (Kanaoka et al. 2008). Our data show incomplete stomatal development in mature leaves of *ice1-2* and amiR-ice1 plants (figure 3.4A). The underdeveloped guard cells were formed as a group of small cells without stomata, and in some instances, a single group contained around 3-4 cells. However, normal stomata could be detected in amiR-ice1 and *ice1-2* (figure 3.4A). Stomatal density was calculated by counting the number of typical pairs of guard cells and grouped underdeveloped cells under a light microscope. Significant differences in the density of normal guard cells and of underdeveloped cells were found between WT and both ICE1 transgenic lines (figure 3.4B). Interestingly, amiR-ice1 contained a higher density of grouped guard cells than in *ice1-2*. These results confirm the efficiency of amiR-ice1 in interfering with ICE1 function during stomata development.

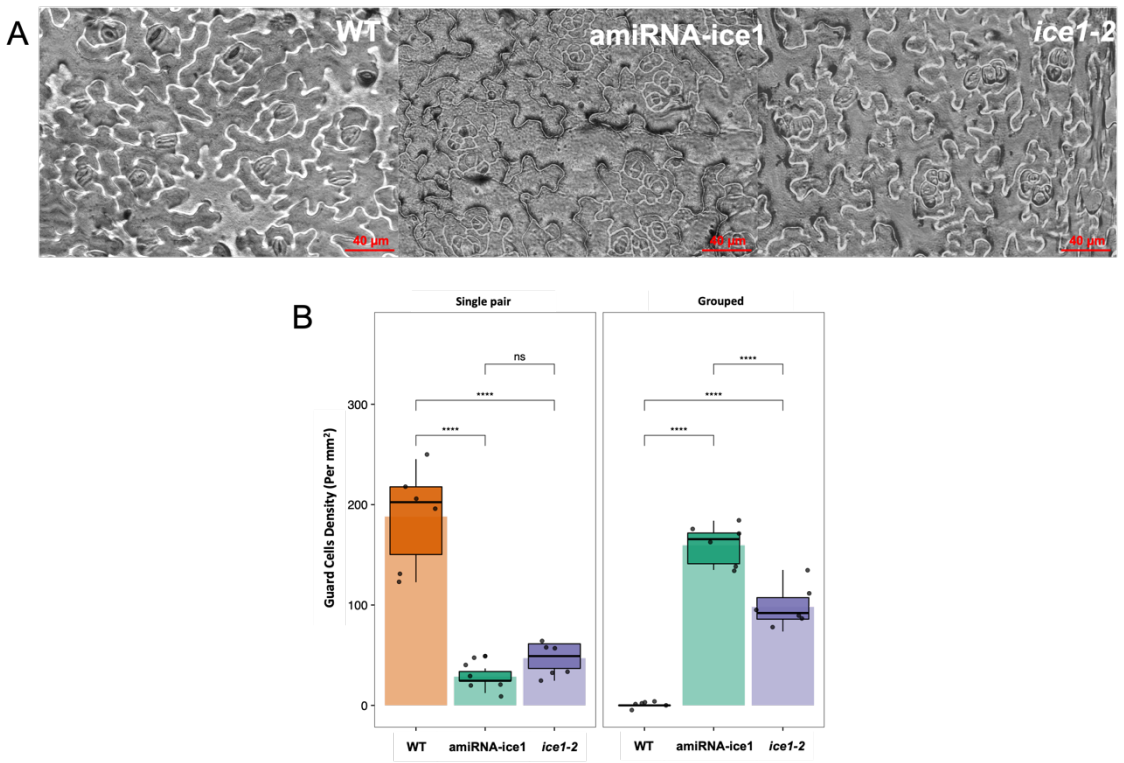

Figure 3.4 Defective stomatal development observed in WT, amiR-ice1, and *ice1-2* (A). The density of single pair and grouped guard cells in WT, amiR-ice1, and *ice1-2* (B). Six different fields of observation were used as replicates to calculate the density per square millimetre (mm^2). Asterisk indicates significant difference between comparison groups (Tukey's HSD test, **** $p < 0.0001$, *** $p < 0.001$, ** $p < 0.01$, and * $p < 0.05$)

To test the role of ICE in adaptation to freezing stress, seed from wild type, amiR-ice1, and *ice1-2*, were stratified for 7-day under dark- and cold-condition to ensure germination was uniform between genotypes. Seeds were sown on media and grown under short-day conditions for 7 d. Then, germinated seedlings with similar development were transferred to 150 mm circular plates. Each plate was divided into three sections, with each section containing 50 seedlings. Seedlings were continually grown until they reached the 14-d stage. These steps were done to avoid unequal growth rates resulting from seed germination phenotypes and to reduce any possible effects that plate location might have within the freezing cabinet. All plates were pre-treated at 0^{o}C for 1 h during the freezing tolerance experiment to achieve cold acclimation. Then, the temperature was lowered at a rate of 1^{o}C·h^{-1} until it reached -7^{o}C. Two days later, after transferring plates to long-day growth conditions, the surviving plants were scored for viability using green (healthy) leaves with no visible damage to the shoot apical meristem area (the central area of rosette leaves) as an indicator. We found no significant difference in survival rates among WT, amiR-ice1, and ice1-2 (figure 3.5). Notably, the survival rates from WT were slightly lower than amiR-ice1 and *ice1-2*. These results suggest that, under our experimental conditions, both amiR-ice1 and *ice1-2* had insignificant effects on freezing tolerance.

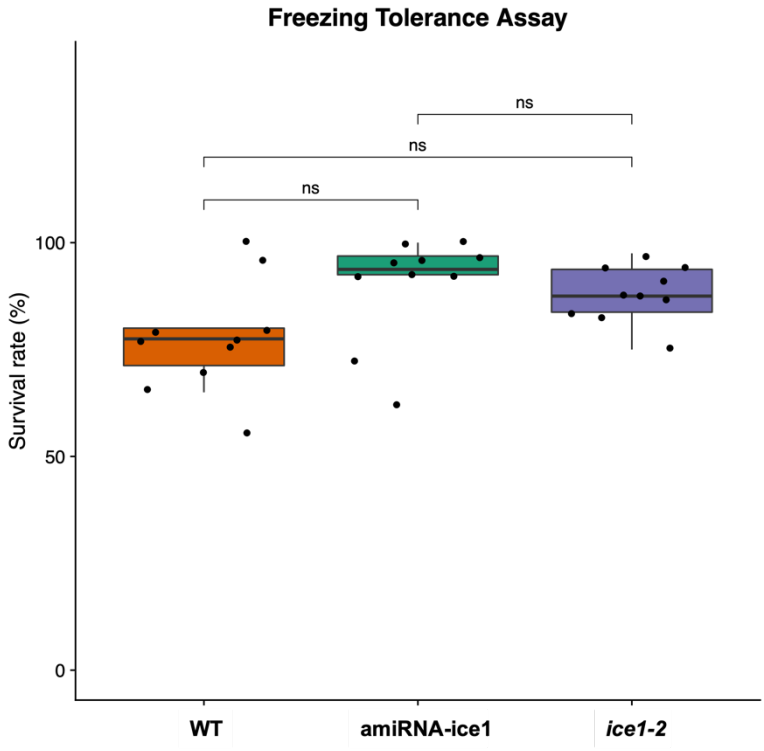

Figure 3.5 Freezing tolerance assay. Survival rates were calculated from recovered plants after being exposed to -7°C. Each data point was calculated from 50 seedlings. Nine replicates were used in the statistical analysis. Asterisk indicates a significant difference between comparison groups (Tukey's HSD test, ** $p < 0.01$, * $p < 0.05$, ns $p > 0.05$)

3.2.2 Transcriptional mis-regulation found in amiR-ice1and *ice1-2* plants.

To further define the role of *ICE1* in cold-mediated transcription, transcriptomic analysis was performed using RNA-seq libraries from WT, amiR-ice1, and *ice1-2* under three conditions and with two biological replicates (table 3.1). Untreated samples were collected at ZT 2; when treated samples were grown for three hours (ZT 5) under control (22°C) or cold (4°C) temperature conditions, differentially expressed genes (DEGs) were identified from pair-wise comparisons with a false discovery rate (FDR) of 0.05, and log2FC ≥1.0 for up-regulated DEGs and log2FC ≤ 1.0 for down-regulated DEGs. The cut-off meant that each differentially expressed gene exhibited a significant difference with an adjusted p-value of 0.05 and had at least a two-fold change in expression level in the treatment condition compared to the

reference condition. The comparison between WT and amiR-ice1 grown under control temperature conditions (22ºC - 3 hours) showed a substantial reduction of *ICE1* expression but no affecting on *ICE2* expression (figure 3.6A). On the other hand, *ice1-2* did not show significant changes in *ICE1* expression level (figure 3.6B). In comparison to WT, the expression level of *ICE1* in both transgenic lines suggested that amiR-ice1 was a proper knock-down mutant. Moreover, amiR-ice1 and *ice1-2* had a different number of computed DEGs, especially in the upregulation direction, with around 5-fold differences (57 from amiR-ice1 and 275 from *ice1-2*). amiR-ice1 and *ice1-2* have a similar number of down-regulated genes, 323 and 390, respectively. Collectively, the results suggested unequal effects in transcription between amiR-ice1 and *ice1-2* under standard growth conditions.

Table 3.1 List of RNA-sequencing Libraries

Sample Name	Genotype	Treatment	Replicates
WT_untreat_1	WT (Col-0)	Untreated (22ºC – ZT2)	1
WT_untreat_2	WT (Col-0)	Untreated (22ºC – ZT2)	2
amiR-ice1_untreat_1	amiR-ice1	Untreated (22ºC – ZT2)	1
amiR-ice1_untreat_2	amiR-ice1	Untreated (22ºC – ZT2)	2
*ice1-2*_untreat_1	*ice1-2*	Untreated (22ºC – ZT2)	1
*ice1-2*_untreat_1	*ice1-2*	Untreated (22ºC – ZT2)	2
WT_22_1	WT (Col-0)	22ºC – ZT5	1
WT_22_2	WT (Col-0)	22ºC - ZT5	2
amiR-ice1_22_1	amiR-ice1	22ºC - ZT5	1
amiR-ice1_22_2	amiR-ice1	22ºC - ZT5	2
*ice1-2*_22_1	*ice1-2*	22ºC - ZT5	1
*ice1-2*_22_1	*ice1-2*	22ºC - ZT5	2
WT_4_1	WT (Col-0)	4ºC - ZT5	1
WT_4_2	WT (Col-0)	4ºC - ZT5	2
amiR-ice1_4_1	amiR-ice1	4ºC - ZT5	1
amiR-ice1_4_2	amiR-ice1	4ºC - ZT5	2
*ice1-2*_4_1	*ice1-2*	4ºC - ZT5	1
*ice1-2*_4_1	*ice1-2*	4ºC - ZT5	2

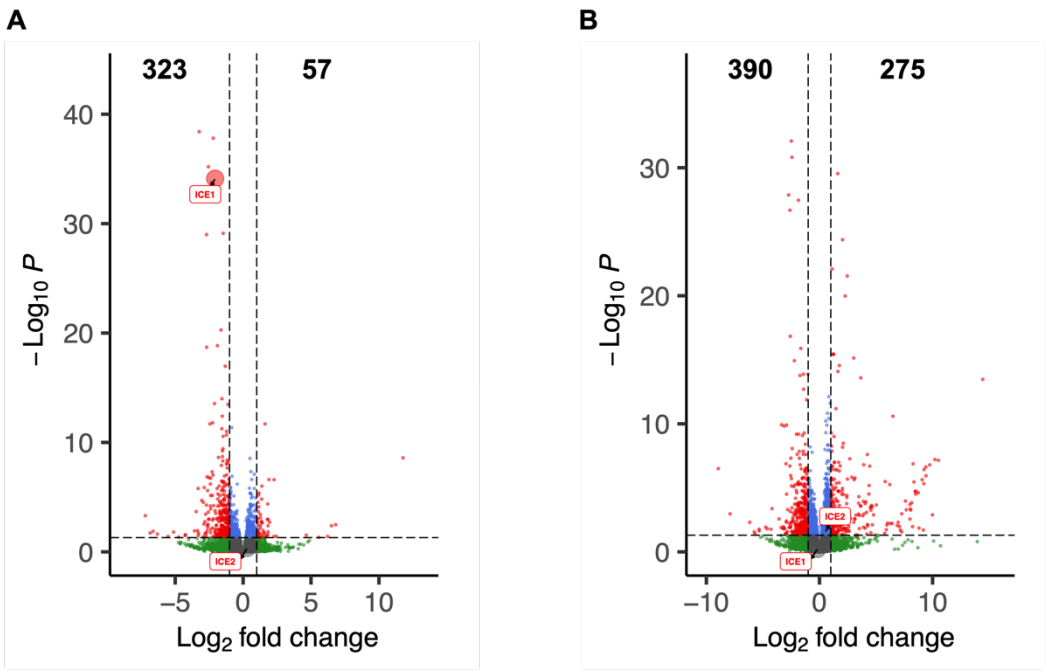

Figure 3.6 Volcano plots showing differential gene expression in amiR-ice1, and *ice1-2* grown at 22°C. (A) DEGs found between WT and amiR-ice1, (B) DEGs found between WT and *ice1-2*. Red dots, genes with significant differences having FDR < 0.5 and log2FC over threshold (log2FC ≥1.0 for up-regulated genes and log2FC ≤ 1.0 for down-regulated genes); Blue dots, genes with significant differences having FDR < 0.05 and log2FC below threshold. Green dots are genes that are not significantly different in the comparisons. *ICE1* and *ICE2* are highlighted in red rectangular boxes. The numbers indicate the number of up-regulated DEGs (right) and down-regulated DEGs (left).

ICE1 was found to be strongly down-regulated in amiR-ice1 lines under cold conditions, confirming the efficiency of our transgenic construct in interfering with ICE1 function (figure 3.7A). On the other hand, *ice1-2* had no effect on *ICE1* after cold treatment (figure 3.7B). The number of DEGs compared to WT under cold showed similar tendencies as in ambient temperature. The number of DEGs from *ice1-2* were 237 and 324, from up-and down-regulated DEGs, respectively, and were higher than the number of DEGs from amiR-ice1, with 87 up-regulated and 209 down-regulated DEGs. The results suggested a greater effect from the presence of *ice1-2* than from the reduced expression of *ICE1* by amiR-ice1. JBrowse, a genome browser, was used to show the different mapped reads in the *ice1-2* gene locus, scaled in counts

per million (CPM) units. Some reads were mapped to the intron of a typical *ICE1* gene structure, suggesting that the T-DNA insertion in *ice1-2* had no effect on expression level but could result in the atypical form of the translated protein (figure 3.8).

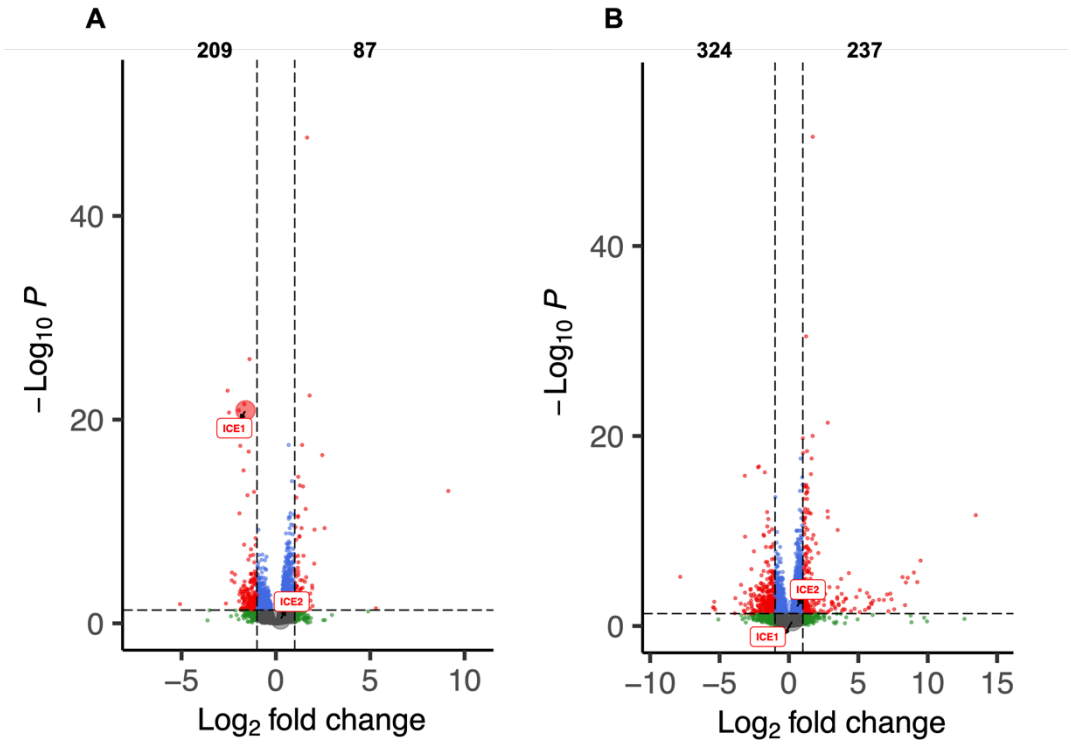

Figure 3.7 Volcano plots showing differential gene expression in amiR-ice1, and *ice1-2* grown at 4ºC. (A) DEGs found between WT and amiR-ice1, (B) DEGs found between WT and *ice1-2*. Red dots, genes with significant differences having FDR < 0.5 and log2FC over threshold (log2FC ≥1.0 for up-regulated genes and log2FC ≤ 1.0 for down-regulated genes); Blue dots, genes with significant differences having FDR < 0.05 and log2FC below threshold. Green dots are genes that are not significantly different in the comparisons. *ICE1* and *ICE2* are highlighted in red rectangles. The numbers indicate the number of up-regulated DEGs (right) and down-regulated DEGs (left).

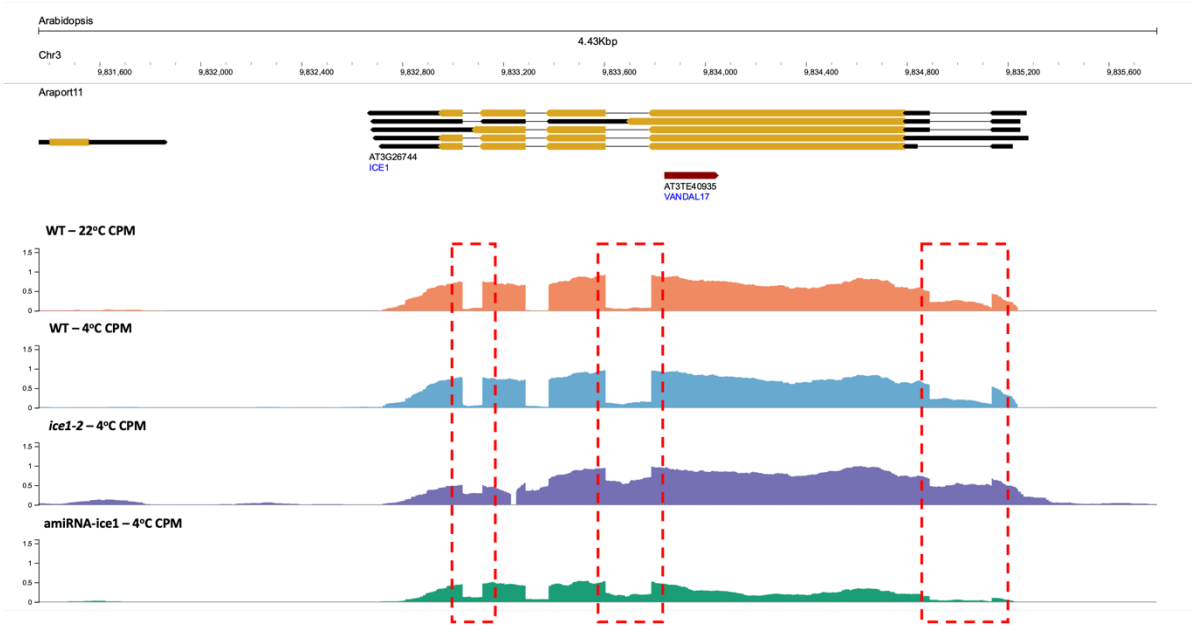

Figure 3.8 Genome Browser View showing the abundance of reads mapping to the ICE1 locus. Mapped reads were scaled to counts per million (CPM) units. First-panel exhibits gene structure from the Araport11 database. The second to fifth panels show the structure of the mapped reads from plants grown at 22°C and 4°C. Red dashed rectangles indicate the location of introns.

3.2.3 Low-Temperature Treatment is the Main Factor Affecting Genome-Wide Gene Expression Regardless of Genotype

In this study, I have shown how *ICE1* expression levels are reduced by amiR-ice1, and the possibility of an atypical ICE1 partially functional protein forming in *ice1-2* mutants. To assess the impacts of the different genotypes (WT, amiR-ice1, and *ice1-2*) under different treatment regimens (untreated, 22°C - 0 h; ambient, 22°C - 3 h; and cold, 4°C - 3 h), principal component analysis (PCA) was performed using log2-transformed counts across all conditions. The replicates were shown separately in the PCA plot (figure 3.9). The first PC (PC1 – with 43% variance) separated the cold-treated samples from other conditions. PC2, with 22% variance, divided untreated- and ambient temperature samples. PC2 also showed that *ice1-2* was detached from WT and amiR-ice1 under ambient temperature treatment. One replicate of WT under cold treatment was dissociated from the rest in PC2. PC3 contributed 12% variance

and exhibited a similar trend as for PC2. Thus, the PCA results suggest that cold treatment was the main factor affecting the transcriptome (PC1), and that it affected all genotypes similarly.

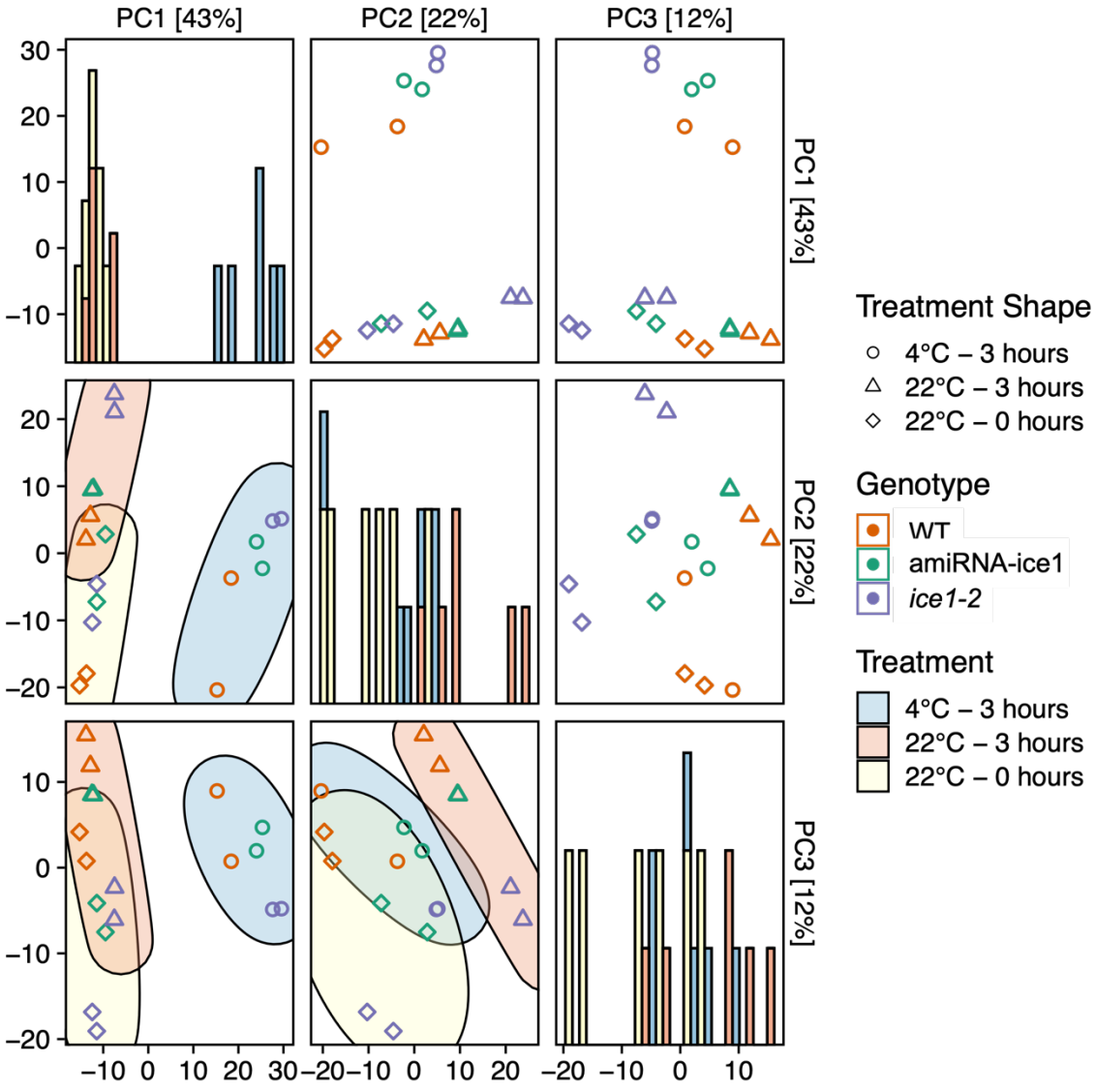

Figure 3.9 Principal component analysis (PCA) plot from WT, amiR-ice1, and *ice1-2* under untreated (22°C - 0 hours), ambient (22°C - 3 hours), and cold (4°C - 3 hours) conditions. The number in the bracket shows the percentage variance contributed by the principal component. The colours of dots represent genotypes. The filled colours of circle indicate the treatments. The histogram in a diagonal matrix shows the distribution of the treatments according to PC in the x-axis.

After observing the general grouping pattern in the PCA, DEGs were calculated by pair-wise comparisons by the DESeq2 pipeline with an FDR of 0.05 and log2FC cut-off value of 1.0. In this instance, untreated samples were excluded to simplify the analysis. Comparisons 1, 2, and 3 indicated the DEGs from the comparisons between samples from control temperature (22ºC) (reference condition) with cold-treated samples (treatment condition) from WT, amiR-ice1, and *ice1-2*, respectively. Comparisons 4 and 5 were the exact comparisons as shown in figure 3.7, showing the effects of transgenic *ICE1* under cold conditions. A similar number of DEGs in both up-and down-regulated genes were found across genotypes, with around a 3-fold difference between up-regulated genes and down-regulated genes. Approximately 900 DEGs were found in the WT comparison, with around 100 and 200 DEGs increased in the comparisons from amiR-ice1, and *ice1-2*, respectively (table 3.2). List of DEGs from comparison 1 is in appendix table 7.1.

Table 3.2 List of Pair-wise comparisons and Numbers of DEGs

Comparison	Reference condition	Treatment condition	Number of DEGs	Up-regulated DEGs	Down-regulated DEGs
1	WT 22ºC	WT 4ºC	889	677	212
2	amiR-ice1 22ºC	amiR-ice1 4ºC	999	732	267
3	*ice1-2* 22ºC	*ice1-2* 4ºC	1,102	755	347
4	WT 4ºC	amiR-ice1 4ºC	296	87	209
5	WT 4ºC	*ice1-2* 4ºC	561	237	324

The similarity in the number of DEGs reflected the general tendency of comparisons. DEGs found in comparisons 1 to 3 allowed us to define a group of cold-responsive DEGs across all genotypes. Moreover, the overlap of DEG list from all comparisons shows that the majority of DEGs were classified as common DEGs, consisting of 467 genes in total (391 up-regulated genes and 76 down-regulated genes, group 1). The second abundant group was a list of DEGs specific to the *ice1-2* comparison (365 DEGs, group 2), followed by the groups 3 and 4 representing cold-regulated DEGs from amiR-ice1 and WT comparisons (264 and 226 DEGs, respectively). Groups 5 – 7, containing the lowest number of DEGs, partially

overlapped between DEGs from two comparisons (figure 3.10A). Similar trends were also found in the overlap between up-regulated DEGs, but the down-regulated DEGs seemed to be independent in different genotypes (figures 3.10B and C). The highest number of DEGs found in the shared group suggested that most genes behaved similarly after 3 h under cold treatment, regardless of the genotypes. However, there were hundreds of genes categorised in unique groups from both transgenic lines suggesting different effects of amiR-ice1 or *ice1-2* under cold treatment. Common cold-regulated DEGs showed a relatively stronger log2FC on both up-regulation and down-regulation together with a more significant adjusted p-value in comparison to genotype-specific DEGs (non-common DEGs). This trend was found in all comparisons confirming the main effect of cold treatment in all genotypes (appendix figure 7.2).

The lists of DEGs in groups 1 to 4 were used for a gene-ontology (GO) analysis, according to annotated terms in the *Arabidopsis* database. The first 20 enriched GO terms based on significance were selected. There were several enriched GO terms related to hypoxia across all groups (figure 3.11). Other general terms related to biotic or abiotic response were also found in multiple groups. However, group 1 or common cold-responsive DEGs was the only group showing the enrichment in terms of 'response to cold' and 'response to temperate stimulus' (figure 3.11A). There were 45 genes with 'response to cold' GO in common cold-regulated DEGs (table 3.3). The results from GO analysis suggested the effect of cold treatment to plant oxygen usage. Different groups with similar GO terms indicated the different pathways of DEGs involved in the same aspect of the cell biological pathway. Specific GO terms related to cold were found only in group 1, confirming that cold was the primary factor affecting gene expression levels regardless of whether *ICE1* was expressed at normal levels.

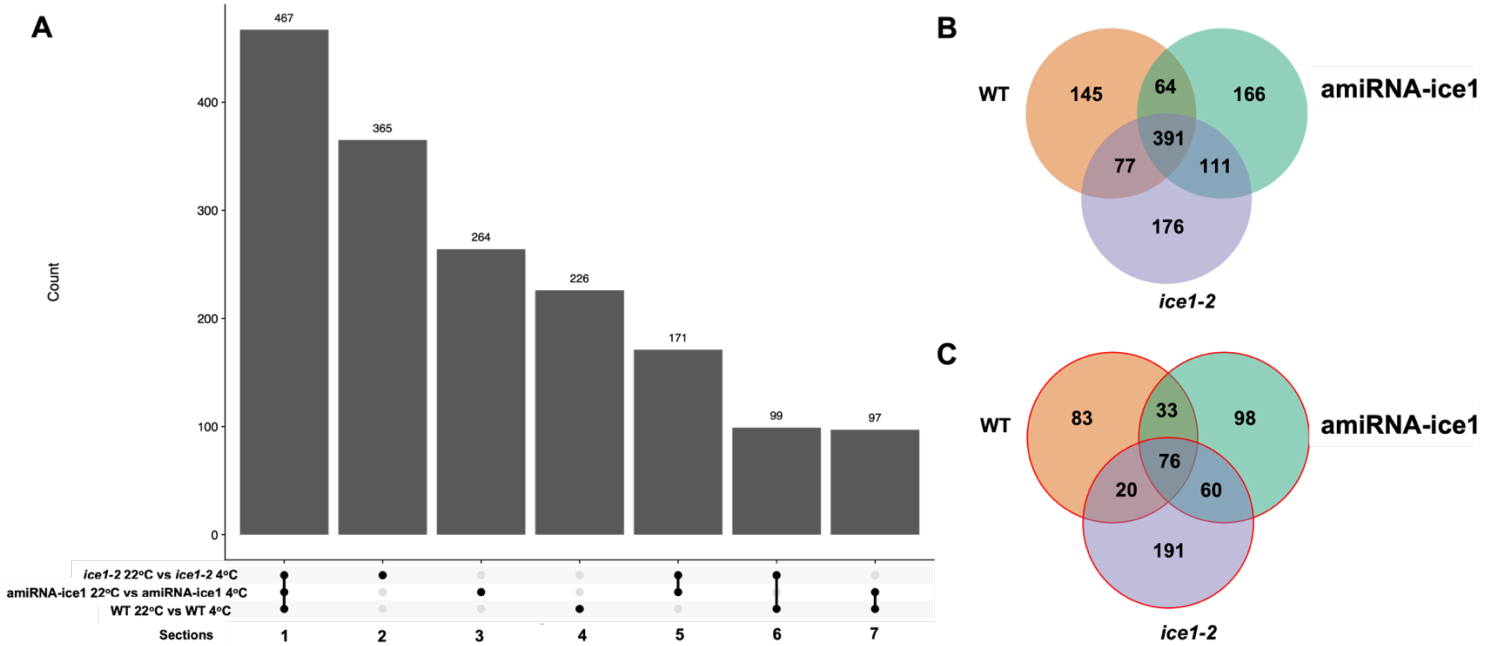

Figure 3.10 The overlap between lists of DEGs from comparison between 22°C treatment and 4°C treatment from WT, amiR-ice1, and *ice1-2*. List of total number of overlapped DEGs (A), Venn-diagram showing overlapping up-regulated genes (B), Venn-diagram showing overlapping down-regulated genes (C). Number above bar charts and inside the group represents the number of genes per group. The connected dots indicate the category of overlap. Each category was designated with a number for further analysis.

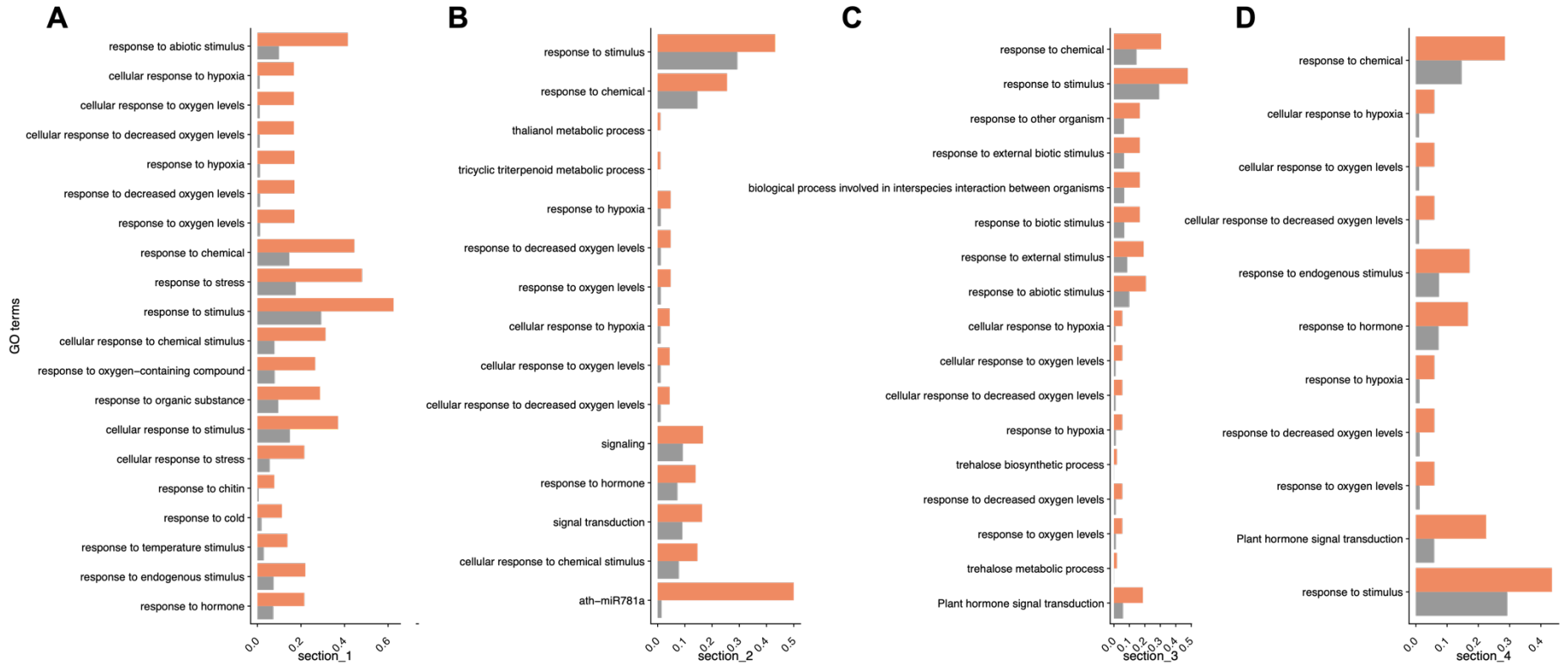

Figure 3.11 Gene ontology (GO) analysis. The enriched GO terms from submitted gene list in group 1 (A), group 2 (B), group 3 (C), and group 4 (D). X-axis indicates the frequency of GO terms between expected value (grey bar) and observed value (orange bar). The expected frequency is calculated from the number of genes with particular GO term divided by the total GO terms in *Arabidopsis* database. The observed value is calculated from the number of genes with the term in an input divided by the number of input genes.

Table 3.3 List of Genes with Cold-Related Gene Ontology from common cold-regulated DEGs

Gene ID	Gene Symbols	Gene ID	Gene Symbols
AT1G01060	*LHY*	AT3G55580	NA
AT1G09350	*GolS3*	AT3G61190	*BAP1*
AT1G10760	*SEX1*	AT4G17090	*CT-BMY*
AT1G12610	*DDF1*	AT4G17615	*CBL1*
AT1G18740	NA	AT4G25470	*CBF2*
AT1G20440	*COR47*	AT4G25480	*CBF3*
AT1G20450	*ERD10*	AT4G25490	*CBF1*
AT1G20620	*CAT3*	AT4G33980	NA
AT1G20823	NA	AT4G34150	NA
AT1G22190	NA	AT4G35985	NA
AT1G27730	*STZ*	AT4G37610	*BT5*
AT2G17840	*ERD7*	AT4G38840	NA
AT2G30250	*WRKY25*	AT5G20230	*BCB*
AT2G37770	*ChlAKR*	AT5G37770	*TCH2*
AT2G38470	*WRKY33*	AT5G40010	*AATP1*
AT2G40140	*CZF1*	AT5G42900	*COR27*
AT2G42530	*COR15B*	AT5G47230	*ERF5*
AT2G46830	*CCA1*	AT5G52310	*LTI78* (*RD29A*)
AT3G23250	*MYB15*	AT5G54470	*BBX29*
AT3G48360	*BT2*	AT5G58770	*cPT4*
AT3G49530	*NAC062*	AT5G59820	*RHL41*
AT3G50310	*MAPKKK20*	AT5G62470	*MYB96*
AT3G50970	*LTI30*		

3.2.4 ICE1 Acts as Transcriptional Activator and Repressor under Cold Treatment but has no effect on *CBF* expression

To define the transcriptional dynamics of common cold-regulated DEGs data was processed by (1) merging replicates of the same condition, (2) applying $\log_2$ transformation, and (3) normalising across all conditions by the 'z-score' method for each gene. The processed counts were plotted in a heatmap to observe the expression level pattern. Hierarchical clustering was applied to arrange the similarity across all genes, and the column representing conditions with genotypes and treatments was put in order (figure 3.12). As shown in figure 3.10 B-C, we found 76 common cold-repressed and 391 common cold-induced genes.

CBF1-4 and two *CBF* regulated genes, *RD29A* and *GolS3*, were highlighted in the heatmap. The appearance of the gene in the *CBF* family in the common cold-regulated DEGs list suggested that expression levels of *CBFs* were detectable under cold treatment in WT, knock-down *ICE1* by amiR-ice1 and *ice1-2*. This might imply that ICE1 has little or no effect on *CBF* regulation. However, the z-scores for several genes under cold conditions were inconsistent, suggesting distinct changes in expression level according to genotype under cold treatment. To further understand the impact of genotypes on common cold-regulated DEGs, the k-means clustering was performed separately using values from WT paired with values from amiR-ice1 or with values from *ice1-2.*

The assigned number of clusters was four, according to the optimal number from the elbow plot (data not shown). All four clusters from values between WT and amiR-ice1, so-called amiR-ice1 clusters, showed similar z-scores under ambient conditions, suggesting that there was no effect of amiR-ice1 on genes in all clusters (figure 3.13A). Therefore, the clustering was based on the differences in expression levels under the cold condition. Clusters 2 and 4 indicate ICE1-independent genes with both directions of expression levels changed by cold. Genes in cluster 1 were induced by cold, and the expression levels were induced in amiR-ice1, suggesting the repressive role of ICE1. By contrast, amiR-ice1 had a negative impact on gene expression levels in cluster 3, implying the active roles of ICE1. The number of genes was almost equal between clusters 1, 3, and 4, with 123 genes, 111 genes, and 157 genes, respectively. Cluster 2, containing 76 genes, represented the cold-repressed DEGs. Genes from clusters 1 – 4 are listed in appendix table 7.2.

In a further analysis in this chapter, groups 1 – 4 were also designated with implied roles of ICE1. Group 1 include ICE1-repressed genes. Group 2 include cold-repressed ICE1-independent genes. Group 3 include ICE1-activated genes. Finally, group 4 include cold-induced ICE1-independent genes.

The clustering method based on values from WT and *ice1-2* showed a similar pattern of clusters with different numbers of DEGs. Cluster 1, with 76 genes, represents the cold-repressed gene cluster. Cluster 2 contained 107 genes showing repressed expression levels in *ice1-2* under cold conditions. Cluster 3 showed a slight increase in expression from ice1-2 in the cold, while cluster 4 exhibited a high increase in expression levels (figure 3.13B). Because *ice1-2* produces atypical transcripts

which could result in a partial loss-of-function proteins, the interpretation of the transcriptomic changes is more complex.

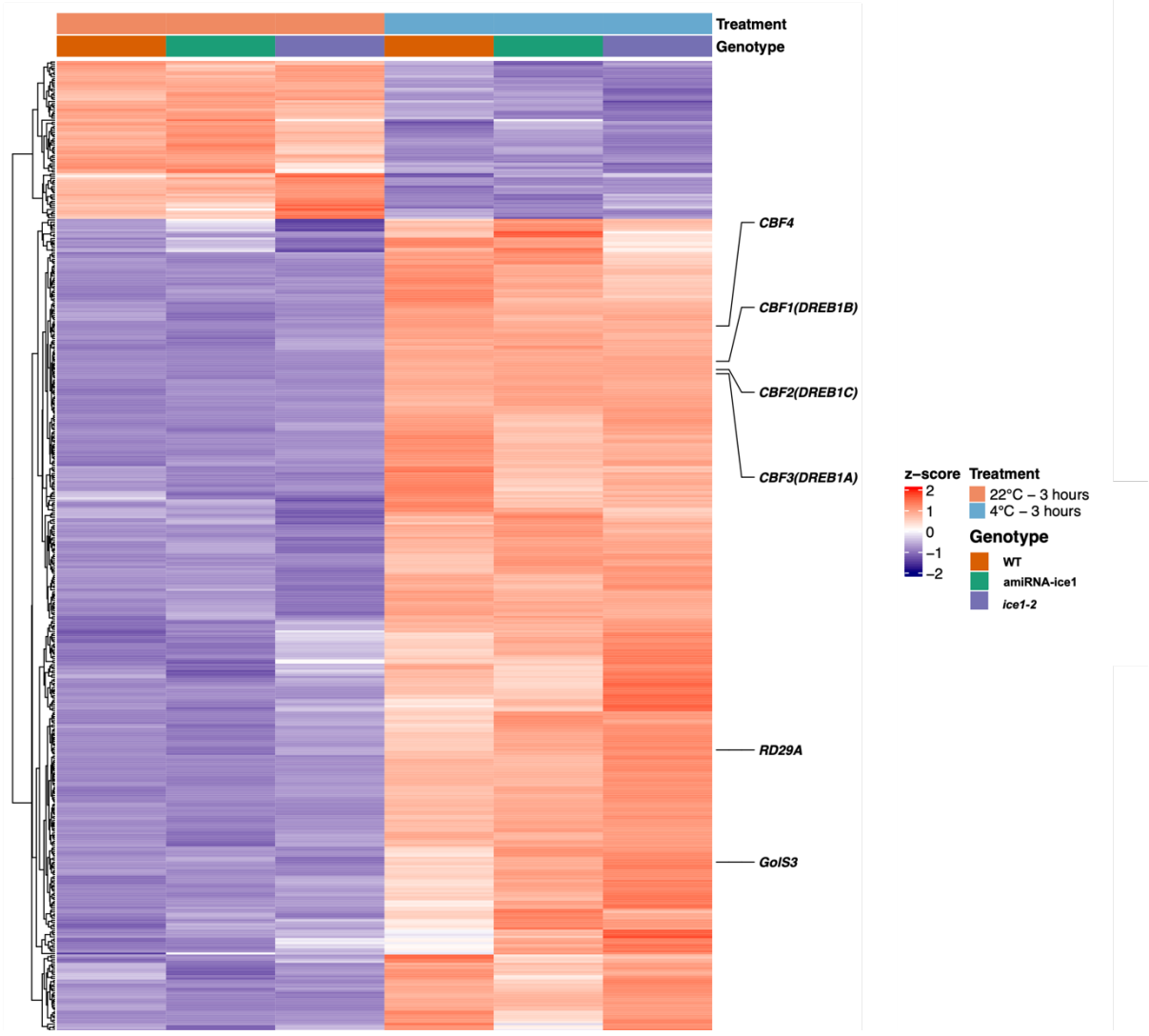

Figure 3.12 Heatmap of expression values from common cold-regulated DEGs. Counts from each gene across all conditions are processed by applying log2 transformation and normalising to generate a z-score. Each row in the heatmap represents the z-score. Columns with colour annotation represent the condition (genotypes and treatments). The lines with gene symbols represent the known cold-regulated genes.

To reduce the complexity of the analysis of common cold-regulated DEGs, we performed a K-means clustering analysis. We also performed a GO analysis for each

cluster, with the aim of finding different characteristics or specific pathways of each cluster. Cluster 2, which represented cold-repressed ICE1-independent genes, had unique GO terms related to carbohydrate metabolism (figure 3.14B). Many of the generic GO terms were enriched in clusters with genes activated by cold, clusters 1, 3, and 4, and the terms were involved in oxygen-related response or response to stimuli. However, biological processes involved in the regulation of transcription, regulation of RNA biosynthetic process, and related terms were found in cluster 1, cold-induced, ICE1-repressed genes, suggesting that a significant proportion of genes in this cluster were involved in transcriptional activities or could be transcription factors (figure 3.14A and table 3.4).

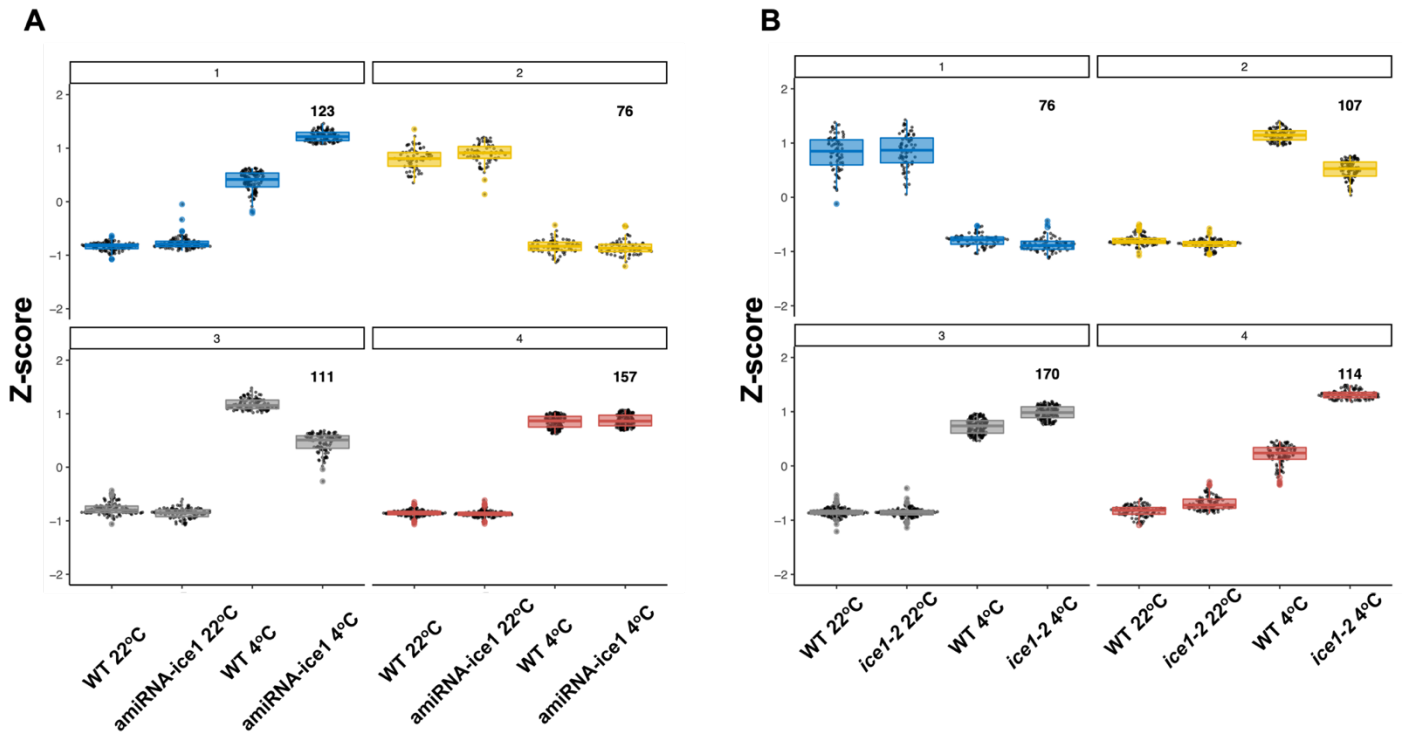

Figure 3.13 K-means clustering based on a list of common cold-regulated DEGs with the processed values (z-score) between WT and amiR-ice1 (A), WT and *ice1-2* (B). The first and second columns are processed normalised counts (z-score) from samples treated with an ambient temperature of WT and transgenic line, respectively. The third and fourth columns are values from the cold treatment. Genes from common cold-regulated DEGs are divided into 4 clusters based on an optimal number of clusters.

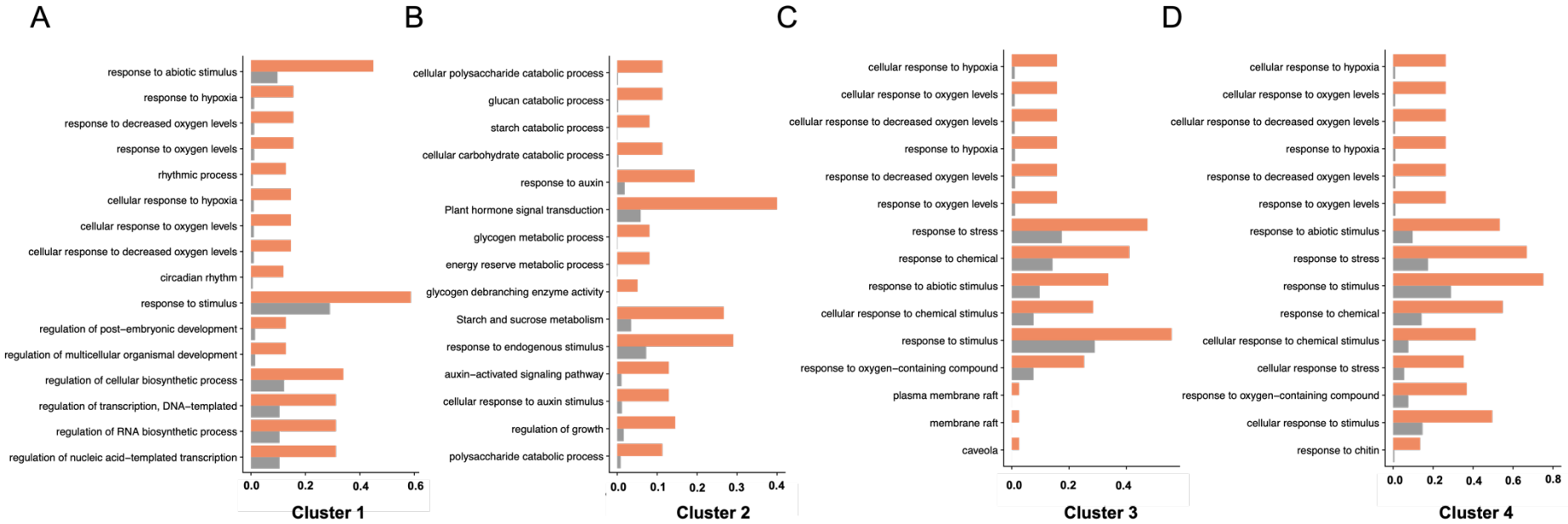

Figure 3.14 Gene ontology (GO) analysis of each cluster from k-means clustering from amiR-ice1. The enriched GO terms are from cluster 1 (A), cluster 2 (B), cluster 3 (C), and cluster 4 (D). X-axis indicates the frequency of GO terms between the expected value (grey bar) and the observed value (orange bar). The expected frequency is calculated from the number of genes with particular GO terms divided by the total GO terms in the *Arabidopsis* database. The observed value is calculated from the number of genes with the term in an input divided by the number of input genes.

Table 3.4 List of Genes with Transcription-Related Gene Ontology in Cluster 1 Genes with cold-related GO are marked with asterisks.

Gene ID	Gene Symbols	Remarks
AT1G01060	*LHY*	*
AT1G07050	NA	
AT1G13260	*RAV1*	
AT1G19050	*ARR7*	
AT1G26790	NA	
AT1G55950	NA	
AT1G68050	*FKF1*	
AT1G69570	NA	
AT1G74890	*ARR15*	
AT2G30040	*MAPKKK14*	
AT2G31380	*STH*	
AT2G40080	*ELF4*	
AT2G46830	*CCA1*	*
AT3G02380	*COL2*	
AT3G07650	*COL9*	
AT3G12320	NA	
AT3G15500	*NAC3*	
AT3G21150	*BBX32*	
AT3G21890	*BBX31*	
AT3G28910	*MYB30*	
AT3G47500	*CDF3*	
AT3G56400	*WRKY70*	
AT3G56710	*SIB1*	
AT4G17490	*ERF6*	
AT4G29190	*OZF2*	
AT4G33980	NA	*
AT5G17300	*RVE1*	
AT5G37260	*RVE2*	
AT5G42900	*COR27*	*
AT5G47220	*ERF2*	
AT5G48250	*BBX8*	
AT5G49330	*MYB111*	
AT5G50360	NA	
AT5G54470	*BBX29*	*
AT5G62430	*CDF1*	

To understand the involvement of ICE1 in k-means clusters, a motif enrichment analysis was performed. The rationale is that the bHLH binding motif domain of ICE1 (i.e. CANNTG where N is any nucleotide), would be found in cluster 1 and cluster 3 with ICE1-dependent genes more than in cluster 2 and cluster 4 containing ICE1-independent genes. To find the enriched motif, XSTREME was used (Bailey 2020). XSTREME is a comprehensive online tool that allows the exploration of enriched motifs in an annotated database or unsupervised *de novo* enrichment analysis by comparing two sets of sequences. The 500bp DNA sequences upstream to the transcription start sites (TSS) from each cluster were used as an input. The equal lengths of sequences from random genes were used as background sequences. With XSTREME, Fisher's exact test is used to find the significance of enrichment in the input sequences compared to background sequences. Table 3.5 contains the cluster number, the implication of clusters, enriched motif sequences, the annotation of motif, and statistical significance from enrichment analysis and *de novo* enrichment analysis. *De novo* enrichment indicates more stringent statistical analysis. Asterisks indicate the motif with significance in enrichment in *de novo* enrichment analysis. Clusters 2 and 3 show no significant enrichment in motif analysis. Cluster 1, indicating repressive roles of ICE1, contains enriched motifs related to bHLH, bZIP, and MYB transcription factors. However, only the bHLH-related motif was statistically significant in *de novo* analysis. Cluster 4 showed the motifs associated with CAMTA transcription factors, NAM (NO APICAL MERISTEM) proteins, and bZIP transcription factors with significance in all enrichment analyses.

Table 3.5 List of Motif Enrichment from amiR-ice1 k-means clusters

Cluster	Implication	Motif	Annotation	Enrichment rank	Enrichment p-value	de novo Enrichment p-value	Note
1	ICE1-repressed, Cold-activated	CACGTGTCT	bHLH	1	2.68E-07	4.70E-03	*
1	ICE1-repressed, Cold-activated	CGACCAAACA	AtIDD11	2	5.99E-07	7.00E-01	
1	ICE1-repressed, Cold-activated	AAATATCT	MYBrelated	3	3.78E-06	-	
1	ICE1-repressed, Cold-activated	KCCACGTGTC	bHLH	4	4.47E-06	-	
1	ICE1-repressed, Cold-activated	AGATATTTT	MYBrelated	5	4.97E-06	-	
1	ICE1-repressed, Cold-activated	ACGTGGC	bZIP	6	7.42E-06	-	
1	ICE1-repressed, Cold-activated	AGATATTTT	MYBrelated	7	1.23E-05	-	
1	ICE1-repressed, Cold-activated	AAATATCT	MYBrelated	8	1.62E-05	-	
1	ICE1-repressed, Cold-activated	ACGTGGC	bZIP	9	3.87E-05	-	
2	ICE1-independent, Cold-repressed	ACAGTCTTAA	-	1	-	5.00E-01	
2	ICE1-independent, Cold-repressed	ATATTGGGC	-	2	-	5.00E-01	
2	ICE1-independent, Cold-repressed	GACCCCTT	-	3	-	5.00E-01	
3	ICE1-activated, Cold-activated	AATATATACG	-	1	-	7.60E-01	
3	ICE1-activated, Cold-activated	AAACAAACAD	-	2	-	3.30E-01	
3	ICE1-activated, Cold-activated	AAAATAAATA	-	3	-	1.00E+00	
4	ICE1-independent, Cold-activated	CGCGT	CAMTA1	1	2.69E-09	1.80E-02	*
4	ICE1-independent, Cold-activated	ACACGGA	NAM, NAP	2	6.76E-08	6.40E-02	*
4	ICE1-independent, Cold-activated	ACGTGTCAT	bZIP (ABF2)	3	1.60E-06	8.40E-03	*

We used publicly available ChIP-seq data for ICE1, which was performed on plants grown under ambient temperature conditions (22^{o}C) using 35S::ICE1-GFP transgenic lines (Tang et al. (2020). A limitation of this study was that the chromatin analysis was carried out in overexpression lines and grown at 22^{o}C.

As shown in figure 3.15, the metaplot showed the ChIP-seq signal across genes with a 3 kb extension. The range of genes from start to end with 3 kb extension was divided into windows, and each window of each gene contained the ChIP-seq signal value. The values plotted in the y-axis were average signals from the same window from all genes in clusters. All clusters showed the ICE1-binding peaks close to the transcription start site of cold-responsive genes, and the signals from all clusters were stronger than signal from random genes. In the range of 1kb upstream to TSS, the average signal from genes in cluster 4 was the highest, followed by clusters 1, 2, and 3. The same tendency was continued towards the genes ending region. The highest abundance of ICE1 ChIP-seq signals in cluster 4 indicated more binding capability of ICE1 than other clusters on average.

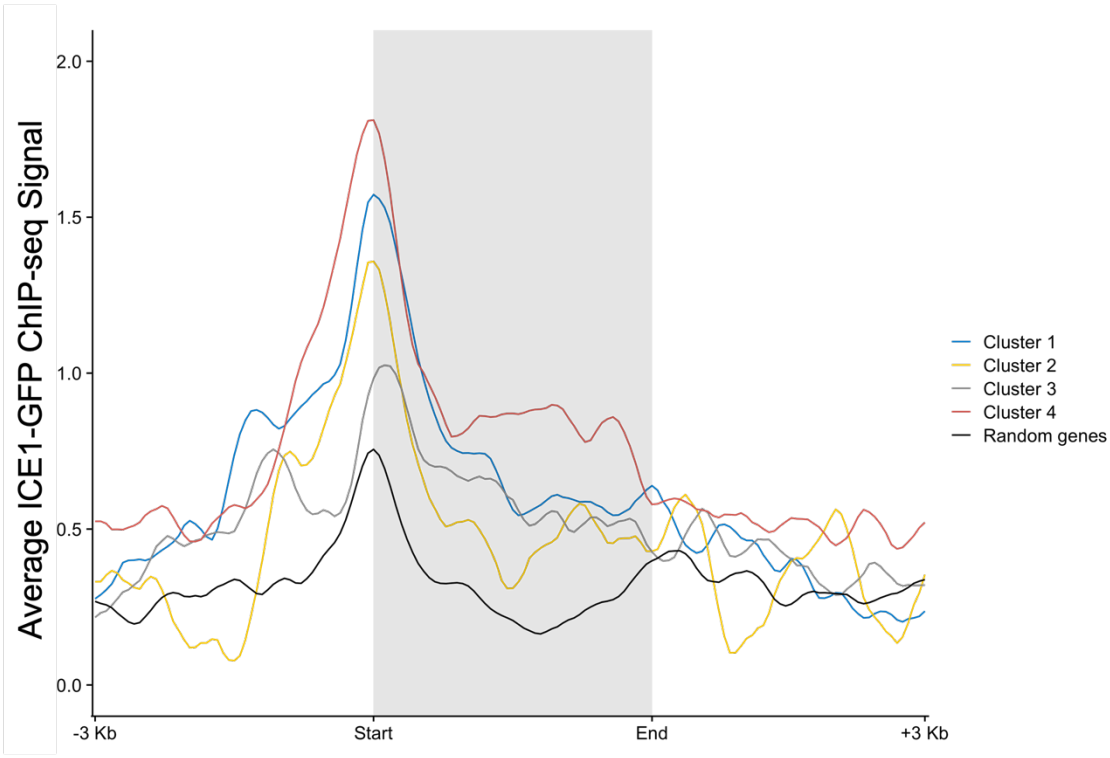

Figure 3.15 Metaplot representing average ICE1-GFP ChIP-seq signal across DEGs found in amiR-ice1 plants. The ChIP-seq signals were detected from the GFP antibody from the overexpression ICE1-GFP transgenic line. The signals were averaged from all genes in the same window. The signals were normalised by the signal in WT, with no expression of ICE1-GFP.

3.2.5 Inducible Overexpression of ICE1 (indICE1) and ICE1^{S278D} is not Sufficient to Resemble the ICE1-Dependent Genes

We determined if ICE1 was necessary in the cold-responsive pathway by analysing amiR-ice1 and *ice1-2* transcriptomes. We found that *CBF1-3* was not regulated by ICE1, however, a small number of genes were dependent on ICE1 activity. To investigate if ICE1 was sufficient to activate a specific transcriptional response we generated chemically inducible overexpression lines. We generated two constructs, one to overexpress the wild-type ICE1 protein (indICE1) and a second carrying an amino acid substitution of serine 278 to aspartate (indICE1^{S278D}) that mimics the phosphorylation of this amino acid, and it is known to increaseICE1 stability upon cold exposure (Ding et al. 2015). Transcriptome analysis was performed

using three genotypes (WT, indICE1, and indICE1^{S278D}) under three different conditions. There was no temperature variable included in this RNA-seq analysis. In the PCA plot, PC1 exhibiting 34% variance indicated the separation between untreated and chemical treatments. PC2 with 24% variance separated the WT from transgenic lines (figure 3.16). The overlap between mock and ß-estradiol treatment indicated that several genes were affected by the treatment and should be removed before gene expression differences are calculated.

Next, we focused on the list of DEGs under the inducible treatment. Table 3.6 contained the information for all pair-wise comparisons. Comparisons 1 and 2 show the differences between genotypes under the untreated condition as a control to check that there was no leaky expression from the inducible promoter (appendix figure 7.3). Comparisons 3 and 4 were to test the effect of the mock and ß-estradiol treatment, respectively. Because DMSO induces membrane rigidification which could trigger low temperature sensory pathway as reported in Örvar et al., (2000), we found 82 overlapping genes between the effects of mock treatment (comparison 3 in table 3.6) and cold-responsive genes in WT plants (comparison 1 in table 3.2) (appendix figure 7.4A). However, there was no specific GO terms related directly to cold found in comparison 3 suggesting that DMSO could partially trigger some cold-responsive genes in the lower degree than the temperature itself (appendix figure 7.4B). Comparisons 5 and 6 exhibited the transgenic inducible lines. However, the number of DEGs was still low even when the least stringent cut-offs were applied (FDR of 0.05, log2FC cut-off value of 0.5). An alternative way to obtain the list of DEGs was by using the untreated samples of each genotype as a normaliser. For the list of normalised DEGs from indICE1, the process was done by excluding DEGs from comparison number 1 or 7 out of comparison 8. A similar process was applied to indICE1^{S278D}. This normalisation method removed the effects of genotypes and the impact of DMSO used as mock treatment. The number of normalised DEGs was shown in comparisons 11 and 12 with 124 genes for indICE1 and 552 genes for indICE1^{S278D}, respectively. The number of normalised DEGs between two genotypes were around 4-fold, which could be because of the difference between the modification and the differences of induced ICE1 expression. The list of normalised DEGs for indICE1 is shown in appendix table 7.3 – 7.4.

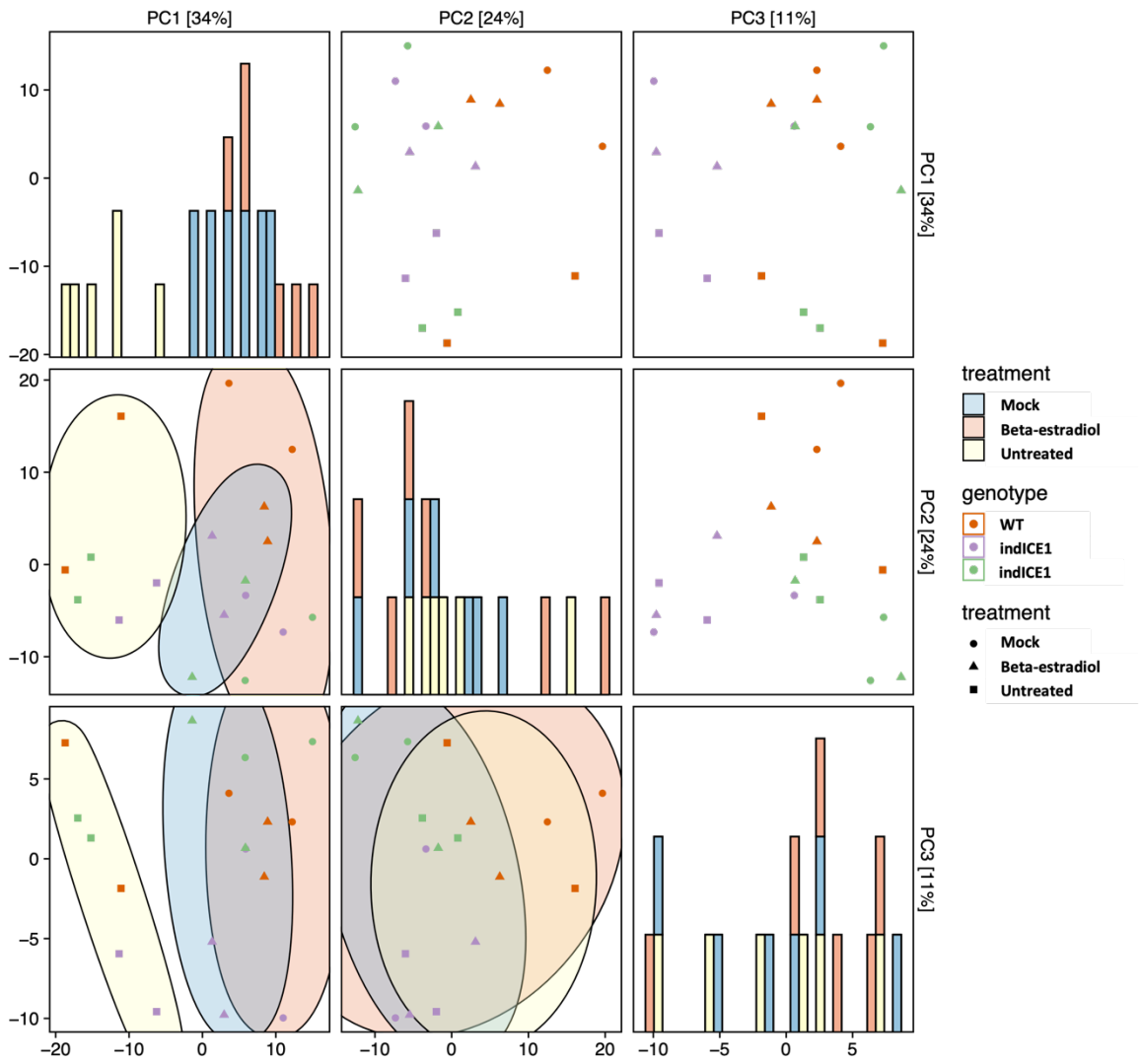

Figure 3.16 Principal component analysis (PCA) plot from WT, indICE1, and indICE1^{S278D} under untreated, mock treatment, and ß-estradiol treatment. The number in the bracket shows the percentage variance contributed by the principal component. Coloured dots represent genotypes. Filled circles indicate the treatments used. The histogram in the diagonal matrix shows the distribution of treatments according to PC on the x-axis.

Table 3.6 List of Pair-wise comparisons and Numbers of DEGs from WT, indICE1, and indICE1^{S278D}

	Reference condition	Treatment condition	Number of DEGs	Up-regulated DEGs	Down-regulated DEGs
1	WT untreated	indICE1 untreated	194	163	31
2	WT untreated	indICE1^{S278D} untreated	40	33	7
3	WT untreated	WT mock	878	553	325
4	WT untreated	WT est	798	345	453
5	indICE1 mock	indICE1 est	59	24	35
6	indICE1^{S278D} mock	indICE1^{S278D}est	83	44	39
7	indICE1 untreated	indICE1 mock	39	24	15
8	indICE1 untreated	indICE1 est	312	213	99
9	indICE1^{S278D} untreated	indICE1^{S278D}mock	410	289	121
10	indICE1^{S278D} untreated	indICE1^{S278D}est	1,233	681	552
11	Normalised indICE1 DEGs	-	124	82	42
12	Normalised indICE1^{S278D} DEGs	-	552	262	290

To investigate whether inducible transgenic lines could resemble ICE1-dependent genes from k-means clusters from amiR-ice1 (figure 3.13), a list of ICE1-dependent genes was used to overlap with the normalised DEGs from indICE1 and indICE1^{S278D}. Figure 3.17A shows the overlapping number of DEGs. Only two genes overlapped with ICE1-dependent genes with up-regulated normalised indICE1 DEGs. However, no genes overlapped with down-regulated genes. The overlap between ICE1-dependent genes and up- and down-regulated DEGs from indICE1^{S278D} were 10 and 2 genes, respectively (figure 3.17B). The statistical analysis from Fisher's exact test showed that there were no significant overlaps in all pairs of intersections. The insignificant overlaps suggest that the inducible transgenic lines were not sufficient to activate or repress ICE1-dependent genes. It is also possible that there are other factors other than transcriptional activation involved in the regulation of ICE1-related cold-responsive genes. All overlapping genes are marked with asterisks in appendix table 7.3 - 7.4.

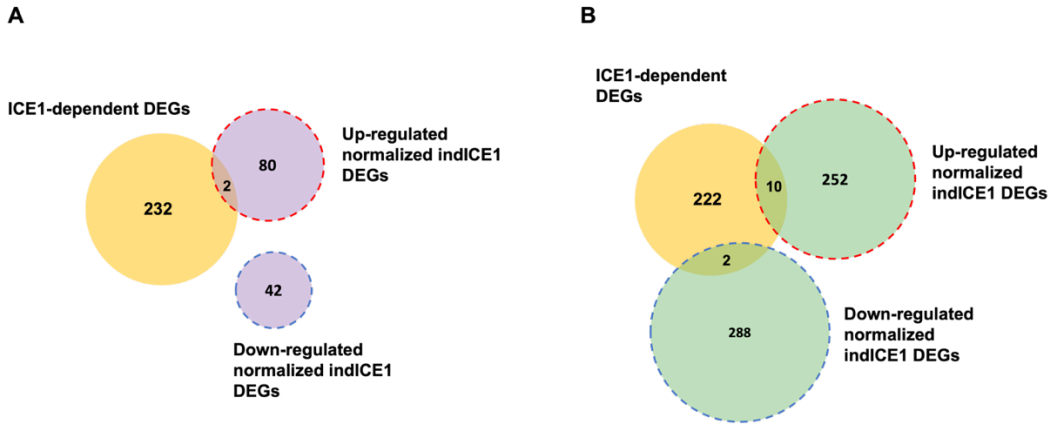

Figure 3.17 Venn diagram of the overlapping genes between ICE1-dependent DEGs, k-means clusters from amiR-ice1, and normalised up- and down-regulated DEGs from indICE1 (A) and indICE1^{S278D} (B). The number in the intersection indicates a number of overlapping genes.

3.2.6 Low Temperature Removes Repressive Histone Marks in ICE1-Dependent Genes

One hypothesis is that the ICE1-related cold response might be regulated epigenetically, which could explain the discrepancy between transcriptome and binding to chromatin. Vernalisation is a good example of how repressive histone modifications accumulate at some loci (e.g., *FLC)* over a long period of cold to regulate their expression. However, it is not fully understood how these repressive marks are put in place or removed upon cold exposure. Our hypothesis is that low-temperature exposure could change the chromatin landscape of ICE1-regulated genes. To test this idea, we used publicly available ChIP-seq data for H3K27me3 performed in wild-type seedlings grown under standard (control) and long cold growth conditions (Xi et al. 2020). Differences in normalised ChIP-seq signal between control and cold-treated plants were compared between common cold-regulated genes and random H3K27me3-containing genes (Zhou et al. 2017b) (Figure 3.18). We found under cold conditions a strong reduction of H3K27me3 at cold-regulated genes when compared to a random gene set. The reduction was found both in the gene region and 1kb extension (figure 3.18A). Statistical analysis was performed to compare the reduction of H3K27me3 at gene flanking regions and showed a significant difference between growth at different temperature conditions. These results show that under prolonged

cold exposure, cold-related genes lose H3K27me3 at proximal gene regulatory regions.

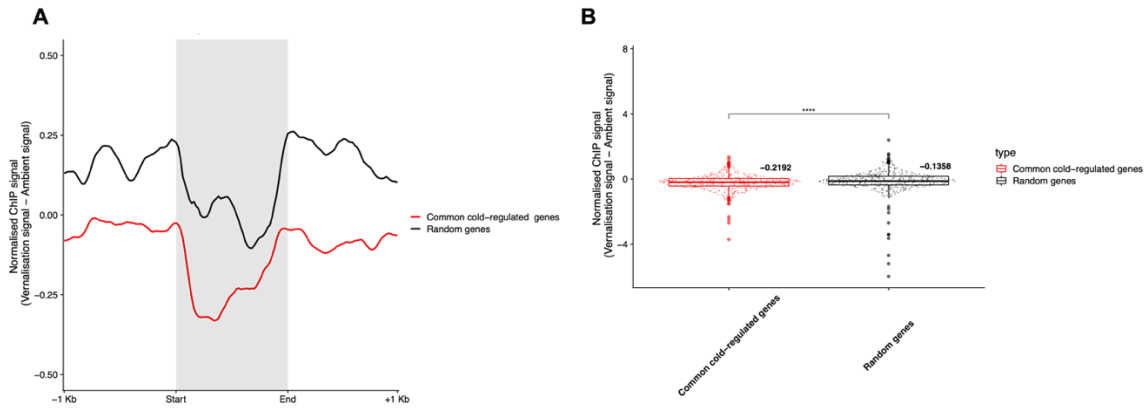

Figure 3.18 Metaplot of normalised H3K27me3 signals at cold-regulated genes. (A) common cold-regulated genes compared to random genes; (B) common cold-regulated genes and random genes. Red line and dots represent the values from common cold-regulated genes. Black line and dots indicate values from random H3K27me3-containing genes obtained from Zhou et al. (2017b). The normalised ChIP-seq signals were calculated from the differences between signals under cold treatment subtracted by the signal under control conditions. The metaplot shows the signal across genes with a 1 kb extension. The numbers above the box plots show the average number of calculated signals. Asterisk indicates significant difference between comparisons (Student's *t*-test, ns – non-significance, **** $p < 0.0001$, *** $p < 0.001$, ** $p < 0.01$, and * $p < 0.05$)

The common cold-regulated DEGs identified were divided into four clusters based on expression values from WT and amiR-ice1 under ambient and cold conditions (figure 3.13). The patterns of expression were different among clusters and can be categorised as ICE1-dependent and ICE1-independent groups. We, then, compared the changes in H3K27me3 accumulation between two groups of genes and the random sets of genes. We found that the cold treatment significantly more reduced H3K27me3 signal from ICE1-dependent genes than from a random gene dataset (figure 3.19A). A similar outcome was found in the comparison between ICE1-independent genes with random genes (figure 3.19B). There was more reduction in

H3K27me3 from ICE1-dependent genes than from ICE1-independent genes. However, the statistical analysis showed no significant difference between the two groups (figure 3.20). The lack of significant difference between signals from ICE1-dependent and ICE1-independent genes suggested that the removal of H3K27me3 generally occurred in the cold and was not specific to ICE1-dependent genes.

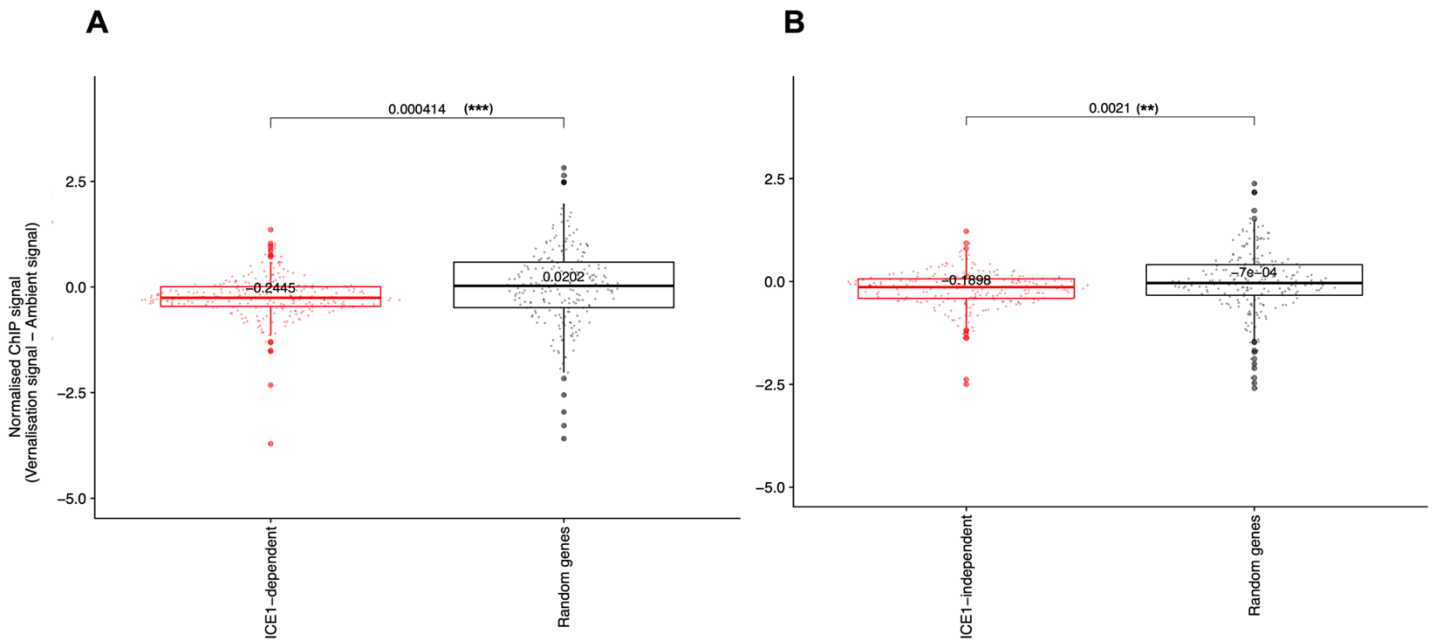

Figure 3.19 Box plots comparing H3K27me3 accumulation at cold responsive gene. (A) ICE1-dependent genes and random genes; (B) ICE1-independent genes and random genes. Red dots represent the values from ICE1-dependent/independent genes. Black dots indicate values from random H3K27me3-containing genes obtained from Zhou et al. (2017b). The normalised ChIP-seq signals were calculated from the differences between signals under cold treatment subtracted by the signal under control conditions. The numbers above the box plots show the average number of calculated signals. Asterisk indicates the significant difference between comparisons (Student's *t*-test, ns – non-significance, **** $p < 0.0001$, *** $p < 0.001$, ** $p < 0.01$, and * $p < 0.05$).

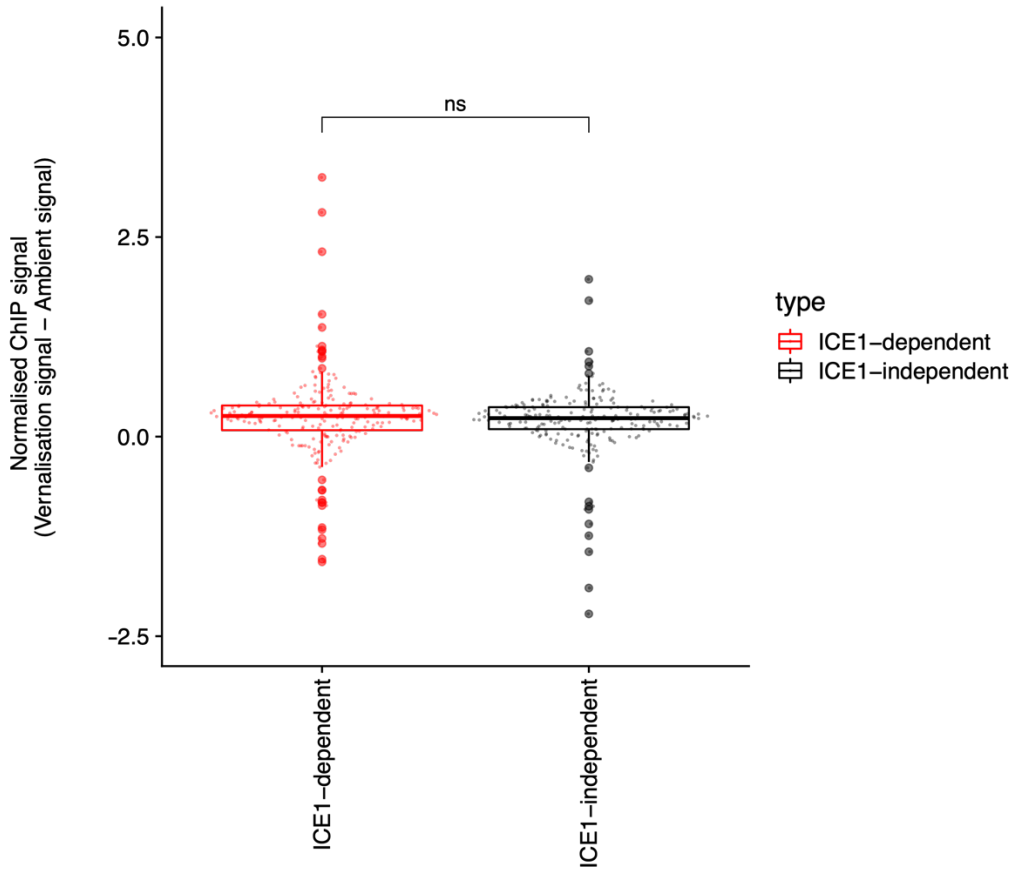

Figure 3.20 Box plots comparing H3K27me3 accumulation at ICE1-dependent and independent genes. Red dots represent the values from ICE1-dependent genes. Black dots indicate values from ICE1-independent genes. The normalised ChIP-seq signals were calculated from the differences between signals under cold treatment subtracted by the signal under control conditions. Asterisks indicate significant differences between comparisons (Student's t-test, ns – non-significance, **** $p < 0.0001$, *** $p < 0.001$, ** $p < 0.01$, and * $p < 0.05$)

The removal of H3K27me3 requires the activity of histone demethylases (Gan et al. 2014; Lu et al. 2011). RELATIVE OF EARLY FLOWERING 6 (REF6) is a Jumonji-type (JMJ) histone demethylase that has been found to play a major role in the removal of H3K27me3 and in genome stability (Lu et al. 2011). We identified REF6 target genes under ambient conditions and overlapped this list with cold-regulated and ICE1-dependent or independent genes. We found 31 REF6 target genes to be ICE1-dependent and 29 to be ICE1-independent (figure 3.21 and table 3.7). To

decipher the possible connection between ICE1 and the removal of H3K27me3, we treated with cold for 3h wild type and *ref6-5* 14-day-old seedlings. We measured the expression of *GolS3* (AT1G093500) and AT5G41740, two ICE1-dependent genes with ICE1-binding motif at their promoter regions, and with low H3K27me3 under low-temperature exposure (appendix figure 7.5). Notably, *GolS3* appears not to be a target of REF6 at ambient temperature when AT5G41740 is (Antunez-Sanchez et al. 2020). Interestingly, the cold-mediated transcriptional response of these genes is impaired in *ref6-5* mutant. In addition, we found that the expression of *GolS3* was significantly reduced (60%) by low temperature when the other gene was not affected (figure 3.22). These results suggest that the cold-mediated epigenetic modifications are involved in the transcriptional activity of some ICE1-dependent genes.

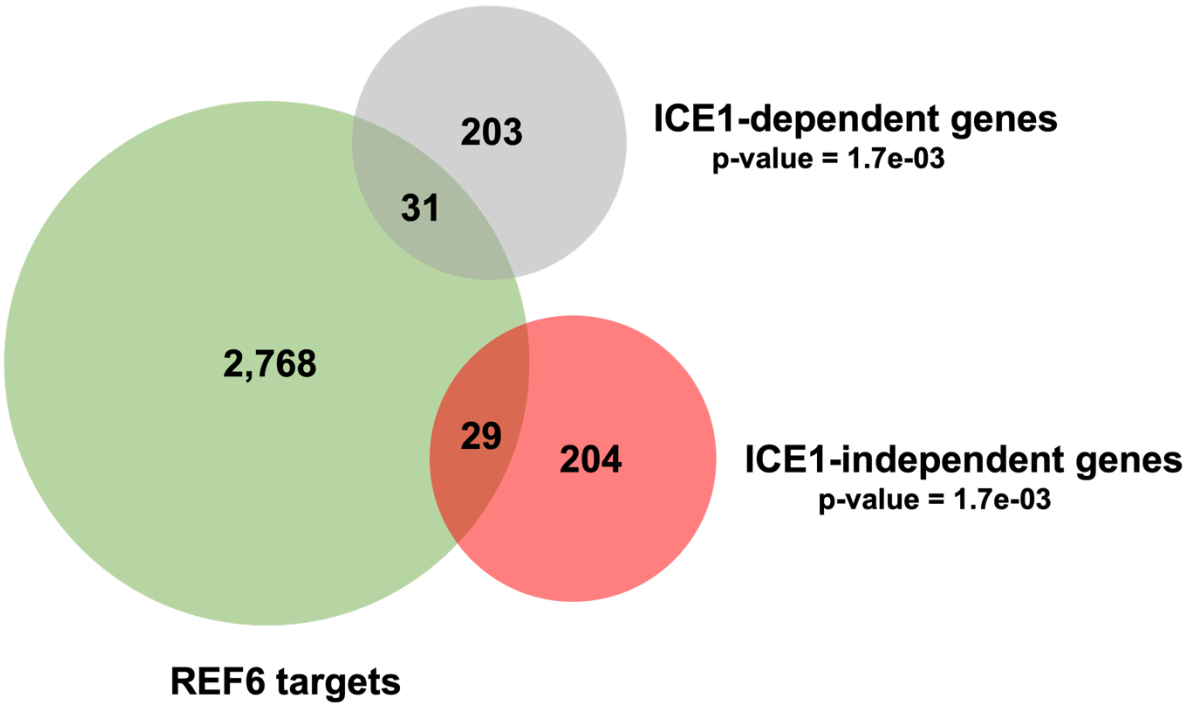

Figure 3.21 Overlap between REF6 targets and both ICE1-dependent genes and ICE1-independent genes. The number of overlapping genes is indicated in the intersection. P-value underneath each diagram indicates the significance of Fisher's exact test.

Table 3.7 Lists of Overlapping Genes between REF6 targets and both ICE1-dependent Genes and ICE1-independent Genes

REF6 targets with ICE1-dependent genes	Symbols	REF6 targets with ICE1-independent genes	Symbols
AT1G01560	*MPK11*	AT1G07330	NA
AT1G04570	NA	AT1G13480	NA
AT1G05330	NA	AT1G28370	*ERF11*
AT1G06030	NA	AT1G60190	*PUB19*
AT1G12610	*DDF1*	AT1G64170	*CHX16*
AT1G19040	NA	AT1G70820	NA
AT1G62000	NA	AT2G33260	NA
AT1G69570	NA	AT2G41640	NA
AT1G70800	*EHB1*	AT3G24600	NA
AT1G74830	NA	AT3G55880	*SUE4*
AT1G74890	*ARR15*	AT3G62750	*BGLU8*
AT2G26480	*UGT76D1*	AT4G18880	*HSF A4A*
AT2G37770	*ChlAKR*	AT4G22758	NA
AT2G40130	NA	AT4G25470	*CBF2*
AT3G02800	*PFA-DSP3*	AT4G25480	*CBF3*
AT3G12960	*SMP1*	AT4G25490	*CBF1*
AT3G14770	*SWEET2*	AT4G26530	*FBA5*
AT3G21660	NA	AT5G04340	*ZAT6*
AT3G50930	*BCS1*	AT5G16960	NA
AT4G19960	*KUP9*	AT5G17850	NA
AT4G25433	NA	AT5G18010	*SAUR19*
AT4G28405	NA	AT5G18020	*SAUR20*
AT4G36950	*MAPKKK21*	AT5G18030	NA
AT4G39070	*BZS1*	AT5G19240	NA
AT4G39320	NA	AT5G37770	*TCH2*
AT5G40010	*AATP1*	AT5G39785	NA
AT5G41740	NA	AT5G45340	*CYP707A3*
AT5G43620	NA	AT5G52050	NA
AT5G51990	*CBF4*	AT5G60100	*PRR3*
AT5G52310	*LTI78*		
AT5G58770	*cPT4*		

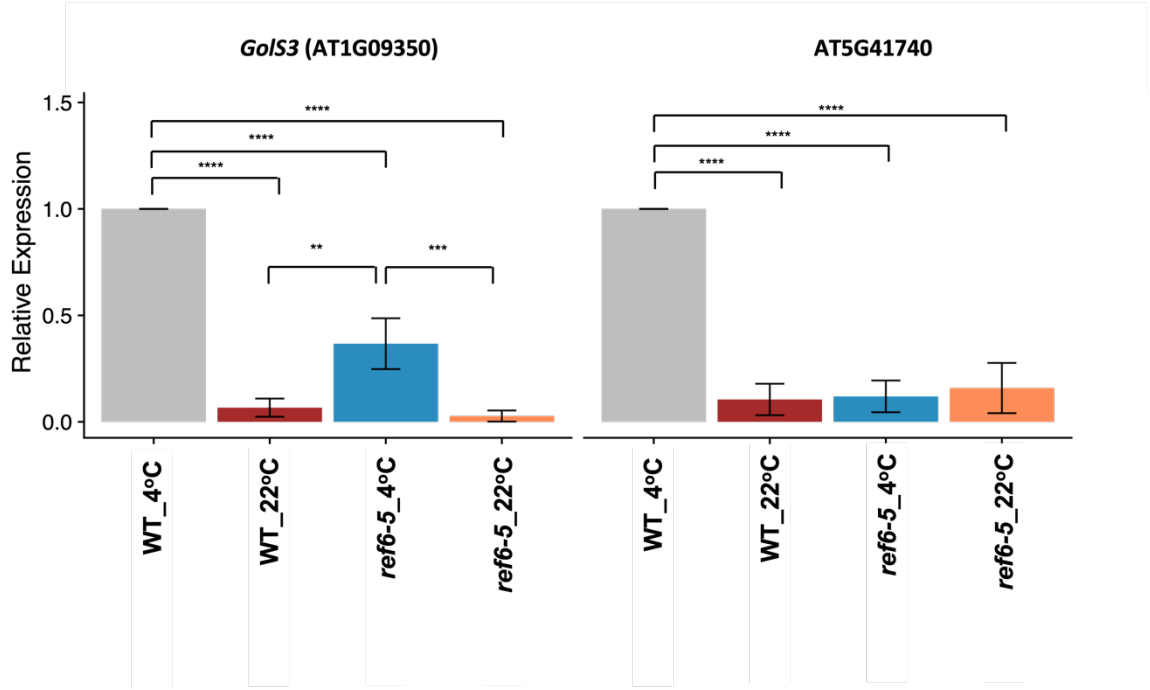

Figure 3.22 qRT-PCR analysis showing relative expression of *GolS3* (AT1G09350), and AT5G41740 in 14 days old seedlings grown under 22°C and exposed to 4°C for three hours. The relative expression was calculated using ΔΔCt method (Schmittgen and Livak 2008). The normalisation was done in comparison with positive control (WT under 4°C) and GAPDH was used as a housekeeping gene in the calculation. The experiment was done with triple replicates. The error bars indicate standard deviation from three replicates. Asterisk indicates the significant difference between comparisons (Tukey's HSD test, **** $p < 0.0001$, *** $p < 0.001$, ** $p < 0.01$, and * $p < 0.05$)

3.3 Discussion

In this study, we developed amiR-ice1 transgenic lines to dissect the roles of ICE1 in cold-responsive transcriptional gene networks. ICE1 plays a major role in seed development and stomatal formation (Denay et al. 2014; MacGregor et al. 2019). We have found that transgenic amiRNA-ice1 plants also have defects in stomata development and subtle effects in seed development. The defects in germination found in amiRNA-ice1 plants are consistent with a previous study carried out with *ice1-2* mutants (MacGregor et al. 2019). However, the seed shape was affected to a lesser extent in amiR-ice1 compared to *ice1-2*, (Denay et al. 2014; MacGregor et al. 2019). The defects in stomata development were stronger in amiR-ice1 than in *ice1-2* mutants, as the number of grouped underdeveloped guard cells was higher. The stomatal phenotype found in amiR-ice1 plants was also consistent with mutants of ICE1 interacting proteins (Kanaoka et al. 2008; Pillitteri et al. 2007). Taken together, our data support preliminary studies indicating that ICE1 plays a role in the seed germination and stomatal development.

Several studies have reported that *ice1-2* is highly sensitive to freezing temperatures either when grown in media or soil (Ding et al. 2015; Kim et al. 2015; Li et al. 2017). However, we found that amiR-ice1 and *ice1-2* plants did not show significant differences from wild-type when exposed to freezing temperatures. Unfortunately, the methodology employed by other studies is not fully documented thus it is difficult to place our observations in context with previous reports (Ding et al. 2015; Li et al. 2017). The discrepancy between our data and previous studies may be caused by differences in the methodology employed to expose plants to freezing or differences in the developmental stage of the plants that affect their recovery after the freezing treatment (Wanner and Junttila 1999). To ensure the latter was not an issue we ensured that all plants tested in freezing assays had uniform germination after long stratification (7 days) and similar size. Other groups have used the electrolyte leakage assay or measured reactive oxygen species in response to freezing (Kawarazaki et al. 2013; Thalhammer et al. 2014). Unfortunately, these assays require a specific freezing facility, which was not available to us.

In addition to phenotypic assays, we conducted a genome-wide transcriptomic analysis under different temperature conditions. This analysis confirmed the efficacy

of the amiR-ice1 construct, which depleted significantly ICE1 expression. We found that *ice1-2,* which contains a T-DNA insertion in the third exon did not alter ICE1 expression and produced atypical transcripts that could result in a partially functional protein. This phenomenon is frequently found in *Arabidopsis* T-DNA mutant collections, where 1% of mutant lines produce truncated and partially functional proteins (Wang 2008). Notably, the transgene insertion in *ice1-2* is located downstream of the bHLH protein interaction domain which could result in a partially functional protein. This hypothesis is supported by the striking differences we have found in the transcriptome of amiR-ice1 and *ice1-2* plants.

In this study, the majority of genes show similar expression changes under cold treatment in WT, amiR-ice1, and *ice1-2*, so-called common cold-regulated genes. This group of genes shows more substantial regulation by cold when compared with other genotype-specific gene lists. Moreover, gene ontology analysis also shows the enriched terms related to cold response specifically in the common cold-regulated list. There are several well-known *CORs* which appear in the list of common cold-regulated genes; for instance, *CBF1/2/3* and the downstream genes such as *GolS3* and *RD29A* (Chinnusamy et al. 2003; Ding et al. 2015; Jiang et al. 2017; Kidokoro et al. 2022). CCA1 and LHY, upstream activators of *CBF1-3, COR47,* and *COR15* (Dong et al. 2011), are also on the list of common cold-regulated genes. The results from our study have shown that several major transcription factors modulating cold response are still expressed in WT and both transgenic lines. The results show no major disruption in cold response in both amiRNA-ice1 and *ice1*-2 suggesting that ICE1 might not be the primary component in the cold-responsive pathway.

Although the common cold-regulated genes show the same induction or repression regardless of the genotypes, the expression profiles of several genes under cold treatment are unequal between WT and transgenic lines. This indicates the amiR-ice1 and *ice1-2* might still have effects on some genes in cold. To observe the unequal changes in more detail, k-means clustering was used to separate common cold-regulated genes into four clusters. We focused only on the clusters based on values from amiR-ice1 and WT to reduce the complexity of the analysis. We have found that four clusters represent two groups of genes, ICE1-dependent and ICE1-independent genes. These groups consist of an almost equal number of genes, indicating that half

of the common cold-regulated genes have changes in expression levels when *ICE1* is not fully expressed under cold conditions. *CBF1/2/3* are in the list of ICE1-independent genes. This result is in line with the study by Kidokoro et al. (2020), which showed an insignificant difference in the expression level of *CBF1-3* in *ice1-2*, *ice2-1*, and *ice1-2 ice2-1* double mutant under the same cold condition used in our study. Collectively, our confirms that transcription of *CBFs* is independent of ICE1 or, at least, is not the target of ICE1 during early cold response.

We found that ICE1 acts as both an activator and a repressor of transcription. ICE1 was thought to be the only transcriptional activator of genes under cold stress (Ding et al. 2015; Hwarari et al. 2022). However, the repressive effects of ICE1 have been reported only under normal temperatures during seed development (MacGregor et al. 2019). ICE1 was also found to repress Jasmonic acid (JA)-related genes in anther during the reproductive growth (Wei et al. 2018). To date, the repressive roles of ICE1 in cold stress have not been described. Our study, using a loss of function amiRNA-ice1line, shows that ICE1 could act as a transcriptional activator or repressor under cold conditions. Moreover, we also identified several genes that are associated with *CBF* regulation in the list of ICE1-repressed genes. CCA1 and LHY are positive regulators of *CBFs* after 6 hours of cold exposure (Dong et al. 2011), which coincides with the repression by REVEILLE1 and 2 (RVE1 and RVE2) in *CBF3* (Kidokoro et al. 2022). ICE1 has a repressive effect on *CCA1*, *LHY*, *RVE1*, and *RVE2,* suggesting a dynamic in the transcriptional regulation upstream of *CBFs* and the integrative function of ICE1 in circadian-related cold response. Given that the peak expression levels of *CBFs* were around 3 h, when we found no effect of ICE1 on *CBFs*, we suspected that the ICE1-regulated upstream regulators of *CBFs* might take part in time-specific regulation of *CBFs* after a long period of cold treatment.

Because *ICE1* encodes a protein with a bHLH and a bZIP domains (Chinnusamy et al. 2003; Kanaoka et al. 2008) and we found the enrichment of the bHLH binding motif only in the 500bp flanking regions upstream of genes in ICE1-repressed cluster, this indicates that a group of ICE1-repressed genes may contain a significant proportion of ICE1 direct targets. However, ICE1-activated genes have no enriched motifs suggesting the indirect effects of ICE1 on this group. The cluster of cold-activated ICE1-independent genes shows the enrichment of the binding motifs

related to CAMTA, NAM, and bZIP but not bHLH confirming ICE1-independent cold response. CAMTA transcription factors have been reported to be the regulators of *CBFs* and other cold-responsive genes (Doherty et al. 2009; Kidokoro et al. 2017; Kim et al. 2013). However, when we re-analysed the ICE1 publicly available chromatin binding data (Tang et al. 2020), we found that genes in the cold-activated ICE1-independent cluster show the highest binding potential followed by the cluster of ICE1-repressed genes. This could be because ICE1 also has a bZIP domain located toward the N-terminal of the protein (Kanaoka et al. 2008). The bZIP domain in plants binds to a motif with an "ACGT" core, either A-box (TACGTA), C-box (GACGTC) and G-box (CACGTG) (Jakoby et al. 2002). In the case of ICE1, its bHLH domain binds to an E-box motif (CANNTG; where N is any nucleotide), which is similar to the G-box motif (Kidokoro et al. 2020). Moreover, The ICE1 chromatin binding experiments were done using a transgenic line that constitutively expresses an *ICE1-GFP* transgene (Tang et al. 2020). Thus, the abundance of the ICE1 signal might be caused by binding to bZIP motifs, which is consistent with the enrichment we found for bZIP motifs in this cluster. However, it must be noted that the ChIP-seq was performed under standard growth conditions, which might not fully reflect the binding of ICE1 to cold-related genes.

In this study, the inducible overexpression of ICE1 and ICE1^{S278D} was used to test the capacity of ICE1 to mimic a cold-directed transcriptional response. Although the downregulation of *ICE1* does not affect the expression level of *CBFs* under short cold treatment, there are still cold-regulated genes affected.

We removed the effects of the mock treatment and used two independent transgenic lines in the analysis. We found that only two genes (*FRIABLE1* (*FRB1*) and *ß-AMYLASE8* (*BMY8*)) were in the intersection between ICE1-dependent and up-regulated DEGs in indICE1 lines. *FRB1* is reported to have a function in cell wall adhesion but is not directly related to the cold stress (Neumetzler et al. 2012), while *BMY8* encodes ß-amylase8 is specific to the chloroplast, where it is involved in maltose metabolism and in protecting the photosystem under cold treatment (Kaplan and Guy 2005). Several known genes were found to overlap between ICE1-dependent and up- and down-regulated DEGs in indICE1^{S278D}, which are *ß-GLUCOSIDASE11 (BGLU11), POLYGALACTURONASE INVOLVED IN EXPANSION3 (PGX3),*

WRKY48, and *WRKY72*. However, none of these genes involved in the major cold-responsive pathway. These results suggest that the activation of *ICE1* is not sufficient to mimic a cold-directed transcriptional response under ambient temperature. These results suggest that low temperature causes chromatin changes that are required for ICE1 action in transcription.

Epigenetic changes in response to cold stress exposure over a short period of time have been reported in plants and involve the removal of histone deacetylase 2C (HD2C) through the interaction with HOS15 and POWERDRESS (PWR) (Park et al. 2018). Upon removal of HD2C, cold-responsive genes such as *COR15A, COR47,* and COR78 display an accessible chromatin conformation (Park et al. 2018). Other studies have shown that in *Arabidopsis* the repressive histone mark H3K27me3 is dynamically affected after long-term cold exposure (De Lucia et al. 2008; Sung and Amasino 2004; Sung et al. 2006). In this study, I hypothesised that removal of the repressive mark under cold treatment occurs before cold-responsive transcription factors, such as ICE1, are activated. We found that the removal of H3K27me3 from cold-regulated genes is significantly stronger than in random genes. However, there was no significant change in the reduction of H3K27me3 between the ICE1-dependent and ICE1-independent groups. There was also an equal number of overlapping genes between ICE1-dependent and ICE1-independent groups with targets of REF6, a key H3K27me3 demethylases (Antunez-Sanchez et al. 2020). Collectively, the results indicate the dynamic role of H3K27me3 under low-temperature growth, which is likely to affect ICE1 transcriptional activity. We found that the removal of H3K27me3 is necessary for the activity of ICE1 in several target genes. The interplay between histone demethylases and transcription factors has been well-studied during plant developmental processes (Hung et al. 2021). It also plays a role in response to environmental stimuli, for instance, PHYTOCHROME INTERACTING FACTOR 4 (PIF4) requires REF6 activity to regulate gene expression under warm growth conditions (He et al. 2021). The connection between chromatin modifications and transcription factors under a short period of the cold response is poorly understood. However, results from our study provide a strong link between the molecular mechanisms and adaptation to low-temperature stress.

3.4 Chapter Conclusion

In this study, we describe the use of classic genetic lesions and newly generated amiR-ice1 lines to study the role of ICE1 in seed germination and stomatal development. Transcriptomic studies revealed that amiR-ice1 lines result in ICE1 loss-of-function when *ice1*-2 produces atypical transcripts which most likely result in truncated protein. Our transcriptomic data shows that ICE1 plays a minor role in the transcriptional regulation of COR genes. Ectopic expression of ICE1 cannot mimic the changes in gene expression of ICE1-dependent genes, pointing to epigenetic regulation of ICE1 function. Notably, we have also found that the removal of H3K27me3 from the promoter of ICE1 targets is required for ICE1 activity.

Chapter 4 Transgenerational Stress Memory in Clonal Plants

4.1 Introduction

4.1.1 Somatic and Transgenerational Stress Memory in Plants

Somatic stress memory in plants can be measured by the transcriptional activity of genes during priming exposure, the recovery stage, and subsequent exposures. These transcriptional changes define three different classes: type I stress memory refers to the sustained induction of transcriptional activity over a long period. Type II memory is characterised by an enhancement from the re-induction process (figure 1.3) (Baurle and Trindade 2020; Oberkofler et al. 2021). The degree of response is not the only aspect of measuring stress memory; the strength of response in primed plants is another factor in the transcriptional stress memory (Lamke and Baurle 2017). Several studies have also proposed that epigenetic modifications mediate a somatic stress memory response in plants. FLC is a type I stress memory gene that accumulates H3K27me3 repressive histone marks that are actively removed upon a long period of cold exposure (De Lucia et al. 2008; Sung and Amasino 2004; Sung et al. 2006). In heat response, the formation of a protein complex consisting of FORGETTER1 (FGT1) with chromatin remodelers, BRM and CHR11/17, maintains the chromatin accessibility of several genes encoding heat-shock proteins up to three days (Brzezinka et al. 2016). A similar mechanism occurs in the cold mediated by PICKLE (PKL), a CHD3-type chromatin remodeler (Yang et al. 2019). Type II stress memory is established by the accumulation of active marks such as H3K4me3, resulting in the hyper-induction of a few genes under subsequent drought stress (Liu et al. 2014). Several studies also show changes in DNA methylation mediated by long non-coding RNA, non-coding RNA, or transposable elements (TEs) in response to environmental stimuli that contribute to stress memory responses (Ariel et al. 2014; Ariel et al. 2015; Gagliardi et al. 2019). Previous work has shown that the salt-induced changes in DNA methylation can persist as a somatic stress memory (Wang et al. 2015). Non-chromatin-related mechanisms such as paused RNA Pol II close to transcription start sites also associates with type II drought memory genes (Ding et al. 2012). The sustained activity of stress-related transcription factors is also one of the mechanisms of a stress memory (Bruce et al. 2007). Apart from the stress memory

mediated by transcriptional activity and/or chromatin-related elements, an accumulation of secondary metabolites in plants by priming stress is also found as a stress memory mechanism. Temperate grass species such as tall fescue (*Festuca arundinacea*) exhibit enhanced levels of cellular lipidomes, including several types of phospholipids and glycolipids, resulting in higher tolerance to subsequent heat stress (Zhang et al. 2019).

Several studies have proposed the existence of a transgenerational stress memory (TSM), which is stable at least through two stress-free generations and thus not affected by stress-mediated parental effects. TSM has been found to occur in heat stress responses and involves a positive feedback loop between HEAT SHOCK TRANSCRIPTION FACTOR A2 (HSFA2) and REF6 (Liu et al. 2019). This protein complex activates HEAT-INDUCED TAS1 TARGET 5 (HTT5) and represses the biosynthesis of siRNA antagonistic to HTT5. Notably, these feedback loops seem to be heritable through multiple generations resulting in early flowering with the adaptive immunity (Liu et al. 2019). Because chromatin marks are actively reset during sexual reproduction, it has been proposed that transgenerational stress memory is likely underpinned by changes in DNA methylation (Crisp et al. 2016; Hauser et al. 2011). Cold-induced transgenerational memory has been associated with changes in leaf-number phenotype and the reactivation of transposons, such as *ONSEN* and *TSI*, suggesting that the heritability is linked to hypomethylated TEs (Migicovsky and Kovalchuk 2015). This form of cold stress memory is lost in DICEL-LIKE 2 AND DICER-LIKE 3 mutants, thus indicating that small RNAs and the RdDM pathway are implicated in this process.

4.1.2 Resetting Mechanisms as a Barrier to Transgenerational Stress Memory

Heritable stress adaptive phenotypes in *Arabidopsis* have been also found in response to drought stress, however, they are not associated with changes in DNA methylation (Ganguly et al. 2017). In a similar vein, the immediate progenies of salt-treated parents exhibit higher survival rates under lethal salt stress and profound changes in DNA methylation, however, these changes are lost after two generations of growth under stress-free conditions (Wibowo et al. 2016). This study also uncovered that one of the resetting mechanisms is associated with the activity of the DNA glycosylase, DEMETER (DME), in the male germlines. Epigenetic resetting

mechanisms have been reported also during both male and female gametogenesis. Male gametogenesis begins with diploid cells in anther, named pollen mother cells. Pollen mother cells (2n) undergo a cycle of meiosis resulting in haploid microspores (n). Male gametocyte or bicellular pollen is formed after a process of mitotic division and consists of a vegetative nucleus (VN) and a generative nucleus (GN). Then, the generative cell undergoes the final round of mitosis, giving two haploid sperm cells, SC (figure 4.1A, (Ono and Kinoshita 2021)). Similarly, female gametogenesis of flowering plants begins with the meiosis of megaspore mother cells, a vegetative diploid cell in the ovary. Only one female meiocyte survives and becomes a megaspore. The megaspore undergoes three rounds of mitotic division generating female gametophyte with seven cells aligning, as shown in figure 4.1B (Ono and Kinoshita 2021). Only two cells are involved in double fertilisation. One sperm cell from pollen fertilises with an egg cell generating a zygote. The other sperm cell fuse with central cell generation triploid endosperm.

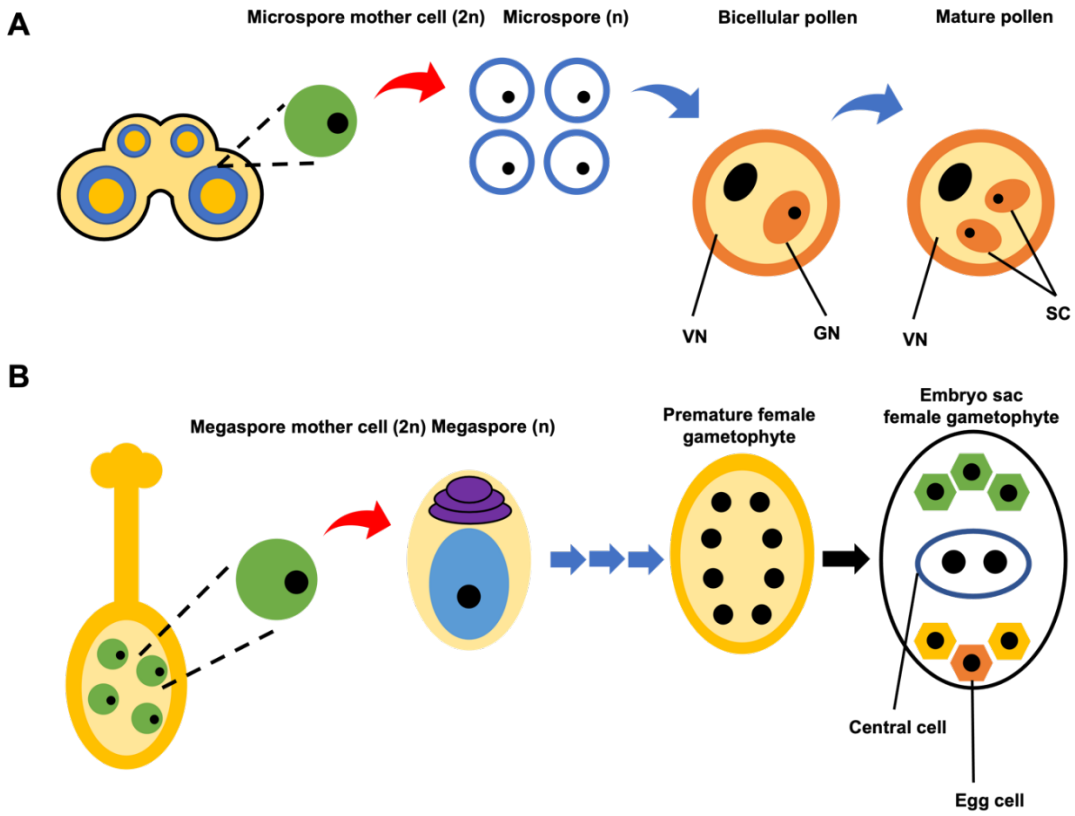

Figure 4.1 Male gametogenesis (A) and female gametogenesis in plant reproduction (B). Male gametogenesis starts from the meiosis of the diploid microspore mother cell resulting in four haploid microspores. A mitosis cycle generates bicellular pollen consisting of vegetative nuclei (VN) and generative nuclei (GN). Finally, GN goes through another process of mitosis, developing two sperm cells (SC). Female gametogenesis starts with a megasporocyte or megaspore mother cell going through meiotic cell division, but only one cell survives and becomes a haploid megaspore. Then, each megaspore undergoes three cycles of mitosis and differentiation, resulting in an embryo sac consisting of three antipodal cells, a central cell, two synergids, and an egg cell (Modified from Ono and Kinoshita 2021).

The reprogramming of DNA methylation marks occurs in different cell types during gametogenesis (Calarco et al. 2012; Feng et al. 2010). The reset DNA methylation mechanisms arise before and after fertilisation as the accumulation of transposon transcripts during male gametogenesis coincides with a decrease in DNA methylation. Moreover, CHH methylation in microspores and sperm cells is reset and associated with the repression of *DRM2*'s expression level (Calarco et al. 2012).

Unlike in sperm cells, *DRM2* is activated again in the vegetative nucleus to restore CHH methylation guided by 24 nt siRNAs from surrounding pollen cells (Calarco et al. 2012; Kawashima and Berger 2014). MET1 activity is stable in microspores and SC resulting in limited CG reprogramming. However, DME and ROS1 DNA demethylase modulate major reprogramming of CG and non-CG methylation in VN targeting a specific type of retrotransposons (figure 4.2) (Calarco et al. 2012; Kawashima and Berger 2014). During female gametogenesis, all contexts of DNA methylation are reset in the central cell associated with the reduced activity of MET1 and with high activity of DME, leading to the accumulation of TE transcripts (Calarco et al. 2012; Kawashima and Berger 2014). In egg cells, the expression levels of *MET1*, *CMT3,* and *DME* are undetectable, but *DRM1* and *DRM2* are highly expressed and coincide with low expression of TEs suggesting that the RdDM pathway is highly active in egg cells (figure 4.3) (Feng et al. 2010).

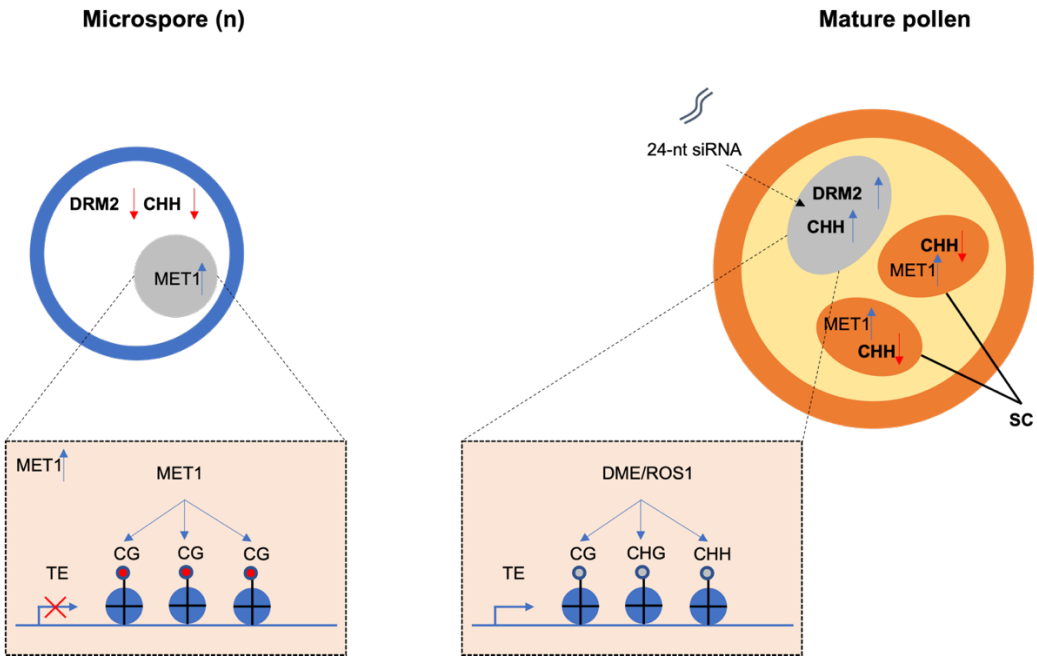

Figure 4.2 Epigenetic reprogramming during male gametogenesis. Reduced expression of *DRM2* is associated with the reprogramming of CHH in microspores. MET1 has a standard function in microspores and sperm cells to maintain DNA methylation in the CG context. The vegetative nucleus has enhanced DRM2 activity guided by 24-nt siRNAs from surrounding cells. DME and ROS1 also demethylate all contexts of specific retrotransposon in the vegetative heart. Vegetative nucleus (VN), Sperm cells (SC) (Modified from Calarco et al. 2012).

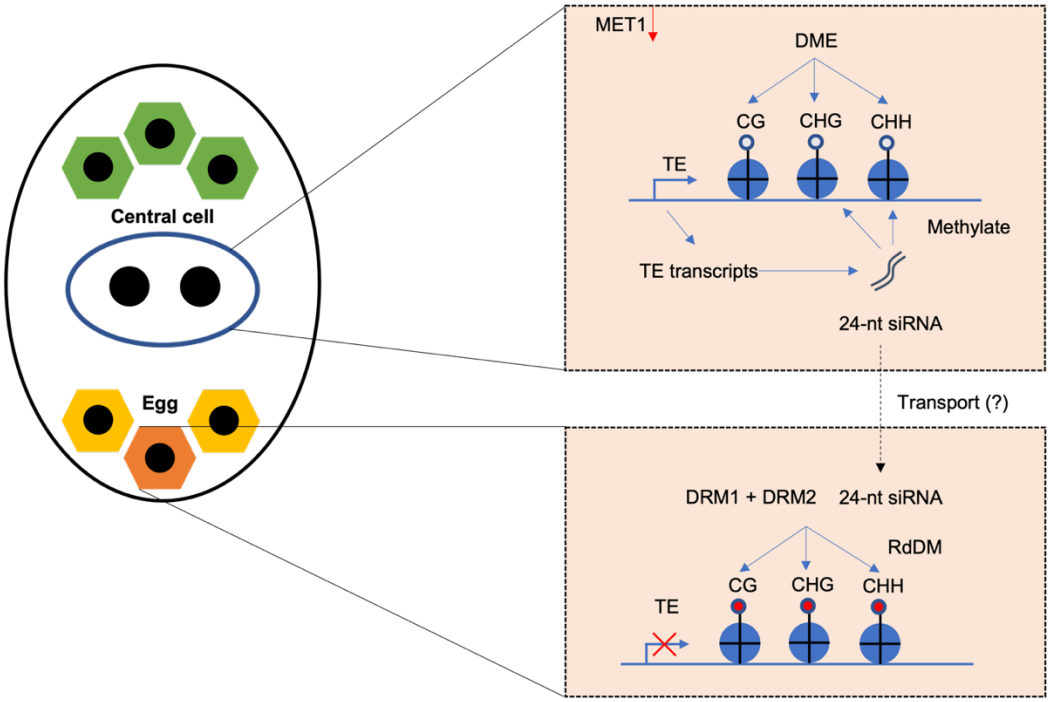

Figure 4.3 Epigenetic reprogramming during female gametogenesis. Demethylation occurs in central cells of the female gametophytes through the function of DME. Reduced MET1 activity in central cells also associates with reset CG methylation resulting in enhanced TE transcripts. Enhanced TE transcripts generate 24-nt siRNAs, which further methylate CHG and CHH context through the RdDM pathway. 24-nt siRNAs also relocate to egg cells to establish DNA methylation to silence TE (Modified from Feng et al. 2010).

The idea that DNA methylation is reset in gametes involves the cell-to-cell motility of siRNA from sister cells of gametes. The accumulation of TE transcripts in the VN generates 21-nt siRNA that have the capacity of moving into sperm cells and activating the RdDM pathway to regain the DNA methylation. Similarly, TE transcripts in a central cell are thought to produce 24-nt siRNA capable of moving to the egg cell to re-establish the DNA methylation. The loss of CHH methylation during male gametogenesis is partially restored using maternal 24-nt siRNA after fertilisation (Calarco et al. 2012; Kawashima and Berger 2014; Martinez and Kohler 2017). The imprinting TE methylation mediated by siRNA could be applied as the mechanism of the epigenetic inheritance (Calarco et al. 2012; Kawashima and Berger 2014; Martinez and Kohler 2017).

4.1.3 Somatic Embryogenesis as a Strategy to Enhance the Stability of Transgenerational Stress Memory

The barriers that sexual reproduction imposes on transgenerational stress memory are overcome in some clonal plants such as white clover (*Trifolium repens*), where stress-induced transgenerational stress memory against drought and herbivorous caterpillars are associated with changes in DNA methylation (Gonzalez et al. 2016; González et al. 2016). The same research group conducted a similar experiment with five environmental stimuli and observed the TSM in clonal progenies white clover (Rendina González et al. 2018). The results have shown the differences in morphology of the second-generation offspring from drought-treated plants, and the differences are associated with DNA methylation changes.

Preliminary work from Putra et al. (2018) using *Arabidopsis* clonal plants propagated from different organs after stress supported the view that clonal progenies displayed strong stress memory responses. Because regenerated plant lines were propagated sexually stress-free over three generations and they showed evidence for adaptive responses, which supported the view that cloning could enhance stress-induced transgenerational memory (figure 4.4). This study also showed that cold and high salinity caused specific transcriptional and phenotypic changes in leaf regenerated lines (LO) and root regenerated lines (RO) respectively. Collectively, the work of Putra et al. (2018) supported the view of an enhanced transgenerational stress memory linked to clonal propagation and tissue of origin.

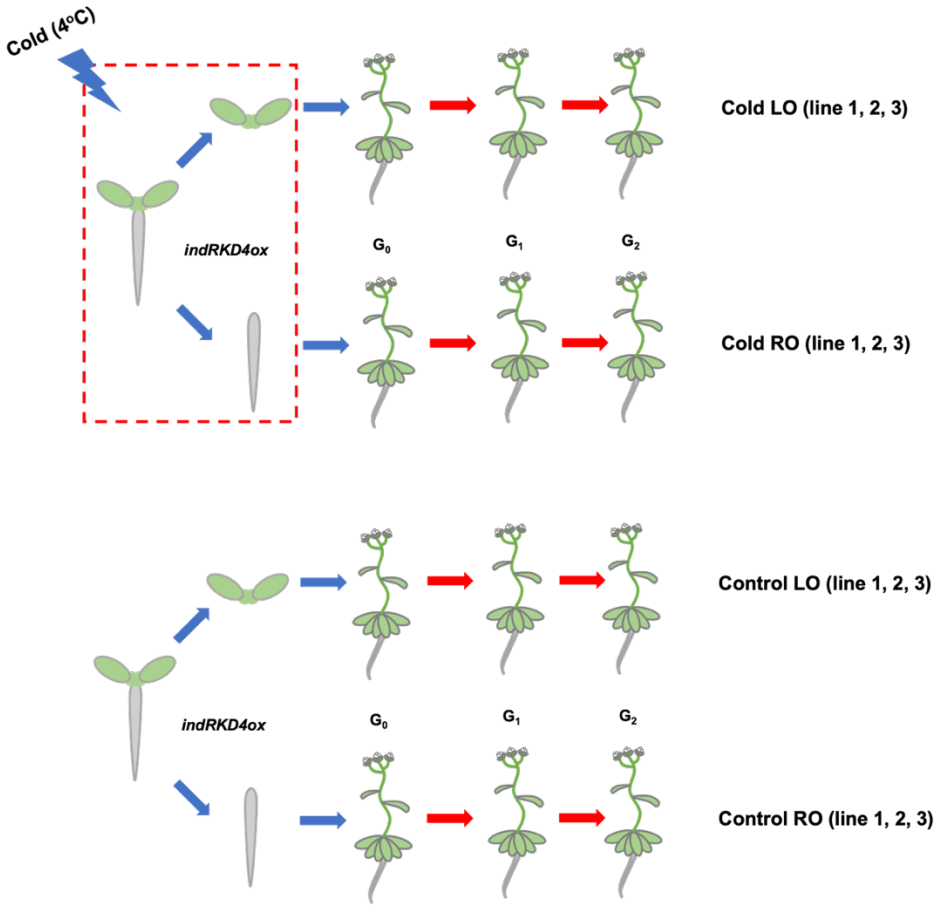

Figure 4.4 Somatic embryogenesis under control and cold- stress treatment. indRKD4 is used to clone plants by somatic embryogenesis under control condition (22°C) and cold treatment (4°C). The first clonal regenerants are designated as G_0 generation consisting of four lineages: Cold-LO, Cold-RO, Control-LO, and Control-RO, with at least three lines per clonal lineage. All plants from G_0 generation are propagated under stress-free conditions for two generations resulting in G_2 generation used in phenotypic, transcriptomic and methylome analysis (modified from Putra et al., (2018)).

4.1.4 Chapter Aims

Previous studies have shown that clonal plants may have the capacity to integrate environmental signals into a stable transgenerational stress memory. However, the precise molecular mechanisms and phenotypic consequences are yet unknown. In this chapter, I describe a genome-wide transcriptomic and epigenomic analysis, which shed light on some of the molecular mechanisms underpinning primed response in clonal plants.

4.2 Results

4.2.1 Transgenerational Transcriptional Memory in Regenerated Plants Primed with Cold

To determine the impact of cloning in TSM, clonal plants were generated from leaves and roots using plants exposed to control (22ºC) and cold stress (4ºC). Each clonal lineage consisted of ten independent lines that were propagated under stress-free conditions for three generations via sexual reproduction (figure 4.4). Leaf and root samples from three randomly selected G_2 lines were collected for molecular analysis by combining samples from ten randomly selected four-week-old plants.

For the transcriptome analysis, each clonal line was considered as a separated biological replicate in order to identify robust molecular changes associated with growth conditions and tissue of origin (Schurch et al. 2016). We identified DEGs from pairwise comparisons between control and stressed clonal lines for each tissue of origin. All biological replicates were plotted against each other in a scatter plot to check the consistency between replicates. Two of the RNA-seq libraries, Control-LO_1 and Cold-RO_3, had a very high level of variance and were removed from the analysis (appendix figure 8.1).

We performed a principal component analysis, which showed that 36% of variance contribution separated samples according to the temperature treatment during the cloning process. However, the second principal component, with 29% of variance contribution, was not able to separate samples by any criteria (figure 4.5). DEGs were calculated using a cut-off of FDR ≤ 0.05 with a log2FC cut-off threshold of 1.0. We performed four possible pair-wise comparisons in the analysis (table 4.1). The first comparison was to determine the effect of cold treatment in LO clones, named LO cold memory (LCM) genes, of which 447 were up-regulated and 480 were down-regulated. The second comparison was to determine the effect of cold treatment in RO clones, named RO cold memory (RCM) genes, of which 60 were up-regulated genes and 193 were down-regulated. Comparisons 3 and 4 aimed to determine the differences between tissue of origin and treatment, respectively. The lists of DEGs with statistical values are shown in appendix tables 8.1 – 8.2.

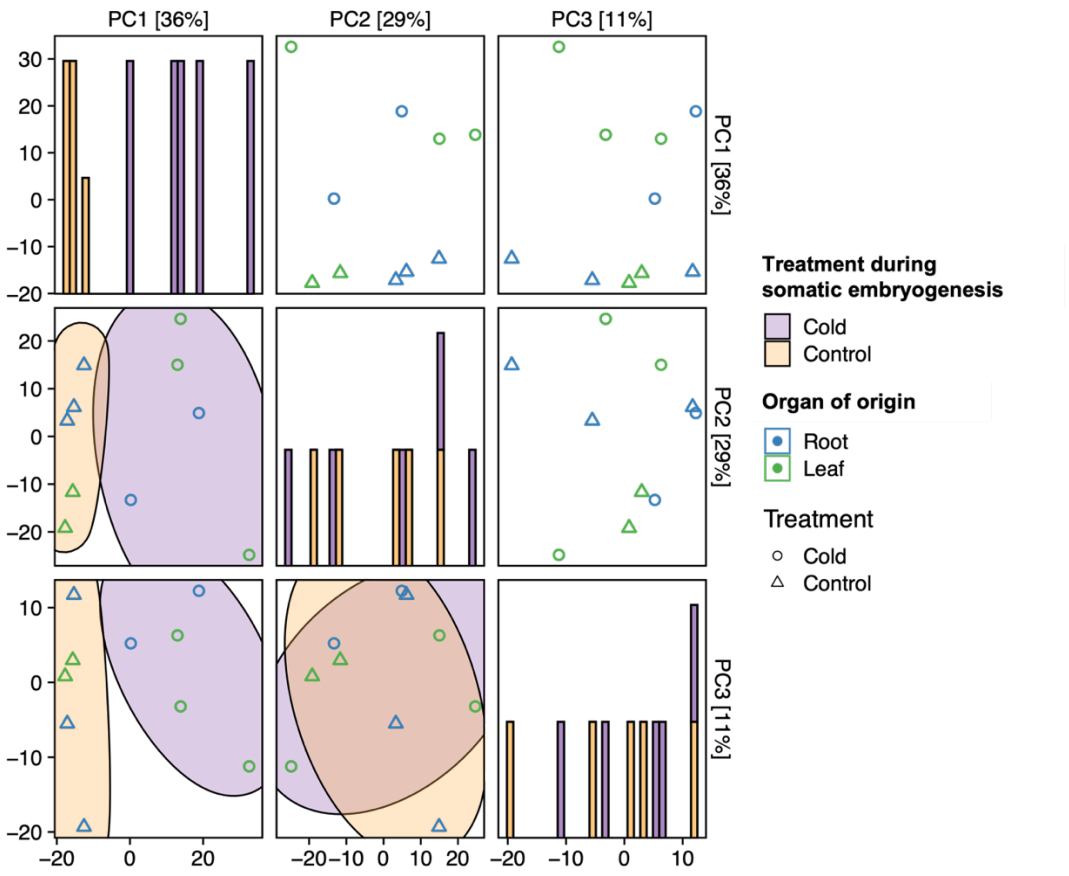

Figure 4.5 Principal component analysis (PCA) plot of clonal plants of G_2 generation from Control-RO, Control-LO, Cold-RO, and Cold-LO clonal lines. The number in the bracket shows the percentage variance contributed by the principal component. The colours of dots indicate organ of origin. The filled colours of circles and shapes of dots indicate the treatments during the somatic embryogenesis. The histogram in a diagonal matrix shows the distribution of the treatments according to PC on the x-axis.

Table 4.1 Pairwise comparisons and Numbers of DEGs between clonal lineages from G_2 generation

Number	Reference condition	Treatment condition	Description	Up-regulated DEGs	Down-regulated DEGs
1	Control-LO	Cold-LO	LO cold memory (LCM)	447	480
2	Control-RO	Cold-RO	RO cold memory (RCM)	60	193
3	Control-RO	Control-LO	-	9	20
4	Cold-RO	Cold-LO	-	21	29

We performed a gene ontology (GO) analysis on the DEGs identified in each comparison. LCM genes were enriched for GO terms related to cell wall organisation, carbohydrate metabolic process, response to water deprivation, and response to abiotic stimulus (figure 4.6A). RCM genes had a smaller number of enriched GO terms, which were related to response to chemical, response to ethylene, cell wall organisation, and response to hypoxia (figure 4.6B). All GO terms show significant enrichment with higher observed values from the input dataset than expected values from the *Arabidopsis* database.

To observe the cold memory genes in detail, the list of early cold-responsive (ECOR) genes containing 889 genes was obtained from transcriptome data from wild-type seedlings treated for 3 hours at 4ºC (see table 3.2). In addition, using publicly available data we identified 5,262 genes from wild-type seedlings treated for 24 hours at 4ºC (Song et al. 2021), which we termed late cold response genes (LCOR). Then, we looked at the overlap between LCM genes and RCM genes with ECOR genes and LCOR genes. Statistical significance of the overlap was calculated with GeneOverlap using a Fisher's exact test. We found 72 genes overlapping between ECOR and LCM genes, while only 27 genes overlap with RCM genes (figure 4.7A-B). For the intersection with LCR genes, 336 and 122 genes overlapped with LCM genes and RCM genes, respectively (figure 4.7C-D). Fisher's exact test indicated lower p-values from the intersection between both early and late cold-responsive genes with LCM genes, indicating a more significant overlap.

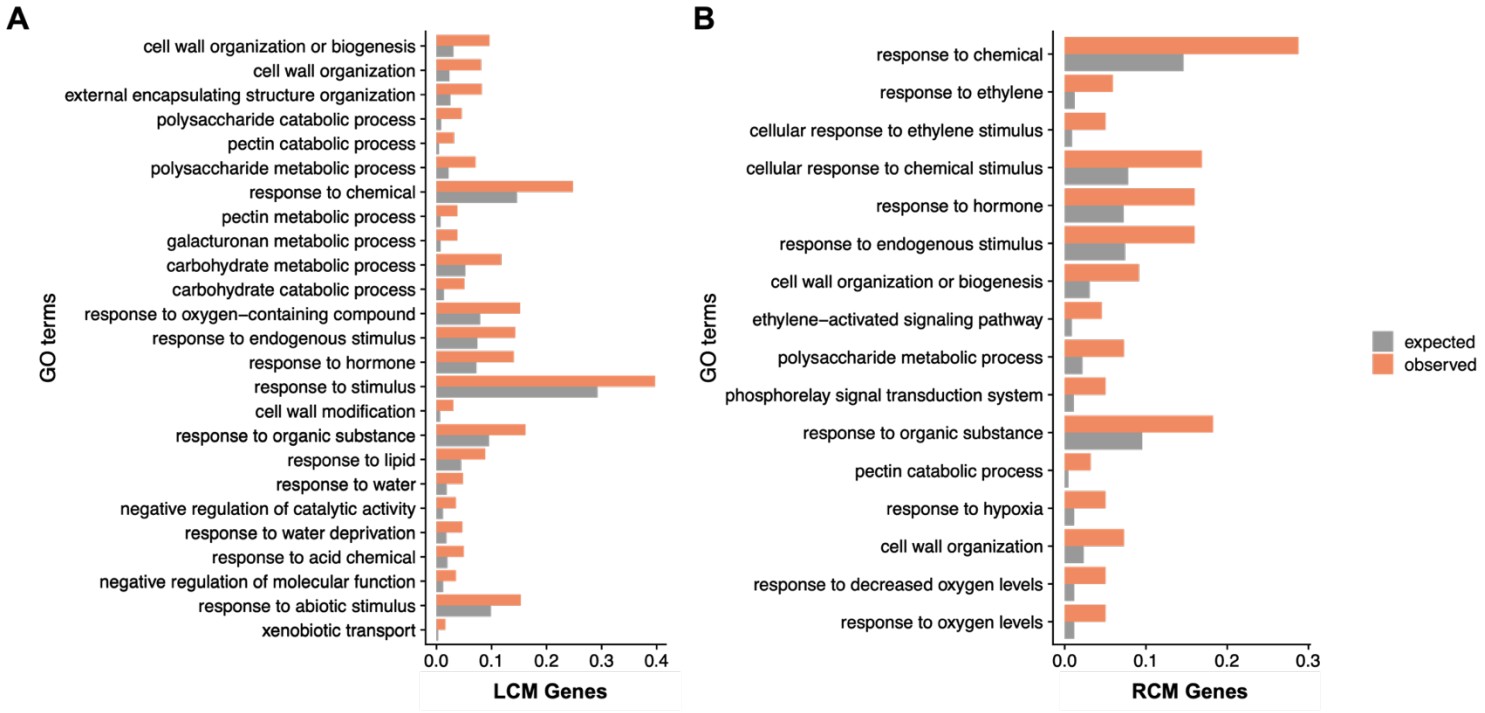

Figure 4.6 Enriched GO terms found in LCM genes (A) and RCM genes (B). The X-axis indicates the frequency of GO terms between the expected value (grey bar) and the observed value (orange bar). The expected frequency is calculated from the number of genes with particular GO terms divided by the total GO terms in the *Arabidopsis* database. The observed value is calculated from the number of genes with the term in an input divided by the number of input genes.

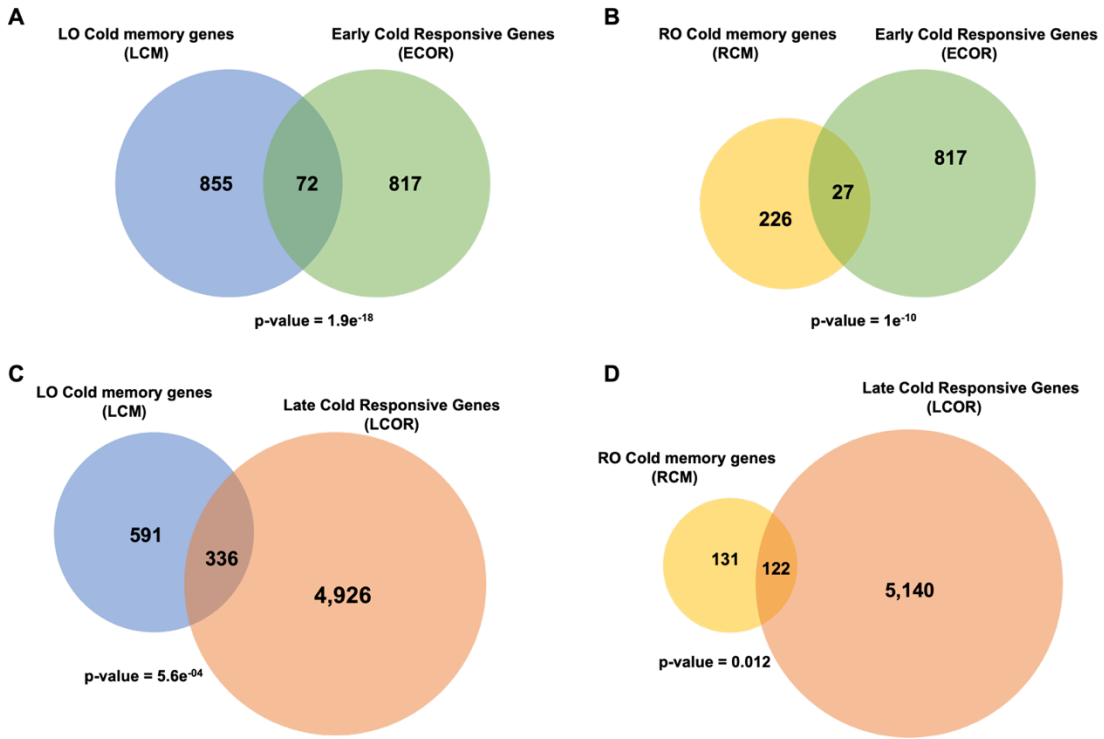

Figure 4.7 Overlap between differentially expressed genes associated with cold responses and cloning. Overlap between ECOR genes with LCM genes (A) and RCM genes (B). Overlap between LCOR genes with LCM genes (C) and RCM genes (D). p-value underneath each diagram indicates the significance of Fisher's exact test.

4.2.2 DNA Methylation Imprints are Stably Inherited in Regenerated Plants Primed with Cold

Results in section 4.2.1 revealed the existence of a transgenerational transcriptional memory in regenerated plants primed with cold. To investigate possible mechanisms underpinning this stress memory, we performed a whole-genome bisulfite sequencing analysis to define changes in DNA methylation that are inherited in the clonal lineages previously used in the transcriptomic analysis.

We calculated the differences in DNA methylation using DMRcaller (Catoni et al. 2018). Quality control analysis identified datasets affected by low sequencing coverage, which could affect the calculation of differentially methylated regions DMRs. To address this issue, we selected for analysis only datasets with good coverage. To determine the differences in DNA methylation at CG and CHG sites we selected a "noise filtering" method (DMRcaller-NF), for CHH sites we selected a "bins" method (DMRcaller-B). Both methods compute DMRs based on the determined bin/window size, minimum proportion difference of the comparison, and adjusted p-values < 0.05. All threshold values were listed in chapter 2.

We compared Control-LO and Control-RO regenerated lines with Cold-LO and Cold-RO samples, respectively. This analysis revealed a gain in CG methylation in DMRs from Cold-LO lines, while a small proportion of DMRs was hypomethylated CG. The gain and loss of DMRs in the CHG context were barely detected in Cold-LO. There were also detectable hypermethylated DMRs in the CHH context. The distribution of DMRs from Cold-LO plants was similar to a normal distribution of DNA methylation in the *Arabidopsis* genome (figure 4.8A, appendix table 8.3). In Cold-RO plants, CG was primarily hypomethylated while hypermethylation at CG sites was indistinguishable from the control group. We did not find DMRs at CHG context in any of the comparisons. The most abundant DMRs were found at hypermethylated CHHs, while a loss of methylation at CHH sites was found in a smaller proportion (appendix table 8.3). Interestingly, in comparison with the normal distribution from the *Arabidopsis* genome, DMRs in the CHH context of Cold-RO plants were found mainly in intergenic regions or in the range of 1kb upstream of Transcription Start Sites (TSS) (figure 4.8B).

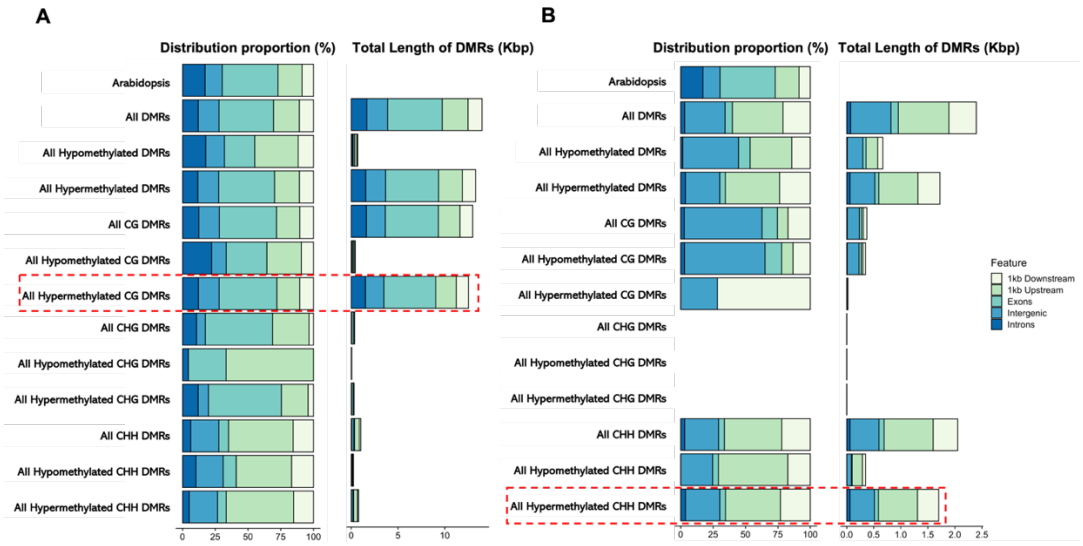

Figure 4.8 The distribution proportion and total length of DMRs in regenerated Plants primed with Cold. (A) Cold-LO DMRs; (B) Cold-RO DMRs. The colour bars show the features of DMRs located in different regions dividing into 1kb downstream and upstream of genes, exons, intergenic, and introns. Dashed red boxes indicate the most enriched DMRs contexts.

After identifying DMRs, we assessed the overlap DMRs to nearby genes, named differentially methylated genes (DMGs), using a 3kb flanking window (table 4.2). The number of DMGs were higher than the number of DMRs indicating that there could be multiple genes affected by the same DMR. In a second step, we intersected DMGs from comparisons between Control-LO/Cold-LO and Control-RO/Cold-RO. There was a total of 1,729 DMGs found in Cold-LO lines, mostly in hypermethylated CG sites, and located both downstream or upstream of DMRs. However, we also found some DMRs inside annotated genes (figure 4.9A). In contrast, in Cold-RO lines we found only 397 DMGs and most of them associated with hypermethylated CHH sites. Notably, only 60 DMGs were found shared between both lists, suggesting the differences in DNA methylation found in clonal lines was tissue-dependent and stronger in those regenerated from cold treated leaves (figure 4.9B).

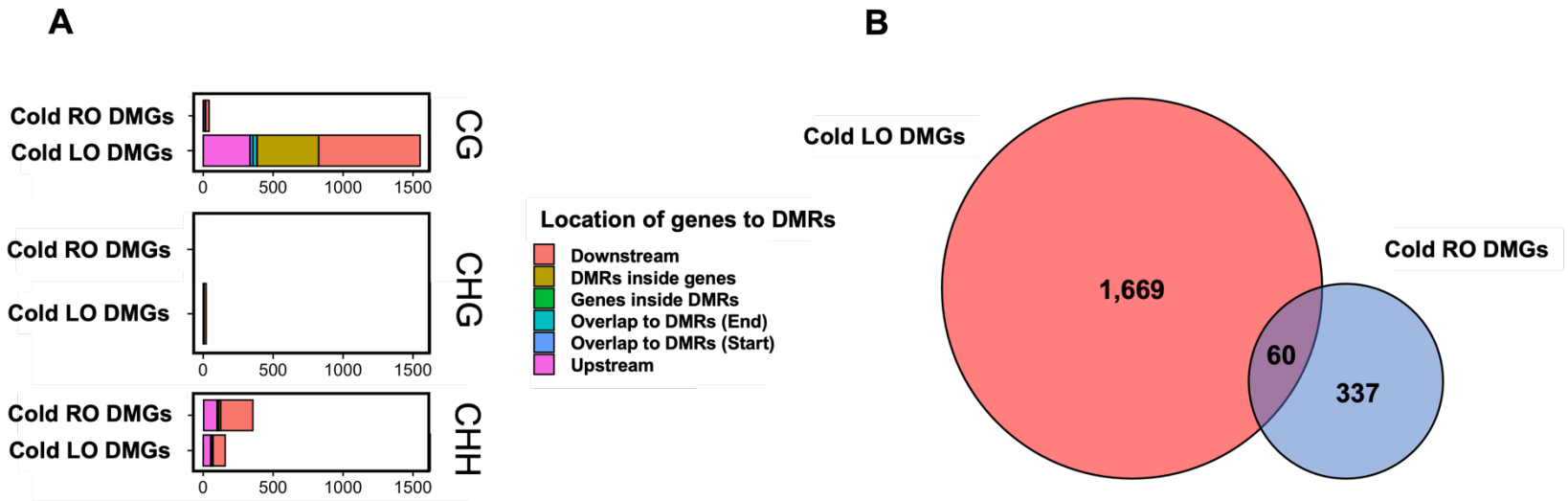

Figure 4.9 The number of differentially methylated genes in Regenerated Plants primed with Cold. (A) DMRs found at different sequence contexts in Cold-LO and Cold-RO lines. (B) Intersection between Cold-LO and Cold-RO DMGs. Colour bars show the features of genes annotated to DMRs, including genes located downstream or upstream of DMRs, DMRs located inside genes, genes located inside DMRs, and genes overlapped with the start site or end site of DMRs.

Table 4.2 Number of DMGs identified in Regenerated Plants primed with Cold.

Number	Type of DMGs	Number of genes annotated to DMRs		
		CG contexts	CHG contexts	CHH contexts
1	Cold-LO	1,551	21	157
2	Cold-RO	42	0	355

We then focused on DMGs from regenerated primed plants to identify the overlap between cold memory and cold-primed genes. In this process, LCM and RCM were calculated with FDR ≤ 0.05 with log2FC≥ 0.5 to define cold memory DEGs, and we found 82 overlapping genes in Cold-LO and 3 in Cold-RO (figure 4.10). We then focused only on Cold-LO lines, where we found a similar number of genes up- and down-regulated overlapping with DMGs. There were 40 up-regulated and 42 down-regulated DEGs overlapping with DMGs. However, the number of genes shared between DMGs and DEGs was not enough to show a significant overlap with Fisher's exact test.

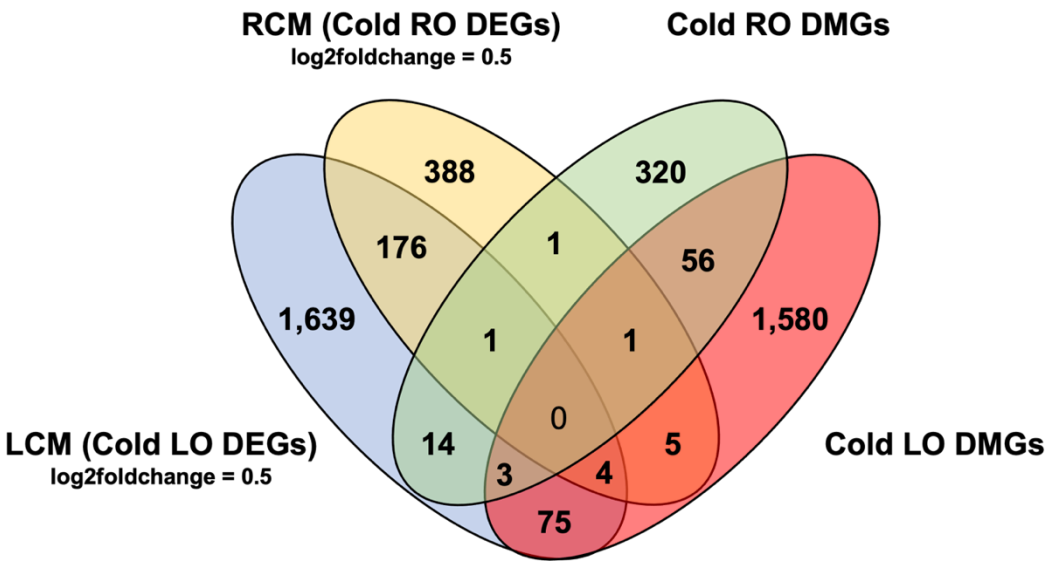

Figure 4.10 Venn diagram representing the overlap between memory and primed genes. In this analysis, LCM and RCM DEGs were calculated with FDR ≤ 0.05 and log2FC cut-off values of 0.5.

4.2.3 Regenerated Plants Primed with Cold Show Enhanced Transgenerational Adaptability to Freezing Stress

The genome-wide transcriptomic analysis revealed the clonal plants regenerated from primed leaves display a cold transcriptional memory. There was only a small set of genes showing transcriptional changes in association with changes in DNA methylation at proximal flanking sequences. This result suggests that DNA methylation is partially involved in TSM, and there could be other epigenetic mechanisms underpinning the cold transcriptional memory. To assess if these molecular changes had a phenotypic consequence, we exposed to freezing two-week-old seedlings from clonal lines (G_2 generation) to determine if they are better adapted to extreme cold conditions. We found that the survival rate to freezing was significantly enhanced in Cold-LO lines than in control lines (figure 4.11, appendix figure 8.2). On the other hand, none of the Cold-RO lines showed evidence of enhanced adaptation to freezing.

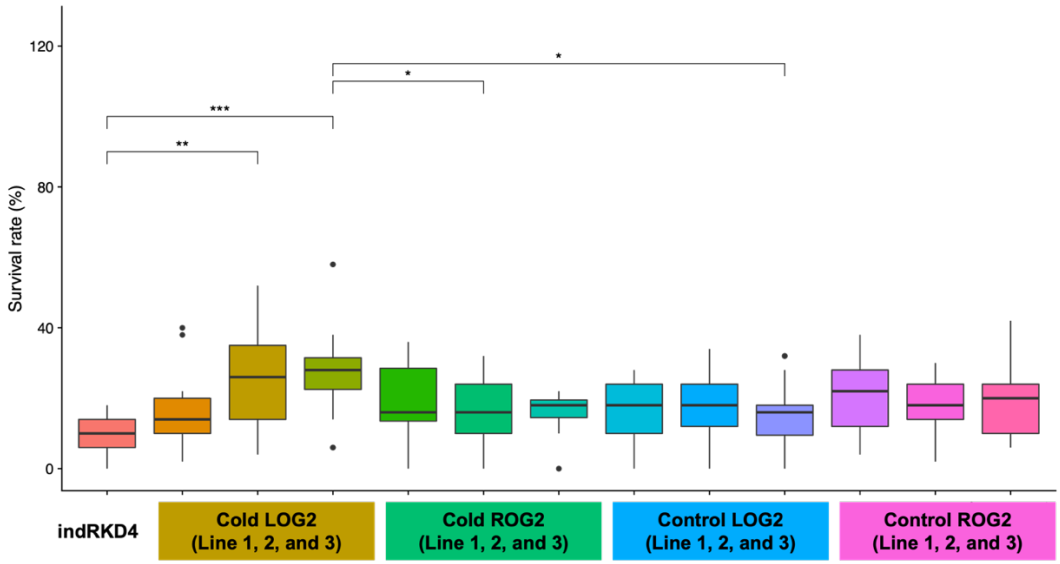

Figure 4.11 Enhanced tolerance to freezing in regenerated plants exposed to cold. Survival rates were calculated from recovered plants after being exposed to -5ºC. Each data point was calculated from 50 seedlings. Non-clonal indRKD4 was used as control. Seven replicates were used in the statical analysis. Asterisk indicates the significant difference between comparisons (Tukey's HSD test, *** $p < 0.001$, ** $p < 0.01$, * $p < 0.05$, ns $p > 0.05$)

4.2.4 Augmented Transcriptional Responses in Regenerated lines Primed with Cold

The augmented response to freezing found in regenerated lines primed with cold may be driven by a poised transcriptional state that is stable across multiple cycles of sexual reproduction. To test this hypothesis, we exposed seedlings from Control-LO and clonal lineages (G_2 generation) to control (22ºC – 1h) and cold (4ºC – 1h) growth temperature conditions (figure 4.12). We collected rosette leaves for transcriptome analysis with three replicates per each condition.

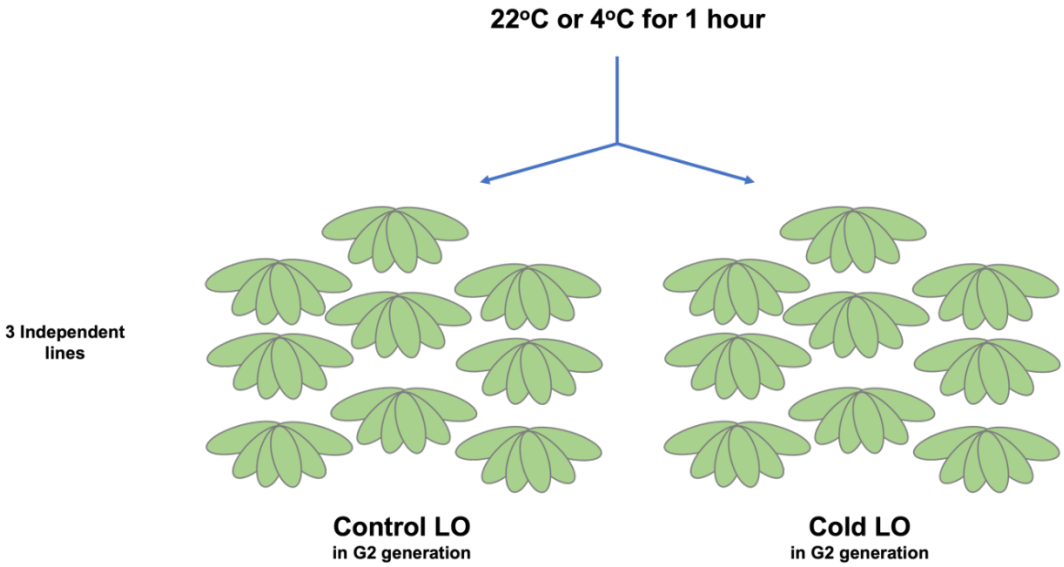

Figure 4.12 Transcriptional analysis of regenerated lines primed with cold in response to recurrent stress. Four-week-old plants from G_2 generation of Control-LO and Cold-LO clonal lineages, three independent lines each, were treated for 1 hour at 4°C or 22°C. Rosette leaf samples were pooled from nine randomly selected plants. Each clonal line was considered a biological replicate.

Principal component analysis revealed that the most important factor in the transcriptional responses was cold exposure, as in PC1 samples were grouped according to the growth conditions regardless of the origin of the clones from cold-treated or untreated tissues. However, PC2 and PC3 separated samples by the tissue of origin and differences were more obvious when these plants were challenged with cold (figure 4.13). We identified DEGs using a stringent cut-off (FDR ≤ 0.05 and log2FC ≥ 1.0) (table 4.3). In a first comparison, we assessed the effect of cold treatment in Control-LO lines to identify Control-LO-cold responsive (22LCR) genes and identified 1,395 up-regulated genes and 607 down-regulated genes. The second comparison identified Cold-LO-cold responsive (4LCR) genes with 1,206 up-regulated genes and 643 down-regulated genes. The third comparison identified the cold memory genes in clonal lines that originated from leaves not exposed to cold (see section 4.2.1). The fourth comparison identified the DEGs between regenerated lines after a 1h challenge with cold.

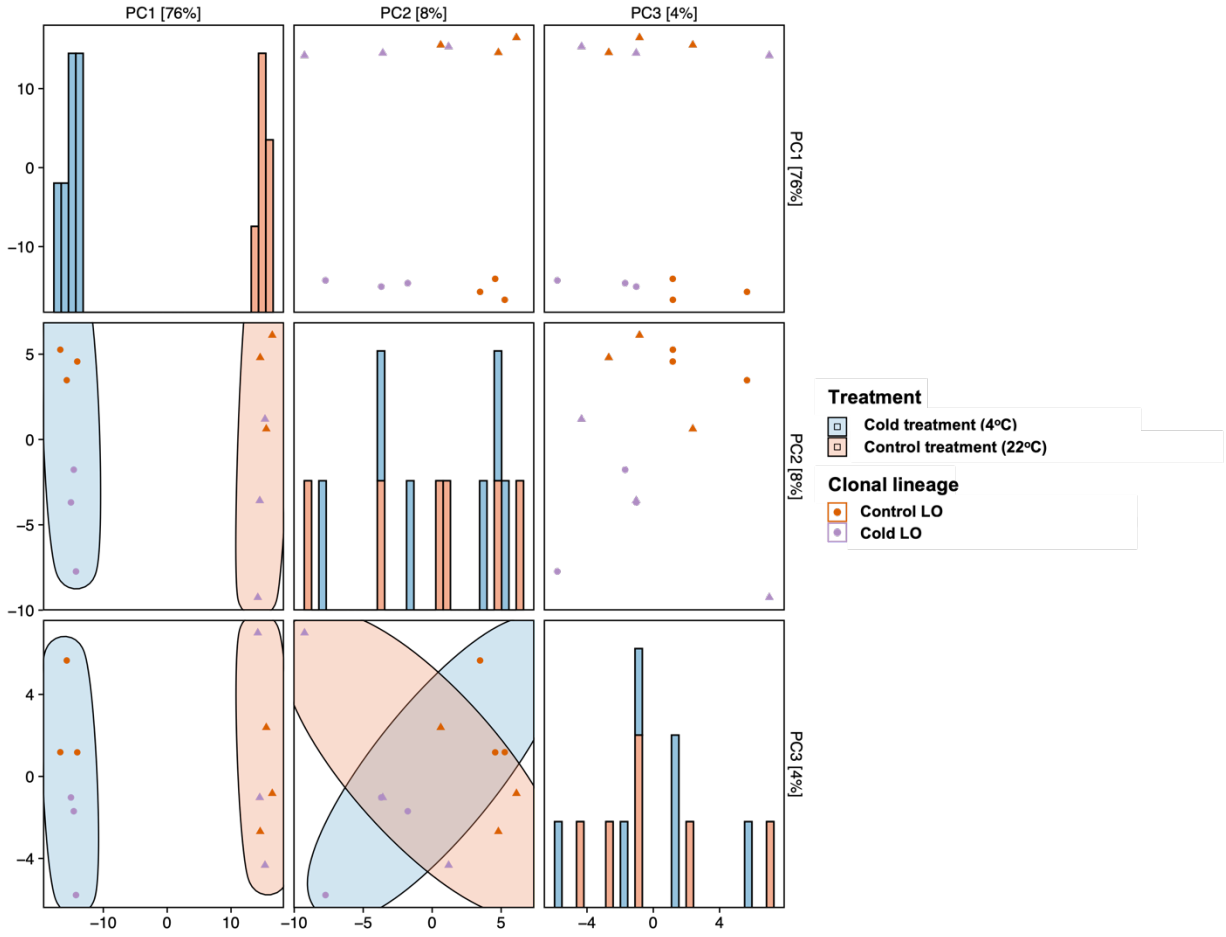

Figure 4.13 Principal component analysis (PCA) plot of RNA-seq samples from regenerated plants primed with and without cold and subjected to different temperature treatments. The number in the bracket shows the percentage variance contributed by the principal component. The colours of dots indicate organs of origin. The filled colours of circles and shapes of dots indicate the treatments during somatic embryogenesis. The histogram in a diagonal matrix shows the distribution of the treatments according to PC on the x-axis.

Table 4.3 List of Pair-wise comparisons and numbers of DEGs between regenerated plants primed with cold and subjected to different temperature treatments.

Number	Reference condition	Treatment condition	Description	Up-regulated DEGs	Down-regulated DEGs
1	22ºC Control-LO	4ºC Control-LO	Control-LO-cold responsive (22LCR)	1,395	607
2	22ºC Cold-LO	4ºC Cold-LO	Cold-LO-cold responsive (4LCR)	1,206	643
3	22ºC Control-LO	22ºC Cold-LO	Cold memory	78	38
4	4ºC Control-LO	4ºC Cold-LO	-	135	79

We also investigated the similarity of 22LCR and 4 LCR genes, with the common cold-responsive genes (figure 4.14). We found 1,246 overlapping genes between them, of which 1,010 were up-regulated DEGs and 234 down-regulated. A total number of 756 genes were unique to 22LCR, and 653 genes were specific to 4LCR genes. We then assessed the difference between common cold-responsive genes and unique genes from both 22LCR and 4 LCR genes (figure 4.15).

We separated genes into three different groups: specific 22LCR, specific 4LCR and shared cold-responsive genes. Genes in the shared cold-responsive group contained similar expression values under untreated and cold-treated conditions. On the other hand, genes in the specific 22LCR group were not altered in the absence of treatment but changed after cold treatment. However, specific 4LCR genes were altered in both untreated and treated conditions, and after treatment the differences were exacerbated. Gene ontology analysis also indicated the enriched terms related to cold response only in the shared group. Specific 22LCR genes had GO terms related to stress response in general and no enriched GO terms were found in the list of specific 4LCR genes (appendix figure 8.3).

Figure 4.14 Venn diagram representing the overlap between up- and down-regulated genes from Control-LO-cold responsive genes (22LCR) and Cold-LO-cold responsive genes (4LCR).

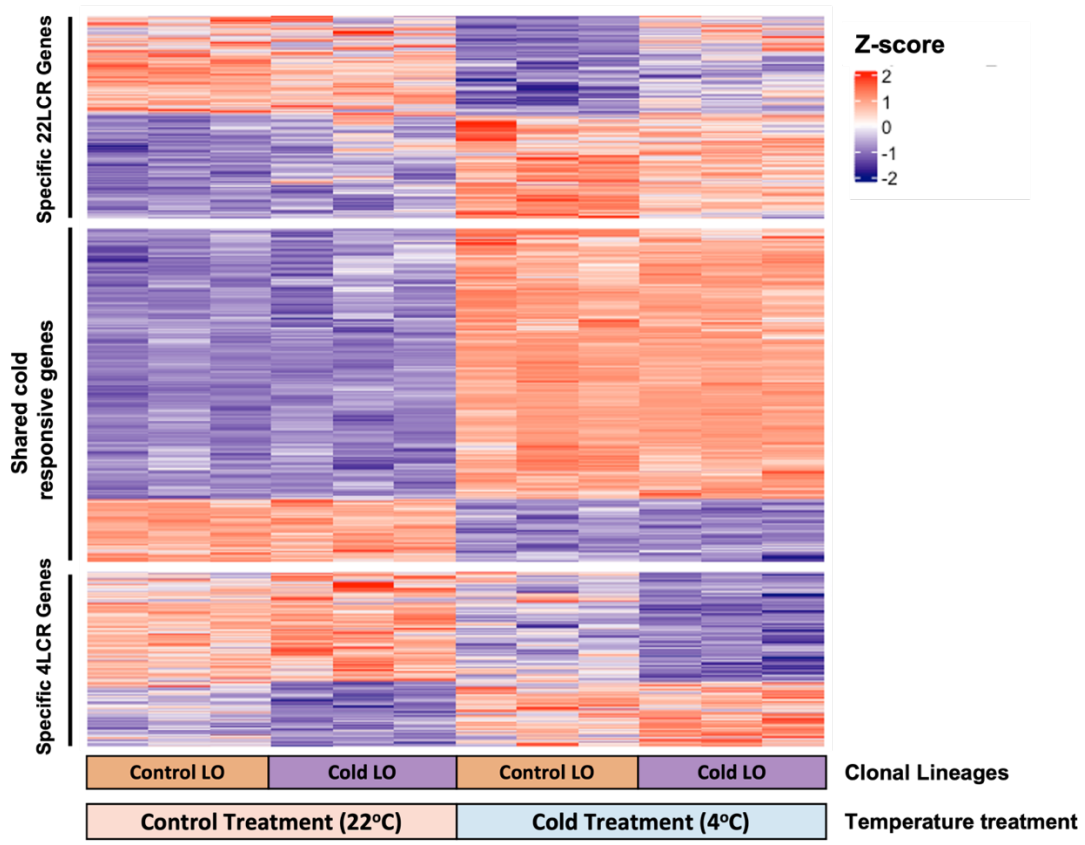

Figure 4.15 Heatmap of expression values from specific 22LCR (top-panel), shared cold-responsive genes (middle panel), and specific 4LCR (bottom panel). Counts from each gene across all conditions are processed by applying log2 transformation and normalising to generate a z-score. The rows of the heatmap represent the z-score of genes. Colour annotation represents the condition (clonal lineages and temperature treatments).

Even though the shared cold-responsive genes displayed similar expression levels between plant lines under both conditions, we investigated the unequal changes of behaviour in different clonal lineages after a cold treatment. K-means clustering was performed based on processed counts (z-score) of genes from all conditions. This analysis identified four clusters, two of them (1 and 3) included genes not affected under ambient temperature but upregulated in response to cold treatment with a stronger response if clonal lines were primed with cold. The other two clusters (2 and

4) contained genes that were misregulated at ambient temperature and affected by the temperature conditions during cloning and downregulated in response to cold.

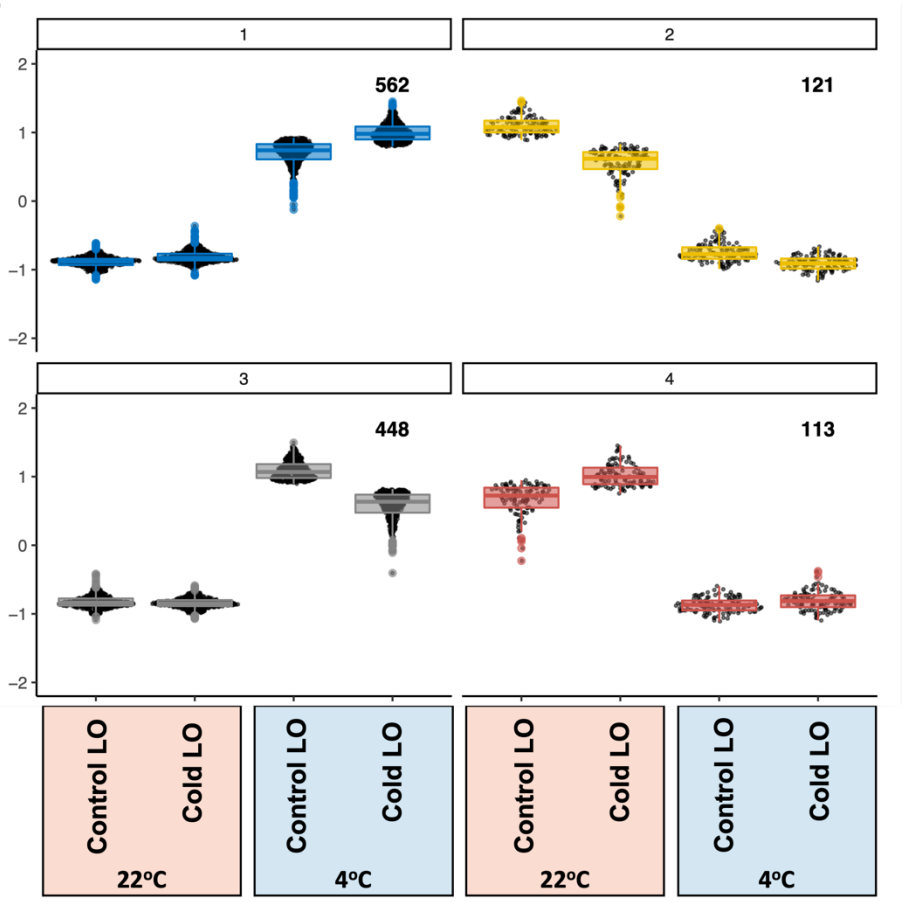

Figure 4.16 K-means clustering based on a list of shared cold-responsive genes after exposure to cold. The first and second columns are processed normalised counts (z-score) from regenerated plants in G_2 generation from Control-LO and Cold-LO lineages treated with 22°C for 1 hour. The third and the fourth columns are processed values from regenerated plants under 4°C. The number of clusters is based on the optimal number from the elbow plot.

Table 4.4 List of DEGs with specific GO term *response to cold* from k-means cluster 1 and cluster 3

Cold-related genes in cluster1	Symbol	Cold-related genes in cluster3	Symbol
AT1G07720	KCS3	AT1G01060	LHY
AT1G09560	GLP5	AT1G01120	KCS1
AT1G16390	ATOCT3	AT1G08930	ERD6
AT1G21910	DREB26	AT1G18740	NA
AT1G22190	NA	AT1G20440	COR47
AT1G22882	NA	AT1G20450	LTI29
AT1G25450	KCS5	AT1G22890	NA
AT1G71960	ABCG25	AT1G27730	STZ
AT2G19620	NDL3	AT1G50460	HKL1
AT2G38470	WRKY33	AT2G16280	KCS9
AT2G40140	CZF1	AT2G16500	ADC1
AT2G47730	ATGSTF8	AT2G26640	KCS11
AT3G08720	ATPK19	AT2G30250	WRKY25
AT3G17390	MTO3	AT2G46830	CCA1
AT3G45640	ATMPK3	AT3G03050	CSLD3
AT3G48360	BT2	AT3G05880	RCI2A
AT3G50260	CEJ1	AT3G49530	ANAC062
AT4G02330	ATPMEPCRB	AT3G53460	CP29
AT4G12470	AZI1	AT3G55580	NA
AT4G34150	NA	AT3G61580	NA
AT4G36020	CSDP1	AT4G08500	MEKK1
AT5G16910	ATCSLD2	AT4G17090	CT-BMY
AT5G20230	ATBCB	AT4G25470	CBF2
AT5G35750	AHK2	AT4G37610	BT5
AT5G37770	TCH2	AT5G20250	DIN10
AT5G57560	TCH4	AT5G42900	COR27
AT5G67450	AZF1	AT5G43760	KCS20
		AT5G62470	MYB96

4.3 Discussions

Stress memory or stress priming in plants is mediated by multiple mechanisms, including modifications in chromatin structure by the accumulation of active or repressive histone marks, changes in DNA methylation, the deposition or pausing of RNA Pol II, and the accumulation of small RNAs and stress-responsive secondary metabolites (Brzezinka et al. 2016; De Lucia et al. 2008; Ding et al. 2012; Gagliardi et al. 2019; Sung and Amasino 2004; Sung et al. 2006; Yang et al. 2019; Zhang et al. 2019). All these mechanisms help plants adapt to recurrent stress exposures by activating stress-specific pathways faster or to a more substantial degree. These changes can be evaluated by measuring the transcriptional stress memory dynamics during and after stress exposure (Baurle and Trindade 2020). Even though the idea of somatic stress memory is supported by multiple studies, the concept of transgenerational stress memory has not yet been fully demonstrated.

In this study, we have used transcriptomic and methylome data derived from clonal plant lineages generated from plants exposed to a stress treatment. We carried out this analysis using plants grown under stress-free conditions, thus the accumulation of stress-related transcripts, secondary metabolites, and RNA Pol II deposition that could be caused by cold stress is assumed to be reset (Crisp et al. 2016). The transcriptomic data show that cold treatment during cloning results in transgenerational effects even after two cycles of sexual reproduction, resulting in the activation of cold-related genes, which we defined as a new form of transgenerational stress memory arising in clonal plants. We found evidence for heritable cold memory present in clones derived from leaves (LCM) and others derived from leaves (RCM). Intriguingly, the number of LCM genes was much higher than RCM suggesting that the tissue of origin has a major impact on transgenerational stress memory. This could be because of the spatial differences in gene expression under low temperatures. Several studies have reported differences in cold response between leaves and roots of *Arabidopsis* (Kreps et al. 2002). Only 14% of the COR genes are shared between cold-treated leaves and roots, and leaves show a higher number of genes differentially expressed in response to cold. Several shared COR genes display differences in expression between organs (Guo et al. 2021). Organ-specific stress responses are common in plants, and sometimes involve the communication between root and shoot resulting in a synergistic response in the whole plant (Li et al. 2021).

Our data also show that LCM and RCM genes show significant overlap with early cold-responsive genes (ECOR) and late cold-responsive genes (LCOR) (Song et al. 2021). Most of the cold memory genes found in clonal plants were found to be associated with carbohydrate metabolic processes and cell wall organisation. These results are consistent with previous studies showing that cold response in plants involves alteration in the cell wall structure and carbohydrate metabolism (Nägele and Heyer 2013; Takahashi et al. 2019). Notably, cold memory genes in clonal plants are also enriched for response to hypoxia or to oxygen-containing compounds, which are commonly found among cold-responsive genes (see chapter 3). Our data also identified genes implicated in other stress-responsive pathways, such as water deprivation (Sharma et al. 2018). Collectively, our transcriptomic data support the view that clonal plants have stable transgenerational stress memory, which is likely underpinned by tissue-specific transcriptional responses.

To reveal the mechanism(s) implicated in the heritable stress memory response found in clonal plants we performed a DNA methylation analysis because this epigenetic mark is known to be mitotically and meiotically stable in plants. Although previous work has shown that DNA methylation changes induced by stress are partially stable in plants (Cong et al. 2019; Wibowo et al. 2016; Zheng et al. 2017).

We found that clonal lines from treated plants displayed heritable DNA hypermethylation imprints, but in different contexts depending on the tissue of origin. Hypermethylated CG is enriched in Cold-LO lineages, while Cold-RO lineages are mainly enriched at CHH hypermethylation sites. The enrichment for heritable DNA hypermethylation marks in cold-treated clonal plants contrasts with results from other studies. For example, cold induces genome-wide hypomethylation in Tartary buckwheat leaves and it is correlated with the activation of cold-regulated genes (Song et al. 2020). In sugar beet and Brassica, cold induces both hypomethylation in CHG and CHH sites and hypermethylation in CG sites (Gutschker et al. 2022; Haake et al. 2002; Liu et al. 2017). The gains of CG and CHH methylation found in clonal lineages derived from cold-primed plants suggested that hypermethylation of symmetrical cytosine sites is also a stable stress memory mark. This idea is supported by the hypermethylation found in transposable elements in salt-mediated intergenerational stress memory (Bilichak et al. 2012; Wibowo et al. 2016).

To investigate the correlation between changes in cold memory genes and possible epigenetic inheritance, we identified differentially methylated genes

(DMGs). Although we did not find a major overlap between RCM and DMGs in Cold-RO plant lines, we found a relatively larger number of LCM that overlap with DMGs in Cold-LO plant lines. However, the number of overlapping genes between DMGs and LCM were still low when compared to the whole set of LCM or DMGs indicating that the changes in DNA methylation found in Cold-LO clonal plants are associated with a subset of misregulated genes, indicating that the regulatory role of DNA methylation in these loci is complex. It has been reported that DNA methylation at the promoter regions is associated with a reduction in gene expression, but there are also examples of hypermethylated promoter regions associated with gene activation (Zhang et al. 2018). Similarly, DNA methylation found in gene bodies shows both positive and negative correlation with the gene expression (Kawakatsu et al. 2016). In this study, we have limited the connection between DNA methylation only to the genes within 3kb range. This analysis method aims mainly to find DNA methylation that acts as *cis*-regulatory elements. However, several studies have shown possible roles of DNA methylation at regulatory elements located far away from genes in both plant and human cells (Zicola et al. 2019, Cho et al. 2022). With the same data we have in our studies, we could expand the search to find more genes associated with changes in distal DNA methylation to reveal comprehensive roles of DNA methylation in TSM.

We found that Cold-LO regenerated lines show a better adaptation to freezing temperatures. This observation is in line with the transcriptome data and indicates clonal lines may display augmented transcriptional responses when regenerated lines are challenged with cold. Our transcriptomic analysis identified several cold-responsive genes from Control-LO clones and Cold-LO lines that displayed augmented transcriptional response after a short cold challenge. We found three distinct transcriptional responses in clonal lines from cold-treated leaves: (1) a group of genes affected similarly by cold regardless of the clonal lines, (2) genes with differences in expression levels between clonal lines in both control and cold temperature, and (3) genes primed at control temperature but displaying an enhanced response after cold exposure. The latter two groups resemble the behaviour of genes associated with a somatic stress memory(Baurle and Trindade 2020; Mozgova et al. 2019). Primed transcriptomic changes resulting from cold exposure have been previously reported in *Arabidopsis* seedlings, affecting 40% of COR genes, and implicated in cold-re-acclimation (Byun et al. 2014).

4.4 Chapter Conclusion

Collectively, molecular analyses reveal the existence of a transgenerational stress memory operating in clonal plants that are associated with epigenetic changes, and that result in adaptive stress responses.

Chapter 5 Transgenerational Stress Memory in Clonal Plants is Underpinned by the Transcriptional Activation of Specific Gene Networks.

5.1 Introduction

5.1.1 Transcriptional-Mediated Epigenetic Modifications

The results from chapter 4 support the existence of a heritable stress memory that can be established before or during somatic embryogenesis. Our analyses have shown that regenerated plants acquire changes in DNA methylation at several proximal flanking sequences near cold memory genes. We have also proposed that these epigenetic changes are stably inherited through multiple generations and are associated with altered transcriptional responses when challenged with cold stress. However, it is not clear how these molecular changes are enriched at cold-responsive genes only in regenerated plants that originate from leaves exposed to cold. A possible explanation for this phenomenon is that epigenetic changes are underpinned by the activation by stress of a discrete transcriptional network.

Most transcription factors (TFs) bind to open chromatin and activate defined gene networks (Fan and Huang 2021). However, some TFs can bind to closed chromatin and recruit other factors to regulate chromatin structure and gene expression (Jin et al. 2021). Some TFs bind to methylated regions to direct demethylation and an active gene expression (Kribelbauer et al. 2020). It has been shown in Arabidopsis that SUVH1/3 proteins bind to methylated DNA and recruit the chromatin proteins to enhance proximal gene expression (Harris et al. 2018). Several studies have also shown the mechanism of changes in DNA methylation mediated by transcription factors. In human cells, some TFs recruit DNMTs, methyl transferase enzymes, to methylate target regions (Héberlé and Bardet 2019). TFs can also recruit the demethylase enzyme to the target sites (Héberlé and Bardet 2019). In plants, DEFECTIVE IN MERISTEM SILENCING 4 (*DMS4*) is a transcription factor required for RNA Pol II-mediated RdDM pathway (Kanno et al. 2009).

Transcription of protein-coding genes or non-protein coding elements can recruit DNA methylation to nearby elements. Wibowo et al. (2016) found that intergenerational hyperosmotic stress memory is associated with changes in genome-

wide DNA methylation. Hyperosmotic stress induces the methylation in a transposable element located downstream of *CNI*. The hypermethylated region acts as a distal regulatory element by repressing the expression of antisense lncRNA of *CNI* (*CNI*-AS) resulting in higher expression of *CNI* compared to control. The heritable methylated DNA from the salt-treated parent results in higher *CNI* expression in the immediate stress-free generation than progenies from the parent under control conditions. Long non-coding RNAs (lncRNAs) also modulate DNA methylation through the RdDM pathway. Under auxin response, the *PID*, an auxin polar transporter gene, and the downstream lncRNA, *APOLO,* are transcribed. The transcription of *APOLO* is mediated by both RNA Pol II and Pol V. *APOLO* transcripts by Pol II interact with LHP1, a component of POLYCOMB REPRESSIVE COMPLEX 1 (PRC1), resulting in the loop formation. The transcripts from Pol V recruit the RdDM pathway leading to the DNA methylation in the *APOLO* locus. Hypermethylated regions are recognised by the PRC2 complex to deposit H3K27me3 marks. Altogether, the chromatin loop is formed between *APOLO* and *PID* and reduces the expression of *PID* (Ariel et al. 2014). The regulation of *PID* by *APOLO* is an example of lncRNA-induced DNA methylation connecting the external stimulus. A similar mechanism is also found in the regulation of *HaWRKY6* in sunflowers (*Helianthus annuus*). The TE-derived inverted repeat (IR) near *HaWRKY6* produces the non-coding RNA transcripts (ncRNAs). ncRNAs are associated with increased DNA methylation and loop formation resulting in repressed *HaWRKY6* in mature leaves (Gagliardi et al. 2019). lncRNA transcribed by Pol V also forms a scaffold RNA and is recognised by AGO4-siRNA. AGO4-siRNA-lncRNA complex targets the sequence complementary with lncRNA and induces the methylation via the DRM2 enzyme (Bohmdorfer and Wierzbicki 2015; Gao et al. 2010; Urquiaga et al. 2020; Wierzbicki et al. 2008). Many abiotic stressors regulate the expression of lncRNAs, for example*,* the lncRNA that *SVALKA* located between *CBF1* and *CBF3,* is transcribed under a long period of cold and it is associated with negative feedback controlling the *CBF1* expression (Kindgren et al. 2018). More than twenty lncRNA transcripts are precursors of siRNAs under heat stress in wheat (Jha et al. 2020; Xin et al. 2011). The siRNA accumulation has been reported in response to environmental stresses independently to the transcription of lncRNAs (Crisp et al. 2016; Khraiwesh et al. 2012).

Collectively, several studies have shown a link between environmental stimuli, non-protein coding genes, and DNA methylation at several loci. Some studies even show the connection between the inheritance of DNA methylation in non-protein coding elements which affect the nearby genes. Since the transcription of lncRNAs and other non-protein coding elements is also regulated by transcription factors, together with various effects of transcription factors at a genome-wide level, this could raise the possibility to observe the action of transcription factors in the heritability of stress-responsive mechanisms.

5.1.2 Experimental Design to Assess the Role of Stress-mediated Transcription in Transgenerational Stress Memory

In this study, I hypothesise that transcriptional activation is necessary for the transgenerational stress memory found in clonal plants. To test this hypothesis, we generated artificial microRNA transgenic lines driven by a constitutive promoter to downregulate the expression of CBF genes (amiR-cbf). CBF1/2/3 transcription factors are known to be major regulators of the transcriptional responses mediated by cold (Gilmour et al. 2004). In addition, we generated chemically inducible lines to ectopically overexpress CBF3 (indCBF3). Both constructs were transformed in indRKD4 so they could be used to generate clonal lineages (figure 5.1). We focused our analysis on leaf-origin (LO) clonal lineages because we previously found that they have shown a stronger effect in the establishment and maintenance of a transgenerational stress memory (see chapter 4). Because the constructs of amiR-cbf generated are dominant, we used heterozygous plants thus enabling the recovery of wild-type sibling, which we termed WT*, and allowing us to assess the impact of manipulating CBF expression in cold-mediated transgenerational stress memory (appendix figure 9.1). The construct to overexpress CBF3 was generated with an inducible promoter without leaky expression, so it can be regulated during cloning.

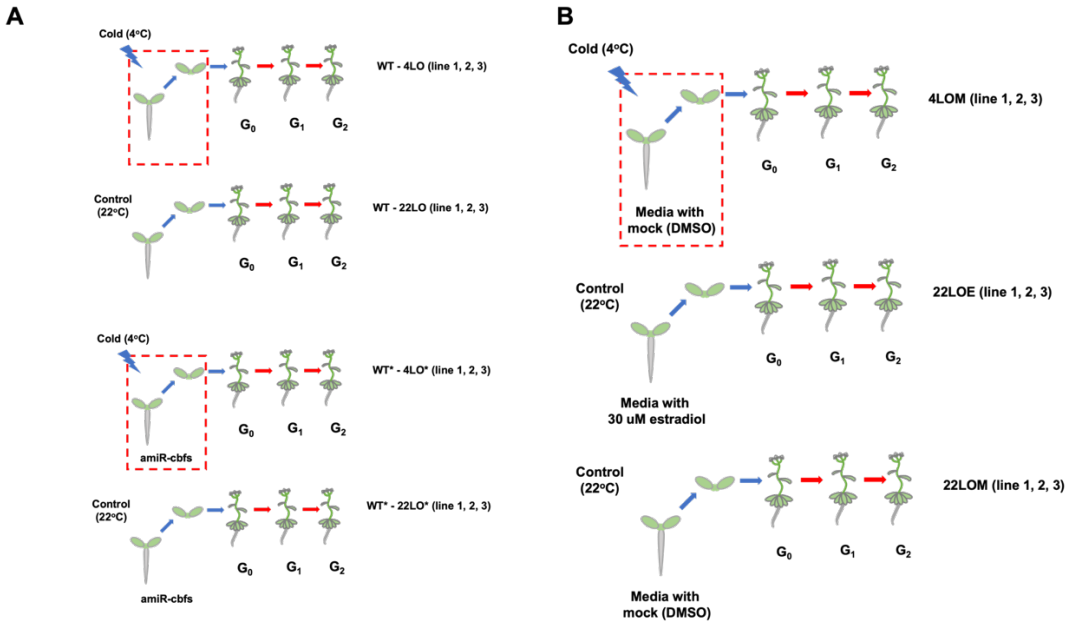

Figure 5.1 Experimental design of the role of *CBFs* in transgenerational cold-stress memory in clonal plants. (A) Schematic diagram of clonal propagation of amiR-cbf; (B) Schematic diagram of clonal propagation of indCBF3 lines. Clonal lines from heterozygous amiR-cbf lines were generated by induced somatic embryogenesis after exposure to two temperature treatments. Clonal lines from heterozygous indCBF3 lines were generated by induced somatic embryogenesis under three different conditions – 4°C with mock (DMSO) treatment, 22°C with 30 µM beta-estradiol condition, and 22°C with mock (DMSO). Root-origin clones were also propagated but were not used in the analysis. amiR-cbf Non-transgenic G_1 plants were selected and grown to produce G_2 progenies that were named WT*. The blue arrow indicates somatic embryogenesis. The red arrow indicates sexual propagation. The red dashed rectangle refers to the cold treatment during the cloning process

5.2 Project Aims

This chapter aims to define the role of CBF transcription factors in transgenerational cold-stress memory of clonal plants. Clonal lineages from amiR-cbf were performed to test the necessity of *CBFs* in transgenerational stress memory, while clonal lineages from indCBF3 were used to investigate the sufficiency of transcription factors in cold-related transgenerational stress memory.

5.3 Results

5.3.1 CBFs are Involved in Transgenerational Cold-Stress Memory in Clonal Plants

Firstly, I investigated the connection between cold memory genes and the *CBF*-transcriptional network. We used publicly available data to identify the cold-responsive genes regulated by *CBFs* (Song et al. 2021). We found 71 genes shared between LO cold memory (LCM) genes and *CBF*-regulated genes, and 14 genes shared with RO cold memory (RCM) genes and *CBF*-regulated genes (figure 5.2A-B). Fisher's exact test showed a greater significance in the overlap with LO cold memory genes indicating that the *CBF* network is connected to tissue-specific transgenerational cold-stress memory found in clonal plants.

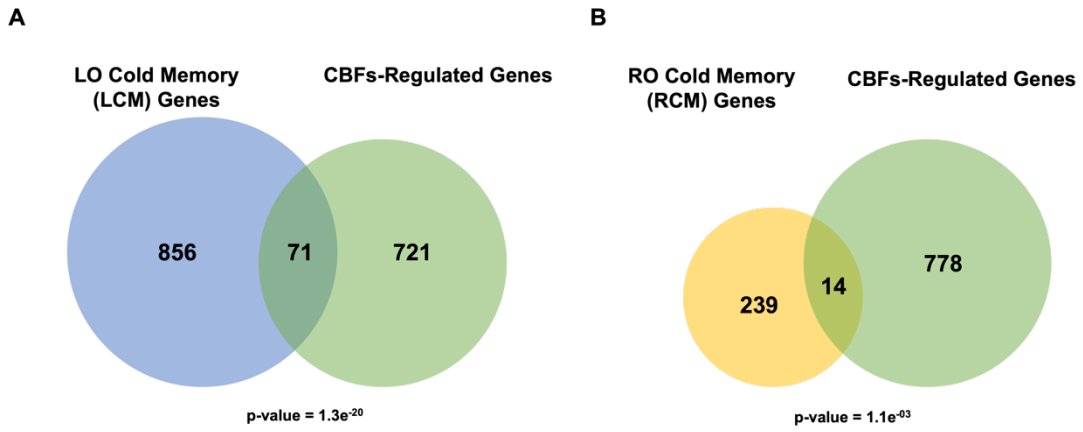

Figure 5.2 Venn diagram of the overlapping lists of genes between LO cold memory genes with *CBF*-regulated cold-responsive genes (A) and RO cold memory genes with *CBF*-regulated cold-responsive genes (B). p-value underneath each diagram indicates the significance of Fisher's exact test.

5.3.2 CBFs are Necessary for the Transgenerational Cold-Stress Memory Found in Clonal Plants

CBFs, also known as *DREB1s,* are a gene family that encodes AP2/ERF-type transcription factors and targets cold-responsive genes with C-repeat/dehydration-responsive elements (G/ACCGAC). *CBFs* consist of four homologous genes *CBF1* (*DREB1B*)*, CBF2* (*DREB1C*)*, CBF3* (*DREB1A*)*,* and *CBF4* (*DREB1D*) (Gilmour et al. 2000; Haake et al. 2002). *CBF4* is implicated in drought stress but not in low-temperature responses (Haake et al. 2002). *CBF1-3* contain high sequence similarity (around 86%) with redundancy in their functions (Jia et al. 2016; Song et al. 2021; Zhao et al. 2016). In this study, an artificial microRNA system was used to downregulate simultaneously *CBF1-3*. After transformation of four different amiR-cbf constructs in indRKD4 plants, we selected homozygous plants to test their efficiency in downregulating the target genes by qRT-PCR (figure 5.3). We found that amiR-cbf line 4.1.3 had an approximate 60% reduction in expression of *CBF1*, 30% reduction in *CBF2*, and 50% reduction in *CBF3* under cold treatment. Also, amiR-cbf line 1.2.1 had lower efficiency and the other two constructs were inefficient in downregulating on at least one member of the *CBF1-3* family (figure 5.3A). We used qRT-PCR to test the impact of each construct on genes known to be regulated by *CBFs*, and found that amiR-cbf lines 1.2.1 and 4.1.3 had similar effect on *GolS3* (figure 5.3B). However, amiR-cbf line 4.1.3 showed a greater reduction of *RD29A* indicating that this line has the greatest efficiency in downregulating *CBFs*.

Next, we tested the efficiency of amiR-cbf lines in somatic embryos exposed to cold, which confirmed the efficacy of line 4.1.3 in downregulating all CBF transcripts (Figure 5.4).

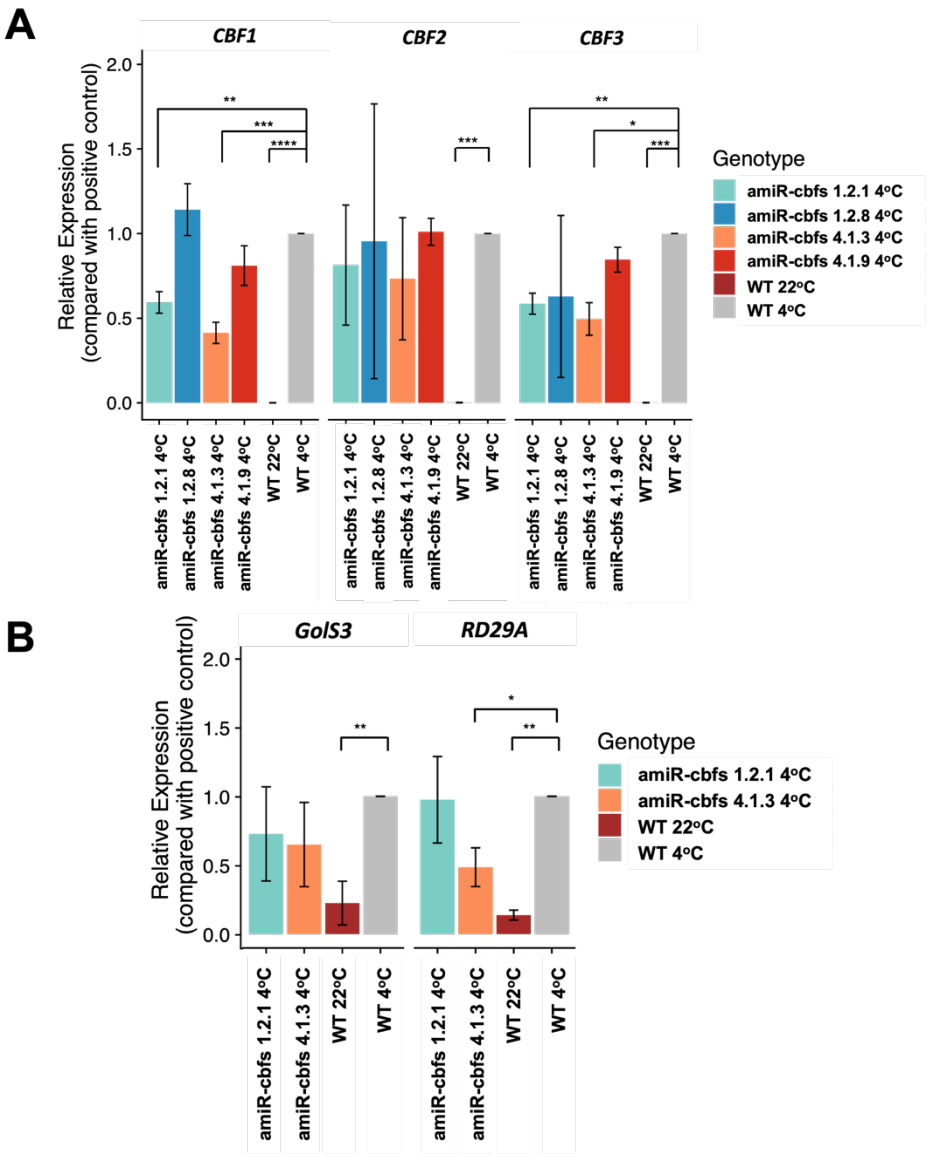

Figure 5.3 qRT-PCR analysis of amiR-cbf lines showing the relative expression of *CBFs* (A) and downstream genes (B). The relative expression was calculated using ΔΔCt method (Schmittgen and Livak 2008). The normalisation was done in comparison with positive control (indRKD4 under 4°C) and GAPDH was used as a housekeeping gene in the calculation. The experiment was done on 10-day old seedlings and with three biological replicates. The error bars indicate standard deviation from three replicates. Asterisk indicates the significant difference between comparisons (t-test, **** $p < 0.0001$, *** $p < 0.001$, ** $p < 0.01$, and * $p < 0.05$)

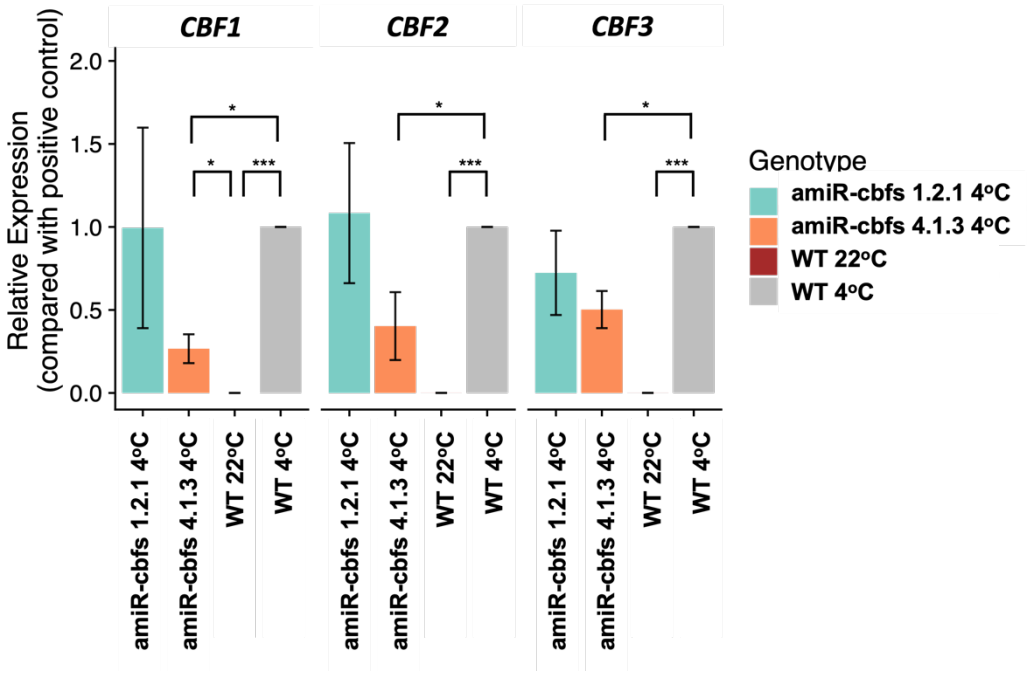

Figure 5.4 qRT-PCR analysis of amiR-cbf lines showing relative expression of *CBF* genes in RKD4-induced somatic embryos. The relative expression was calculated using ΔΔCt method. The normalisation was done in comparison with the positive control (indRKD4 (WT) under 4°C) and GAPDH was used as a housekeeping gene in the calculation. The experiment was done with triple replicates. The error bars indicate the standard deviation from three replicates. (t-test, **** $p < 0.0001$, *** $p < 0.001$, ** $p < 0.01$, and * $p < 0.05$)

We selected amiR-cbf 4.1.3 to interfere with CBF function during exposure to cold or ambient temperature, before somatic embryogenesis and plant regeneration. As a control, we regenerated wild-type plants using the same methodology and growth conditions. Clonal plants from heterozygous amiR-cbf 4.1.3 plants were propagated by self-pollination, which allowed us to select seeds where CBF function was restored, which we named WT*. For each clonal line, we pooled seeds from 3 G_0 plants to generate G_1 and pooled seeds from 5 G_1 plants to generate G_2 progenies (table 2.3). Seeds from G_2 progenies were sown in soil for four weeks under stress-free conditions before sample collection. We analysed leaf-origin (LO) clones only because they exhibited an enhanced cold stress memory when compared to root-origin (RO) clones. We collected leaf samples, three replicas for each condition, for transcriptome analysis using the strategy shown in figure 2.3D.

For the transcriptome analysis, we used clonal progenies regenerated after exposure to two different temperatures – 22LO (22^{o}C growth) and 4LO (4^{o}C growth), and clonal progenies from heterozygous amiR-cbf 4.1.3 plants that had CBF function restored after cloning – 22LO* and 4LO* (table 2.3). Principal component analysis of transcriptome data showed that PC1 separated samples by the temperature conditions before plant regeneration – 4LO* replicates grouped with 4LO, and 22LO* grouped with 22LO. The distance between the first group was closer than between the second, indicating a higher variance contribution in the control LO lines. In the PC2 samples were separated by genotype of the plants used for cloning (figure 5.5). We calculated DEGs using a stringent cut-off via (FDR ≤ 0.05 with log2FC cut-off values of 1.0). We performed four possible pair-wise comparisons (table 5.1). These comparisons can inform on the role of CBFs on cold-mediated transgenerational stress memory. We found that a cold treatment during somatic embryogenesis resulted in more affected transcripts in 22LO/4LO (408 DEGs – LCM genes) than in 22LO*/4LO* (100 DEGs – L*CM genes). On the other hand, a small number of transcripts were affected in 4LO/4LO* (12 DEGs) and 22LO/22LO* (24 DEGs) comparisons (table 5.1). These results support the view that CBF activity is necessary for a stable cold transcriptional memory in clonal plants. Lists of DEGs with statistical values from LCM genes and L*CM genes are shown in appendix table 9.1 – 9.2.

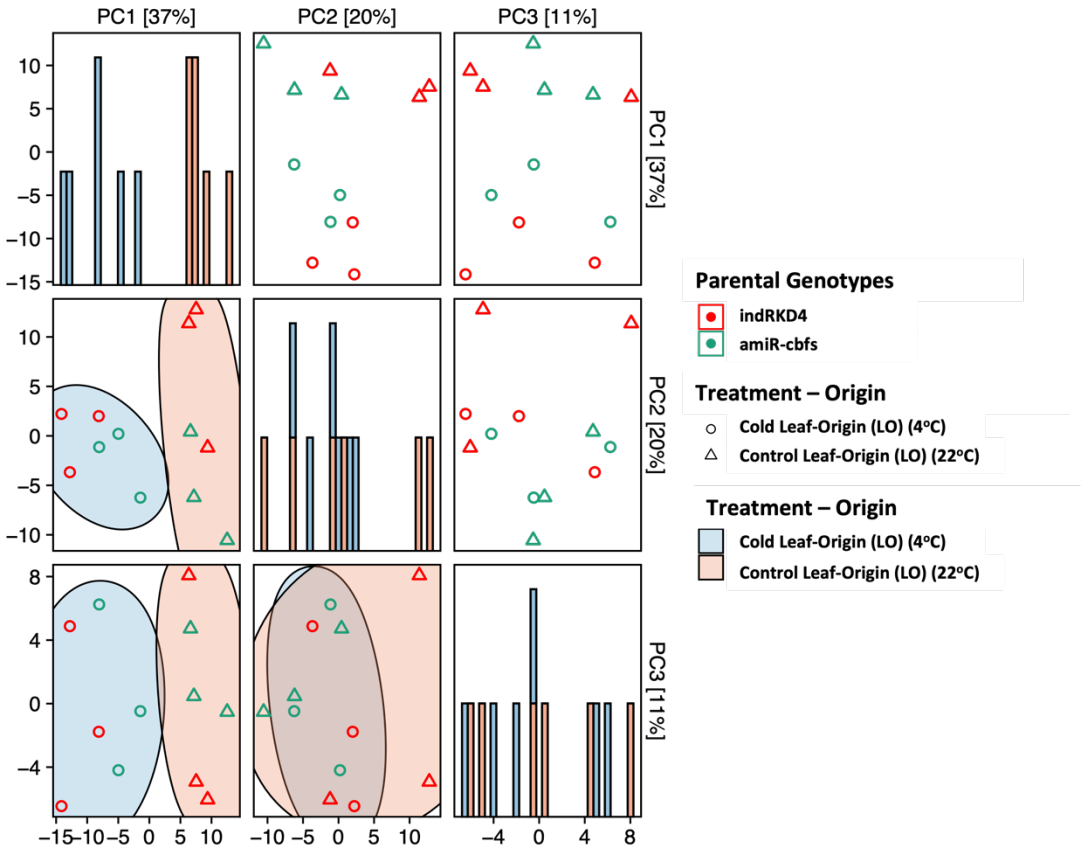

Figure 5.5 Principal component analysis (PCA) plot of transcriptomes from control and amiR-cbf plants exposed to different temperature conditions. The number in the bracket shows the percentage variance contributed by the principal component. The colours of dots represent parental genotypes. The filled colours of circle indicate the treatments during cloning process. The histogram in a diagonal matrix shows the distribution of the treatments according to PC in the x-axis.

Table 5.1 List of Pair-wise comparisons and Numbers of DEGs from wild-type and amiR-cbf plants exposed to different temperature conditions.

	Reference lineages	Treatment lineages	Description	DEGs	Up-regulated DEGs	Down-regulated DEGs
1	22LO	4LO	LO cold memory (LCM)	408	157	251
2	22LO*	4LO*	LO* cold memory (L*CM)	100	23	77
3	4LO	4LO*	-	12	11	1
4	22 LO	22LO*	-	24	17	7

Gene ontology analysis was performed to look at enriched GO terms in all comparisons. As in our previous analyses described in chapter 4, we found that DEGs from the 22LO/4LO comparison showed the term 'response to abiotic stimulus' enriched with the lowest p-value, followed by GO terms related to chemicals and stimulus. Several GO terms were related to hypoxia or decreased oxygen levels. Interestingly, there was a significant enrichment related to cold response (figure 5.6A). GO terms from the comparison between 22LO*/4LO* showed several terms related to cell wall organisation and carbohydrate metabolism. However, no term was directly related to cold response (figure 5.6B). These data suggest that a CBF-mediated transcriptional response activated during somatic embryogenesis is critical for a heritable transcriptional cold memory in clonal plants.

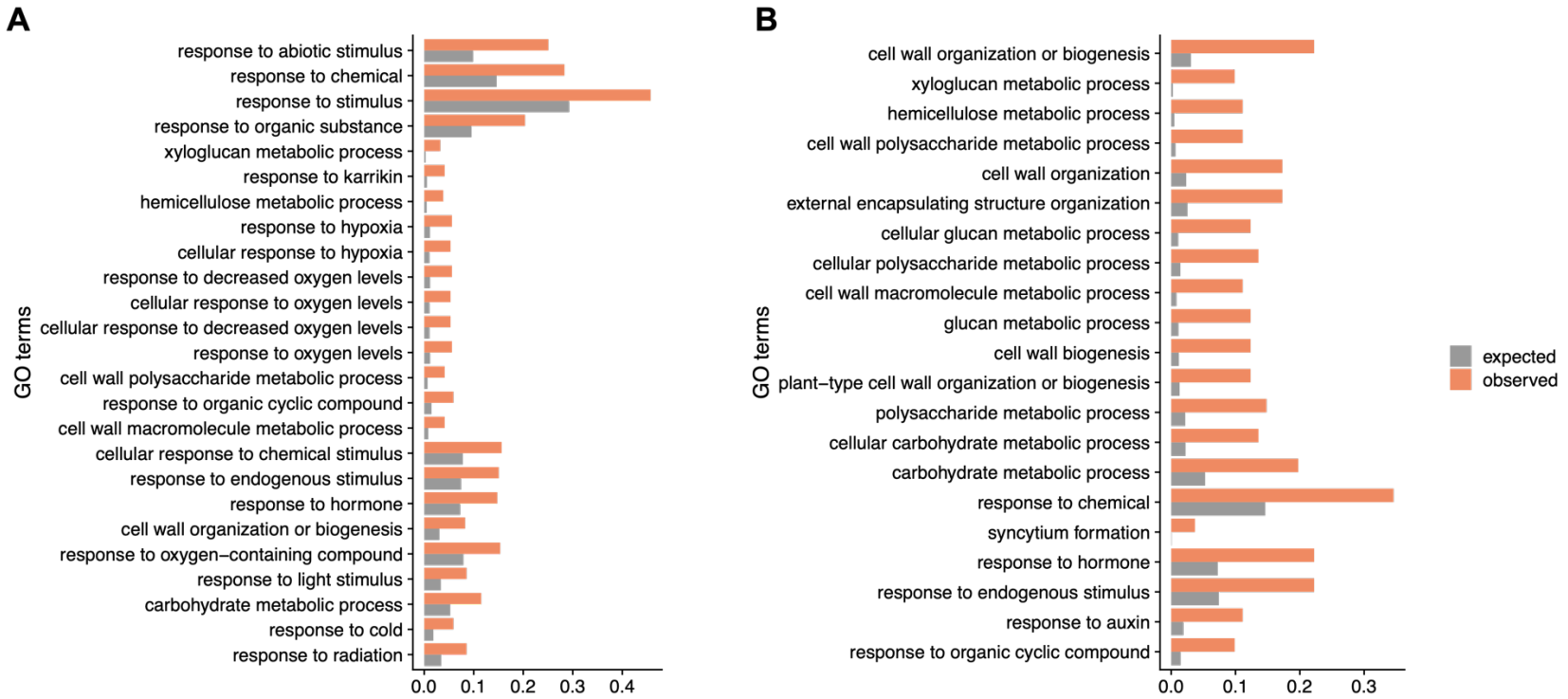

Figure 5.6 Gene ontology (GO) analysis showing the enriched GO terms from submitted DEGs in pair-wise comparisons between 22LO/4LO or LCM genes (A) and 22LO*/4LO* or L*CM genes (B). The X-axis indicates GO terms' frequency between the expected value (grey bar) and the observed value (orange bar). The expected frequency is calculated from the number of genes with particular GO terms divided by the total GO terms in the *Arabidopsis* database. The observed value is calculated from the number of genes with the term in an input divided by the number of input genes.

5.3.3 Cold Memory Genes are Shared Between RKD4- and *cbf*-clonal lineages

Hierarchical clustering of normalised expression on LO cold memory, LCM and L*CM, genes revealed two distinct groups of upregulated and downregulated transcripts. Notably, the transcriptional response of these transcripts in clonal progenies was affected when the expression of CBFs was reduced during somatic embryogenesis when plants were exposed to cold (figure 5.7A). We looked at overlap between LCM and L*CM and found 13 common genes in up-regulated cold memory genes, and 65 common genes in down-regulated cold memory genes. However, we did not find an overlap between up- and down-regulated from both clonal lineages (figure 5.7B).

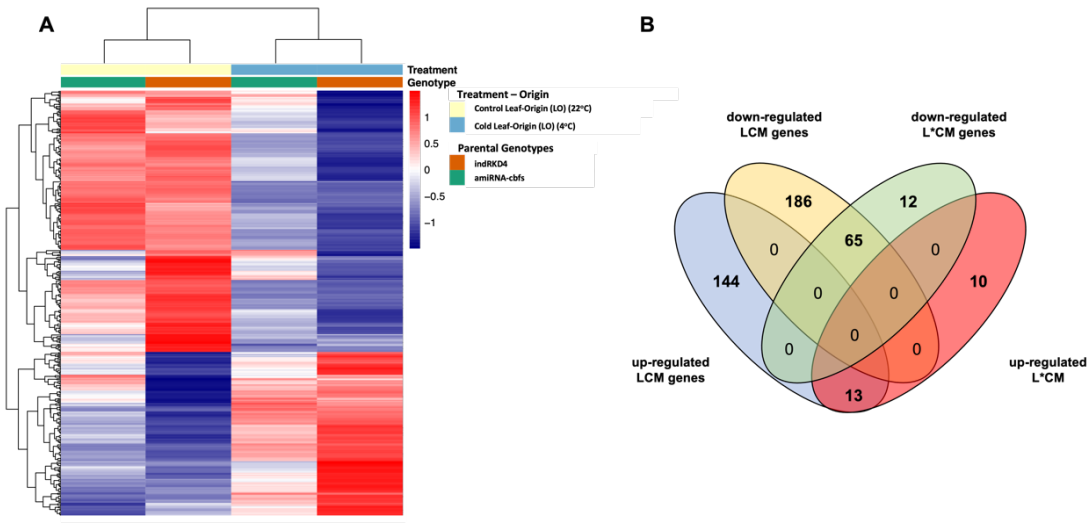

Figure 5.7 Heatmap of expression values from LCM genes (A), Venn diagram of up- and down-regulated DEGs between LCM and L*CM cold memory genes (B). The rows of the heatmap represent the z-score of genes. Columns with colour annotation represent the condition (parental genotypes and treatments during the cloning process).

5.3.4 Transgenerational Cold Stress Memory is Underlined by a CBF-Activated Network.

To define further the role of *CBFs* in the establishment of a cold stress memory in clonal plants, we looked at the overlap between cold memory genes from LCM and L*CM lineages and genes known to be regulated upon cold exposure by *CBFs*. We found 41 LCM genes and 15 L*CM genes that were *CBF* targets, and 12 common genes that were *CBF* targets (appendix table 9.3). The significant overlap between *CBF*-regulated genes and LCM genes (p-value = $2.3e^{-16}$, figure 5.8) reinforces our previous findings revealing the existence of cold memory genes inherited in clonal progenies of cold-treated plants (figure 5.2A).

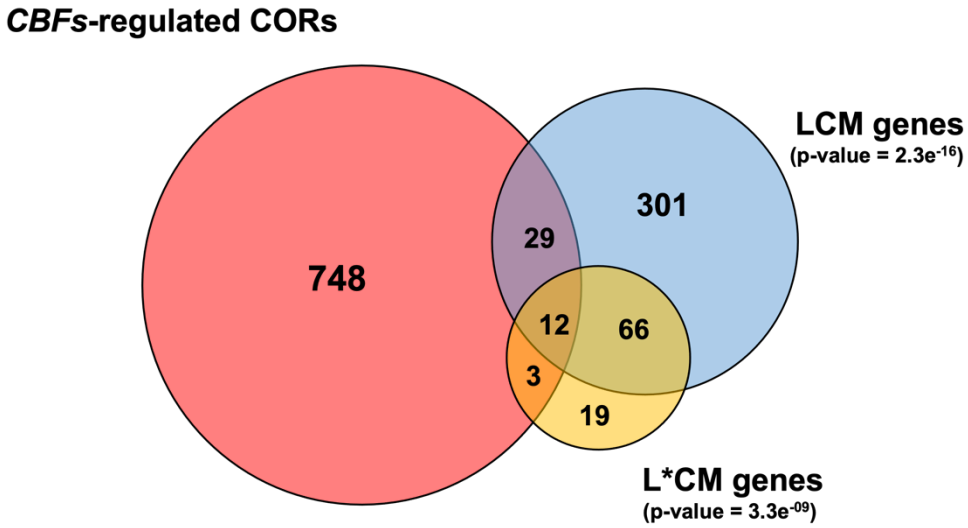

Figure 5.8 Venn diagram of the overlapping lists of genes between *CBF*-regulated genes (red), LCM genes (blue) and L*CM genes (yellow). The P-value for each diagram indicates the significance of Fisher's exact test.

5.3.5 Ectopic *CBF3* Expression Partially Phenocopies the Cold Memory Response Found in Clonal Plants.

Our data suggested that CBFs are necessary to establish a cold memory response in clonal plants. We then decided to test if the transcriptional cascade regulated by CBFs is sufficient to mediate this stress memory response. To test this hypothesis, we generated transgenic lines with a chemically inducible (Estradiol) construct that could enable the controlled expression of *CBF3* (indCBF3) during somatic embryo induction. To minimise the risk of silencing endogenous CBF genes we engineer a codon optimised CBF3 construct. We identified one line (indCBF3 4.10) that activated CBF3 expression at high levels upon exposure to β-estradiol but showed a low basal expression after mock (DMSO) treatment (figure 5.9). We then tested in leaf and callus samples the expression of three known CBF3 targets, *COR15A, RD29A,* and *GolS3,* and found that they all were expressed in indCBF3 4.10 upon β-estradiol treatment (figure 5.9). Notably, the endogenous CBF3 gene was not affected by the chemical induction of the transgene thus indicating that CBF3 is not self-regulated. Collectively, our data demonstrates that it is possible to manipulate the CBF3-mediated transcriptional network in absence of a cold treatment.

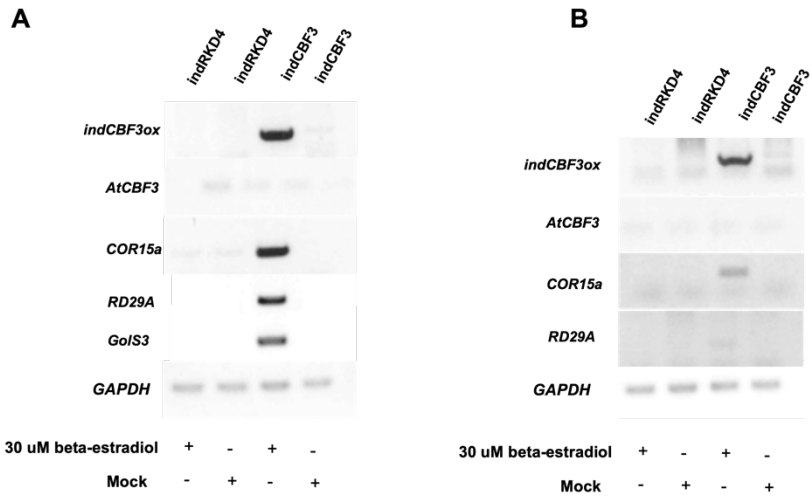

Figure 5.9 Semi-quantitative RT-PCR to test the efficiency of *indCBF3* 4.10 after being treated with β-estradiol or mock solutions. Seedling from 10 day old plants (A) RKD4-induced callus (B). Genes tested are shown on the left side. indCBF3 refers to the estradiol-inducible CBF3 transgene. *AtCBF3* refers to endogenous *CBF3* gene. *COR15a*, *RD29A*, and *GolS3* are activated by *CBFs* in response to cold stress.

Next, we generated clonal lines from indCBF3 transgenic plants using the methodology described previously. To simplify the analysis, we generated leaf-origin (LO) clonal lines from indCBF3 that were grown at 22ºC and treated with mock solution (22LOM) or treated with β-estradiol to ectopically express CBF3 (22LOE). In addition, we generated clonal lines exposed to cold (4ºC) and treated them with a mock solution (4LOM). For each condition, we generated three independent clonal lines that were propagated to G_2 using the same strategy employed in previous chapters. To quantify the transcriptional changes in each group we used replicated RNA-seq data from independent clonal lines, thus increasing the stringency of the analysis. To determine the impact of *CBF3* overexpression and cold on stress memory, we measured the transcriptional differences found between 22LOM and 22LOE or 4LOM (figure 5.1B). Quality control analysis revealed that two RNA-seq datasets had poor sequence quality and they were removed from the analysis (appendix figure 9.2). Principal component analysis of RNA-seq data showed a clear separation between the three experiments (PC1 with 40% and PC2 with 20% variance contribution) (figure 5.10). Notably, the 22LOE lines were separated in PC3 with a 13% variance

contribution. We calculated DEGs from pair-wise comparisons (FDR < 0.05 with log2FC cut-off values of 0.5, table 5.3). We compared 22LOM and 4LOM to measure the impact of the cold treatment on cold-induced memory in clonal plants. We also compared 22LOM and 22LOE to measure the effect of CBF3l overexpression to mimic a cold-induced memory in clonal plants.

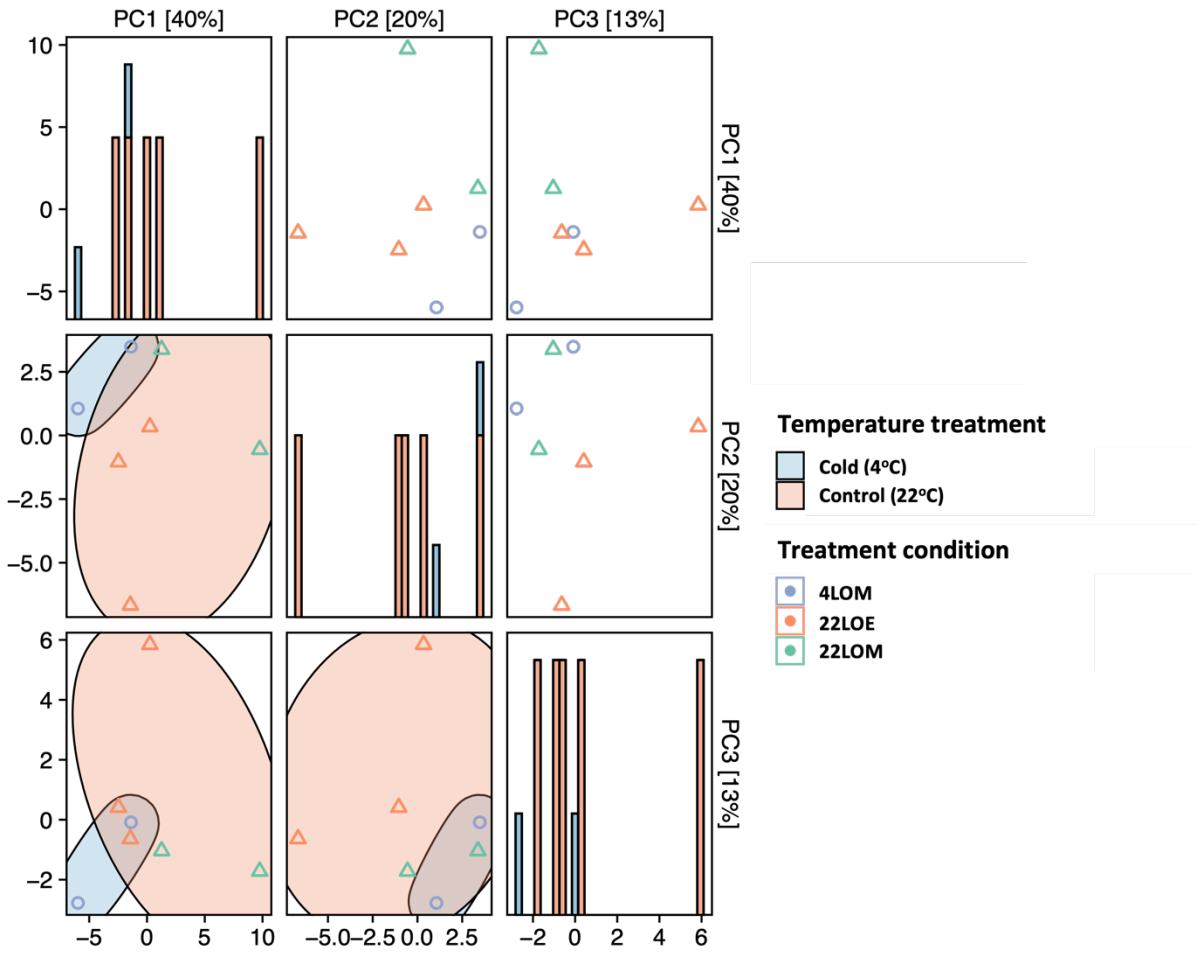

Figure 5.10 Principal component analysis (PCA) plot of RNA-seq data from clonal lines generated from indCBF3 plants treated with mock and β-estradiol during somatic embryo induction. The number in the bracket shows the percentage variance contributed by the principal component. The colours of dots represent treatment during somatic embryogenesis process. The filled colours of circle indicate the temperature treatments during cloning process. The histogram in a diagonal matrix shows the distribution of the treatments according to PC in the x-axis.

Table 5.3 List of Pair-wise comparisons and Numbers of DEGs from G_2 generation of clonal lineages from indCBF3 under different conditions

	Reference lineages	Treatment lineages	Description	DEGs	Up-regulated DEGs	Down-regulated DEGs
1	22LOM	4LOM	Cold-induced memory genes	106	38	68
2	22LOM	4LOE	CBF3-induced memory genes	48	26	22

This analysis uncovered 106 DEGs in clonal lineages generated from plants exposed to cold during regeneration. Notably, we found 48 DEGs in clonal lineages generated from indCBF3 plants treated with β-estradiol. As previously found, cold-induced memory genes were enriched in GO terms related to stress response, response to hypoxia, and response to a biotic stimulus (figure 5.11A). CBF3-induced memory genes were enriched in GO terms such as the amino acid biosynthetic process or small molecule synthetic process (figure 5.11B). Notably, 13 genes were shared between the two comparisons and showing a significant statistical intersection (p-value = $6.4e^{-23}$, figure 5.12A) (appendix table 9.4). We also found a small intersection between cold-induced and CBF-induced memory genes with genes regulated by CBF in response to cold (figure 5.12B).

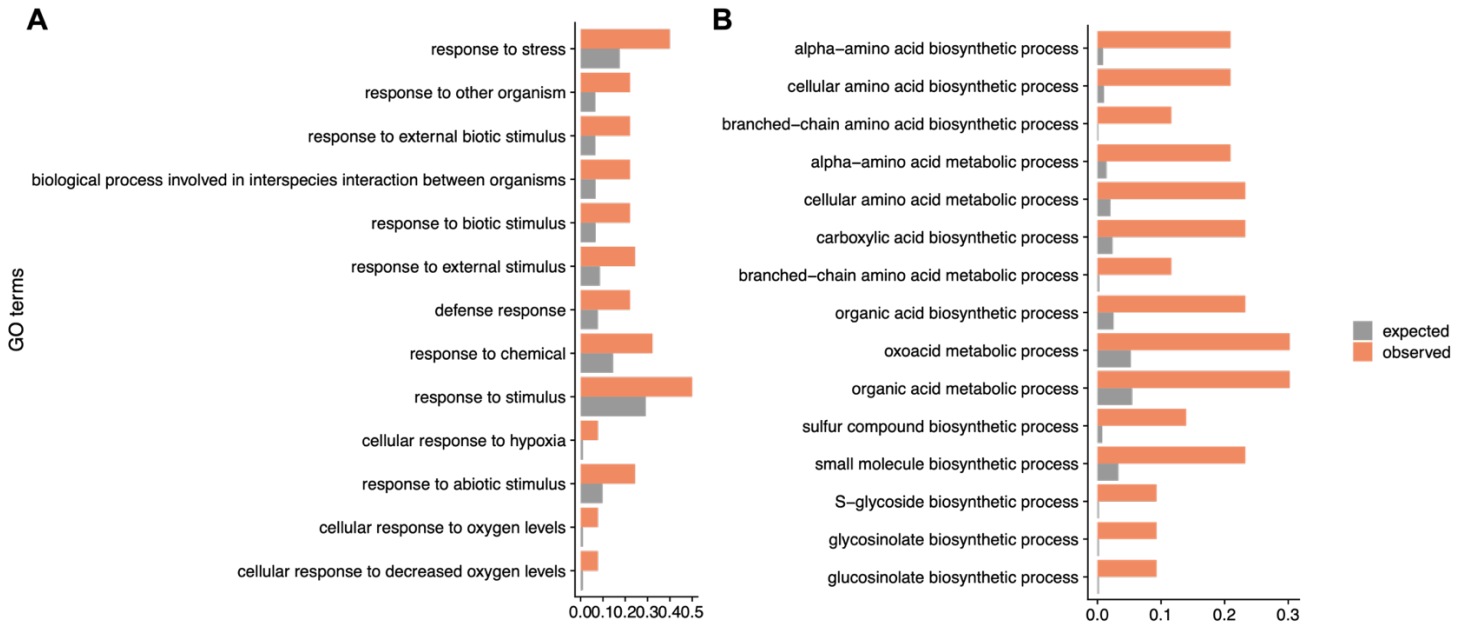

Figure 5.11 Gene ontology (GO) analysis shows the enriched GO terms from submitted DEGs from pair-wise comparisons between cold-induced memory genes (A) and CBF3-induced memory genes (B). X-axis indicates the frequency of GO terms between expected value (grey bar) and observed value (orange bar). The expected frequency is calculated from the number of genes with particular GO term divided by the total GO terms in *Arabidopsis* database. The observed value is calculated from the number of genes with the term in an input divided by the number of input genes.

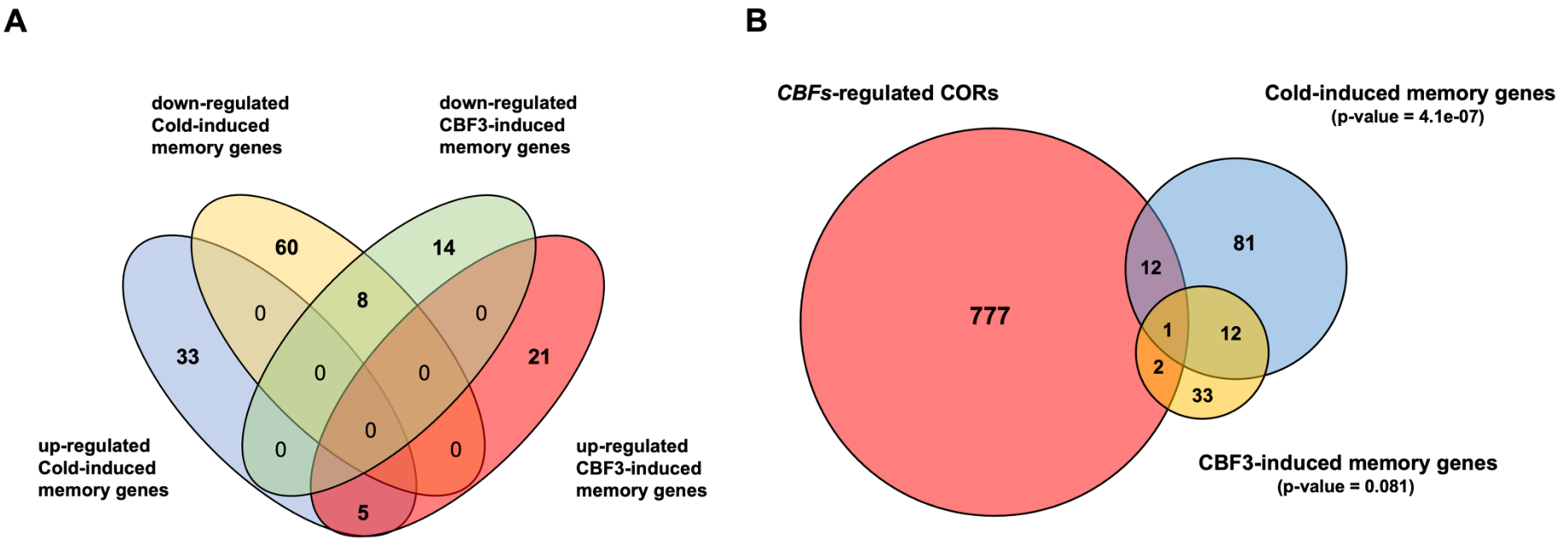

Figure 5.12 Venn diagram representing the overlap between up-and down-regulated genes from cold-induced memory genes and CBF3-induced memory genes (A) and the intersection between cold-induced and CBF3-induced memory genes with *CBF*-regulated CORs (B).

5.4 Discussion

We have shown in the previous chapter evidence for a stable transgenerational cold memory associated with cloning and that this memory is primarily maintained in clonal plants derived from leaf tissues. As such, the transcriptomic changes found in clonal plants are associated with DNA methylation changes at flanking regions of stress memory genes.

In this chapter, we show that a large number of cold memory genes in clonal plants are also components of the transcriptional network regulated by *CBF* transcription factors. We then hypothesised that activation of these cold transcriptional pathways is necessary for the establishment of a stable stress memory. This may be possible because several studies have shown that transcription factors implicated in stress responses can direct epigenetic changes at discrete loci (Fan and Huang 2021; Héberlé and Bardet 2019; Kribelbauer et al. 2020).

To test our hypothesis, we interfered with *CBF1-3* function, using a dominant amiR-cbf transgene, during cold exposure and plant regeneration. We screened several amiR-cbf constructs to select a transgenic line that strongly downregulates most *CBFs*. Our results show that *CBF* expression is strongly activated in somatic cells and also in somatic embryos after exposure to cold. The cold-induced *CBF* expression is also reported in barley embryogenic calli (Vashegyi et al. 2013). Similarly, the expression of HEAT SHOCK FACTOR A2, HSFA2, is activated in embryogenic calli in response to heat (Liu and Charng 2013). To determine if CBFs are specifically required for a stress memory response established during cloning we restored CBF function when propagating lines over multiple sexual generations. We found differences in the number of cold memory genes present in clonal lines of control and amiR-cbf plants treated with cold. We found that in these lines most cold memory genes were downregulated under normal growth temperature conditions, as was the case in experiments shown in the previous chapter. Our results contrast with the transcriptomic profile of *Arabidopsis* seedlings when exposed to cold typically resulting in gene upregulation (Lee et al. 2005; Song et al. 2021). Similar results were found in studies on salt-induced intergenerational memory in Arabidopsis that showed a greater number of down-regulated genes in the next generation after salt-stress, when stressed plants showed mostly upregulated genes (Boyko et al. 2010; Seok et al. 2020). The downregulation may be associated with hypermethylation of gene

regulatory regions that results in a transcriptional repression (Bilichak et al. 2012; Zhang et al. 2018). The different transcriptional dynamics observed between cold memory and cold-responsive genes suggest the regulatory mechanisms implicated in these two responses are different.

We also found a greater reduction in the number of stress memory genes, in particular those enriched for GO terms related to cold responses, in clonal plants derived from plants with reduced CBF activity. However, several *CBF*-regulated genes were found in these clonal lines, which may be caused by the partial loss of CBF function in our amiR-cbf lines. Loss-of-function *CBF* mutants are defective in cold acclimation. A triple mutant of *CBF1-3* shows reduced survival rates under freezing temperature even after being pre-treated with non-lethal cold (Jia et al. 2016). Similar effect on stress acclimation to heat response is also observed in several *Arabidopsis* mutants (Hong et al. 2003). Loss-of-function mutations on ATAF-1, a transcription factor associated with heat response show reduced primed responses of several heat-responsive genes upon a heat stress challenge (Alshareef et al. 2022). Collectively, our data and published work support the view that the activation of a stress-mediated network is critical for transgenerational stress memory in clonal plants.

We then wondered if *CBFs* are sufficient for the establishment of transgenerational stress memory. To test this hypothesis, we ectopically overexpressed CBF3 during cloning but in the absence of cold treatment. Transcriptomic analysis showed that these clonal lines had a small number of cold memory genes but were significantly smaller in number compared to cold-treated clonal lines. This could be explained by the inefficient upregulation of CBF3 during cloning and/or the necessity of a chromatin change directed by cold. Cold is known to change chromatin structure, removing repressive histone marks in several cold-regulated genes, to increase the accessibility of transcription factors (Kwon et al. 2009). Nevertheless, when we compared cold-induced and CBF3-induced memory genes we found a significant overlap, thus suggesting that CBF3 activity is sufficient to direct a transgenerational cold memory response. However, most of these genes do not seem to be known components of the CBF transcriptional pathway.

Collectively, our results indicate that *CBF3* is partially sufficient to establish a transgenerational cold memory response in clonal plants.

5.4 Chapter Conclusion

In this chapter, we have discovered that the transcriptional activity of cold transcriptional networks is necessary for establishing a transgenerational cold memory response in clonal plants.

Chapter 6 General Discussion

6.1 The Roles of ICE1 Transcription Factor in Cold-Responsive Pathways

As sessile organisms, plants have developed stress-responsive pathways to withstand changes in the environment. The core components of stress-responsive pathways are transcription factors that modulate a plethora of regulatory gene networks (Singh et al. 2002). Under low-temperature conditions, cold-responsive genes (*CORs*) contribute to the regulation of multiple physiological components, from stabilising proteins to regulating RNA-chaperone mechanisms (Ding et al. 2019; Kang et al. 2016; Karlson et al. 2002). In *Arabidopsis*, CCAAT MOTIF-BINDING FACTOR (CATMA) and (CBF) TRANSCRIPTION FACTORS regulate approximately 20% of the *COR* genes (Jia et al. 2016). Several studies have revealed that multiple transcription factors regulate the expression of COR genes – including *CBFs*, CAMTAs, CCA1/LHY, and ICE1 (Chinnusamy et al. 2003; Dong et al. 2011; Kidokoro et al. 2017). While CAMTAs and CCA1/LHY are involved in Ca^{2+} signalling and responses to photoperiod, respectively, the role of ICE1 seems to be restricted to the cold-responsive pathway. For over two decades, the *ICE1-CBFs-CORs* transcriptional cascade has been considered the core regulatory pathway in cold responses in plants (Liu et al. 2010; Verma et al. 2020). However, recent data have questioned the role of ICE1 in COR responses and in *CBF* regulation (Kidokoro et al. 2020). The first described ICE1 mutant in Arabidopsis, *ice1-1*, contains a transgenic reporter that is associated with the silencing of the promoter of endogenous *CBF3* (Kidokoro et al. 2020). Moreover, analysis of several independent *ICE1* mutants do not show defects in *CBF1 – 3* expression during cold treatment.

One of the objectives of our study was to define the precise role of *ICE1* in cold responses by using a genome-wide transcriptome approach to measure the transcriptional changes in a T-DNA insertion mutant (*ice1-2*) and artificial microRNA lines (amiRNA-ice1) that strongly downregulate *ICE1* expression. Our data shows that *ice1-2* and amiRNA-ice1 plants display similar defects in seed germination and stomatal development (Denay et al. 2014; Kanaoka et al. 2008). However, we found profound differences in the transcriptome of these mutants. Under both control and cold growth conditions, amiRNA-ice1 plants show a strong reduction in ICE1 transcripts, but *ice1-2* plants show a normal number of truncated transcripts. These

results suggest that amiRNA-ice1 efficiently interfere with ICE1 function, but *ice1-2* likely produces partially functional ICE1 proteins. The transcriptomic analysis also shows that most cold-responsive genes are not affected in both *ice1-2* and amiR-ice1 plants, reinforcing the view that ICE1 is not a major regulator of *CBF* expression and downstream targets (Kidokoro et al. 2020). Although these mutants do not show major defects in the cold-responsive pathway, they display defects in the transcription of a large number of genes associated with oxygen sensing and cell wall function. Previous studies have hypothesised that ICE1 is a transcription activator (Chinnusamy et al. 2003; Zhan et al. 2015) while others have proposed that it acts as a transcriptional repressor (Benedict et al. 2006; Miura et al. 2007). Our data shows that ICE1 has a dual role, repressing and activating the transcription of genes in the cold-responsive pathway. We also found that the ectopic expression of *ICE1* and a phosphomimic $ICE1^{S278D}$ that increases protein stability are unable to mimic the effects that cold imposes on the transcription of ICE1-dependent genes. These data reveal the existence of additional regulatory layers modulating ICE1 function.

Notably, we found that this one layer of regulation may be underpinned epigenetically because the regulatory regions of most cold-responsive and in particular ICE1 targets are enriched on H3K27me3, a repressive histone mark deposited by the PRC2 complex and removed by histone demethylases. We also found the removal of H3K27me3 from cold-responsive genes after cold exposure. Moreover, the activity of the histone demethylase REF6 was necessary for the removal of this histone mark from the promoter regions of several ICE1 targets. The interplay between the chromatin structure and the activity of transcription factors has been well-studied in heat stress response. The activity of HEAT SHOCK TRANSCRIPTION FACTOR A2 (HSFA2) associates with the deposition of active histone marks, H3K4me3, to regulate several HEAT SHOCK PROTEIN (*HSP*) genes (Lämke et al. 2016). JMJ proteins, H3K27me3 demethylases, are also necessary for the heat-induced expression of *HSP22* and *HSP17.6*, and this demethylation is sustained for over three days, resulting in heat acclimation (Yamaguchi et al. 2021). Transcriptional activity of PHYTOCHROME INTERACTING FACTOR4 (PIF4) requires the removal of H3K27me3 by REF6 in the promoter region of several downstream genes during heat stress to regulate the thermomorphogenesis process (He et al. 2021). In cold, the interaction between histone modifications and transcriptional regulation has been

found to be critical during vernalisation (Hung et al. 2022; Kim et al. 2017; Tian et al. 2019). Prolonged low temperatures promote flowering in plants by repressing FLOWERING LOCUS C (FLC), a repressor of floral promoter FLOWERING LOCUS T (*FT*) (Searle et al. 2006). This process occurs from the cold-induced expression of *COOLAIR*, *FLC* antisense lncRNA transcripts, and *COLDAIR*, lncRNA at 3' end of *FLC*, and both lncRNAs recruit PRC2 to accumulate H3K27me3 in *FLC* locus (Kim et al. 2017; Tian et al. 2019). The expression of *COOLAIR* and *COLDAIR* is regulated by the upstream transcription factor WRKY63 (Hung et al. 2022). In short-term cold response, the removal of H3K27me3 has been reported for several downstream targets of *CBFs* in response to cold, but the connection to transcriptional activity is not fully understood (Kwon et al. 2009).

Based on our data and previously published work we proposed a model for ICE1 functions in development and response to cold (Figure 6.1). It is clear that ICE1 plays an important role in embryo and stomatal development (Denay et al. 2014; Kanaoka et al. 2008). Cold does not induce the expression of ICE1, but it activates the post-translational modifications that modulate the stability and activity of ICE1 protein (Ding et al. 2015; Zhao et al. 2017). Our data show that ICE1 does not play a significant role in the regulation of *CBF* expression and has limited effects in *COR* genes. However, it has a potential role in oxygen sensing and cell wall function, which are important components of cold acclimation responses. Our results also indicate that ICE1 has both active and repressive roles in different groups of *COR* genes. Interestingly, ICE1 and CBFs share several downstream genes, for example, *GolS3*. The observations indicate that there is an interaction between the *ICE1* and *CBF* transcriptional networks. To dissect the possible crosstalk between these transcription factors in cold-mediated transcriptional networks, the expression dynamics of *COR* genes in *ICE1* and *CBF* mutants should be carefully investigated.

Our data have also revealed that ICE activity is modulated epigenetically and underpinned by dynamic changes in chromatin in response to cold. To comprehensively dissect the interplay between *ICE1* and the removal of H3K27me3, it would be useful to investigate the transcriptional and chromatin dynamics in plants with genetic lesions interfering with both pathways.

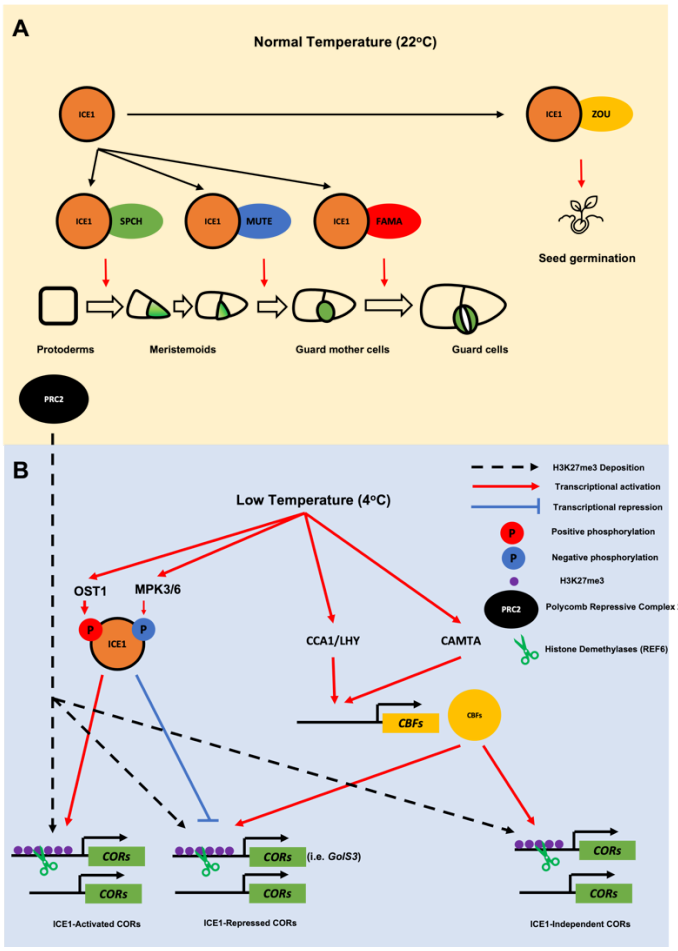

Figure 6.1 Hypothetical models for the different roles of ICE1 in plant development and the cold-responsive pathways. (A) During seed development, ICE1 forms the heterodimer protein complex with ZOU to regulate embryo development. ICE1 also forms protein complexes with SPCH, FAMA, and MUTE to control stomata formation. (B) Under low-temperature conditions, ICE1 undergoes post-translational modifications that regulate protein stability. ICE1 exhibits both active and repressive functions on a group of cold-responsive genes. Several genes are common targets of ICE1 and CBFs. Moreover, cold directs the removal of H3K27me3 which is accumulated under control temperatures by PRC2 in the regulatory elements of genes targeted by ICE1 and CBF. Red arrows indicate transcriptional activation. Blue lines indicate transcriptional repression. Black dashed arrows indicate H3K27me3 deposition by PRC2. The red circle with designated P refers to positive phosphorylation. The blue circle with designated P refers to negative phosphorylation. Scissors refer to the removal of H3K27me3 by histone demethylases.

6.2 Molecular changes associated with a transgenerational cold stress memory in clonal plants

Plants adapt to recurring changes in the environment by maintaining their cellular activity through the activation of specific transcriptional gene networks that can last over multiple mitotic divisions, a process known as stress memory (Crisp et al. 2016; Baurle and Trindade, 2020). The molecular mechanisms implicated in stress memory involve changes in metabolites, protein activity, transcription and epigenetic modifications (Crisp 2016). Most studies have focused on the analysis of short-term stress memory, or somatic stress memory, in response to biotic or abiotic stressors (Baurle and Trindade, 2020). The idea that this form of stress memory may be inherited across meiosis and over multiple generations is more challenging because plants have a wide range of mechanisms to reset epigenetic marks during sexual reproduction (Kawashima and Berger, 2014). It has been hypothesised that DNA methylation is most likely the main contributor to a heritable stress memory in plants because it is stable across mitotic and meiotic cell divisions (Crisp 2016).

To form the stable transgenerational stress memory, the stress information is proposed to be established in the meristem cells and maintained in reproductive tissues, and ultimately transmitted to gametes (Kumar 2018). The integration of stress-induced epigenetic marks is most likely restricted in the shoot apical meristem (SAM), as it has been reported that it is protected from epigenetic changes directed by both internal and external stimuli (Gutzat et al. 2020; Nguyen and Gutzat 2022). However, recent studies have shown that SAMs can integrate and transmit genetic and epigenetic modifications. Epigenetic silencing pathways, mostly linked to *de novo* DNA methylation, is activated in SAM to repress the activity of transposable elements (TEs) (Baubec et al. 2014; Higo et al. 2020). Furthermore, the activity of the RdDM pathway is necessary for the protection of SAM against transmission of the viral genome after infection (Bradamante et al. 2021). These silencing mechanisms are thought to be critical to maintaining the genetic and epigenetic integrity of SAMs before reproductive organs are formed. However, during inflorescent development and more specifically during male gametogenesis CHH methylation at TEs is strongly reduced, as part of epigenetic reprogramming occurring during fertilisation (Gutzat et al. 2020; Walker et al. 2018). Several studies also reveal that meristem cells have small transcriptomic and epigenetic changes when plants are exposed to elevated

temperatures, confirming the protective mechanisms against changes caused by abiotic stress (Bilichak et al. 2015; Pecinka et al. 2010). These studies indicated that meristematic cells may be (i) protected from the integration of epigenetic modification and/or (ii) have active mechanisms to remove these imprints. Although the precise mechanisms are unknown, they may be important to restrict the stability of a transgenerational stress memory in plants.

Previous studies have shown that hyperosmotic stress caused by exposure to high concentrations of salt induces DNA methylation changes that are also found in the subsequent stress-free generation (Boyko et al. 2010; Wibowo et al. 2016). The intra-generational stress-induced DNA methylation changes are associated with changes in gene expression, which may have an adaptive value in plants (Wibowo et al. 2016). Similar responses have been reported for a wide range of biotic stressors (Hannan Parker et al. 2022). Progenies of plants that experienced recurring exposures to pathogens exhibit adaptive resistance responses, which correlate with the enhanced expression of resistance gene and DNA hypomethylation (Luna et al. 2011). Moreover, the heritable adaptive responses to herbivore attack are impaired in plants impaired on small RNA production, suggesting that changes in DNA methylation directed by small RNAs are required for a transgenerational biotic stress memory in plants (Rasmann et al. 2011).

However, detailed molecular and phenotypic analyses carried out in Arabidopsis revealed that the active resetting of DNA methylation marks that takes place during sexual reproduction restricts transgenerational stress memory in plants (Wibowo et al. 2016). Thus, sexual reproduction constitutes a major barrier to the stable inheritance of stress memory in plants.

To address some of these unresolved questions and to overcome some of the restrictions that meristematic cells have to restrict the integration and propagation of stress-mediated imprints we undertook a new experimental approach. We took advantage of the methodology established in our group to generate clonal progenies, via somatic embryogenesis, from different tissues (Wibowo et al. 2018). To determine the stability of these imprints we propagated clonal plants via sexual reproduction over two generations thus limiting potential parent-of-origin environmental effects. We then undertook a genome-wide transcriptomic and epigenomic approach to identify the molecular changes and measure their stability.

We found that cold had a greater impact on the transmission of imprints in clonal plants regenerated from leaves (leaf-origin, LO) than from roots (root-origin, RO). These differences may be linked to the different transcriptional responses of these tissues to cold stress (Guo et al. 2021; Kreps et al. 2002). Our transcriptomic data indicates that the cold memory genes from clonal plants overlap significantly with cold-responsive genes identified in previous studies (Song et al. 2021). These results reveal that (i) somatic cells have the capacity to integrate epigenetic imprints in response to stress, (ii) these imprints are somatically stable after cloning and (ii) are meiotically stable over several generations. Notably, we found that clonal plants from LO lineages accumulated more changes in DNA methylation than RO lineages. The increases in DNA methylation found in cold-primed LO (Cold-LO) lines were mainly on CG sites, while in cold-primed RO (Cold-RO) lines were mainly on CHH sites. Our results contrast with previous studies carried out on leaves of different plant species, which have shown that cold stress induces DNA hypomethylation in all cytosine contexts (Gutschker et al. 2022; Song et al. 2020). However, it is likely that not all cold-induced DNA methylation changes are meiotically stable. We favour the hypothesis that cold induces both hyper- and hypomethylation in all contexts, but only hypermethylated DMRs are stable during cloning and sexual reproduction. In *Arabidopsis*, salt stress has been linked to the intergenerational transmission of DNA hypermethylation (Bilichak et al. 2012) and DNA hypomethylation (Wibowo et al. 2016). Recent studies have shown that aphid feeding induces the loss of DNA methylation, mostly at TEs, that alters the expression of plant immunity genes (Annacondia et al. 2021). Similarly, several studies have shown a correlation between DNA hypomethylation at TEs and the activity of pathogen resistance genes that is associated with heritable resistance against bacterial and fungal pathogens (Cooper and Ton 2022; López Sánchez et al. 2016). Recent studies have shown that the hypomethylation of TEs is linked to transgenerational adaptive responses against pathogen attack (Furci et al. 2019).

In *Arabidopsis*, DNA methylation is mainly found at transposable elements and repetitive sequences, and only 5% is found in upstream promoter regions (Zilberman et al. 2007). Our methylome data shows that the differentially methylated regions (DMRs) associated with transgenerational memory are found primarily in intergenic regions or inside genes. We found that hypermethylated CGs in Cold-LO clones are more enriched in the intergenic regions followed by gene bodies, and

hypermethylated CHHs in Cold-RO clones were mainly found upstream or downstream of genes. We identified differentially methylated genes (DMGs) that were found near DMRs and found that this overlap was greater in LO clonal lineages than in RO clonal lineages. Our data also showed a stronger correlation between DNA hypermethylation and transcriptional changes in LO clonal lines than in RO clonal lines. Our data also reinforce the view that in plants DNA methylation of intergenic sequences, primarily transposable elements and repeats, has a dynamic role in modulating gene expression (Zhang et al. 2018). Intriguingly, we found that several cold memory genes accumulate gene-body DNA methylation, which has been also implicated in gene regulation (Kawakatsu et al. 2016).

Our analysis has revealed that Cold-LO clonal lineages display profound transcriptional changes under stress-free conditions, affecting several known COR genes, which we defined as memory genes (Baurle and Trindade 2020; Byun et al. 2014) (figure 6.2A). We also found evidence for primed or augmented transcriptional response genes after clonal plants were challenged with a brief cold treatment. While some genes displayed the expected transcriptional response to cold, some others showed the characteristic of primed response genes with substantial changes in expression in response to a brief cold challenge (figure 6.2B). Our data suggest that cold-primed genes in clonal plants have acquired distinct epigenetic modifications that could affect transcription. Some of these modifications may include changes in chromatin, as reported for transgenerational thermomemory in Arabidopsis (Liu et al. 2019). Therefore, it would be interesting to measure the epigenetic changes, DNA methylation and histone modifications, present in cold-primed genes before and after stress challenge. Also, to prove that all changes in both transcriptomic and epigenetic levels increase plant adaptability in response to cold stress, the phenotypic measurements, such as freezing tolerance assays or electrolyte leakage assays, are also necessary.

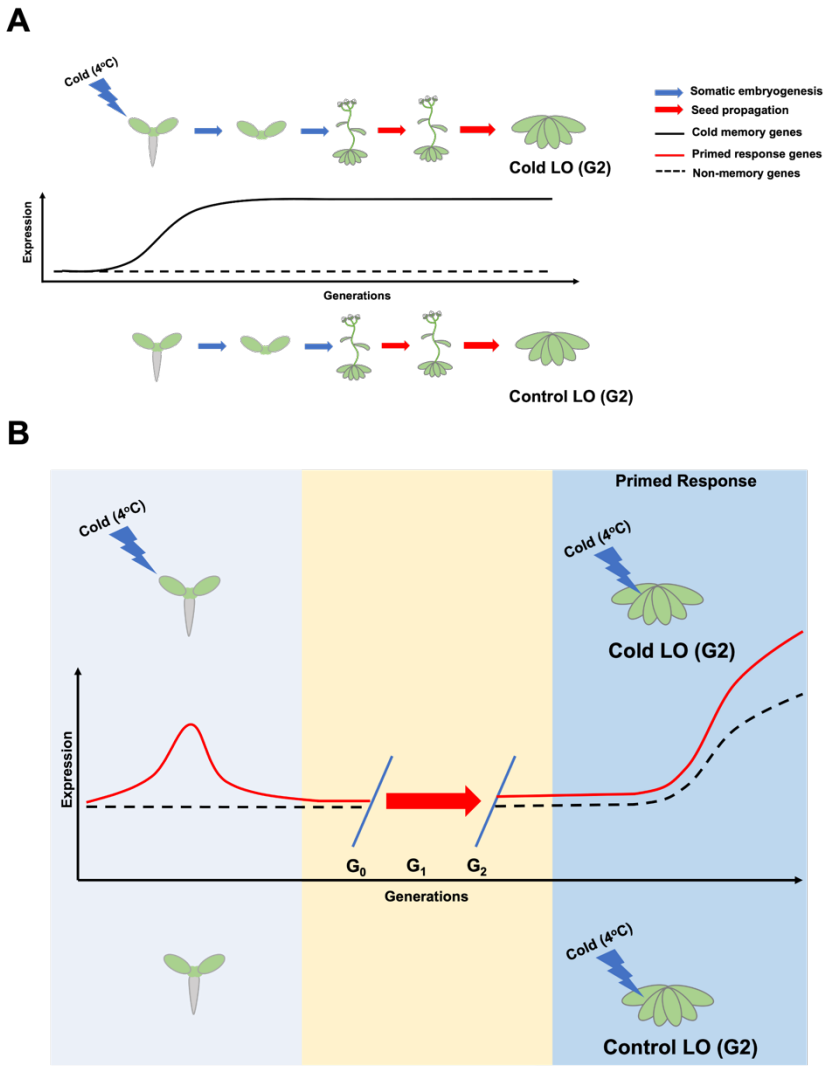

Figure 6.2 The schematic diagram showing the hypothetical models for transgenerational cold memory genes (A) and primed response genes (B) from regenerated plant lineages from cold-treated parents. Cold treatment during somatic embryogenesis induces transcriptomic and epigenetic changes, which could be integrated as cold memory. Cold memory genes are identified by quantifying expression differences in independent clonal lineages (G2) grown under stress-free conditions. Primed response genes are identified by quantifying expression differences in independent clonal lineages (G2) challenged with cold. This approach will also assess the transgenerational stability in clonal lineages of cold memory and primed response genes. Blue arrows indicate somatic embryogenesis. Red arrows indicate reproduction by seed propagation. The black line refers to the expression profile of cold memory genes. The Red line refers to the primed response genes. Black dashed lines indicate non-memory genes.

6.3 CBF Activity is Necessary for a Transgenerational Cold Stress Memory Response in Clonal Plants

Our study shows that cold treatment during clonal propagation via somatic embryogenesis results in a stable transgenerational cold stress memory associated with epigenetic inheritance. The necessity of de novo DNA methylation directed by the RdDM pathway to establish a heritable stress memory has been reported in previous studies (Boyko et al. 2010). However, the capacity of somatic cells to integrate and transmit epigenetic changes directed by environmental stress has never been investigated. We hypothesised that in somatic cells, stress could activate defined transcriptional networks and enable epigenetic changes that can be propagated to clonal plants ultimately via sexual reproduction across multiple generations. This hypothesis is supported by previous studies that have shown that some transcription factors can direct epigenetic modifications (Fan and Huang 2021; Héberlé and Bardet 2019; Kribelbauer et al. 2020). To dissect the necessity of transcription to establish a heritable stress memory, we generated amiRNA-cbf lines to interfere with *CBF1-3* (*CBFs*) during cold stress and cloning but allowed us to restore CBF function in subsequent sexual generations. Our results confirmed our previous work that showed that LO cold memory (LCM) genes are stable across two cycles of sexual reproduction (See Chapter 4). LCM genes contained a significant proportion of cold-regulated genes, some of which are also regulated by *CBF* transcription factors (Song et al. 2021). However, the number of LCM genes was profoundly reduced when we cloned lines using cold-treated amiRNA-cbf plants and CBF function was later restored (L*CM genes). Notably, L*CM genes were substantially depleted in *COR* genes and *CBF*-regulated genes. Our results indicate *CBF* action is necessary to establish a heritable cold stress memory. Notably, the activity of *CBFs* is also necessary for cold acclimation and freezing tolerance (Jia et al. 2016). Similar effects have been reported for transcription factors that modulate light-mediated responses and are necessary for stress memory (Hong et al. 2003). However, the changes in transcriptomic levels of these studies have not been elucidated. A clear example would be the requirement of ATAF-1 transcription factor activity for heat acclimation (Alshareef et al. 2022).

To independently validate our observations, we generated transgenic lines that could enable the inducible ectopic activation of CBF3 (indCBF3). We found that indCBF3 had the ability to induce several CBF3 downstream target genes (Fowler and Thomashow 2002; Gilmour et al. 2000) but independently of cold treatment. We found

that the number of LCM genes misregulated in clonal lines derived from plants expressing CBF3 under control temperature conditions was significantly lower than wild-type plants treated with cold. This incomplete stress memory response may be because the expression of *CBF1-2* is required to activate a broader number of genes in the cold-responsive pathway. Moreover, cold stress may be required to introduce chromatin changes to license transcription factor activity (see Chapter 3) (Kwon et al. 2009).

6.4 Concluding Remarks and Future Works

In summary, our data reveal two important components of the cold adaptation response in plants – (i) ICE1 has a minor role in the cold-responsive pathway and (ii) clonal plants have the capacity of integrating transgenerational stress memory responses to enhance their tolerance to cold-mediated stress.

Although our data show that ICE1 has a minor role in regulating the activation of CBFs in response to cold, it has the capacity to modulate COR genes. Intriguingly, some COR genes appear to be independently regulated by ICE1 and CBFs, thus pointing to a complex interplay of regulatory components in the cold-responsive pathway. We found that low temperatures induce the removal of repressive histone marks that accumulate in cold-regulated genes under control temperature conditions. The removal of these chromatin marks is necessary for the transcriptional activity of ICE1 on direct targets. To uncover the relationship between ICE1 activity and histone modifications, future experiments should investigate the transcriptional and chromatin changes in amiR-ice1 and histone demethylases.

Our study also revealed the existence of a stable transgenerational cold memory in clonal plants that are associated with enhanced transcriptional and phenotypic responses to cold challenges. Intriguingly, this stress memory was greater in clonal lines derived from cold-treated leaves than roots, indicating that the capacity to integrate epigenetic imprints directed by stress differs between cell types. The model of transgenerational cold memory and primed response genes agrees with recent reports on somatic stress memory. Notably, our data suggest that induced stress memory in clonal plants requires the transcriptional activation of cold transcriptional pathways. Further studies should focus on elucidating the characteristics of cold memory genes and the interplay between transcriptional and epigenetic regulation in stress memory responses.

References

Alberts, B., Johnson, A., Lewis, J., Raff, M., Roberts, K., & Walter, P. (2002). Molecular Biology of the Cell. New York: Garland Science.

Alshareef NO, Otterbach SL, Allu AD, Woo YH, de Werk T, Kamranfar I, Mueller-Roeber B, Tester M, Balazadeh S, Schmöckel SM (2022) NAC transcription factors ATAF1 and ANAC055 affect the heat stress response in Arabidopsis. Scientific Reports 12 (1):11264. doi:10.1038/s41598-022-14429-x

Annacondia ML, Markovic D, Reig-Valiente JL, Scaltsoyiannes V, Pieterse CMJ, Ninkovic V, Slotkin RK, Martinez G (2021) Aphid feeding induces the relaxation of epigenetic control and the associated regulation of the defense response in Arabidopsis. New Phytologist 230 (3):1185-1200. doi:https://doi.org/10.1111/nph.17226

Antunez-Sanchez J, Naish M, Ramirez-Prado JS, Ohno S, Huang Y, Dawson A, Opassathian K, Manza-Mianza D, Ariel F, Raynaud C, Wibowo A, Daron J, Ueda M, Latrasse D, Slotkin RK, Weigel D, Benhamed M, Gutierrez-Marcos J (2020a) A new role for histone demethylases in the maintenance of plant genome integrity. eLife 9:e58533. doi:10.7554/eLife.58533

Antunez-Sanchez J, Naish M, Ramirez-Prado JS, Ohno S, Huang Y, Dawson A, Opassathian K, Manza-Mianza D, Ariel F, Raynaud C, Wibowo A, Daron J, Ueda M, Latrasse D, Slotkin RK, Weigel D, Benhamed M, Gutierrez-Marcos J (2020b) A new role for histone demethylases in the maintenance of plant genome integrity. Elife 9. doi:10.7554/eLife.58533

Ariel F, Jegu T, Latrasse D, Romero-Barrios N, Christ A, Benhamed M, Crespi M (2014) Noncoding transcription by alternative RNA polymerases dynamically regulates an auxin-driven chromatin loop. Mol Cell 55 (3):383-396. doi:10.1016/j.molcel.2014.06.011

Ariel F, Romero-Barrios N, Jégu T, Benhamed M, Crespi M (2015) Battles and hijacks: noncoding transcription in plants. Trends Plant Sci 20 (6):362-371. doi:10.1016/j.tplants.2015.03.003

Bailey T (2020) STREME: Accurate and versatile sequence motif discovery. doi:10.1101/2020.11.23.394619

Baubec T, Finke A, Mittelsten Scheid O, Pecinka A (2014) Meristem-specific expression of epigenetic regulators safeguards transposon silencing in Arabidopsis. EMBO reports 15 (4):446-452. doi:https://doi.org/10.1002/embr.201337915

Baurle I, Trindade I (2020) Chromatin regulation of somatic abiotic stress memory. J Exp Bot 71 (17):5269-5279. doi:10.1093/jxb/eraa098

Bell O, Tiwari VK, Thomä NH, Schübeler D (2011) Determinants and dynamics of genome accessibility. Nature Reviews Genetics 12 (8):554-564. doi:10.1038/nrg3017

Benedict C, Geisler M, Trygg J, Huner N, Hurry V (2006) Consensus by Democracy. Using Meta-Analyses of Microarray and Genomic Data to Model the Cold

Acclimation Signaling Pathway in Arabidopsis. Plant Physiology 141 (4):1219-1232. doi:10.1104/pp.106.083527

Bicknell RA, Koltunow AM (2004) Understanding apomixis: recent advances and remaining conundrums. Plant Cell 16 Suppl:S228-245. doi:10.1105/tpc.017921

Bilichak A, Ilnystkyy Y, Hollunder J, Kovalchuk I (2012) The Progeny of Arabidopsis thaliana Plants Exposed to Salt Exhibit Changes in DNA Methylation, Histone Modifications and Gene Expression. PLOS ONE 7 (1):e30515. doi:10.1371/journal.pone.0030515

Bilichak A, Ilnytskyy Y, Wóycicki R, Kepeshchuk N, Fogen D, Kovalchuk I (2015) The elucidation of stress memory inheritance in Brassica rapa plants. Frontiers in Plant Science 6. doi:10.3389/fpls.2015.00005

Bohmdorfer G, Wierzbicki AT (2015) Control of Chromatin Structure by Long Noncoding RNA. Trends Cell Biol 25 (10):623-632. doi:10.1016/j.tcb.2015.07.002

Boycheva I, Vassileva V, Iantcheva A (2014) Histone acetyltransferases in plant development and plasticity. Current genomics 15 (1):28-37. doi:10.2174/1389202915011403061127 42

Boyko A, Blevins T, Yao Y, Golubov A, Bilichak A, Ilnytskyy Y, Hollander J, Meins F, Jr., Kovalchuk I (2010) Transgenerational Adaptation of Arabidopsis to Stress Requires DNA Methylation and the Function of Dicer-Like Proteins. PLOS ONE 5 (3):e9514. doi:10.1371/journal.pone.0009514

Bradamante G, Mittelsten Scheid O, Incarbone M (2021) Under siege: virus control in plant meristems and progeny. The Plant Cell 33 (8):2523-2537. doi:10.1093/plcell/koab140

Bruce TJA, Matthes MC, Napier JA, Pickett JA (2007) Stressful "memories" of plants: Evidence and possible mechanisms. Plant Science 173 (6):603-608. doi:https://doi.org/10.1016/j.plantsci.2007.09.002

Brzezinka K, Altmann S, Czesnick H, Nicolas P, Gorka M, Benke E, Kabelitz T, Jähne F, Graf A, Kappel C, Bäurle I (2016) Arabidopsis FORGETTER1 mediates stress-induced chromatin memory through nucleosome remodeling. eLife 5:e17061. doi:10.7554/eLife.17061

Byun Y-J, Koo M-Y, Joo H-J, Ha-Lee Y-M, Lee D-H (2014) Comparative analysis of gene expression under cold acclimation, deacclimation and reacclimation in Arabidopsis. Physiologia Plantarum 152 (2):256-274. doi:https://doi.org/10.1111/ppl.12163

Calarco JP, Borges F, Donoghue MT, Van Ex F, Jullien PE, Lopes T, Gardner R, Berger F, Feijo JA, Becker JD, Martienssen RA (2012) Reprogramming of DNA methylation in pollen guides epigenetic inheritance via small RNA. Cell 151 (1):194-205. doi:10.1016/j.cell.2012.09.001

Catoni M, Tsang JM, Greco AP, Zabet Nicolae R (2018) DMRcaller: a versatile R/Bioconductor package for detection and visualization of differentially methylated regions in CpG and non-CpG contexts. Nucleic Acids Research 46 (19):e114-e114. doi:10.1093/nar/gky602

Chan Z, Wang Y, Cao M, Gong Y, Mu Z, Wang H, Hu Y, Deng X, He X-J, Zhu J-K (2016) RDM4 modulates cold stress resistance in Arabidopsis partially through the CBF-mediated pathway. New Phytologist 209 (4):1527-1539. doi:https://doi.org/10.1111/nph.13727

Chen S, Zhou Y, Chen Y, Gu J (2018) fastp: an ultra-fast all-in-one FASTQ preprocessor. Bioinformatics 34 (17):i884-i890

Chinnusamy V, Ohta M, Kanrar S, Lee BH, Hong X, Agarwal M, Zhu JK (2003) ICE1: a regulator of cold-induced transcriptome and freezing tolerance in Arabidopsis. Genes Dev 17 (8):1043-1054. doi:10.1101/gad.1077503

Chinnusamy V, Zhu JK (2009) Epigenetic regulation of stress responses in plants. Curr Opin Plant Biol 12 (2):133-139. doi:10.1016/j.pbi.2008.12.006

Cho, JW., Shim, H.S., Lee, C.Y. *et al.* The importance of enhancer methylation for epigenetic regulation of tumorigenesis in squamous lung cancer. *Exp Mol Med* **54**, 12–22 (2022). https://doi.org/10.1038/s12276-021-00718-4

Choi Y, Gehring M, Johnson L, Hannon M, Harada JJ, Goldberg RB, Jacobsen SE, Fischer RL (2002) DEMETER, a DNA glycosylase domain protein, is required for endosperm gene imprinting and seed viability in arabidopsis. Cell 110 (1):33-42

Clapier CR, Cairns BR (2009) The biology of chromatin remodeling complexes. Annu Rev Biochem 78:273-304. doi:10.1146/annurev.biochem.77.062706.153223

Cong W, Miao Y, Xu L, Zhang Y, Yuan C, Wang J, Zhuang T, Lin X, Jiang L, Wang N, Ma J, Sanguinet KA, Liu B, Rustgi S, Ou X (2019) Transgenerational memory of gene expression changes induced by heavy metal stress in rice (Oryza sativa L.). BMC Plant Biology 19 (1):282. doi:10.1186/s12870-019-1887-7

Cooper A, Ton J (2022) Immune priming in plants: from the onset to transgenerational maintenance. Essays in Biochemistry 66 (5):635-646. doi:10.1042/ebc20210082

Crisp PA, Ganguly D, Eichten SR, Borevitz JO, Pogson BJ (2016) Reconsidering plant memory: Intersections between stress recovery, RNA turnover, and epigenetics. Science Advances 2 (2):e1501340. doi:doi:10.1126/sciadv.1501340

De Lucia F, Crevillen P, Jones AM, Greb T, Dean C (2008) A PHD-polycomb repressive complex 2 triggers the epigenetic silencing of FLC during vernalization. Proc Natl Acad Sci U S A 105 (44):16831-16836. doi:10.1073/pnas.0808687105

Denay G, Creff A, Moussu S, Wagnon P, Thevenin J, Gerentes MF, Chambrier P, Dubreucq B, Ingram G (2014) Endosperm breakdown in Arabidopsis requires heterodimers of the basic helix-loop-helix proteins ZHOUPI and INDUCER OF CBP EXPRESSION 1. Development 141 (6):1222-1227. doi:10.1242/dev.103531

Ding Y, Fromm M, Avramova Z (2012) Multiple exposures to drought 'train' transcriptional responses in Arabidopsis. Nature Communications 3 (1):740. doi:10.1038/ncomms1732

Ding Y, Li H, Zhang X, Xie Q, Gong Z, Yang S (2015a) OST1 kinase modulates freezing tolerance by enhancing ICE1 stability in Arabidopsis. Dev Cell 32 (3):278-289. doi:10.1016/j.devcel.2014.12.023

Ding Y, Li H, Zhang X, Xie Q, Gong Z, Yang S (2015b) OST1 Kinase Modulates Freezing Tolerance by Enhancing ICE1 Stability in Arabidopsis. Developmental Cell 32 (3):278-289. doi:https://doi.org/10.1016/j.devcel.2014.12.023

Ding Y, Shi Y, Yang S (2019) Advances and challenges in uncovering cold tolerance regulatory mechanisms in plants. New Phytol 222 (4):1690-1704. doi:10.1111/nph.15696

Dobin A, Davis CA, Schlesinger F, Drenkow J, Zaleski C, Jha S, Batut P, Chaisson M, Gingeras TR (2013) STAR: ultrafast universal RNA-seq aligner. Bioinformatics 29 (1):15-21

Doherty CJ, Van Buskirk HA, Myers SJ, Thomashow MF (2009) Roles for Arabidopsis CAMTA transcription factors in cold-regulated gene expression and freezing tolerance. Plant Cell 21 (3):972-984. doi:10.1105/tpc.108.063958

Dong CH, Agarwal M, Zhang Y, Xie Q, Zhu JK (2006) The negative regulator of plant cold responses, HOS1, is a RING E3 ligase that mediates the ubiquitination and degradation of ICE1. Proc Natl Acad Sci U S A 103 (21):8281-8286. doi:10.1073/pnas.0602874103

Dong MA, Farré EM, Thomashow MF (2011) Circadian clock-associated 1 and late elongated hypocotyl regulate expression of the C-repeat binding factor (CBF) pathway in Arabidopsis. Proc Natl Acad Sci U S A 108 (17):7241-7246. doi:10.1073/pnas.1103741108

Ewels P, Magnusson M, Lundin S, Käller M (2016) MultiQC: summarize analysis results for multiple tools and samples in a single report. Bioinformatics 32 (19):3047-3048

Fan T, Huang Y (2021) Accessible chromatin reveals regulatory mechanisms underlying cell fate decisions during early embryogenesis. Scientific Reports 11 (1):7896. doi:10.1038/s41598-021-86919-3

Feng S, Jacobsen SE, Reik W (2010) Epigenetic reprogramming in plant and animal development. Science 330 (6004):622-627. doi:10.1126/science.1190614

Fowler S, Thomashow MF (2002) Arabidopsis transcriptome profiling indicates that multiple regulatory pathways are activated during cold acclimation in addition to the CBF cold response pathway. Plant Cell 14 (8):1675-1690. doi:10.1105/tpc.003483

Furci L, Jain R, Stassen J, Berkowitz O, Whelan J, Roquis D, Baillet V, Colot V, Johannes F, Ton J (2019) Identification and characterisation of hypomethylated DNA loci controlling quantitative resistance in Arabidopsis. eLife 8:e40655. doi:10.7554/eLife.40655

Gagliardi D, Cambiagno DA, Arce AL, Tomassi AH, Giacomelli JI, Ariel FD, Manavella PA (2019) Dynamic regulation of chromatin topology and transcription by inverted repeat-derived small RNAs in sunflower.

Proceedings of the National Academy of Sciences 116 (35):17578-17583. doi:doi:10.1073/pnas.1903131116

Gan E-S, Xu Y, Wong J-Y, Geraldine Goh J, Sun B, Wee W-Y, Huang J, Ito T (2014) Jumonji demethylases moderate precocious flowering at elevated temperature via regulation of FLC in Arabidopsis. Nature Communications 5 (1):5098. doi:10.1038/ncomms6098

Ganguly DR, Crisp PA, Eichten SR, Pogson BJ (2017) The Arabidopsis DNA Methylome Is Stable under Transgenerational Drought Stress. Plant Physiol 175 (4):1893-1912. doi:10.1104/pp.17.00744

Gao Z, Liu HL, Daxinger L, Pontes O, He X, Qian W, Lin H, Xie M, Lorkovic ZJ, Zhang S, Miki D, Zhan X, Pontier D, Lagrange T, Jin H, Matzke AJ, Matzke M, Pikaard CS, Zhu JK (2010) An RNA polymerase II- and AGO4-associated protein acts in RNA-directed DNA methylation. Nature 465 (7294):106-109. doi:10.1038/nature09025

Gilmour SJ, Fowler SG, Thomashow MF (2004a) Arabidopsis Transcriptional Activators CBF1, CBF2, and CBF3 have Matching Functional Activities. Plant Molecular Biology 54 (5):767-781. doi:10.1023/B:PLAN.0000040902.06881.d4

Gilmour SJ, Fowler SG, Thomashow MF (2004b) Arabidopsis transcriptional activators CBF1, CBF2, and CBF3 have matching functional activities. Plant molecular biology 54 (5):767-781. doi:10.1023/B:PLAN.0000040902.06881.d4

Gilmour SJ, Sebolt AM, Salazar MP, Everard JD, Thomashow MF (2000) Overexpression of the Arabidopsis CBF3 transcriptional activator mimics multiple biochemical changes associated with cold acclimation. Plant Physiol 124 (4):1854-1865. doi:10.1104/pp.124.4.1854

Gilmour SJ, Zarka DG, Stockinger EJ, Salazar MP, Houghton JM, Thomashow MF (1998) Low temperature regulation of the Arabidopsis CBF family of AP2 transcriptional activators as an early step in cold-induced COR gene expression. Plant J 16 (4):433-442. doi:10.1046/j.1365-313x.1998.00310.x

Gong Z, Morales-Ruiz T, Ariza RR, Roldan-Arjona T, David L, Zhu JK (2002) ROS1, a repressor of transcriptional gene silencing in Arabidopsis, encodes a DNA glycosylase/lyase. Cell 111 (6):803-814

Gonzalez AP, Chrtek J, Dobrev PI, Dumalasova V, Fehrer J, Mraz P, Latzel V (2016) Stress-induced memory alters growth of clonal offspring of white clover (Trifolium repens). Am J Bot 103 (9):1567-1574. doi:10.3732/ajb.1500526

González APR, Dumalasová V, Rosenthal J, Skuhrovec J, Latzel V (2016) The role of transgenerational effects in adaptation of clonal offspring of white clover (Trifolium repens) to drought and herbivory. Evolutionary Ecology 31 (3):345-361. doi:10.1007/s10682-016-9844-5

Grimanelli D, Ingouff M (2020) DNA Methylation Readers in Plants. Journal of Molecular Biology 432 (6):1706-1717. doi:https://doi.org/10.1016/j.jmb.2019.12.043

Gu Z, Eils R, Schlesner M, Ishaque N (2018) EnrichedHeatmap: an R/Bioconductor package for comprehensive visualization of genomic signal associations. BMC genomics 19 (1):1-7

Guo M, Liu X, Jiang Y, Yu J, Meng T (2021) Identification Of Arabidopsis genes associated with cold tolerance based on integrated bioinformatics analysis. Journal of Plant Interactions 16 (1):344-353. doi:10.1080/17429145.2021.1955164

Gutschker S, Corral JM, Schmiedl A, Ludewig F, Koch W, Fiedler-Wiechers K, Czarnecki O, Harms K, Keller I, Martins Rodrigues C, Pommerrenig B, Neuhaus HE, Zierer W, Sonnewald U, Müdsam C (2022) Multi-omics data integration reveals link between epigenetic modifications and gene expression in sugar beet (Beta vulgaris subsp. vulgaris) in response to cold. BMC Genomics 23 (1):144. doi:10.1186/s12864-022-08312-2

Gutzat R, Rembart K, Nussbaumer T, Hofmann F, Pisupati R, Bradamante G, Daubel N, Gaidora A, Lettner N, Donà M, Nordborg M, Nodine M, Mittelsten Scheid O (2020) Arabidopsis shoot stem cells display dynamic transcription and DNA methylation patterns. The EMBO Journal 39 (20):e103667. doi:https://doi.org/10.15252/embj.2019103667

Haake V, Cook D, Riechmann JL, Pineda O, Thomashow MF, Zhang JZ (2002) Transcription factor CBF4 is a regulator of drought adaptation in Arabidopsis. Plant Physiol 130 (2):639-648. doi:10.1104/pp.006478

Han M, Grunstein M (1988) Nucleosome loss activates yeast downstream promoters in vivo. Cell 55 (6):1137-1145

Hannah MA, Heyer AG, Hincha DK (2005) A Global Survey of Gene Regulation during Cold Acclimation in Arabidopsis thaliana. PLOS Genetics 1 (2):e26. doi:10.1371/journal.pgen.0010026

Hannan Parker A, Wilkinson SW, Ton J (2022) Epigenetics: a catalyst of plant immunity against pathogens. New Phytologist 233 (1):66-83. doi:https://doi.org/10.1111/nph.17699

Harris CJ, Scheibe M, Wongpalee SP, Liu W, Cornett EM, Vaughan RM, Li X, Chen W, Xue Y, Zhong Z, Yen L, Barshop WD, Rayatpisheh S, Gallego-Bartolome J, Groth M, Wang Z, Wohlschlegel JA, Du J, Rothbart SB, Butter F, Jacobsen SE (2018) A DNA methylation reader complex that enhances gene transcription. Science 362 (6419):1182-1186. doi:10.1126/science.aar7854

Hassan MA, Xiang C, Farooq M, Muhammad N, Yan Z, Hui X, Yuanyuan K, Bruno AK, Lele Z, Jincai L (2021) Cold Stress in Wheat: Plant Acclimation Responses and Management Strategies. Frontiers in Plant Science 12. doi:10.3389/fpls.2021.676884

Hauser M-T, Aufsatz W, Jonak C, Luschnig C (2011a) Transgenerational epigenetic inheritance in plants. Biochimica et Biophysica Acta (BBA) - Gene Regulatory Mechanisms 1809 (8):459-468. doi:https://doi.org/10.1016/j.bbagrm.2011.03.007

Hauser MT, Aufsatz W, Jonak C, Luschnig C (2011b) Transgenerational epigenetic inheritance in plants. Biochim Biophys Acta 1809 (8):459-468. doi:10.1016/j.bbagrm.2011.03.007

He K, Mei H, Zhu J, Qiu Q, Cao X, Deng X (2021) The histone H3K27 demethylase REF6/JMJ12 promotes thermomorphogenesis in Arabidopsis. National Science Review 9 (5). doi:10.1093/nsr/nwab213

He XJ, Chen T, Zhu JK (2011) Regulation and function of DNA methylation in plants and animals. Cell Res 21 (3):442-465. doi:10.1038/cr.2011.23

Héberlé É, Bardet AF (2019) Sensitivity of transcription factors to DNA methylation. Essays Biochem 63 (6):727-741. doi:10.1042/ebc20190033

Higo A, Saihara N, Miura F, Higashi Y, Yamada M, Tamaki S, Ito T, Tarutani Y, Sakamoto T, Fujiwara M, Kurata T, Fukao Y, Moritoh S, Terada R, Kinoshita T, Ito T, Kakutani T, Shimamoto K, Tsuji H (2020) DNA methylation is reconfigured at the onset of reproduction in rice shoot apical meristem. Nature Communications 11 (1):4079. doi:10.1038/s41467-020-17963-2

Hong S-W, Lee U, Vierling E (2003) Arabidopsis hot Mutants Define Multiple Functions Required for Acclimation to High Temperatures. Plant Physiology 132 (2):757-767. doi:10.1104/pp.102.017145

Hung F-Y, Lai Y-C, Wang J, Feng Y-R, Shih Y-H, Chen J-H, Sun H-C, Yang S, Li C, Wu K (2021) The Arabidopsis histone demethylase JMJ28 regulates CONSTANS by interacting with FBH transcription factors. The Plant Cell 33 (4):1196-1211. doi:10.1093/plcell/koab014

Hung F-Y, Shih Y-H, Lin P-Y, Feng Y-R, Li C, Wu K (2022) WRKY63 transcriptional activation of COOLAIR and COLDAIR regulates vernalization-induced flowering. Plant Physiology 190 (1):532-547. doi:10.1093/plphys/kiac295

Hwarari D, Guan Y, Ahmad B, Movahedi A, Min T, Hao Z, Lu Y, Chen J, Yang L (2022) ICE-CBF-COR Signaling Cascade and Its Regulation in Plants Responding to Cold Stress. Int J Mol Sci 23 (3). doi:10.3390/ijms23031549

Jakoby M, Weisshaar B, Dröge-Laser W, Vicente-Carbajosa J, Tiedemann J, Kroj T, Parcy F, b ZIPRG (2002) bZIP transcription factors in Arabidopsis. Trends in plant science 7 (3):106-111. doi:10.1016/s1360-1385(01)02223-3

Jha UC, Nayyar H, Jha R, Khurshid M, Zhou M, Mantri N, Siddique KHM (2020) Long non-coding RNAs: emerging players regulating plant abiotic stress response and adaptation. BMC Plant Biol 20 (1):466. doi:10.1186/s12870-020-02595-x

Jia Y, Ding Y, Shi Y, Zhang X, Gong Z, Yang S (2016) The cbfs triple mutants reveal the essential functions of CBFs in cold acclimation and allow the definition of CBF regulons in Arabidopsis. New Phytologist 212 (2):345-353. doi:https://doi.org/10.1111/nph.14088

Jiang B, Shi Y, Zhang X, Xin X, Qi L, Guo H, Li J, Yang S (2017) PIF3 is a negative regulator of the *CBF* pathway and freezing tolerance in *Arabidopsis*. Proceedings of the National Academy of Sciences 114 (32):E6695-E6702. doi:doi:10.1073/pnas.1706226114

Jin R, Klasfeld S, Zhu Y, Fernandez Garcia M, Xiao J, Han S-K, Konkol A, Wagner D (2021) LEAFY is a pioneer transcription factor and licenses cell reprogramming to floral fate. Nature Communications 12 (1):626. doi:10.1038/s41467-020-20883-w

Jung JH, Domijan M, Klose C, Biswas S, Ezer D, Gao M, Khattak AK, Box MS, Charoensawan V, Cortijo S, Kumar M, Grant A, Locke JC, Schäfer E, Jaeger KE, Wigge PA (2016) Phytochromes function as thermosensors in Arabidopsis. Science 354 (6314):886-889. doi:10.1126/science.aaf6005

Kanaoka MM, Pillitteri LJ, Fujii H, Yoshida Y, Bogenschutz NL, Takabayashi J, Zhu JK, Torii KU (2008) SCREAM/ICE1 and SCREAM2 specify three cell-state transitional steps leading to arabidopsis stomatal differentiation. Plant Cell 20 (7):1775-1785. doi:10.1105/tpc.108.060848

Kang CH, Lee YM, Park JH, Nawkar GM, Oh HT, Kim MG, Lee SI, Kim WY, Yun D-J, Lee SY (2016) Ribosomal P3 protein AtP3B of Arabidopsis acts as both protein and RNA chaperone to increase tolerance of heat and cold stresses. Plant, Cell & Environment 39 (7):1631-1642. doi:https://doi.org/10.1111/pce.12742

Kanno T, Bucher E, Daxinger L, Huettel B, Kreil D, Breinig F, Lind M, Schmitt M, Simon S, Gurazada G, Meyers B, Lorković Z, Matzke A, Matzke M (2009) RNA-directed DNA methylation and plant development require an IWR1-type transcription factor. EMBO reports 11:65-71. doi:10.1038/embor.2009.246

Kaplan F, Guy CL (2005) RNA interference of Arabidopsis beta-amylase8 prevents maltose accumulation upon cold shock and increases sensitivity of PSII photochemical efficiency to freezing stress. The Plant Journal 44 (5):730-743. doi:https://doi.org/10.1111/j.1365-313X.2005.02565.x

Karlson D, Nakaminami K, Toyomasu T, Imai R (2002) A Cold-regulated Nucleic Acid-binding Protein of Winter Wheat Shares a Domain with Bacterial Cold Shock Proteins*. Journal of Biological Chemistry 277 (38):35248-35256. doi:https://doi.org/10.1074/jbc.M205774200

Kawakatsu T, Huang S-sC, Jupe F, Sasaki E, Schmitz RJ, Urich MA, Castanon R, Nery JR, Barragan C, He Y, Chen H, Dubin M, Lee C-R, Wang C, Bemm F, Becker C, O'Neil R, O'Malley RC, Quarless DX, Alonso-Blanco C, Andrade J, Becker C, Bemm F, Bergelson J, Borgwardt K, Chae E, Dezwaan T, Ding W, Ecker JR, Expósito-Alonso M, Farlow A, Fitz J, Gan X, Grimm DG, Hancock A, Henz SR, Holm S, Horton M, Jarsulic M, Kerstetter RA, Korte A, Korte P, Lanz C, Lee C-R, Meng D, Michael TP, Mott R, Muliyati NW, Nägele T, Nagler M, Nizhynska V, Nordborg M, Novikova P, Picó FX, Platzer A, Rabanal FA, Rodriguez A, Rowan BA, Salomé PA, Schmid K, Schmitz RJ, Seren Ü, Sperone FG, Sudkamp M, Svardal H, Tanzer MM, Todd D, Volchenboum SL, Wang C, Wang G, Wang X, Weckwerth W, Weigel D, Zhou X, Schork NJ, Weigel D, Nordborg M, Ecker JR (2016) Epigenomic Diversity in a Global Collection of Arabidopsis thaliana Accessions. Cell 166 (2):492-505. doi:10.1016/j.cell.2016.06.044

Kawarazaki T, Kimura S, Iizuka A, Hanamata S, Nibori H, Michikawa M, Imai A, Abe M, Kaya H, Kuchitsu K (2013) A low temperature-inducible protein AtSRC2 enhances the ROS-producing activity of NADPH oxidase AtRbohF. Biochimica et Biophysica Acta (BBA) - Molecular Cell Research 1833 (12):2775-2780. doi:https://doi.org/10.1016/j.bbamcr.2013.06.024

Kawashima T, Berger F (2014) Epigenetic reprogramming in plant sexual reproduction. Nat Rev Genet 15 (9):613-624. doi:10.1038/nrg3685

Khraiwesh B, Zhu JK, Zhu J (2012) Role of miRNAs and siRNAs in biotic and abiotic stress responses of plants. Biochim Biophys Acta 1819 (2):137-148. doi:10.1016/j.bbagrm.2011.05.001

Kidokoro S, Kim J-S, Ishikawa T, Suzuki T, Shinozaki K, Yamaguchi-Shinozaki K (2020) DREB1A/CBF3 Is Repressed by Transgene-Induced DNA Methylation in the Arabidopsis ice1-1 Mutant[OPEN]. The Plant Cell 32 (4):1035-1048. doi:10.1105/tpc.19.00532

Kidokoro S, Shinozaki K, Yamaguchi-Shinozaki K (2022) Transcriptional regulatory network of plant cold-stress responses. Trends Plant Sci 27 (9):922-935. doi:10.1016/j.tplants.2022.01.008

Kidokoro S, Yoneda K, Takasaki H, Takahashi F, Shinozaki K, Yamaguchi-Shinozaki K (2017) Different Cold-Signaling Pathways Function in the Responses to Rapid and Gradual Decreases in Temperature. Plant Cell 29 (4):760-774. doi:10.1105/tpc.16.00669

Kim DH, Xi Y, Sung S (2017) Modular function of long noncoding RNA, COLDAIR, in the vernalization response. PLoS Genet 13 (7):e1006939. doi:10.1371/journal.pgen.1006939

Kim JM, Sasaki T, Ueda M, Sako K, Seki M (2015a) Chromatin changes in response to drought, salinity, heat, and cold stresses in plants. Front Plant Sci 6:114. doi:10.3389/fpls.2015.00114

Kim Y, Park S, Gilmour SJ, Thomashow MF (2013) Roles of CAMTA transcription factors and salicylic acid in configuring the low-temperature transcriptome and freezing tolerance of Arabidopsis. The Plant Journal 75 (3):364-376. doi:https://doi.org/10.1111/tpj.12205

Kim YS, Lee M, Lee J-H, Lee H-J, Park C-M (2015b) The unified ICE–CBF pathway provides a transcriptional feedback control of freezing tolerance during cold acclimation in Arabidopsis. Plant Molecular Biology 89 (1):187-201. doi:10.1007/s11103-015-0365-3

Kindgren P, Ard R, Ivanov M, Marquardt S (2018a) Transcriptional read-through of the long non-coding RNA SVALKA governs plant cold acclimation. Nat Commun 9 (1):4561. doi:10.1038/s41467-018-07010-6

Kindgren P, Ard R, Ivanov M, Marquardt S (2018b) Transcriptional read-through of the long non-coding RNA SVALKA governs plant cold acclimation. Nature Communications 9 (1):4561. doi:10.1038/s41467-018-07010-6

Knight H, Trewavas AJ, Knight MR (1996) Cold calcium signaling in Arabidopsis involves two cellular pools and a change in calcium signature after acclimation. Plant Cell 8 (3):489-503. doi:10.1105/tpc.8.3.489

Knight MR, Campbell AK, Smith SM, Trewavas AJ (1991) Transgenic plant aequorin reports the effects of touch and cold-shock and elicitors on cytoplasmic calcium. Nature 352 (6335):524-526. doi:10.1038/352524a0

Knight MR, Knight H (2012a) Low-temperature perception leading to gene expression and cold tolerance in higher plants. New Phytol 195 (4):737-751. doi:10.1111/j.1469-8137.2012.04239.x

Knight MR, Knight H (2012b) Low-temperature perception leading to gene expression and cold tolerance in higher plants. New Phytol 195 (4):737-751. doi:10.1111/j.1469-8137.2012.04239.x

Koi S, Hisanaga T, Sato K, Shimamura M, Yamato KT, Ishizaki K, Kohchi T, Nakajima K (2016) An Evolutionarily Conserved Plant RKD Factor Controls Germ Cell Differentiation. Curr Biol 26 (13):1775-1781. doi:10.1016/j.cub.2016.05.013

Kolberg L, Raudvere U, Kuzmin I, Vilo J, Peterson H (2020) gprofiler2--an R package for gene list functional enrichment analysis and namespace conversion toolset g: Profiler. F1000Research 9

Kolde R, Kolde MR (2018) Package 'pheatmap'. R Package 1

Kreps JA, Wu Y, Chang HS, Zhu T, Wang X, Harper JF (2002) Transcriptome changes for Arabidopsis in response to salt, osmotic, and cold stress. Plant Physiol 130 (4):2129-2141. doi:10.1104/pp.008532

Kribelbauer JF, Lu X-J, Rohs R, Mann RS, Bussemaker HJ (2020) Toward a Mechanistic Understanding of DNA Methylation Readout by Transcription Factors. Journal of Molecular Biology 432 (6):1801-1815. doi:https://doi.org/10.1016/j.jmb.2019.10.021

Kumar S (2018) Epigenetic memory of stress responses in plants. J Phytochem Biochem 2 (1)

Kwon CS, Lee D, Choi G, Chung WI (2009) Histone occupancy-dependent and -independent removal of H3K27 trimethylation at cold-responsive genes in Arabidopsis. Plant J 60 (1):112-121. doi:10.1111/j.1365-313X.2009.03938.x

Lafos M, Kroll P, Hohenstatt ML, Thorpe FL, Clarenz O, Schubert D (2011) Dynamic Regulation of H3K27 Trimethylation during Arabidopsis Differentiation. PLOS Genetics 7 (4):e1002040. doi:10.1371/journal.pgen.1002040

Lamke J, Baurle I (2017) Epigenetic and chromatin-based mechanisms in environmental stress adaptation and stress memory in plants. Genome Biol 18 (1):124. doi:10.1186/s13059-017-1263-6

Lämke J, Brzezinka K, Altmann S, Bäurle I (2016) A hit-and-run heat shock factor governs sustained histone methylation and transcriptional stress memory. The EMBO Journal 35 (2):162-175. doi:https://doi.org/10.15252/embj.201592593

Laugesen A, Højfeldt JW, Helin K (2019) Molecular Mechanisms Directing PRC2 Recruitment and H3K27 Methylation. Mol Cell 74 (1):8-18. doi:10.1016/j.molcel.2019.03.011

Lauria M, Rossi V (2011) Epigenetic control of gene regulation in plants. Biochimica et Biophysica Acta (BBA) - Gene Regulatory Mechanisms 1809 (8):369-378. doi:10.1016/j.bbagrm.2011.03.002

Law JA, Jacobsen SE (2010) Establishing, maintaining and modifying DNA methylation patterns in plants and animals. Nat Rev Genet 11 (3):204-220. doi:10.1038/nrg2719

Lawrence II S, Pang Q, Kong W, Chen S (2018) Stomata tape-peel: an improved method for guard cell sample preparation. JoVE (Journal of Visualized Experiments) (137):e57422

Lee BH, Henderson DA, Zhu JK (2005) The Arabidopsis cold-responsive transcriptome and its regulation by ICE1. Plant Cell 17 (11):3155-3175. doi:10.1105/tpc.105.035568

Li H, Ding Y, Shi Y, Zhang X, Zhang S, Gong Z, Yang S (2017) MPK3- and MPK6-Mediated ICE1 Phosphorylation Negatively Regulates ICE1 Stability and Freezing Tolerance in Arabidopsis. Developmental Cell 43 (5):630-642.e634. doi:https://doi.org/10.1016/j.devcel.2017.09.025

Li H, Testerink C, Zhang Y (2021) How roots and shoots communicate through stressful times. Trends in Plant Science 26 (9):940-952. doi:10.1016/j.tplants.2021.03.005

Li Y, Quan C, Yang S, Wu S, Shi M, Wang J, Tian W (2022) Functional Identification of ICE Transcription Factors in Rubber Tree. Forests 13 (1). doi:10.3390/f13010052

Liang CH, Yang CC (2015) Identification of ICE1 as a negative regulator of ABA-dependent pathways in seeds and seedlings of Arabidopsis. Plant Mol Biol 88 (4-5):459-470. doi:10.1007/s11103-015-0335-9

Lim CJ, Park J, Shen M, Park HJ, Cheong MS, Park KS, Baek D, Bae MJ, Ali A, Jan M, Lee SY, Lee B-h, Kim W-Y, Pardo JM, Yun D-J (2020) The Histone-Modifying Complex PWR/HOS15/HD2C Epigenetically Regulates Cold Tolerance Plant Physiology 184 (2):1097-1111. doi:10.1104/pp.20.00439

Liu C, Lu F, Cui X, Cao X (2010a) Histone methylation in higher plants. Annu Rev Plant Biol 61:395-420. doi:10.1146/annurev.arplant.043008.091939

Liu H-c, Charng Y-y (2013) Common and Distinct Functions of Arabidopsis Class A1 and A2 Heat Shock Factors in Diverse Abiotic Stress Responses and Development Plant Physiology 163 (1):276-290. doi:10.1104/pp.113.221168

Liu J, Feng L, Gu X, Deng X, Qiu Q, Li Q, Zhang Y, Wang M, Deng Y, Wang E, He Y, Baurle I, Li J, Cao X, He Z (2019a) An H3K27me3 demethylase-HSFA2 regulatory loop orchestrates transgenerational thermomemory in Arabidopsis. Cell Res 29 (5):379-390. doi:10.1038/s41422-019-0145-8

Liu L, Duan L, Zhang J, Zhang Z, Mi G, Ren H (2010b) Cucumber (Cucumis sativus L.) over-expressing cold-induced transcriptome regulator ICE1 exhibits changed morphological characters and enhances chilling tolerance. Scientia Horticulturae 124 (1):29-33. doi:10.1016/j.scienta.2009.11.018

Liu N, Fromm M, Avramova Z (2014) H3K27me3 and H3K4me3 Chromatin Environment at Super-Induced Dehydration Stress Memory Genes of Arabidopsis thaliana. Molecular Plant 7 (3):502-513. doi:https://doi.org/10.1093/mp/ssu001

Liu T, Li Y, Duan W, Huang F, Hou X (2017) Cold acclimation alters DNA methylation patterns and confers tolerance to heat and increases growth rate in Brassica rapa. J Exp Bot 68 (5):1213-1224. doi:10.1093/jxb/erw496

Liu Y, Dang P, Liu L, He C (2019b) Cold acclimation by the CBF-COR pathway in a changing climate: Lessons from Arabidopsis thaliana. Plant Cell Rep 38 (5):511-519. doi:10.1007/s00299-019-02376-3

Llorente F, Oliveros JC, Martínez-Zapater JM, Salinas J (2000) A freezing-sensitive mutant of Arabidopsis, frs1, is a new aba3 allele. Planta 211 (5):648-655. doi:10.1007/s004250000340

López Sánchez A, Stassen JH, Furci L, Smith LM, Ton J (2016) The role of DNA (de)methylation in immune responsiveness of Arabidopsis. Plant J 88 (3):361-374. doi:10.1111/tpj.13252

Lorch Y, LaPointe JW, Kornberg RD (1987) Nucleosomes inhibit the initiation of transcription but allow chain elongation with the displacement of histones. Cell 49 (2):203-210

Love MI, Huber W, Anders S (2014) Moderated estimation of fold change and dispersion for RNA-seq data with DESeq2. Genome biology 15 (12):1-21

Lu F, Cui X, Zhang S, Jenuwein T, Cao X (2011) Arabidopsis REF6 is a histone H3 lysine 27 demethylase. Nature Genetics 43 (7):715-719. doi:10.1038/ng.854

Luger K, Mader AW, Richmond RK, Sargent DF, Richmond TJ (1997) Crystal structure of the nucleosome core particle at 2.8 A resolution. Nature 389 (6648):251-260. doi:10.1038/38444

Luna E, Bruce TJ, Roberts MR, Flors V, Ton J (2012) Next-generation systemic acquired resistance. Plant Physiol 158 (2):844-853. doi:10.1104/pp.111.187468

Ma Y, Dai X, Xu Y, Luo W, Zheng X, Zeng D, Pan Y, Lin X, Liu H, Zhang D, Xiao J, Guo X, Xu S, Niu Y, Jin J, Zhang H, Xu X, Li L, Wang W, Qian Q, Ge S, Chong K (2015) COLD1 confers chilling tolerance in rice. Cell 160 (6):1209-1221. doi:10.1016/j.cell.2015.01.046

MacGregor DR, Zhang N, Iwasaki M, Chen M, Dave A, Lopez-Molina L, Penfield S (2019) ICE1 and ZOU determine the depth of primary seed dormancy in Arabidopsis independently of their role in endosperm development. Plant J 98 (2):277-290. doi:10.1111/tpj.14211

Mantyla E, Lang V, Palva ET (1995) Role of Abscisic Acid in Drought-Induced Freezing Tolerance, Cold Acclimation, and Accumulation of LT178 and RAB18 Proteins in Arabidopsis thaliana. Plant Physiology 107 (1):141-148. doi:10.1104/pp.107.1.141

Martinez G, Kohler C (2017) Role of small RNAs in epigenetic reprogramming during plant sexual reproduction. Curr Opin Plant Biol 36:22-28. doi:10.1016/j.pbi.2016.12.006

Maruyama K, Todaka D, Mizoi J, Yoshida T, Kidokoro S, Matsukura S, Takasaki H, Sakurai T, Yamamoto YY, Yoshiwara K, Kojima M, Sakakibara H, Shinozaki K, Yamaguchi-Shinozaki K (2012) Identification of cis-acting promoter elements in cold- and dehydration-induced transcriptional pathways in

Arabidopsis, rice, and soybean. DNA Res 19 (1):37-49. doi:10.1093/dnares/dsr040

Matzke MA, Mosher RA (2014) RNA-directed DNA methylation: an epigenetic pathway of increasing complexity. Nat Rev Genet 15 (6):394-408. doi:10.1038/nrg3683

Migicovsky Z, Kovalchuk I (2015) Transgenerational inheritance of epigenetic response to cold in Arabidopsis thaliana. Biocatalysis and Agricultural Biotechnology 4 (1):1-10. doi:10.1016/j.bcab.2014.09.001

Miura K, Furumoto T (2013) Cold signaling and cold response in plants. Int J Mol Sci 14 (3):5312-5337. doi:10.3390/ijms14035312

Miura K, Jin JB, Lee J, Yoo CY, Stirm V, Miura T, Ashworth EN, Bressan RA, Yun D-J, Hasegawa PM (2007a) SIZ1-Mediated Sumoylation of ICE1 Controls CBF3/DREB1A Expression and Freezing Tolerance in Arabidopsis. The Plant Cell 19 (4):1403-1414. doi:10.1105/tpc.106.048397

Miura K, Jin JB, Lee J, Yoo CY, Stirm V, Miura T, Ashworth EN, Bressan RA, Yun DJ, Hasegawa PM (2007b) SIZ1-mediated sumoylation of ICE1 controls CBF3/DREB1A expression and freezing tolerance in Arabidopsis. Plant Cell 19 (4):1403-1414. doi:10.1105/tpc.106.048397

Miura K, Ohta M, Nakazawa M, Ono M, Hasegawa PM (2011) ICE1 Ser403 is necessary for protein stabilization and regulation of cold signaling and tolerance. Plant J 67 (2):269-279. doi:10.1111/j.1365-313X.2011.04589.x

Moore LD, Le T, Fan G (2013) DNA Methylation and Its Basic Function. Neuropsychopharmacology 38 (1):23-38. doi:10.1038/npp.2012.112

Mozgova I, Mikulski P, Pecinka A, Farrona S (2019) Epigenetic Mechanisms of Abiotic Stress Response and Memory in Plants. In: Alvarez-Venegas R, De-la-Peña C, Casas-Mollano JA (eds) Epigenetics in Plants of Agronomic Importance: Fundamentals and Applications: Transcriptional Regulation and Chromatin Remodelling in Plants. Springer International Publishing, Cham, pp 1-64. doi:10.1007/978-3-030-14760-0_1

Murgia I, Giacometti S, Balestrazzi A, Paparella S, Pagliano C, Morandini P (2015) Analysis of the transgenerational iron deficiency stress memory in Arabidopsis thaliana plants. Frontiers in Plant Science 6. doi:10.3389/fpls.2015.00745

Nadeau JA, Sack FD (2002) Stomatal development in Arabidopsis. Arabidopsis Book 1:e0066. doi:10.1199/tab.0066

Nägele T, Heyer AG (2013) Approximating subcellular organisation of carbohydrate metabolism during cold acclimation in different natural accessions of Arabidopsis thaliana. New Phytol 198 (3):777-787. doi:10.1111/nph.12201

Nakamichi N, Kusano M, Fukushima A, Kita M, Ito S, Yamashino T, Saito K, Sakakibara H, Mizuno T (2009) Transcript Profiling of an Arabidopsis PSEUDO RESPONSE REGULATOR Arrhythmic Triple Mutant Reveals a Role for the Circadian Clock in Cold Stress Response. Plant and Cell Physiology 50 (3):447-462. doi:10.1093/pcp/pcp004

Neumetzler L, Humphrey T, Lumba S, Snyder S, Yeats TH, Usadel B, Vasilevski A, Patel J, Rose JK, Persson S, Bonetta D (2012) The FRIABLE1 gene product

affects cell adhesion in Arabidopsis. PLoS One 7 (8):e42914. doi:10.1371/journal.pone.0042914

Nguyen V, Gutzat R (2022) Epigenetic regulation in the shoot apical meristem. Current Opinion in Plant Biology 69:102267. doi:https://doi.org/10.1016/j.pbi.2022.102267

Novillo F, Alonso JM, Ecker JR, Salinas J (2004) CBF2/DREB1C is a negative regulator of CBF1/DREB1B and CBF3/DREB1A expression and plays a central role in stress tolerance in <em>Arabidopsis</em&gt. Proceedings of the National Academy of Sciences of the United States of America 101 (11):3985. doi:10.1073/pnas.0303029101

Novillo F, Medina J, Salinas J (2007) Arabidopsis CBF1 and CBF3 have a different function than CBF2 in cold acclimation and define different gene classes in the CBF regulon. Proc Natl Acad Sci U S A 104 (52):21002-21007. doi:10.1073/pnas.0705639105

O'Kane D, Gill V, Boyd P, Burdon R (1996) Chilling, oxidative stress and antioxidant responses inArabidopsis thaliana callus. Planta 198 (3):371-377. doi:10.1007/BF00620053

Oberkofler V, Pratx L, Baurle I (2021) Epigenetic regulation of abiotic stress memory: maintaining the good things while they last. Curr Opin Plant Biol 61:102007. doi:10.1016/j.pbi.2021.102007

Ojolo SP, Cao S, Priyadarshani S, Li W, Yan M, Aslam M, Zhao H, Qin Y (2018) Regulation of Plant Growth and Development: A Review From a Chromatin Remodeling Perspective. Front Plant Sci 9:1232. doi:10.3389/fpls.2018.01232

Ono A, Kinoshita T (2021) Epigenetics and plant reproduction: Multiple steps for responsibly handling succession. Curr Opin Plant Biol 61:102032. doi:10.1016/j.pbi.2021.102032

Örvar BL, Sangwan V, Omann F, Dhindsa RS (2000) Early steps in cold sensing by plant cells: the role of actin cytoskeleton and membrane fluidity. The Plant Journal 23 (6):785-794. doi:https://doi.org/10.1046/j.1365-313x.2000.00845.x

Park J, Lim CJ, Shen M, Park HJ, Cha J-Y, Iniesto E, Rubio V, Mengiste T, Zhu J-K, Bressan RA, Lee SY, Lee B-h, Jin JB, Pardo JM, Kim W-Y, Yun D-J (2018a) Epigenetic switch from repressive to permissive chromatin in response to cold stress. Proceedings of the National Academy of Sciences 115 (23):E5400. doi:10.1073/pnas.1721241115

Park S, Lee CM, Doherty CJ, Gilmour SJ, Kim Y, Thomashow MF (2015) Regulation of the Arabidopsis CBF regulon by a complex low-temperature regulatory network. Plant J 82 (2):193-207. doi:10.1111/tpj.12796

Pecinka A, Dinh HQ, Baubec T, Rosa M, Lettner N, Mittelsten Scheid O (2010) Epigenetic regulation of repetitive elements is attenuated by prolonged heat stress in Arabidopsis. Plant Cell 22 (9):3118-3129. doi:10.1105/tpc.110.078493

Peirats-Llobet M, Han SK, Gonzalez-Guzman M, Jeong CW, Rodriguez L, Belda-Palazon B, Wagner D, Rodriguez PL (2016) A Direct Link between Abscisic Acid Sensing and the Chromatin-Remodeling ATPase BRAHMA via Core ABA Signaling Pathway Components. Mol Plant 9 (1):136-147. doi:10.1016/j.molp.2015.10.003

Peterson CL, Dingwall A, Scott MP (1994) Five SWI/SNF gene products are components of a large multisubunit complex required for transcriptional enhancement. Proc Natl Acad Sci U S A 91 (8):2905-2908

Pfluger J, Wagner D (2007) Histone modifications and dynamic regulation of genome accessibility in plants. Curr Opin Plant Biol 10 (6):645-652. doi:10.1016/j.pbi.2007.07.013

Pillitteri LJ, Sloan DB, Bogenschutz NL, Torii KU (2007) Termination of asymmetric cell division and differentiation of stomata. Nature 445 (7127):501-505. doi:10.1038/nature05467

Putra, Hadi Lanang (2018) Enhanced Epigenetic Inheritance in *Arabidopsis thaliana* (Doctural dissertation). Retrieved from Department of Life Sciences, The University of Warwick

Rasmann S, De Vos M, Casteel CL, Tian D, Halitschke R, Sun JY, Agrawal AA, Felton GW, Jander G (2011) Herbivory in the Previous Generation Primes Plants for Enhanced Insect Resistance Plant Physiology 158 (2):854-863. doi:10.1104/pp.111.187831

Rendina González AP, Preite V, Verhoeven KJF, Latzel V (2018) Transgenerational Effects and Epigenetic Memory in the Clonal Plant Trifolium repens. Frontiers in Plant Science 9. doi:10.3389/fpls.2018.01677

Rinne P, Welling A, Kaikuranta P (1998) Onset of freezing tolerance in birch (Betula pubescens Ehrh.) involves LEA proteins and osmoregulation and is impaired in an ABA-deficient genotype. Plant, Cell & Environment 21 (6):601-611. doi:https://doi.org/10.1046/j.1365-3040.1998.00306.x

Ritonga FN, Chen S (2020) Physiological and Molecular Mechanism Involved in Cold Stress Tolerance in Plants. Plants (Basel) 9 (5). doi:10.3390/plants9050560

Sangwan V, Foulds I, Singh J, Dhindsa RS (2001) Cold-activation of Brassica napus BN115 promoter is mediated by structural changes in membranes and cytoskeleton, and requires Ca2+ influx. The Plant Journal 27 (1):1-12. doi:https://doi.org/10.1046/j.1365-313x.2001.01052.x

Schmittgen TD, Livak KJ (2008a) Analyzing real-time PCR data by the comparative C(T) method. Nat Protoc 3 (6):1101-1108. doi:10.1038/nprot.2008.73

Schmittgen TD, Livak KJ (2008b) Analyzing real-time PCR data by the comparative CT method. Nature protocols 3 (6):1101-1108

Schurch NJ, Schofield P, Gierliński M, Cole C, Sherstnev A, Singh V, Wrobel N, Gharbi K, Simpson GG, Owen-Hughes T, Blaxter M, Barton GJ (2016) How many biological replicates are needed in an RNA-seq experiment and which differential expression tool should you use? Rna 22 (6):839-851. doi:10.1261/rna.053959.115

Schwab R, Ossowski S, Riester M, Warthmann N, Weigel D (2006) Highly specific gene silencing by artificial microRNAs in Arabidopsis. The Plant Cell 18 (5):1121-1133

Searle I, He Y, Turck F, Vincent C, Fornara F, Kröber S, Amasino RA, Coupland G (2006) The transcription factor FLC confers a flowering response to vernalization by repressing meristem competence and systemic signaling in Arabidopsis. Genes Dev 20 (7):898-912. doi:10.1101/gad.373506

Seo PJ, Park M-J, Lim M-H, Kim S-G, Lee M, Baldwin IT, Park C-M (2012) A Self-Regulatory Circuit of CIRCADIAN CLOCK-ASSOCIATED1 Underlies the Circadian Clock Regulation of Temperature Responses in Arabidopsis The Plant Cell 24 (6):2427-2442. doi:10.1105/tpc.112.098723

Seok HY, Nguyen LV, Van Nguyen D, Lee SY, Moon YH (2020) Investigation of a Novel Salt Stress-Responsive Pathway Mediated by Arabidopsis DEAD-Box RNA Helicase Gene AtRH17 Using RNA-Seq Analysis. Int J Mol Sci 21 (5). doi:10.3390/ijms21051595

Shahbazian MD, Grunstein M (2007) Functions of site-specific histone acetylation and deacetylation. Annu Rev Biochem 76:75-100. doi:10.1146/annurev.biochem.76.052705.162114

Sharma R, Singh G, Bhattacharya S, Singh A (2018) Comparative transcriptome meta-analysis of Arabidopsis thaliana under drought and cold stress. PLOS ONE 13 (9):e0203266. doi:10.1371/journal.pone.0203266

Sharma VK, Fletcher JC (2002) Maintenance of shoot and floral meristem cell proliferation and fate. Plant Physiol 129 (1):31-39. doi:10.1104/pp.010987

Shen L (2014) GeneOverlap: An R package to test and visualize gene overlaps. R Package 3

Shen Q, Lin Y, Li Y, Wang G (2021) Dynamics of H3K27me3 Modification on Plant Adaptation to Environmental Cues. Plants (Basel) 10 (6). doi:10.3390/plants10061165

Shi Y, Tian S, Hou L, Huang X, Zhang X, Guo H, Yang S (2012) Ethylene signaling negatively regulates freezing tolerance by repressing expression of CBF and type-A ARR genes in Arabidopsis. The Plant Cell 24 (6):2578-2595

Shi Y, Yang S (2014) ABA Regulation of the Cold Stress Response in Plants. In: Abscisic Acid: Metabolism, Transport and Signaling. pp 337-363. doi:10.1007/978-94-017-9424-4_17

Silvertown J (2008) The Evolutionary Maintenance of Sexual Reproduction: Evidence from the Ecological Distribution of Asexual Reproduction in Clonal Plants. International Journal of Plant Sciences 169 (1):157-168. doi:10.1086/523357

Singh KB, Foley RC, Oñate-Sánchez L (2002) Transcription factors in plant defense and stress responses. Current Opinion in Plant Biology 5 (5):430-436. doi:https://doi.org/10.1016/S1369-5266(02)00289-3

Song J, Angel A, Howard M, Dean C (2012) Vernalization - a cold-induced epigenetic switch. J Cell Sci 125 (Pt 16):3723-3731. doi:10.1242/jcs.084764

Song Y, Jia Z, Hou Y, Ma X, Li L, Jin X, An L (2020) Roles of DNA Methylation in Cold Priming in Tartary Buckwheat. Frontiers in Plant Science 11. doi:10.3389/fpls.2020.608540

Song Y, Zhang X, Li M, Yang H, Fu D, Lv J, Ding Y, Gong Z, Shi Y, Yang S (2021) The direct targets of CBFs: In cold stress response and beyond. Journal of Integrative Plant Biology 63 (11):1874-1887. doi:https://doi.org/10.1111/jipb.13161

Stone SL, Braybrook SA, Paula SL, Kwong LW, Meuser J, Pelletier J, Hsieh T-F, Fischer RL, Goldberg RB, Harada JJ (2008) *Arabidopsis* LEAFY COTYLEDON2 induces maturation traits and auxin activity: Implications for somatic embryogenesis. Proceedings of the National Academy of Sciences 105 (8):3151-3156. doi:doi:10.1073/pnas.0712364105

Stroud H, Do T, Du J, Zhong X, Feng S, Johnson L, Patel DJ, Jacobsen SE (2014) Non-CG methylation patterns shape the epigenetic landscape in Arabidopsis. Nat Struct Mol Biol 21 (1):64-72. doi:10.1038/nsmb.2735

Sung S, Amasino RM (2004a) Vernalization and epigenetics: how plants remember winter. Current Opinion in Plant Biology 7 (1):4-10. doi:10.1016/j.pbi.2003.11.010

Sung S, Amasino RM (2004b) Vernalization and epigenetics: how plants remember winter. Curr Opin Plant Biol 7 (1):4-10. doi:10.1016/j.pbi.2003.11.010

Sung S, He Y, Eshoo TW, Tamada Y, Johnson L, Nakahigashi K, Goto K, Jacobsen SE, Amasino RM (2006) Epigenetic maintenance of the vernalized state in Arabidopsis thaliana requires LIKE HETEROCHROMATIN PROTEIN 1. Nat Genet 38 (6):706-710. doi:10.1038/ng1795

Takahashi D, Gorka M, Erban A, Graf A, Kopka J, Zuther E, Hincha DK (2019) Both cold and sub-zero acclimation induce cell wall modification and changes in the extracellular proteome in Arabidopsis thaliana. Sci Rep 9 (1):2289. doi:10.1038/s41598-019-38688-3

Takahashi D, Li B, Nakayama T, Kawamura Y, Uemura M (2013) Plant plasma membrane proteomics for improving cold tolerance. Front Plant Sci 4:90. doi:10.3389/fpls.2013.00090

Tang K, Zhao L, Ren Y, Yang S, Zhu JK, Zhao C (2020a) The transcription factor ICE1 functions in cold stress response by binding to the promoters of CBF and COR genes. Journal of integrative plant biology 62 (3):258-263

Tang K, Zhao L, Ren Y, Yang S, Zhu JK, Zhao C (2020b) The transcription factor ICE1 functions in cold stress response by binding to the promoters of CBF and COR genes. J Integr Plant Biol 62 (3):258-263. doi:10.1111/jipb.12918

Thalhammer A, Hincha DK, Zuther E (2014) Measuring Freezing Tolerance: Electrolyte Leakage and Chlorophyll Fluorescence Assays. In: Hincha DK, Zuther E (eds) Plant Cold Acclimation: Methods and Protocols. Springer New York, New York, NY, pp 15-24. doi:10.1007/978-1-4939-0844-8_3

Tian Y, Zheng H, Zhang F, Wang S, Ji X, Xu C, He Y, Ding Y (2019) PRC2 recruitment and H3K27me3 deposition at *FLC* require FCA binding of

COOLAIR. Science Advances 5 (4):eaau7246. doi:doi:10.1126/sciadv.aau7246

Trap-Gentil MV, Hebrard C, Lafon-Placette C, Delaunay A, Hagege D, Joseph C, Brignolas F, Lefebvre M, Barnes S, Maury S (2011) Time course and amplitude of DNA methylation in the shoot apical meristem are critical points for bolting induction in sugar beet and bolting tolerance between genotypes. J Exp Bot 62 (8):2585-2597. doi:10.1093/jxb/erq433

Urquiaga MCO, Thiebaut F, Hemerly AS, Ferreira PCG (2020) From Trash to Luxury: The Potential Role of Plant LncRNA in DNA Methylation During Abiotic Stress. Front Plant Sci 11:603246. doi:10.3389/fpls.2020.603246

Vashegyi I, Marozsán-Tóth Z, Galiba G, Dobrev PI, Vankova R, Tóth B (2013) Cold response of dedifferentiated barley cells at the gene expression, hormone composition, and freezing tolerance levels: studies on callus cultures. Mol Biotechnol 54 (2):337-349. doi:10.1007/s12033-012-9569-9

Verma RK, Kumar VVS, Yadav SK, Kumar TS, Rao MV, Chinnusamy V (2020) Overexpression of Arabidopsis ICE1 enhances yield and multiple abiotic stress tolerance in indica rice. Plant Signal Behav 15 (11):1814547. doi:10.1080/15592324.2020.1814547

Visioni A, Tondelli A, Francia E, Pswarayi A, Malosetti M, Russell J, Thomas W, Waugh R, Pecchioni N, Romagosa I, Comadran J (2013) Genome-wide association mapping of frost tolerance in barley (Hordeum vulgare L.). BMC Genomics 14 (1):424. doi:10.1186/1471-2164-14-424

Waki T, Hiki T, Watanabe R, Hashimoto T, Nakajima K (2011) The Arabidopsis RWP-RK protein RKD4 triggers gene expression and pattern formation in early embryogenesis. Curr Biol 21 (15):1277-1281. doi:10.1016/j.cub.2011.07.001

Walker J, Gao H, Zhang J, Aldridge B, Vickers M, Higgins JD, Feng X (2018) Sexual-lineage-specific DNA methylation regulates meiosis in Arabidopsis. Nature Genetics 50 (1):130-137. doi:10.1038/s41588-017-0008-5

Wang W, Huang F, Qin Q, Zhao X, Li Z, Fu B (2015) Comparative analysis of DNA methylation changes in two rice genotypes under salt stress and subsequent recovery. Biochem Biophys Res Commun 465 (4):790-796. doi:10.1016/j.bbrc.2015.08.089

Wang YH (2008) How effective is T-DNA insertional mutagenesis in Arabidopsis? Journal of Biochemical Technology 1 (1):11-20

Wanner LA, Junttila O (1999) Cold-induced freezing tolerance in Arabidopsis. Plant Physiol 120 (2):391-400. doi:10.1104/pp.120.2.391

Wei D, Liu M, Chen H, Zheng Y, Liu Y, Wang X, Yang S, Zhou M, Lin J (2018) INDUCER OF CBF EXPRESSION 1 is a male fertility regulator impacting anther dehydration in Arabidopsis. PLoS Genetics 14:e1007695. doi:10.1371/journal.pgen.1007695

Wibowo A, Becker C, Durr J, Price J, Spaepen S, Hilton S, Putra H, Papareddy R, Saintain Q, Harvey S, Bending GD, Schulze-Lefert P, Weigel D, Gutierrez-Marcos J (2018) Partial maintenance of organ-specific epigenetic marks during

plant asexual reproduction leads to heritable phenotypic variation. Proceedings of the National Academy of Sciences 115 (39):E9145-E9152. doi:doi:10.1073/pnas.1805371115

Wibowo A, Becker C, Marconi G, Durr J, Price J, Hagmann J, Papareddy R, Putra H, Kageyama J, Becker J, Weigel D, Gutierrez-Marcos J (2016) Hyperosmotic stress memory in Arabidopsis is mediated by distinct epigenetically labile sites in the genome and is restricted in the male germline by DNA glycosylase activity. Elife 5. doi:10.7554/eLife.13546

Wierzbicki AT, Haag JR, Pikaard CS (2008) Noncoding transcription by RNA polymerase Pol IVb/Pol V mediates transcriptional silencing of overlapping and adjacent genes. Cell 135 (4):635-648. doi:10.1016/j.cell.2008.09.035

Xi Y, Park S-R, Kim D-H, Kim E-D, Sung S (2020a) Transcriptome and epigenome analyses of vernalization in Arabidopsis thaliana. The Plant Journal 103 (4):1490-1502. doi:https://doi.org/10.1111/tpj.14817

Xi Y, Park SR, Kim DH, Kim ED, Sung S (2020b) Transcriptome and epigenome analyses of vernalization in Arabidopsis thaliana. The Plant Journal 103 (4):1490-1502

Xie H, Sun Y, Cheng B, Xue S, Cheng D, Liu L, Meng L, Qiang S (2018) Variation in ICE1 Methylation Primarily Determines Phenotypic Variation in Freezing Tolerance in Arabidopsis thaliana. Plant and Cell Physiology 60 (1):152-165. doi:10.1093/pcp/pcy197

Xin M, Wang Y, Yao Y, Song N, Hu Z, Qin D, Xie C, Peng H, Ni Z, Sun Q (2011) Identification and characterization of wheat long non-protein coding RNAs responsive to powdery mildew infection and heat stress by using microarray analysis and SBS sequencing. BMC Plant Biology 11 (1):61. doi:10.1186/1471-2229-11-61

Yamaguchi N, Matsubara S, Yoshimizu K, Seki M, Hamada K, Kamitani M, Kurita Y, Nomura Y, Nagashima K, Inagaki S, Suzuki T, Gan E-S, To T, Kakutani T, Nagano AJ, Satake A, Ito T (2021) H3K27me3 demethylases alter HSP22 and HSP17.6C expression in response to recurring heat in Arabidopsis. Nature Communications 12 (1):3480. doi:10.1038/s41467-021-23766-w

Yan W, Chen D, Smaczniak C, Engelhorn J, Liu H, Yang W, Graf A, Carles CC, Zhou D-X, Kaufmann K (2018) Dynamic and spatial restriction of Polycomb activity by plant histone demethylases. Nature Plants 4 (9):681-689. doi:10.1038/s41477-018-0219-5

Yang R, Hong Y, Ren Z, Tang K, Zhang H, Zhu J-K, Zhao C (2019a) A Role for PICKLE in the Regulation of Cold and Salt Stress Tolerance in Arabidopsis. Frontiers in Plant Science 10. doi:10.3389/fpls.2019.00900

Yang R, Hong Y, Ren Z, Tang K, Zhang H, Zhu JK, Zhao C (2019b) A Role for PICKLE in the Regulation of Cold and Salt Stress Tolerance in Arabidopsis. Front Plant Sci 10:900. doi:10.3389/fpls.2019.00900

Yuan HM, Sheng Y, Chen WJ, Lu YQ, Tang X, Ou-Yang M, Huang X (2017) Overexpression of Hevea brasiliensis HbICE1 Enhances Cold Tolerance in Arabidopsis. Front Plant Sci 8:1462. doi:10.3389/fpls.2017.01462

Zarka DG, Vogel JT, Cook D, Thomashow MF (2003) Cold Induction of Arabidopsis CBF Genes Involves Multiple ICE (Inducer of CBF Expression) Promoter Elements and a Cold-Regulatory Circuit That Is Desensitized by Low Temperature. Plant Physiology 133 (2):910-918. doi:10.1104/pp.103.027169

Zhan X, Zhu J-K, Lang Z (2015) Increasing Freezing Tolerance: Kinase Regulation of ICE1. Developmental Cell 32 (3):257-258. doi:https://doi.org/10.1016/j.devcel.2015.01.004

Zhang H, Lang Z, Zhu JK (2018) Dynamics and function of DNA methylation in plants. Nat Rev Mol Cell Biol 19 (8):489-506. doi:10.1038/s41580-018-0016-z

Zhang Q, Chen Q, Wang S, Hong Y, Wang Z (2014) Rice and cold stress: methods for its evaluation and summary of cold tolerance-related quantitative trait loci. Rice (N Y) 7 (1):24. doi:10.1186/s12284-014-0024-3

Zhang T, Zhang W, Jiang J (2015) Genome-Wide Nucleosome Occupancy and Positioning and Their Impact on Gene Expression and Evolution in Plants. Plant Physiol 168 (4):1406-1416. doi:10.1104/pp.15.00125

Zhang X, Xu Y, Huang B (2019) Lipidomic reprogramming associated with drought stress priming-enhanced heat tolerance in tall fescue (Festuca arundinacea). Plant, Cell & Environment 42 (3):947-958. doi:https://doi.org/10.1111/pce.13405

Zhang X, Yazaki J, Sundaresan A, Cokus S, Chan SW, Chen H, Henderson IR, Shinn P, Pellegrini M, Jacobsen SE, Ecker JR (2006) Genome-wide high-resolution mapping and functional analysis of DNA methylation in arabidopsis. Cell 126 (6):1189-1201. doi:10.1016/j.cell.2006.08.003

Zhang Y, Liu T, Meyer CA, Eeckhoute J, Johnson DS, Bernstein BE, Nusbaum C, Myers RM, Brown M, Li W (2008) Model-based analysis of ChIP-Seq (MACS). Genome biology 9 (9):1-9

Zhao C, Wang P, Si T, Hsu CC, Wang L, Zayed O, Yu Z, Zhu Y, Dong J, Tao WA, Zhu JK (2017a) MAP Kinase Cascades Regulate the Cold Response by Modulating ICE1 Protein Stability. Dev Cell 43 (5):618-629 e615. doi:10.1016/j.devcel.2017.09.024

Zhao C, Wang P, Si T, Hsu CC, Wang L, Zayed O, Yu Z, Zhu Y, Dong J, Tao WA, Zhu JK (2017b) MAP Kinase Cascades Regulate the Cold Response by Modulating ICE1 Protein Stability. Dev Cell 43 (5):618-629.e615. doi:10.1016/j.devcel.2017.09.024

Zhao C, Zhang Z, Xie S, Si T, Li Y, Zhu J-K (2016) Mutational Evidence for the Critical Role of CBF Transcription Factors in Cold Acclimation in Arabidopsis. Plant Physiology 171 (4):2744-2759. doi:10.1104/pp.16.00533

Zheng X, Chen L, Xia H, Wei H, Lou Q, Li M, Li T, Luo L (2017) Transgenerational epimutations induced by multi-generation drought imposition mediate rice plant's adaptation to drought condition. Sci Rep 7:39843. doi:10.1038/srep39843

Zhou M, Chen H, Wei D, Ma H, Lin J (2017a) Arabidopsis CBF3 and DELLAs positively regulate each other in response to low temperature. Scientific Reports 7 (1):39819. doi:10.1038/srep39819

Zhou X, Muhammad I, Lan H, Xia C (2022) Recent Advances in the Analysis of Cold Tolerance in Maize. Frontiers in Plant Science 13. doi:10.3389/fpls.2022.866034

Zhou Y, Tergemina E, Cui H, Förderer A, Hartwig B, Velikkakam James G, Schneeberger K, Turck F (2017b) Ctf4-related protein recruits LHP1-PRC2 to maintain H3K27me3 levels in dividing cells in Arabidopsis thaliana. Proc Natl Acad Sci U S A 114 (18):4833-4838. doi:10.1073/pnas.1620955114

Zicola, J., Liu, L., Tänzler, P. *et al.* Targeted DNA methylation represses two enhancers of *FLOWERING LOCUS T* in *Arabidopsis thaliana*. *Nat. Plants* **5**, 300–307 (2019). https://doi.org/10.1038/s41477-019-0375-2

Zilberman D, Gehring M, Tran RK, Ballinger T, Henikoff S (2007) Genome-wide analysis of Arabidopsis thaliana DNA methylation uncovers an interdependence between methylation and transcription. Nat Genet 39 (1):61-69. doi:10.1038/ng1929

Zimmerman JL (1993) Somatic Embryogenesis: A Model for Early Development in Higher Plants. Plant Cell 5 (10):1411-1423. doi:10.1105/tpc.5.10.1411

Zuo Z-F, Kang H-G, Park M-Y, Jeong H, Sun H-J, Yang D-H, Lee Y-E, Song P-S, Lee H-Y (2019) Overexpression of ICE1, a Regulator of Cold-Induced Transcriptome, Confers Cold Tolerance to Transgenic Zoysia japonica. Journal of Plant Biology 62 (2):137-146. doi:10.1007/s12374-018-0330-1

Appendix 7

Appendix table 7.1 DEGs and values from the pair-wise comparison between WT 22ºC and WT 4ºC

Gene ID	baseMean	log2FoldChange	lfcSE	padj	Symbol	Gene ID	baseMean	log2FoldChange	lfcSE	padj	Symbol
AT2G03965	6.267	-4.835	1.402	0.006	None	AT1G10585	113.993	1.445	0.338	0.000	BHLH167
AT4G08505	5.978	-3.764	1.376	0.041	None	AT3G62550	2056.241	1.447	0.310	0.000	AT3G62550
AT2G29170	60.819	-3.220	0.418	0.000	None	AT5G39785	203.712	1.449	0.173	0.000	None
AT5G02515	127.829	-2.915	0.345	0.000	None	AT1G51620	29.458	1.453	0.477	0.019	AT1G51620
AT2G18010	11.820	-2.853	0.926	0.017	SAUR10	AT3G57520	7947.355	1.455	0.484	0.021	RFS2
AT3G03830	22.071	-2.766	0.708	0.001	SAUR28	AT1G32900	5854.793	1.455	0.194	0.000	GBSS1
AT3G61898	44.625	-2.597	0.452	0.000	None	AT5G59330	32.741	1.460	0.519	0.034	AT5G59330
AT5G09805	12.053	-2.426	0.827	0.025	IDL3	AT3G50800	42.121	1.461	0.391	0.002	AT3G50800
AT5G45830	36.523	-2.398	0.662	0.003	DOG1	AT4G17230	894.449	1.461	0.136	0.000	None
AT3G18773	26.345	-2.398	0.660	0.003	ATL77	AT2G43620	539.675	1.462	0.436	0.008	AT2G43620
AT3G16670	815.029	-2.302	0.620	0.003	AT3G16670	AT5G41740	468.055	1.470	0.147	0.000	AT5G41740
AT3G44765	10.607	-2.244	0.834	0.045	None	AT3G01350	64.141	1.472	0.323	0.000	NPF5.9
AT4G15680	88.851	-2.204	0.378	0.000	GRXS4	AT1G73500	461.029	1.480	0.186	0.000	MKK9
AT4G16880	449.855	-2.162	0.202	0.000	None	AT3G06520	72.452	1.481	0.360	0.001	None
AT1G70820	1772.104	-2.151	0.166	0.000	AT1G70820	AT1G09575	171.824	1.481	0.247	0.000	AT1G09575
AT4G12900	60.618	-2.097	0.363	0.000	None	AT5G47060	555.631	1.482	0.146	0.000	AT5G47060
AT2G43375	15.529	-2.058	0.669	0.017	None	AT5G65320	30.769	1.486	0.520	0.030	BHLH99
AT4G04330	98.770	-2.037	0.309	0.000	RBCX1	AT3G45970	461.023	1.496	0.228	0.000	EXLA1
AT3G53800	285.050	-2.017	0.302	0.000	Fes1B	AT5G42760	354.615	1.499	0.297	0.000	AT5G42760
AT3G46370	80.954	-2.007	0.318	0.000	AT3G46370	AT2G25460	86.224	1.499	0.294	0.000	AT2G25460
AT5G20710	40.230	-2.003	0.454	0.000	BGAL7	AT2G35070	52.152	1.504	0.429	0.005	None
AT4G38860	781.571	-1.987	0.139	0.000	AT4G38860	AT3G55880	234.956	1.507	0.197	0.000	SUE4
AT1G76610	28.758	-1.968	0.498	0.001	None	AT1G13260	2699.146	1.507	0.353	0.000	RAV1
AT4G15690	117.620	-1.922	0.369	0.000	GRXS5	AT1G66160	319.599	1.508	0.238	0.000	PUB20
AT3G46970	1777.260	-1.899	0.145	0.000	PHS2	AT2G31141	24.801	1.508	0.543	0.036	AT2G31141
AT5G18050	63.732	-1.857	0.389	0.000	SAUR22	AT5G24590	853.467	1.510	0.129	0.000	NAC091
AT1G22770	768.393	-1.827	0.131	0.000	GI	AT5G13320	156.249	1.510	0.427	0.005	PBS3
AT3G42800	34.361	-1.826	0.546	0.008	None	AT2G26480	93.778	1.512	0.323	0.000	UGT76D1
AT3G49970	24.118	-1.818	0.520	0.005	AT3G49970	AT2G46940	77.719	1.513	0.312	0.000	None
AT2G32100	322.537	-1.790	0.170	0.000	OFP16	AT4G30280	598.648	1.515	0.231	0.000	XTH18

Gene ID	baseMean	log2FoldChange	lfcSE	padj	Symbol	Gene ID	baseMean	log2FoldChange	lfcSE	padj	Symbol
AT4G34510	19.725	-1.779	0.574	0.016	KCS17	AT3G06020	63.126	1.516	0.403	0.002	FAF4
AT1G75960	187.482	-1.777	0.199	0.000	AAE8	AT3G50060	477.004	1.516	0.194	0.000	MYB77
AT5G18060	87.620	-1.752	0.364	0.000	SAUR23	AT1G65500	251.862	1.516	0.363	0.001	AT1G65500
AT5G05320	27.253	-1.723	0.475	0.003	MO3	AT5G60680	2619.888	1.519	0.282	0.000	AT5G60680
AT4G25250	55.298	-1.711	0.535	0.012	PMEI4	AT3G46620	835.559	1.535	0.128	0.000	RDUF1
AT2G47560	37.636	-1.711	0.503	0.007	ATL64	AT5G37770	829.655	1.536	0.138	0.000	CML24
AT5G24240	72.175	-1.709	0.532	0.012	PI4KG3	AT4G39670	73.997	1.537	0.407	0.002	AT4G39670
AT4G15670	54.804	-1.705	0.385	0.000	GRXS7	AT1G21250	545.344	1.537	0.262	0.000	WAK1
AT1G05660	59.533	-1.702	0.390	0.000	AT1G05660	AT3G52800	1714.482	1.542	0.104	0.000	SAP6
AT2G39120	24.371	-1.685	0.491	0.006	WTF9	AT4G15480	128.965	1.544	0.346	0.000	UGT84A1
AT3G13277	53.167	-1.668	0.390	0.000	None	AT1G36370	2291.091	1.551	0.195	0.000	SHM7
AT3G18080	3553.357	-1.665	0.114	0.000	BGLU44	AT5G62470	465.202	1.552	0.125	0.000	MYB96
AT5G18010	45.136	-1.657	0.496	0.008	SAUR19	AT1G19020	214.618	1.552	0.319	0.000	AT1G19020
AT1G14430	139.376	-1.656	0.248	0.000	AT1G14430	AT4G06536	60.358	1.555	0.348	0.000	None
AT5G54190	213.202	-1.653	0.520	0.013	PORA	AT3G15500	147.884	1.561	0.357	0.000	NAC055
AT5G05810	41.392	-1.651	0.431	0.002	ATL43	AT3G62260	410.532	1.562	0.130	0.000	AT3G62260
AT1G22340	23.509	-1.632	0.546	0.022	UGT85A7	AT1G77120	676.244	1.576	0.272	0.000	ADH1
AT5G18020	159.503	-1.631	0.245	0.000	SAUR20	AT4G35640	112.965	1.587	0.391	0.001	SAT4
AT5G35738	32.021	-1.630	0.517	0.014	None	AT4G39070	82.682	1.590	0.408	0.001	BBX20
AT1G69830	2229.255	-1.630	0.094	0.000	AMY3	AT3G23250	58.807	1.594	0.356	0.000	MYB15
AT2G47460	83.548	-1.623	0.339	0.000	MYB12	AT5G16200	167.045	1.598	0.213	0.000	None
AT3G29320	3282.212	-1.617	0.083	0.000	PHS1	AT2G16890	501.669	1.599	0.254	0.000	UGT90A1
AT4G34760	359.687	-1.616	0.154	0.000	SAUR50	AT1G70800	96.369	1.599	0.305	0.000	CAR6
AT1G53887	19.096	-1.616	0.590	0.040	None	AT1G02610	366.694	1.605	0.425	0.002	AT1G02610
AT1G10760	3230.248	-1.612	0.122	0.000	GWD1	AT5G41590	43.333	1.606	0.403	0.001	AT5G41590
AT4G38840	643.756	-1.596	0.151	0.000	AT4G38840	AT2G25735	132.502	1.608	0.378	0.000	AT2G25735
AT5G02810	2759.584	-1.582	0.178	0.000	APRR7	AT5G26920	303.320	1.608	0.459	0.005	CBP60G
AT5G18030	203.309	-1.580	0.276	0.000	SAUR21	AT1G35210	23.432	1.609	0.561	0.030	AT1G35210
AT3G07215	175.700	-1.563	0.266	0.000	None	AT5G16960	28.864	1.617	0.444	0.003	AT5G16960
AT1G70880	82.280	-1.563	0.283	0.000	AT1G70880	AT1G17420	468.104	1.619	0.175	0.000	LOX3
AT2G46790	680.849	-1.561	0.167	0.000	APRR9	AT5G61600	370.566	1.619	0.250	0.000	ERF104
AT4G23240	27.249	-1.520	0.498	0.018	CRK16	AT2G27500	916.321	1.623	0.188	0.000	AT2G27500
AT5G60100	31.556	-1.519	0.447	0.007	PRR3	AT1G02400	174.640	1.624	0.270	0.000	GA2OX6

Gene ID	baseMean	log2FoldChange	lfcSE	padj	Symbol	Gene ID	baseMean	log2FoldChange	lfcSE	padj	Symbol
AT5G64860	603.591	-1.513	0.118	0.000	DPE1	AT1G73890	94.152	1.624	0.297	0.000	AT1G73890
AT2G05518	27.071	-1.513	0.504	0.021	None	AT3G14440	428.531	1.625	0.282	0.000	NCED3
AT2G33790	203.138	-1.507	0.564	0.047	AGP30	AT1G65490	1684.995	1.631	0.171	0.000	AT1G65490
AT3G25905	20.104	-1.501	0.522	0.029	CLE27	AT5G57010	74.299	1.631	0.309	0.000	IQM5
AT4G14230	458.138	-1.493	0.125	0.000	CBSDUF2	AT3G45060	22.619	1.632	0.520	0.014	NRT2.6
AT4G26530	4619.828	-1.493	0.299	0.000	FBA5	AT3G23170	349.239	1.633	0.271	0.000	AT3G23170
AT5G43440	237.083	-1.492	0.189	0.000	AT5G43440	AT1G68520	7984.297	1.640	0.118	0.000	COL6
AT4G03060	669.439	-1.490	0.380	0.001	None	AT2G24600	271.407	1.643	0.244	0.000	AT2G24600
AT1G48330	74.430	-1.481	0.349	0.000	AT1G48330	AT3G48390	179.174	1.645	0.339	0.000	AT3G48390
AT5G50760	183.070	-1.481	0.250	0.000	AT5G50760	AT4G12470	1974.559	1.645	0.456	0.004	AZI1
AT3G18070	50.108	-1.474	0.376	0.001	BGLU43	AT3G45960	57.328	1.646	0.355	0.000	EXLA3
AT2G45560	536.466	-1.465	0.226	0.000	CYP76C1	AT4G11000	26.020	1.647	0.555	0.023	AT4G11000
AT3G14200	312.830	-1.463	0.190	0.000	AT3G14200	AT1G32920	694.748	1.653	0.257	0.000	AT1G32920
AT3G01310	1266.070	-1.448	0.118	0.000	AT3G01310	AT3G49530	781.731	1.654	0.138	0.000	NAC062
AT2G06925	265.526	-1.444	0.241	0.000	PLA2-ALPHA	AT5G51390	100.121	1.657	0.388	0.000	None
AT2G23770	133.915	-1.436	0.258	0.000	LYK4	AT3G15450	11709.449	1.658	0.562	0.024	AT3G15450
AT3G28370	81.436	-1.422	0.278	0.000	AT3G28370	AT4G33985	60.040	1.658	0.357	0.000	None
AT2G32390	156.447	-1.418	0.216	0.000	GLR3.5	AT5G38240	45.160	1.661	0.430	0.002	None
AT5G47240	210.835	-1.418	0.324	0.000	atnudt8	AT4G36850	7394.866	1.663	0.410	0.001	AT4G36850
AT2G45040	23.603	-1.408	0.471	0.022	4MMP	AT5G17050	1869.316	1.669	0.224	0.000	UGT78D2
AT4G15700	106.374	-1.403	0.363	0.002	GRXS3	AT4G17615	389.078	1.673	0.249	0.000	CBL1
AT5G15290	23.854	-1.402	0.489	0.029	CASP5	AT2G15880	605.519	1.674	0.373	0.000	PEX3
AT5G04470	19.588	-1.402	0.521	0.045	SIM	AT2G08435	36.788	1.677	0.423	0.001	None
AT2G03310	321.726	-1.396	0.185	0.000	AT2G03310	AT2G17036	76.889	1.678	0.369	0.000	None
AT3G16660	781.528	-1.389	0.343	0.001	AT3G16660	AT3G22910	43.981	1.678	0.368	0.000	ACA13
AT1G09467	57.915	-1.387	0.358	0.002	None	AT5G18670	3615.737	1.682	0.186	0.000	BAM9
AT3G03850	49.487	-1.386	0.420	0.009	AT3G03850	AT4G12490	112.348	1.687	0.469	0.004	AT4G12490
AT2G21210	706.263	-1.360	0.182	0.000	AT2G21210	AT4G37610	1249.323	1.690	0.501	0.008	BT5
AT5G06690	237.751	-1.355	0.328	0.001	WCRKC1	AT1G72760	18.198	1.691	0.573	0.024	None
AT5G22794	53.807	-1.351	0.368	0.003	AT5G22794	AT5G17040	64.380	1.692	0.497	0.007	UGT78D4
AT4G18240	1126.036	-1.348	0.115	0.000	SS4	AT3G30775	6682.370	1.703	0.625	0.041	POX1
AT1G14200	183.918	-1.347	0.219	0.000	AT1G14200	AT4G26200	100.328	1.706	0.322	0.000	ACS7
AT5G41400	193.469	-1.339	0.250	0.000	None	AT5G19560	26.976	1.707	0.461	0.003	ATROPGEF10

Gene ID	baseMean	log2FoldChange	lfcSE	padj	Symbol	Gene ID	baseMean	log2FoldChange	lfcSE	padj	Symbol
AT2G40840	2750.427	-1.339	0.144	0.000	DPE2	AT4G01250	210.538	1.710	0.296	0.000	WRKY22
AT4G16870	644.455	-1.333	0.216	0.000	None	AT3G46080	44.187	1.715	0.451	0.002	ZAT8
AT1G68330	41.510	-1.333	0.399	0.008	None	AT4G35985	163.663	1.731	0.210	0.000	P85
AT3G26290	1861.391	-1.323	0.167	0.000	CYP71B26	AT1G80130	940.631	1.732	0.412	0.000	AT1G80130
AT3G13240	54.710	-1.320	0.395	0.008	None	AT5G39890	94.531	1.743	0.395	0.000	PCO2
AT5G54064	26.803	-1.315	0.494	0.048	None	AT4G31800	378.977	1.745	0.242	0.000	WRKY18
AT3G25495	287.903	-1.314	0.184	0.000	None	AT5G47230	290.040	1.747	0.238	0.000	ERF5
AT4G24350	370.218	-1.312	0.180	0.000	AT4G24350	AT1G68500	80.162	1.749	0.374	0.000	None
AT1G08550	1123.159	-1.307	0.166	0.000	VDE1	AT2G30040	692.147	1.751	0.167	0.000	MAPKKK14
AT3G60220	87.176	-1.305	0.290	0.000	ATL4	AT5G22920	2887.405	1.752	0.570	0.017	RZPF34
AT4G38850	64.965	-1.300	0.293	0.000	SAUR15	AT1G74830	26.275	1.757	0.514	0.007	MYOB6
AT4G16447	47.900	-1.298	0.392	0.009	AT4G16447	AT3G28580	59.119	1.757	0.474	0.003	AT3G28580
AT2G12170	36.361	-1.292	0.398	0.011	None	AT5G35777	120.679	1.766	0.363	0.000	None
AT1G70990	24.575	-1.285	0.444	0.028	None	AT1G09500	276.951	1.767	0.312	0.000	AT1G09500
AT5G20790	275.605	-1.281	0.259	0.000	AT5G20790	AT5G24510	14.991	1.769	0.638	0.037	AT5G24510
AT4G32340	756.008	-1.277	0.198	0.000	AT4G32340	AT1G22380	25.612	1.773	0.606	0.026	UGT85A3
AT2G23840	617.804	-1.275	0.179	0.000	AT2G23840	AT2G04050	172.842	1.774	0.340	0.000	DTX3
AT3G05730	2759.263	-1.272	0.356	0.004	AT3G05730	AT5G64905	29.616	1.776	0.587	0.020	PEP3
AT3G62750	1588.267	-1.266	0.101	0.000	BGLU8	AT3G47875	21.825	1.786	0.553	0.011	None
AT1G78955	34.323	-1.265	0.429	0.024	CAMS1	AT3G48100	369.592	1.791	0.208	0.000	ARR5
AT2G34430	43065.717	-1.258	0.161	0.000	LHB1B1	AT4G15430	656.414	1.793	0.146	0.000	AT4G15430
AT5G11610	135.821	-1.253	0.273	0.000	None	AT4G02380	6464.712	1.793	0.301	0.000	SAG21
AT1G36940	67.234	-1.246	0.302	0.001	None	AT5G15120	166.276	1.796	0.339	0.000	PCO1
AT1G61500	144.228	-1.239	0.237	0.000	AT1G61500	AT4G21680	247.772	1.799	0.513	0.005	NPF7.2
AT2G26515	32.112	-1.239	0.422	0.025	None	AT1G29290	14.277	1.800	0.630	0.030	CEP14
AT1G12845	213.217	-1.233	0.260	0.000	None	AT5G64660	266.268	1.804	0.205	0.000	PUB27
AT5G01550	49.476	-1.232	0.387	0.013	None	AT1G35290	33.561	1.806	0.571	0.014	ALT1
AT4G22560	66.169	-1.231	0.298	0.001	None	AT3G52400	954.981	1.808	0.182	0.000	SYP122
AT3G25870	84.983	-1.231	0.272	0.000	AT3G25870	AT1G09350	80.260	1.811	0.370	0.000	GOLS3
AT5G28262	27.906	-1.230	0.441	0.036	None	AT3G50770	67.427	1.812	0.508	0.004	CML41
AT1G74453	32.524	-1.228	0.453	0.043	None	AT4G24110	115.771	1.818	0.325	0.000	AT4G24110
AT2G28720	649.815	-1.224	0.141	0.000	AT2G28720	AT4G25810	347.022	1.822	0.231	0.000	XTH23
AT4G16860	1715.966	-1.218	0.212	0.000	RPP4	AT1G22570	678.075	1.826	0.247	0.000	NPF5.15

Gene ID	baseMean	log2FoldChange	lfcSE	padj	Symbol	Gene ID	baseMean	log2FoldChange	lfcSE	padj	Symbol
AT1G17700	46.040	-1.212	0.354	0.006	PRA1F1	AT5G48850	538.602	1.827	0.670	0.041	SDI1
AT1G64590	112.130	-1.198	0.317	0.002	AT1G64590	AT5G66650	233.261	1.835	0.185	0.000	AT5G66650
AT4G09020	492.471	-1.196	0.148	0.000	ISA3	AT1G19380	436.614	1.836	0.282	0.000	AT1G19380
AT3G61460	884.884	-1.196	0.131	0.000	BRH1	AT3G22961	31.256	1.841	0.460	0.001	None
AT1G06460	644.174	-1.195	0.133	0.000	ACD32.1	AT4G36820	37.281	1.849	0.555	0.008	AT4G36820
AT2G07042	52.413	-1.195	0.402	0.022	None	AT2G41010	361.421	1.855	0.173	0.000	CAMBP25
AT3G60490	41.470	-1.190	0.354	0.008	ERF035	AT1G22190	1448.727	1.860	0.158	0.000	RAP2-13
AT5G60880	73.204	-1.188	0.338	0.005	BASL	AT4G02330	538.896	1.861	0.201	0.000	PME41
AT4G31320	82.734	-1.187	0.325	0.003	AT4G31320	AT3G02140	423.100	1.865	0.258	0.000	AFP4
AT3G06120	76.745	-1.177	0.383	0.017	MUTE	AT2G41100	813.194	1.870	0.561	0.008	CML12
AT5G26040	127.637	-1.173	0.214	0.000	HDA2	AT1G76600	335.924	1.872	0.293	0.000	AT1G76600
AT3G13270	54.882	-1.160	0.362	0.012	None	AT2G42540	1288.001	1.876	0.694	0.043	COR15A
AT2G26220	56.311	-1.159	0.392	0.024	None	AT5G19240	932.504	1.877	0.151	0.000	AT5G19240
AT2G40610	1693.140	-1.155	0.193	0.000	EXPA8	AT2G32210	50.177	1.889	0.439	0.000	AT2G32210
AT4G27440	7071.929	-1.150	0.135	0.000	PORB	AT2G36220	55.079	1.890	0.430	0.000	AT2G36220
AT1G22030	146.410	-1.149	0.213	0.000	None	AT5G40010	40.503	1.891	0.571	0.009	AATP1
AT2G38460	206.875	-1.149	0.217	0.000	IREG1	AT4G18880	555.913	1.893	0.154	0.000	HSFA4A
AT3G61550	203.376	-1.142	0.178	0.000	None	AT5G63350	39.222	1.894	0.610	0.016	AT5G63350
AT5G02160	4038.516	-1.140	0.194	0.000	AT5G02160	AT1G77640	29.562	1.894	0.503	0.002	ERF013
AT4G12320	858.219	-1.140	0.146	0.000	CYP706A6	AT5G13170	800.331	1.895	0.441	0.000	SWEET15
AT5G03960	52.058	-1.136	0.370	0.017	IQD12	AT1G62420	100.945	1.897	0.349	0.000	AT1G62420
AT3G04530	64.458	-1.135	0.344	0.009	PPCK2	AT3G56400	313.327	1.908	0.332	0.000	WRKY70
AT1G72645	143.104	-1.135	0.239	0.000	AT1G72645	AT5G63160	4286.004	1.916	0.390	0.000	BT1
AT3G47830	28.925	-1.127	0.419	0.045	AT3G47830	AT4G08040	98.616	1.922	0.379	0.000	ACS11
AT1G73750	556.677	-1.121	0.175	0.000	None	AT5G15190	152.045	1.922	0.271	0.000	AT5G15190
AT4G28240	1148.464	-1.119	0.145	0.000	None	AT4G27360	65.139	1.933	0.583	0.009	AT4G27360
AT2G01170	348.286	-1.114	0.170	0.000	BAT1	AT3G47660	14.909	1.936	0.661	0.025	AT3G47660
AT5G45820	1035.310	-1.111	0.334	0.009	CIPK20	AT4G08250	17.979	1.938	0.564	0.006	SCL26
AT1G64170	221.172	-1.109	0.210	0.000	CHX16	AT1G28480	25.537	1.938	0.583	0.009	GRXC9
AT2G23410	35.009	-1.109	0.398	0.035	DPS	AT3G55840	56.969	1.939	0.366	0.000	HSPRO1
AT4G27820	522.223	-1.109	0.155	0.000	BGLU9	AT2G20142	37.810	1.939	0.482	0.001	AT2G20142
AT3G16870	157.642	-1.103	0.242	0.000	GATA17	AT1G09380	73.109	1.946	0.649	0.021	AT1G09380
AT4G31050	154.320	-1.100	0.216	0.000	LIP2P	AT2G35930	128.014	1.957	0.293	0.000	PUB23

Gene ID	baseMean	log2FoldChange	lfcSE	padj	Symbol	Gene ID	baseMean	log2FoldChange	lfcSE	padj	Symbol
AT5G24100	76.889	-1.095	0.380	0.028	AT5G24100	AT3G54000	258.669	1.961	0.182	0.000	None
AT1G75580	49.993	-1.095	0.340	0.012	AT1G75580	AT5G52310	2853.881	1.963	0.311	0.000	RD29A
AT2G18650	39.478	-1.094	0.360	0.019	ATL49	AT4G33920	1188.196	1.964	0.131	0.000	AT4G33920
AT4G27840	196.170	-1.092	0.203	0.000	PHYL2.1	AT5G28630	108.078	1.966	0.384	0.000	None
AT2G39681	292.376	-1.092	0.159	0.000	None	AT2G35290	67.908	1.978	0.381	0.000	None
AT3G25700	124.869	-1.092	0.231	0.000	AT3G25700	AT5G17460	629.696	1.980	0.200	0.000	None
AT5G07700	57.134	-1.088	0.401	0.043	MYB76	AT4G36110	39.828	1.985	0.475	0.000	AT4G36110
AT1G51080	167.946	-1.083	0.201	0.000	None	AT1G72660	11.981	1.986	0.751	0.050	DRG2
AT3G10520	858.733	-1.082	0.138	0.000	AHB2	AT2G40000	4894.051	1.994	0.477	0.000	HSPRO2
AT1G20020	9472.091	-1.079	0.121	0.000	LFNR2	AT3G19030	2723.298	1.998	0.122	0.000	None
AT1G09750	1924.622	-1.077	0.176	0.000	AED3	AT1G65890	72.812	2.002	0.543	0.003	AAE12
AT5G02180	338.835	-1.075	0.186	0.000	AVT1D	AT5G14570	2488.875	2.006	0.206	0.000	NRT2.7
AT2G43550	422.695	-1.074	0.237	0.000	ATTI6	AT3G02380	2483.110	2.008	0.170	0.000	COL2
AT3G15840	2849.330	-1.072	0.124	0.000	PIFI	AT5G40790	21.406	2.010	0.748	0.045	AT5G40790
AT4G13410	79.039	-1.070	0.336	0.013	CSLA15	AT4G34150	2131.692	2.020	0.124	0.000	AT4G34150
AT4G39780	209.428	-1.069	0.248	0.000	ERF060	AT2G17830	105.337	2.021	0.394	0.000	None
AT1G12090	6749.670	-1.068	0.164	0.000	ELP	AT4G14365	133.665	2.023	0.273	0.000	XBAT34
AT4G31730	291.168	-1.067	0.182	0.000	GDU1	AT2G22500	658.931	2.035	0.192	0.000	PUMP5
AT4G37160	68.554	-1.067	0.324	0.010	sks15	AT5G58840	64.130	2.036	0.371	0.000	SBT4.9
AT1G14920	1012.014	-1.065	0.126	0.000	GAI	AT2G17840	1767.472	2.041	0.205	0.000	ERD7
AT2G22450	187.106	-1.064	0.187	0.000	RIBA2	AT1G72950	27.930	2.043	0.526	0.001	AT1G72950
AT3G13065	180.704	-1.063	0.253	0.000	SRF4	AT3G06435	28.140	2.044	0.530	0.002	None
AT1G57590	107.915	-1.057	0.254	0.001	PAE2	AT3G60670	24.436	2.045	0.498	0.001	AT3G60670
AT5G67390	199.340	-1.053	0.209	0.000	AT5G67390	AT2G38470	1130.991	2.049	0.182	0.000	WRKY33
AT3G03265	114.989	-1.052	0.366	0.029	None	AT3G03280	28.191	2.065	0.467	0.000	AT3G03280
AT3G26580	1687.725	-1.051	0.132	0.000	AT3G26580	AT1G21910	337.979	2.070	0.252	0.000	ERF012
AT3G23730	498.935	-1.050	0.187	0.000	XTH16	AT2G23810	2293.114	2.075	0.144	0.000	TET8
AT5G36120	476.799	-1.050	0.180	0.000	CCB3	AT4G36950	19.073	2.082	0.672	0.016	MAPKKK21
AT1G10060	205.816	-1.048	0.250	0.000	ATBCAT-1	AT2G16060	533.681	2.087	0.257	0.000	AHB1
AT5G49015	59.389	-1.046	0.354	0.023	None	AT5G49330	74.803	2.087	0.367	0.000	MYB111
AT5G63810	464.341	-1.044	0.150	0.000	BGAL10	AT4G23215	14.770	2.091	0.716	0.026	None
AT1G07450	84.107	-1.044	0.314	0.009	AT1G07450	AT3G04800	27.566	2.093	0.525	0.001	TIM23-3
AT1G20620	33774.042	-1.043	0.157	0.000	CAT3	AT4G29190	1726.268	2.096	0.143	0.000	AT4G29190

Gene ID	baseMean	log2FoldChange	lfcSE	padj	Symbol	Gene ID	baseMean	log2FoldChange	lfcSE	padj	Symbol
AT1G20010	2359.472	-1.043	0.126	0.000	TUBB5	AT5G25250	148.974	2.098	0.346	0.000	FLOT1
AT1G51940	484.945	-1.033	0.193	0.000	LYK3	AT3G03025	18.328	2.106	0.638	0.009	None
AT3G47860	373.268	-1.027	0.164	0.000	CHL	AT5G01100	127.333	2.108	0.262	0.000	FRB1
AT3G03370	77.598	-1.025	0.291	0.005	AT3G03370	AT4G11890	115.716	2.116	0.714	0.023	AT4G11890
AT4G33625	890.769	-1.024	0.133	0.000	AT4G33625	AT4G30350	982.753	2.117	0.153	0.000	SMXL2
AT5G13920	59.119	-1.020	0.319	0.012	None	AT4G27280	574.014	2.118	0.214	0.000	KRP1
AT2G45210	157.880	-1.018	0.249	0.001	SAUR36	AT2G45570	73.761	2.122	0.499	0.000	CYP76C2
AT4G04840	976.818	-1.018	0.141	0.000	MSRB6	AT1G49450	220.685	2.125	0.388	0.000	AT1G49450
AT5G22580	1296.317	-1.015	0.181	0.000	AT5G22580	AT1G09070	7203.989	2.127	0.120	0.000	SRC2
AT2G24220	108.257	-1.015	0.239	0.000	ATPUP5	AT1G23710	620.763	2.128	0.145	0.000	AT1G23710
AT1G79460	194.603	-1.013	0.245	0.001	GA2	AT5G52750	80.842	2.141	0.398	0.000	HIPP13
AT4G30690	1152.279	-1.011	0.126	0.000	IF3-4	AT5G48250	253.326	2.144	0.238	0.000	COL10
AT2G42800	69.089	-1.009	0.359	0.034	AtRLP29	AT1G69890	323.363	2.144	0.455	0.000	AT1G69890
AT1G66080	91.362	-1.008	0.256	0.001	AT1G66080	AT3G43850	37.061	2.145	0.749	0.030	AT3G43850
AT2G39040	43.193	-1.005	0.376	0.047	PER24	AT5G17540	32.335	2.147	0.505	0.000	AT5G17540
AT3G45230	151.220	-1.002	0.197	0.000	AT3G45230	AT2G27080	295.946	2.162	0.233	0.000	NHL13
AT2G31010	291.482	-1.002	0.250	0.001	AT2G31010	AT3G59350	831.246	2.166	0.231	0.000	AT3G59350
AT3G29670	149.252	1.001	0.236	0.000	PMAT2	AT3G63060	41.752	2.173	0.562	0.002	EDL3
AT1G48100	171.332	1.001	0.327	0.018	AT1G48100	AT5G08770	206.981	2.173	0.187	0.000	None
AT3G49790	624.637	1.002	0.272	0.003	AT3G49790	AT2G47770	92.216	2.176	0.734	0.023	TSPO
AT5G37550	70.951	1.002	0.297	0.007	AT5G37550	AT1G20823	285.755	2.186	0.216	0.000	ATL80
AT3G17770	1531.635	1.004	0.175	0.000	AT3G17770	AT1G06540	13.230	2.201	0.791	0.036	None
AT2G32540	1580.906	1.005	0.146	0.000	CSLB4	AT1G01060	5237.773	2.202	0.091	0.000	LHY
AT1G16850	84.714	1.006	0.300	0.008	AT1G16850	AT3G44900	21.431	2.203	0.594	0.003	CHX4
AT2G27830	660.837	1.006	0.224	0.000	AT2G27830	AT1G18200	127.587	2.204	0.229	0.000	RABA6B
AT1G34420	91.856	1.007	0.294	0.006	AT1G34420	AT5G15950	3745.150	2.212	0.201	0.000	SAMDC2
AT5G22390	438.263	1.013	0.197	0.000	AT5G22390	AT1G19180	751.963	2.224	0.179	0.000	TIFY10A
AT3G18560	524.991	1.016	0.140	0.000	None	AT5G49520	194.188	2.233	0.285	0.000	WRKY48
AT5G58620	672.849	1.018	0.116	0.000	AT5G58620	AT3G15740	10.610	2.237	0.736	0.019	None
AT4G18010	2105.063	1.020	0.168	0.000	IP5P2	AT5G17850	166.119	2.238	0.246	0.000	CCX2
AT5G59550	464.704	1.020	0.126	0.000	AT5G59550	AT3G09520	68.994	2.239	0.331	0.000	ATEXO70H4
AT1G12420	350.149	1.020	0.257	0.001	ACR8	AT1G55950	19.461	2.244	0.809	0.037	None
AT4G06880	52.584	1.022	0.341	0.021	None	AT4G09820	37.162	2.249	0.703	0.012	TT8

Gene ID	baseMean	log2FoldChange	lfcSE	padj	Symbol	Gene ID	baseMean	log2FoldChange	lfcSE	padj	Symbol
AT4G14550	749.434	1.023	0.172	0.000	IAA14	AT5G65350	50.759	2.254	0.389	0.000	HTR11
AT1G27770	1706.240	1.027	0.096	0.000	ACA1	AT3G21890	205.097	2.255	0.344	0.000	MIP1B
AT5G42460	102.347	1.027	0.269	0.002	None	AT1G52890	143.748	2.264	0.376	0.000	NAC019
AT5G01700	91.107	1.029	0.234	0.000	AT5G01700	AT5G49070	15.237	2.264	0.696	0.011	KCS21
AT5G47910	2142.478	1.029	0.155	0.000	RBOHD	AT1G69570	24.503	2.290	0.637	0.004	CDF5
AT2G31880	559.855	1.029	0.170	0.000	SOBIR1	AT1G66090	70.172	2.293	0.390	0.000	AT1G66090
AT3G11460	43.084	1.032	0.390	0.050	PCMP-H52	AT5G64750	35.196	2.295	0.704	0.010	ABR1
AT5G46050	151.060	1.032	0.360	0.029	NPF5.2	AT3G48510	74.487	2.302	0.524	0.000	AT3G48510
AT3G07720	1363.250	1.033	0.197	0.000	AT3G07720	AT3G56880	1631.294	2.313	0.118	0.000	AT3G56880
AT1G07150	133.629	1.033	0.272	0.002	MAPKKK13	AT2G32020	98.788	2.317	0.318	0.000	AT2G32020
AT1G43910	286.536	1.036	0.252	0.001	AT1G43910	AT5G64870	68.818	2.319	0.343	0.000	FLOT3
AT2G29710	45.102	1.036	0.380	0.041	None	AT1G65390	122.383	2.320	0.394	0.000	PP2A5
AT1G74890	50.392	1.038	0.345	0.021	ARR15	AT3G16860	124.781	2.320	0.300	0.000	COBL8
AT3G01290	2163.148	1.040	0.349	0.022	HIR3	AT5G65300	85.119	2.322	0.341	0.000	AT5G65300
AT3G28910	560.965	1.042	0.165	0.000	MYB30	AT1G20450	7482.388	2.322	0.119	0.000	ERD10
AT2G48080	103.034	1.042	0.335	0.016	AT2G48080	AT1G10400	23.543	2.335	0.555	0.000	UGT90A2
AT4G38480	195.828	1.043	0.179	0.000	AT4G38480	AT5G52050	198.102	2.337	0.263	0.000	DTX50
AT5G13700	39.471	1.043	0.390	0.046	PAO1	AT3G20520	23.422	2.349	0.569	0.001	GDPDL5
AT1G19050	402.451	1.045	0.189	0.000	ARR7	AT2G33260	16.969	2.360	0.682	0.006	AT2G33260
AT2G01020	67.141	1.046	0.352	0.022	None	AT3G28340	130.503	2.372	0.292	0.000	GATL10
AT4G15530	6080.275	1.047	0.184	0.000	PPDK	AT5G54490	113.244	2.374	0.272	0.000	PBP1
AT3G23920	3566.061	1.047	0.121	0.000	BAM1	AT5G46710	161.652	2.374	0.283	0.000	AT5G46710
AT2G38250	83.117	1.049	0.353	0.023	GT-3B	AT1G09287	9.913	2.380	0.873	0.041	None
AT2G30230	247.483	1.049	0.264	0.001	AT2G30230	AT3G24780	53.987	2.388	0.456	0.000	None
AT5G43890	48.348	1.049	0.375	0.035	YUC5	AT2G42530	790.484	2.389	0.714	0.008	COR15B
AT4G19960	718.211	1.051	0.147	0.000	KUP9	AT5G41750	180.905	2.389	0.359	0.000	AT5G41750
AT2G18700	2195.905	1.051	0.353	0.022	TPS11	AT1G13480	56.288	2.405	0.434	0.000	None
AT5G47640	490.363	1.052	0.284	0.003	NFYB2	AT4G01985	24.312	2.429	0.672	0.004	AT4G01985
AT1G62300	624.458	1.053	0.168	0.000	WRKY6	AT1G56660	1600.707	2.435	0.212	0.000	AT1G56660
AT5G04720	1129.126	1.053	0.143	0.000	ADR1-L2	AT3G18300	44.451	2.439	0.433	0.000	None
AT3G62720	780.731	1.053	0.160	0.000	XXT1	AT1G01560	39.212	2.445	0.456	0.000	MPK11
AT5G47370	1334.733	1.054	0.180	0.000	HAT2	AT1G17380	89.176	2.446	0.395	0.000	TIFY11A
AT4G34131	406.558	1.055	0.204	0.000	UGT73B3	AT4G29610	42.041	2.454	0.457	0.000	CDA6

Gene ID	baseMean	log2FoldChange	lfcSE	padj	Symbol	Gene ID	baseMean	log2FoldChange	lfcSE	padj	Symbol
AT4G18340	405.489	1.056	0.248	0.000	AT4G18340	AT5G64810	26.681	2.461	0.580	0.000	WRKY51
AT3G57530	1565.608	1.058	0.131	0.000	CPK32	AT3G29000	33.693	2.470	0.558	0.000	CML45
AT4G15760	3218.651	1.060	0.207	0.000	None	AT5G04340	408.367	2.473	0.270	0.000	ZAT6
AT2G34650	119.059	1.065	0.298	0.004	PID	AT2G40140	1968.184	2.475	0.094	0.000	CZF1
AT3G59750	39.782	1.065	0.374	0.031	LECRK58	AT3G50930	307.416	2.485	0.296	0.000	HSR4
AT4G36500	604.366	1.073	0.279	0.002	AT4G36500	AT3G55500	93.820	2.489	0.475	0.000	EXPA16
AT1G27200	627.077	1.074	0.128	0.000	None	AT5G57560	1521.725	2.503	0.433	0.000	XTH22
AT4G25620	905.262	1.075	0.154	0.000	AT4G25620	AT2G30020	516.893	2.507	0.175	0.000	AT2G30020
AT4G15233	305.242	1.078	0.246	0.000	ABCG42	AT3G01795	69.904	2.508	0.376	0.000	None
AT3G47500	3488.724	1.078	0.123	0.000	CDF3	AT2G35710	197.696	2.509	0.266	0.000	PGSIP8
AT5G52570	1316.282	1.078	0.171	0.000	BETA-OHASE 2	AT4G07195	10.393	2.529	0.813	0.016	None
AT5G15240	100.076	1.085	0.312	0.005	AVT1J	AT1G21210	23.467	2.538	0.545	0.000	WAK4
AT3G25250	167.725	1.088	0.260	0.000	OXI1	AT1G66500	193.419	2.544	0.197	0.000	PCFS1
AT1G67880	347.516	1.089	0.136	0.000	AT1G67880	AT1G73805	51.272	2.551	0.429	0.000	SARD1
AT5G06400	38.352	1.090	0.409	0.047	None	AT5G11070	1339.707	2.552	0.206	0.000	None
AT1G13340	146.945	1.093	0.294	0.003	AT1G13340	AT5G39660	1387.002	2.566	0.125	0.000	CDF2
AT3G17510	4543.921	1.094	0.103	0.000	CIPK1	AT1G02660	1247.856	2.566	0.395	0.000	PLIP2
AT1G07985	92.752	1.097	0.348	0.014	AT1G07985	AT1G07330	10.769	2.579	0.893	0.028	AT1G07330
AT2G40080	268.509	1.097	0.204	0.000	ELF4	AT5G11290	18.597	2.583	0.609	0.000	None
AT5G22250	104.692	1.097	0.262	0.000	CAF1-11	AT1G18710	351.480	2.602	0.710	0.003	AtMYB47
AT1G56540	52.743	1.099	0.389	0.033	AT1G56540	AT5G44420	43.348	2.621	0.765	0.006	PDF1.2A
AT3G09600	1513.381	1.100	0.150	0.000	RVE8	AT3G10930	54.124	2.623	0.402	0.000	AT3G10930
AT1G27100	1739.703	1.100	0.126	0.000	AT1G27100	AT5G39580	405.623	2.645	0.449	0.000	PER62
AT1G02810	283.381	1.100	0.199	0.000	PME7	AT4G24170	7.801	2.659	1.000	0.048	KIN7I
AT4G21480	55.694	1.101	0.376	0.025	None	AT3G07650	305.058	2.660	0.265	0.000	COL9
AT2G23100	102.553	1.103	0.254	0.000	None	AT5G06320	317.280	2.672	0.190	0.000	NHL3
AT5G67370	3038.137	1.103	0.215	0.000	CGLD27	AT5G58310	12.855	2.682	0.959	0.035	MES18
AT3G18950	215.527	1.103	0.341	0.011	AT3G18950	AT4G14690	659.004	2.699	0.445	0.000	ELIP2
AT5G09570	72.261	1.103	0.329	0.008	AT5G09570	AT1G72520	228.835	2.715	0.274	0.000	LOX4
AT1G14480	77.333	1.104	0.281	0.001	AT1G14480	AT4G36010	345.933	2.730	0.275	0.000	AT4G36010
AT5G11650	738.986	1.105	0.105	0.000	AT5G11650	AT1G18740	1613.153	2.735	0.166	0.000	AT1G18740
AT5G48070	120.258	1.107	0.290	0.002	XTH20	AT2G41640	510.483	2.746	0.205	0.000	AT2G41640
AT1G70290	4149.742	1.108	0.204	0.000	TPS8	AT3G44260	400.302	2.757	0.255	0.000	CAF1-9

Gene ID	baseMean	log2FoldChange	lfcSE	padj	Symbol	Gene ID	baseMean	log2FoldChange	lfcSE	padj	Symbol
AT3G02150	573.341	1.109	0.175	0.000	TCP13	AT5G42800	612.617	2.765	0.839	0.009	DFRA
AT4G15248	172.832	1.112	0.281	0.001	MIP1A	AT1G07587	13.961	2.782	0.757	0.003	None
AT1G10370	2054.265	1.112	0.133	0.000	GSTU17	AT4G18280	602.720	2.790	0.222	0.000	AT4G18280
AT4G32800	132.728	1.113	0.289	0.002	ERF043	AT5G54470	989.404	2.794	0.142	0.000	AT5G54470
AT2G26190	951.135	1.114	0.141	0.000	IQM4	AT2G28500	84.068	2.804	0.388	0.000	LBD11
AT5G21940	3122.153	1.115	0.412	0.043	AT5G21940	AT3G50310	58.454	2.814	0.620	0.000	MAPKKK20
AT3G14770	945.528	1.117	0.259	0.000	SWEET2	AT4G33970	60.628	2.817	0.479	0.000	PEX4
AT5G02780	167.371	1.118	0.318	0.005	GSTL1	AT5G50360	72.922	2.817	0.576	0.000	AT5G50360
AT1G66180	2151.118	1.118	0.358	0.015	AT1G66180	AT1G70420	865.609	2.864	0.227	0.000	AT1G70420
AT5G13370	1048.430	1.119	0.138	0.000	AT5G13370	AT1G05675	26.467	2.880	0.694	0.001	UGT74E1
AT4G16780	768.491	1.119	0.209	0.000	HAT4	AT5G26700	8.589	2.888	0.888	0.011	None
AT5G47960	50.308	1.122	0.311	0.004	RABA4C	AT5G01760	21.837	2.893	0.604	0.000	TOL7
AT5G14760	631.338	1.123	0.136	0.000	AO	AT1G35140	601.426	2.911	0.440	0.000	EXL1
AT1G02850	2250.837	1.124	0.175	0.000	BGLU11	AT1G09930	7.483	2.930	1.088	0.044	OPT2
AT3G54150	83.054	1.125	0.416	0.044	AT3G54150	AT3G20600	186.308	2.942	0.269	0.000	NDR1
AT3G53960	375.439	1.125	0.157	0.000	NPF5.7	AT5G50450	639.220	2.960	0.281	0.000	None
AT4G05070	2612.515	1.126	0.198	0.000	AT4G05070	AT5G42900	77.348	2.969	0.465	0.000	COR27
AT3G46600	1276.143	1.126	0.124	0.000	SCL30	AT4G17490	438.003	2.970	0.238	0.000	ERF6
AT5G13930	6477.570	1.128	0.307	0.003	CHS	AT1G07050	57.986	2.999	0.554	0.000	AT1G07050
AT5G50915	288.056	1.132	0.304	0.003	BHLH137	AT1G73540	857.259	3.000	0.187	0.000	NUDT21
AT4G00080	123.688	1.135	0.310	0.003	UNE11	AT4G11280	1168.175	3.002	0.177	0.000	ACS6
AT1G19770	1315.644	1.144	0.188	0.000	PUP14	AT2G01300	52.014	3.003	0.513	0.000	AT2G01300
AT4G22758	88.940	1.146	0.333	0.006	None	AT5G17300	2485.036	3.021	0.190	0.000	RVE1
AT4G32480	1202.880	1.148	0.397	0.028	AT4G32480	AT1G09950	28.120	3.026	0.597	0.000	RAS1
AT3G19580	169.112	1.150	0.193	0.000	AZF2	AT1G04570	122.545	3.029	0.699	0.000	None
AT5G14650	96.594	1.153	0.411	0.034	AT5G14650	AT3G48650	13.066	3.036	0.750	0.001	None
AT1G19610	171.247	1.159	0.335	0.006	PDF1.4	AT1G58420	36.617	3.071	0.516	0.000	AT1G58420
AT1G16130	118.769	1.161	0.340	0.007	WAKL2	AT2G14247	254.805	3.084	1.084	0.031	AT2G14247
AT1G72940	425.756	1.161	0.151	0.000	AT1G72940	AT1G12030	118.061	3.104	1.159	0.046	AT1G12030
AT3G11410	2517.931	1.162	0.333	0.005	PP2CA	AT4G18650	7.587	3.106	1.051	0.024	DOGL4
AT2G43820	2860.933	1.166	0.168	0.000	UGT74F2	AT2G46400	82.576	3.107	0.399	0.000	WRKY46
AT5G49480	4384.074	1.168	0.131	0.000	ATCP1	AT3G55580	119.348	3.193	0.380	0.000	AT3G55580
AT4G06534	119.575	1.170	0.325	0.004	None	AT1G74450	871.048	3.193	0.153	0.000	AT1G74450

Gene ID	baseMean	log2FoldChange	lfcSE	padj	Symbol	Gene ID	baseMean	log2FoldChange	lfcSE	padj	Symbol
AT5G44568	74.092	1.171	0.375	0.015	None	AT3G48360	4246.596	3.197	0.445	0.000	BT2
AT5G65207	714.706	1.172	0.259	0.000	None	AT5G40000	22.412	3.211	0.636	0.000	AT5G40000
AT1G02640	1282.408	1.180	0.403	0.025	BXL2	AT1G50745	27.743	3.228	0.649	0.000	None
AT3G52520	31.791	1.182	0.421	0.034	None	AT1G49230	114.041	3.293	0.327	0.000	ATL78
AT1G58410	48.360	1.185	0.423	0.035	RXW24L	AT3G45660	44.312	3.326	0.496	0.000	AT3G45660
AT4G02075	208.763	1.185	0.218	0.000	PIT1	AT2G45760	21.294	3.336	0.749	0.000	BAP2
AT4G01950	810.313	1.186	0.155	0.000	ATGPAT3	AT3G02840	16.185	3.347	0.926	0.004	AT3G02840
AT2G37970	50.244	1.188	0.334	0.004	SOUL-1	AT4G14368	5.422	3.353	1.191	0.034	AT4G14368
AT5G14120	6908.288	1.191	0.348	0.006	AT5G14120	AT3G21660	45.686	3.361	0.589	0.000	AT3G21660
AT5G38450	27.321	1.191	0.447	0.047	CYP735A1	AT2G24681	6.132	3.406	1.178	0.028	REM11
AT4G27450	2877.814	1.193	0.420	0.031	AT4G27450	AT5G03210	115.884	3.423	0.380	0.000	None
AT3G62070	284.869	1.194	0.293	0.001	None	AT4G13395	46.418	3.449	0.587	0.000	DVL10
AT5G63130	99.512	1.195	0.278	0.000	None	AT1G15010	123.211	3.454	0.485	0.000	AT1G15010
AT5G49360	14789.871	1.196	0.437	0.040	BXL1	AT3G48520	227.804	3.486	0.336	0.000	CYP94B3
AT1G31355	40.436	1.198	0.407	0.024	None	AT2G31590	5.824	3.570	1.218	0.025	None
AT1G29690	689.956	1.201	0.166	0.000	CAD1	AT5G17350	162.794	3.630	0.271	0.000	AT5G17350
AT1G63090	894.575	1.206	0.215	0.000	PP2A11	AT5G43620	172.702	3.633	0.332	0.000	PCFS5
AT1G77990	455.302	1.210	0.191	0.000	SULTR2;2	AT1G80840	257.186	3.648	0.335	0.000	WRKY40
AT5G64310	838.602	1.211	0.171	0.000	AGP1	AT3G55980	2841.813	3.676	0.127	0.000	SZF1
AT1G11260	5311.772	1.215	0.457	0.048	STP1	AT3G51400	24.853	3.702	0.882	0.000	AT3G51400
AT2G43290	829.251	1.218	0.108	0.000	CML5	AT2G17850	12.876	3.731	1.357	0.039	AT2G17850
AT3G51895	1899.124	1.224	0.202	0.000	SULTR3;1	AT5G05410	525.061	3.735	0.258	0.000	DREB2A
AT1G72920	124.577	1.224	0.287	0.000	AT1G72920	AT2G20825	7.119	3.759	1.263	0.022	ULT2
AT4G24230	1516.189	1.228	0.446	0.039	ACBP3	AT1G06030	24.244	3.769	0.890	0.000	AT1G06030
AT2G02100	2579.114	1.230	0.156	0.000	PDF2.2	AT3G24600	4.902	3.806	1.410	0.044	None
AT3G01960	63.337	1.230	0.367	0.008	None	AT4G27652	309.954	3.817	0.256	0.000	AT4G27652
AT3G15210	873.394	1.231	0.157	0.000	ERF4	AT1G73066	45.144	3.817	0.527	0.000	None
AT5G45110	781.820	1.234	0.135	0.000	NPR3	AT2G41280	13.020	3.830	1.177	0.011	M10
AT5G24210	1010.795	1.234	0.332	0.003	AT5G24210	AT1G28370	110.987	3.845	0.323	0.000	ERF11
AT5G08790	1220.729	1.235	0.110	0.000	NAC081	AT4G17090	10453.908	3.866	0.147	0.000	BAM3
AT4G24380	168.743	1.236	0.191	0.000	AT4G24380	AT1G25400	777.503	3.895	0.421	0.000	AT1G25400
AT5G05365	51.164	1.236	0.435	0.031	None	AT5G20230	2023.136	3.896	0.412	0.000	BCB
AT5G67480	1193.792	1.237	0.184	0.000	BT4	AT3G61190	167.197	3.901	0.396	0.000	BAP1

Gene ID	baseMean	log2FoldChange	lfcSE	padj	Symbol	Gene ID	baseMean	log2FoldChange	lfcSE	padj	Symbol
AT2G23120	5140.618	1.239	0.129	0.000	AT2G23120	AT1G18300	593.173	3.904	0.286	0.000	NUDT4
AT1G72910	154.264	1.240	0.311	0.001	AT1G72910	AT4G28405	7.053	3.913	1.111	0.005	None
AT3G28270	1513.396	1.241	0.333	0.003	AT3G28270	AT4G27657	134.652	3.915	0.338	0.000	AT4G27657
AT3G17225	32.358	1.243	0.421	0.024	None	AT4G01360	46.067	3.917	0.661	0.000	AT4G01360
AT5G54720	70.508	1.246	0.327	0.002	AT5G54720	AT1G30190	18.869	3.960	0.966	0.001	None
AT2G30250	565.430	1.247	0.229	0.000	WRKY25	AT3G02515	6.622	3.973	1.364	0.026	None
AT2G39350	425.094	1.249	0.178	0.000	ABCG1	AT3G17980	10.786	3.975	1.136	0.005	CAR4
AT4G24260	38.358	1.251	0.405	0.017	KOR3	AT3G04640	836.637	3.979	0.207	0.000	AT3G04640
AT4G05050	13951.043	1.251	0.105	0.000	UBQ11	AT4G09030	4.656	3.988	1.455	0.040	AGP10
AT2G36690	206.972	1.252	0.352	0.004	AT2G36690	AT4G33980	187.587	4.114	0.427	0.000	AT4G33980
AT4G12480	3635.804	1.252	0.336	0.003	EARLI1	AT4G24570	661.457	4.117	0.203	0.000	PUMP4
AT1G74350	73.661	1.268	0.295	0.000	None	AT5G24470	1759.626	4.174	0.194	0.000	APRR5
AT1G33610	151.879	1.270	0.281	0.000	AT1G33610	AT3G49130	25.294	4.178	0.674	0.000	AT3G49130
AT5G08760	399.512	1.270	0.262	0.000	None	AT1G50750	45.720	4.195	0.495	0.000	None
AT4G25700	2078.854	1.271	0.183	0.000	BETA-OHASE 1	AT5G46295	15.976	4.220	0.846	0.000	None
AT1G03610	1342.449	1.274	0.209	0.000	AT1G03610	AT4G25433	32.869	4.281	0.918	0.000	AT4G25433
AT5G38350	56.888	1.275	0.381	0.008	AT5G38350	AT5G62520	89.409	4.303	0.521	0.000	SRO5
AT5G26340	993.092	1.277	0.170	0.000	STP13	AT4G03505	6.082	4.324	1.486	0.027	AT4G03505
AT5G53290	128.713	1.277	0.285	0.000	CRF3	AT1G61340	376.438	4.406	0.230	0.000	None
AT2G31380	2461.759	1.279	0.143	0.000	BBX25	AT4G29780	887.275	4.508	0.183	0.000	AT4G29780
AT5G59340	55.931	1.279	0.327	0.001	WOX2	AT1G06417	5.408	4.586	1.709	0.045	None
AT2G47780	41.911	1.282	0.441	0.027	AT2G47780	AT1G27730	1044.411	4.587	0.220	0.000	ZAT10
AT4G39320	94.614	1.288	0.248	0.000	AT4G39320	AT1G11210	1115.410	4.601	0.214	0.000	AT1G11210
AT3G16510	80.625	1.289	0.296	0.000	None	AT1G51090	179.262	4.622	0.395	0.000	AT1G51090
AT1G64065	51.785	1.291	0.367	0.005	AT1G64065	AT1G07135	603.425	4.627	0.198	0.000	AT1G07135
AT1G61800	95.778	1.301	0.465	0.035	GPT2	AT5G62360	503.971	4.655	0.296	0.000	AT5G62360
AT1G16530	53.145	1.301	0.322	0.001	LBD3	AT3G12960	7.156	4.667	1.323	0.005	AT3G12960
AT5G02020	1004.977	1.302	0.196	0.000	SIS	AT1G34050	6.564	4.706	1.623	0.027	AT1G34050
AT2G46830	5854.465	1.304	0.117	0.000	CCA1	AT1G68050	543.140	4.732	0.299	0.000	ADO3
AT1G64760	265.019	1.305	0.229	0.000	AT1G64760	AT5G59820	1057.400	4.756	0.390	0.000	ZAT12
AT1G23870	2170.655	1.305	0.290	0.000	TPS9	AT1G33760	35.816	4.769	0.628	0.000	ERF022
AT5G58120	397.077	1.310	0.157	0.000	AT5G58120	AT3G12900	117.471	4.788	1.419	0.007	AT3G12900
AT2G39980	393.537	1.311	0.243	0.000	AT2G39980	AT4G27654	22.848	4.832	0.763	0.000	AT4G27654

Gene ID	baseMean	log2FoldChange	lfcSE	padj	Symbol	Gene ID	baseMean	log2FoldChange	lfcSE	padj	Symbol
AT5G15130	247.798	1.311	0.231	0.000	WRKY72	AT1G05330	12.329	4.917	1.040	0.000	None
AT2G40130	253.387	1.316	0.346	0.002	SMXL8	AT1G01310	6.532	4.930	1.438	0.006	AT1G01310
AT3G59080	341.552	1.320	0.208	0.000	AT3G59080	AT2G40925	5.651	4.954	1.785	0.037	None
AT1G69490	449.766	1.322	0.435	0.019	NAC029	AT5G05220	7.373	5.018	1.793	0.035	None
AT1G21050	870.230	1.323	0.157	0.000	None	AT5G42380	78.444	5.024	0.889	0.000	CML37
AT1G19640	74.877	1.323	0.413	0.012	JMT	AT1G68765	5.728	5.036	1.626	0.016	IDA
AT5G16360	137.356	1.325	0.235	0.000	AT5G16360	AT3G22830	144.954	5.082	0.383	0.000	HSFA6B
AT5G54710	285.076	1.329	0.233	0.000	AT5G54710	AT5G17030	9.130	5.088	1.725	0.024	UGT78D3
AT5G56795	84.215	1.329	0.324	0.001	None	AT1G75945	58.093	5.211	1.508	0.006	None
AT3G12320	3193.023	1.329	0.119	0.000	LNK3	AT5G37250	25.168	5.288	1.006	0.000	None
AT4G37260	1053.772	1.330	0.163	0.000	MYB73	AT5G06520	8.697	5.291	1.347	0.001	AT5G06520
AT4G23220	58.277	1.335	0.376	0.004	CRK14	AT3G11020	72.180	5.295	0.576	0.000	DREB2B
AT1G78070	1267.935	1.336	0.231	0.000	AT1G78070	AT3G60930	1288.630	5.322	0.168	0.000	None
AT3G16720	261.965	1.338	0.207	0.000	ATL2	AT1G60190	2439.402	5.332	0.441	0.000	PUB19
AT2G37770	728.042	1.340	0.259	0.000	AKR4C9	AT1G56060	9.434	5.414	1.694	0.012	None
AT5G58770	991.621	1.348	0.227	0.000	AT5G58770	AT5G45340	731.102	5.485	0.246	0.000	CYP707A3
AT4G19191	39.014	1.348	0.376	0.004	PCMP-E1	AT5G37260	4380.361	5.518	0.154	0.000	RVE2
AT1G20440	11391.239	1.357	0.141	0.000	COR47	AT2G35670	6.846	5.621	1.694	0.009	FIS2
AT2G04032	74.813	1.362	0.417	0.010	ZIP7	AT3G25225	5.157	5.702	1.702	0.008	None
AT1G67470	153.424	1.362	0.229	0.000	None	AT1G54750	4.507	5.784	1.943	0.022	None
AT2G33510	326.879	1.366	0.167	0.000	AT2G33510	AT3G56790	18.752	5.795	1.004	0.000	AT3G56790
AT1G64500	4170.470	1.370	0.114	0.000	AT1G64500	AT3G11773	9.623	5.804	1.561	0.003	AT3G11773
AT2G39650	123.794	1.373	0.242	0.000	AT2G39650	AT5G45105	5.903	5.814	1.998	0.026	None
AT1G10340	66.639	1.376	0.450	0.018	AT1G10340	AT5G45630	71.689	5.903	0.705	0.000	AT5G45630
AT4G11300	334.623	1.383	0.151	0.000	None	AT4G08145	11.661	5.963	1.644	0.003	None
AT1G21670	1104.689	1.384	0.170	0.000	AT1G21670	AT2G32050	4.408	5.987	1.883	0.013	AT2G32050
AT1G01130	79.898	1.385	0.329	0.000	AT1G01130	AT2G17660	66.604	6.059	0.790	0.000	AT2G17660
AT5G13210	86.753	1.386	0.379	0.003	AT5G13210	AT1G70390	5.720	6.154	1.697	0.003	None
AT5G62430	1078.596	1.386	0.220	0.000	CDF1	AT4G33860	5.167	6.294	1.800	0.005	AT4G33860
AT1G05575	49.553	1.386	0.442	0.015	AT1G05575	AT1G24159	4.678	6.343	1.887	0.008	None
AT2G19810	663.062	1.388	0.153	0.000	AT2G19810	AT1G70640	260.153	6.356	0.747	0.000	None
AT1G56430	341.966	1.389	0.509	0.041	NAS4	AT1G76650	608.387	6.374	0.669	0.000	CML38
AT5G39610	345.971	1.389	0.491	0.032	NAC92	AT5G20260	13.009	6.643	1.545	0.000	None

Gene ID	baseMean	log2FoldChange	lfcSE	padj	Symbol	Gene ID	baseMean	log2FoldChange	lfcSE	padj	Symbol
AT5G47220	476.946	1.391	0.206	0.000	ERF2	AT1G47405	12.287	6.713	2.351	0.030	None
AT5G05190	154.880	1.393	0.224	0.000	EDR4	AT1G33160	5.418	6.760	1.877	0.004	None
AT3G56710	88.013	1.398	0.433	0.011	SIB1	AT1G62000	5.134	6.778	1.827	0.003	None
AT1G10810	48.267	1.401	0.390	0.004	AT1G10810	AT1G73190	29.647	6.818	1.587	0.000	TIP3-1
AT5G10750	549.083	1.402	0.136	0.000	None	AT2G23808	6.388	7.041	1.723	0.001	None
AT3G02800	62.959	1.403	0.349	0.001	DSP3	AT1G73510	30.882	7.130	1.179	0.000	None
AT3G21150	148.134	1.403	0.397	0.005	BBX32	AT4G18422	206.589	7.220	0.598	0.000	None
AT4G19420	4381.114	1.405	0.317	0.000	AT4G19420	AT2G31100	19.959	7.230	1.528	0.000	None
AT1G02470	111.095	1.406	0.433	0.011	AT1G02470	AT1G30390	51.007	7.311	1.450	0.000	None
AT5G66210	1019.664	1.415	0.103	0.000	CPK28	AT1G12610	21.917	7.509	1.592	0.000	DREB1F
AT1G52640	25.074	1.416	0.450	0.014	AT1G52640	AT4G25480	3728.434	7.759	0.214	0.000	DREB1A
AT5G15970	3352.805	1.420	0.184	0.000	KIN2	AT5G13655	19.657	8.109	1.608	0.000	None
AT4G38340	48.531	1.423	0.400	0.004	NLP3	AT1G29680	15.130	8.307	1.644	0.000	OBAP2C
AT5G20670	127.460	1.427	0.297	0.000	AT5G20670	AT2G05441	17.984	8.356	1.595	0.000	None
AT4G22710	34.585	1.430	0.429	0.008	CYP706A2	AT1G26790	642.221	8.578	0.613	0.000	None
AT2G41250	4509.364	1.430	0.137	0.000	AT2G41250	AT4G25470	6343.032	8.978	0.210	0.000	DREB1C
AT3G50970	1293.356	1.433	0.099	0.000	XERO2	AT1G19040	27.374	9.217	1.584	0.000	None
AT5G58650	293.079	1.434	0.281	0.000	PSY1	AT4G25490	2202.626	10.258	0.456	0.000	DREB1B
						AT5G51990	252.155	12.462	1.463	0.000	DREB1D

Appendix table 7.2 List of Genes in K-means clustering

Gene ID	Symbol	Clusters	Gene ID	Symbol	Clusters
AT1G01060	LHY	1	AT1G09750	NA	2
AT1G02470	NA	1	AT1G10760	SEX1	2
AT1G02850	BGLU11	1	AT1G14200	NA	2
AT1G04570	NA	1	AT1G14430	NA	2
AT1G07050	NA	1	AT1G14920	GAI	2
AT1G07150	MAPKKK13	1	AT1G20620	CAT3	2
AT1G09350	GolS3	1	AT1G36940	NA	2
AT1G12420	ACR8	1	AT1G61500	NA	2
AT1G13260	RAV1	1	AT1G64170	CHX16	2
AT1G19050	ARR7	1	AT1G69830	AMY3	2
AT1G19640	JMT	1	AT1G70820	NA	2
AT1G21670	NA	1	AT1G72645	NA	2
AT1G22570	NA	1	AT1G73750	NA	2
AT1G26790	NA	1	AT1G09467	NA	2
AT1G48100	NA	1	AT1G75960	NA	2
AT1G49230	NA	1	AT1G76610	NA	2
AT1G07587	NA	1	AT1G79460	GA2	2
AT1G51090	NA	1	AT2G01170	BAT1	2
AT1G55950	NA	1	AT2G06925	PLA2-ALPHA	2
AT1G56430	NAS4	1	AT2G23770	LYK4	2
AT1G63090	PP2-A11	1	AT2G26220	#N/A	2
AT1G64500	NA	1	AT2G26515	NA	2
AT1G67470	NA	1	AT2G29170	NA	2
AT1G68050	FKF1	1	AT2G32100	OFP16	2
AT1G68500	NA	1	AT2G32390	GLR3.5	2
AT1G69570	NA	1	AT2G34430	LHB1B1	2
AT1G70420	NA	1	AT2G40610	EXPA8	2
AT1G70640	NA	1	AT2G40840	DPE2	2
AT1G70800	EHB1	1	AT2G47460	MYB12	2
AT1G72910	NA	1	AT3G01310	NA	2
AT1G72920	NA	1	AT3G03830	SAUR28	2
AT1G72940	NA	1	AT3G03850	SAUR26	2
AT1G74890	ARR15	1	AT3G07215	NA	2
AT2G15880	NA	1	AT3G13277	NA	2
AT2G16890	NA	1	AT3G03265	NA	2
AT2G17660	NA	1	AT3G16870	GATA17	2
AT2G30040	MAPKKK14	1	AT3G18080	BGLU44	2
AT2G30230	NA	1	AT3G18773	NA	2
AT2G31380	STH	1	AT3G25495	#N/A	2
AT2G35290	NA	1	AT3G28370	NA	2
AT2G36220	NA	1	AT3G29320	PHS1	2
AT2G37770	ChlAKR	1	AT3G45230	NA	2
AT2G40080	ELF4	1	AT3G46370	NA	2
AT2G40130	NA	1	AT3G46970	PHS2	2
AT2G42530	COR15B	1	AT3G53800	Fes1B	2
AT2G46830	CCA1	1	AT3G60220	ATL4	2
AT2G46940	NA	1	AT3G61460	BRH1	2
AT3G02380	COL2	1	AT3G61898	NA	2
AT3G01795	NA	1	AT3G62750	BGLU8	2
AT3G06020	FAF4	1	AT4G09020	ISA3	2
AT3G06520	NA	1	AT4G12900	NA	2
AT3G07650	COL9	1	AT4G14230	NA	2
AT3G07720	NA	1	AT4G16870	#N/A	2
AT3G12320	NA	1	AT4G16880	NA	2

Gene ID	Symbol	Clusters	Gene ID	Symbol	Clusters
AT3G14770	SWEET2	1	AT4G26530	FBA5	2
AT3G15500	NAC3	1	AT4G27440	PORB	2
AT3G18950	NA	1	AT4G27840	NA	2
AT3G21150	BBX32	1	AT4G28240	NA	2
AT3G21890	BBX31	1	AT4G34760	NA	2
AT3G23170	NA	1	AT4G38840	NA	2
AT3G23920	BAM1	1	AT4G38850	SAUR15	2
AT3G28910	MYB30	1	AT4G38860	NA	2
AT3G47500	CDF3	1	AT5G02160	NA	2
AT3G50310	MAPKKK20	1	AT5G02810	PRR7	2
AT3G51400	NA	1	AT5G11610	NA	2
AT3G55580	NA	1	AT5G02515	NA	2
AT3G56400	WRKY70	1	AT5G18010	SAUR19	2
AT3G56710	SIB1	1	AT5G18020	SAUR20	2
AT3G63060	EDL3	1	AT5G18030	NA	2
AT4G05070	NA	1	AT5G18050	SAUR22	2
AT4G13395	RTFL12	1	AT5G18060	SAUR23	2
AT4G14690	ELIP2	1	AT5G22794	NA	2
AT4G15248	BBX30	1	AT5G41400	NA	2
AT4G15430	NA	1	AT5G43440	NA	2
AT4G17090	CT-BMY	1	AT5G60100	PRR3	2
AT4G17490	ERF6	1	AT5G64860	DPE1	2
AT4G18422	NA	1	AT1G02660	NA	4
AT4G06880	NA	1	AT1G07135	NA	4
AT4G19960	KUP9	1	AT1G07330	NA	4
AT4G25433	NA	1	AT1G09070	SRC2	4
AT4G25700	BETA-OHASE 1	1	AT1G09950	RAS1	4
AT4G27360	NA	1	AT1G11210	NA	4
AT4G29190	OZF2	1	AT1G13480	NA	4
AT4G29610	NA	1	AT1G15010	NA	4
AT4G33980	NA	1	AT1G17380	JAZ5	4
AT4G36010	NA	1	AT1G18300	NUDT4	4
AT4G36110	SAUR9	1	AT1G18740	NA	4
AT4G36950	MAPKKK21	1	AT1G20440	COR47	4
AT5G08760	NA	1	AT1G20450	ERD10	4
AT5G10750	NA	1	AT1G21050	NA	4
AT5G14760	AO	1	AT1G23710	NA	4
AT5G15190	NA	1	AT1G25400	NA	4
AT5G15240	NA	1	AT1G27100	NA	4
AT5G15950	NA	1	AT1G27730	STZ	4
AT5G17050	UGT78D2	1	AT1G28370	ERF11	4
AT5G17300	RVE1	1	AT1G29690	CAD1	4
AT5G18670	BMY3	1	AT1G30390	#N/A	4
AT5G20230	BCB	1	AT1G06417	NA	4
AT5G24470	PRR5	1	AT1G33610	NA	4
AT5G26340	MSS1	1	AT1G49450	NA	4
AT5G37260	RVE2	1	AT1G54750	#N/A	4
AT5G41590	NA	1	AT1G56660	NA	4
AT5G41740	NA	1	AT1G60190	PUB19	4
AT5G42760	NA	1	AT1G61340	FBS1	4
AT5G42900	COR27	1	AT1G62300	WRKY6	4
AT5G45630	NA	1	AT1G65490	NA	4
AT5G46710	NA	1	AT1G66090	NA	4
AT5G47060	NA	1	AT1G69890	NA	4
AT5G47220	ERF2	1	AT1G72520	LOX4	4
AT5G48250	BBX8	1	AT1G73066	NA	4
AT5G49330	MYB111	1	AT1G73500	MKK9	4

Gene ID	Symbol	Clusters	Gene ID	Symbol	Clusters
AT5G49480	CP1	1	AT1G73540	NUDT21	4
AT5G50360	NA	1	AT1G73805	SARD1	4
AT5G50450	NA	1	AT1G73890	NA	4
AT5G52310	LTI78	1	AT1G74450	NA	4
AT5G52570	BETA-OHASE 2	1	AT1G76650	CML38	4
AT5G54470	BBX29	1	AT1G78070	NA	4
AT5G58120	NA	1	AT1G80130	NA	4
AT5G58770	cPT4	1	AT1G80840	WRKY40	4
AT5G60680	NA	1	AT2G02100	LCR69	4
AT5G62360	NA	1	AT2G16060	HB1	4
AT5G62430	CDF1	1	AT2G17036	NA	4
AT5G63130	NA	1	AT2G17840	ERD7	4
AT1G01310	NA	3	AT2G22500	UCP5	4
AT1G01560	MPK11	3	AT2G23120	NA	4
AT1G02610	NA	3	AT2G23810	TET8	4
AT1G05330	NA	3	AT2G28500	LBD11	4
AT1G06030	NA	3	AT2G30250	WRKY25	4
AT1G12610	DDF1	3	AT2G32050	NA	4
AT1G18200	RABA6b	3	AT2G33260	NA	4
AT1G19020	NA	3	AT2G34650	PID	4
AT1G19040	NA	3	AT2G35710	PGSIP7	4
AT1G19180	JAZ1	3	AT2G37970	SOUL-1	4
AT1G20823	NA	3	AT2G38470	WRKY33	4
AT1G22190	NA	3	AT2G40000	HSPRO2	4
AT1G23870	TPS9	3	AT2G40140	CZF1	4
AT1G24159	NA	3	AT2G40925	NA	4
AT1G32920	NA	3	AT2G41010	CAMBP25	4
AT1G33160	NA	3	AT2G41250	NA	4
AT1G33760	NA	3	AT2G41640	NA	4
AT1G35210	NA	3	AT3G02140	TMAC2	4
AT1G50745	NA	3	AT3G02515	#N/A	4
AT1G50750	NA	3	AT3G04640	NA	4
AT1G58420	NA	3	AT3G04800	TIM23-3	4
AT1G62000	NA	3	AT3G09520	EXO70H4	4
AT1G66500	NA	3	AT3G09600	RVE8	4
AT1G73510	NA	3	AT3G11020	DREB2B	4
AT1G74830	NA	3	AT3G15210	ERF4	4
AT1G76600	NA	3	AT3G16510	NA	4
AT2G01300	NA	3	AT3G16720	ATL2	4
AT2G05441	NA	3	AT3G17980	C2	4
AT2G23808	NA	3	AT3G19030	NA	4
AT2G25460	NA	3	AT3G20600	NDR1	4
AT2G26480	UGT76D1	3	AT3G22830	HSFA6B	4
AT2G27080	NA	3	AT3G24600	NA	4
AT2G27500	NA	3	AT3G45660	NA	4
AT2G30020	NA	3	AT3G46620	RDUF1	4
AT2G31100	NA	3	AT3G47660	NA	4
AT2G08435	NA	3	AT3G48360	BT2	4
AT2G31590	NA	3	AT3G48510	NA	4
AT2G32020	NA	3	AT3G48520	CYP94B3	4
AT2G32210	NA	3	AT3G48650	#N/A	4
AT2G35670	FIS2	3	AT3G49530	NAC062	4
AT2G43290	MSS3	3	AT3G51895	SULTR3;1	4
AT2G45760	BAP2	3	AT3G52800	NA	4
AT2G46400	WRKY46	3	AT3G55880	SUE4	4
AT3G02800	PFA-DSP3	3	AT3G55980	SZF1	4
AT3G02840	NA	3	AT3G56880	NA	4

Gene ID	Symbol	Clusters	Gene ID	Symbol	Clusters
AT3G03280	NA	3	AT3G57530	CPK32	4
AT3G10930	NA	3	AT3G59350	NA	4
AT3G12960	SMP1	3	AT3G60930	#N/A	4
AT3G15450	NA	3	AT3G61190	BAP1	4
AT3G15740	NA	3	AT3G62260	NA	4
AT3G16860	COBL8	3	AT3G62550	NA	4
AT3G18300	NA	3	AT4G01250	WRKY22	4
AT3G19580	ZF2	3	AT4G05050	UBQ11	4
AT3G21660	NA	3	AT4G08145	#N/A	4
AT3G22961	NA	3	AT4G11280	ACS6	4
AT3G23250	MYB15	3	AT4G11300	NA	4
AT3G24780	NA	3	AT4G17615	CBL1	4
AT3G25250	AGC2-1	3	AT4G18280	NA	4
AT3G28340	GATL10	3	AT4G18880	HSF A4A	4
AT3G29000	NA	3	AT4G19191	NA	4
AT3G44260	CAF1a	3	AT4G22758	NA	4
AT3G45060	NRT2.6	3	AT4G24380	NA	4
AT3G45960	EXLA3	3	AT4G24570	DIC2	4
AT3G48100	RR5	3	AT4G25470	CBF2	4
AT3G49130	NA	3	AT4G25480	DREB1A	4
AT3G50930	BCS1	3	AT4G25490	CBF1	4
AT3G50970	LTI30	3	AT4G27657	NA	4
AT3G52400	SYP122	3	AT4G30350	NA	4
AT3G54000	NA	3	AT4G33920	NA	4
AT3G56790	NA	3	AT4G33985	NA	4
AT4G01360	BPS3	3	AT4G34150	NA	4
AT4G08040	ACS11	3	AT4G36820	NA	4
AT4G17230	SCL13	3	AT4G37260	MYB73	4
AT4G27280	NA	3	AT4G37610	BT5	4
AT4G27652	NA	3	AT5G03210	DIP2	4
AT4G27654	NA	3	AT5G04340	ZAT6	4
AT4G28405	NA	3	AT5G04720	ADR1-L2	4
AT4G29780	NA	3	AT5G05410	DREB2A	4
AT4G33970	NA	3	AT5G06320	NHL3	4
AT4G35985	NA	3	AT5G08790	ATAF2	4
AT4G39070	BZS1	3	AT5G11070	NA	4
AT4G39320	NA	3	AT5G11650	NA	4
AT5G01100	FRB1	3	AT5G13655	NA	4
AT5G01760	NA	3	AT5G14570	NRT2.7	4
AT5G08770	NA	3	AT5G16200	NA	4
AT5G15130	WRKY72	3	AT5G16960	NA	4
AT5G15970	KIN2	3	AT5G17350	NA	4
AT5G16360	NA	3	AT5G17460	NA	4
AT5G17540	NA	3	AT5G17850	NA	4
AT5G20260	NA	3	AT5G19240	NA	4
AT5G20670	NA	3	AT5G24510	NA	4
AT5G25250	FLOT1	3	AT5G24590	TIP	4
AT5G26920	CBP60G	3	AT5G37770	TCH2	4
AT5G28630	NA	3	AT5G38350	NA	4
AT5G37250	NA	3	AT5G39660	CDF2	4
AT5G40000	NA	3	AT5G39785	NA	4
AT5G40010	AATP1	3	AT5G45110	NPR3	4
AT5G41750	NA	3	AT5G45340	CYP707A3	4
AT5G42380	CML37	3	AT5G47230	ERF5	4
AT5G43620	NA	3	AT5G51390	NA	4
AT5G46295	NA	3	AT5G52050	NA	4
AT5G49520	WRKY48	3	AT5G54490	PBP1	4

Gene ID	Symbol	Clusters	Gene ID	Symbol	Clusters
AT5G51990	CBF4	3	AT5G58650	PSY1	4
AT5G52750	NA	3	AT5G59340	WOX2	4
AT5G61600	ERF104	3	AT5G59820	RHL41	4
AT5G62520	SRO5	3	AT5G62470	MYB96	4
AT5G63160	BT1	3	AT5G64660	CMPG2	4
AT5G64870	NA	3	AT5G64810	WRKY51	4
AT5G65207	NA	3	AT5G65300	NA	4
AT5G65350	HTR11	3	AT5G66210	CPK28	4
AT5G66650	NA	3			

Appendix table 7.3 List of Normalised DEGs from indICE1. Asterisks indicate genes overlapped with ICE1-dependent genes from K-means clustering

Gene ID	Regulated by indICE1	Symbol	Gene ID	Regulated by indICE1	Symbol
AT1G05560	up-regulation	UGT1	AT4G25810	up-regulation	XTH23
AT1G05562	up-regulation	None	AT4G28450	up-regulation	AT4G28450
AT1G08090	up-regulation	NRT2.1	AT4G34590	up-regulation	BZIP11
AT1G09310	up-regulation	AT1G09310	AT4G36020	up-regulation	CSP1
AT1G14060	up-regulation	AT1G14060	AT4G36880	up-regulation	None
AT1G14120	up-regulation	AT1G14120	AT4G37370	up-regulation	CYP81D8
AT1G18810	up-regulation	PKS3	AT4G38770	up-regulation	PRP4
AT1G29660	up-regulation	AT1G29660	AT4G38775	up-regulation	None
AT1G31580	up-regulation	ECS1	AT5G01100	up-regulation	FRB1 *
AT1G33600	up-regulation	AT1G33600	AT5G01790	up-regulation	None
AT1G48000	up-regulation	MYB112	AT5G05990	up-regulation	AT5G05990
AT1G49750	up-regulation	AT1G49750	AT5G12110	up-regulation	AT5G12110
AT1G49860	up-regulation	GSTF14	AT5G25450	up-regulation	QCR7-2
AT1G52930	up-regulation	BRIX1-2	AT5G33370	up-regulation	AT5G33370
AT1G63840	up-regulation	AT1G63840	AT5G43330	up-regulation	MDH2
AT1G66580	up-regulation	RPL10C	AT5G48570	up-regulation	FKBP65
AT1G72600	up-regulation	None	AT5G53400	up-regulation	BOB1
AT1G72610	up-regulation	GLP1	AT5G55620	up-regulation	AT5G55620
AT1G76470	up-regulation	AT1G76470	AT5G57180	up-regulation	CIA2
AT1G78380	up-regulation	GSTU19	AT5G59820	up-regulation	ZAT12
AT1G79160	up-regulation	None	AT1G04790	down-regulation	None
AT2G01670	up-regulation	NUDT17	AT1G05570	down-regulation	CALS1
AT2G15050	up-regulation	LTP7	AT1G06150	down-regulation	EMB1444
AT2G16900	up-regulation	None	AT1G14960	down-regulation	AT1G14960
AT2G19310	up-regulation	HSP18.5	AT1G21310	down-regulation	EXT3
AT2G24500	up-regulation	REIL2	AT1G52060	down-regulation	JAL9
AT2G29420	up-regulation	GSTU7	AT1G52760	down-regulation	CSE
AT2G08340	up-regulation	None	AT1G61810	down-regulation	BGLU45
AT2G36792	up-regulation	None	AT1G80050	down-regulation	APT2
AT2G36790	up-regulation	UGT73C6	AT2G01830	down-regulation	AHK4
AT2G36950	up-regulation	HIPP05	AT2G03890	down-regulation	PI4KG7
AT2G37710	up-regulation	LECRK41	AT2G16980	down-regulation	AT2G16980
AT2G41090	up-regulation	CML10	AT2G27370	down-regulation	CASP3
AT2G42710	up-regulation	AT2G42710	AT2G28671	down-regulation	AT2G28671

Gene ID	Regulated by indICE1	Symbol	Gene ID	Regulated by indICE1	Symbol
AT2G47730	up-regulation	GSTF8	AT2G36100	down-regulation	CASP1
AT3G01790	up-regulation	AT3G01790	AT2G39040	down-regulation	PER24
AT3G04000	up-regulation	ChlADR2	AT3G09940	down-regulation	MDAR3
AT3G04710	up-regulation	TPR10	AT3G14540	down-regulation	TPS19
AT3G08590	up-regulation	AT3G08590	AT3G16340	down-regulation	ABCG29
AT3G08950	up-regulation	HCC1	AT3G08405	down-regulation	None
AT3G03095	up-regulation	None	AT4G02290	down-regulation	AtGH9B13
AT3G26744	up-regulation	SCRM	AT4G02970	down-regulation	None
AT3G27540	up-regulation	AT3G27540	AT4G04970	down-regulation	CALS11
AT3G27880	up-regulation	AT3G27880	AT4G12520	down-regulation	AT4G12520
AT3G50910	up-regulation	AT3G50910	AT4G15393	down-regulation	CYP702A5
AT3G52870	up-regulation	IQM3	AT4G15910	down-regulation	ATDI21
AT3G53230	up-regulation	CDC48D	AT4G19030	down-regulation	NIP1-1
AT3G54420	up-regulation	EP3	AT4G22750	down-regulation	PAT13
AT3G59010	up-regulation	PME35	AT4G26120	down-regulation	AT4G26120
AT3G62270	up-regulation	BOR2	AT4G26320	down-regulation	AGP13
AT4G01250	up-regulation	WRKY22	AT4G30170	down-regulation	PER45
AT4G04020	up-regulation	PAP1	AT5G15180	down-regulation	PER56
AT4G12400	up-regulation	HOP3	AT5G15230	down-regulation	GASA4
AT4G15620	up-regulation	AT4G15620	AT5G23980	down-regulation	FRO4
AT4G15770	up-regulation	AT4G15770	AT5G23990	down-regulation	ATFRO5
AT4G17090	up-regulation	BAM3 *	AT5G38150	down-regulation	PMI15
AT4G06665	up-regulation	None	AT5G38212	down-regulation	None
AT4G20020	up-regulation	MORF1	AT5G40730	down-regulation	AGP24
AT4G20835	up-regulation	None	AT5G56540	down-regulation	AGP14
AT4G20860	up-regulation	FAD-OXR	AT5G60570	down-regulation	AT5G60570
AT4G22610	up-regulation	AT4G22610	AT5G60660	down-regulation	PIP2-4
AT4G23670	up-regulation	AT4G23670	AT5G63090	down-regulation	LOB

Appendix table 7.4 List of Normalised DEGs from indICE1^{S278D}. Asterisks indicate genes overlapped with ICE1-dependent genes from K-means clustering.

Gene ID	Direction	Symbol	Gene ID	Direction	Symbol
AT1G01720	up-regulation	NAC002	AT1G10470	down-regulation	ARR4
AT1G02850	up-regulation	BGLU11*	AT1G11545	down-regulation	XTH8
AT1G02880	up-regulation	TPK1	AT1G11670	down-regulation	None
AT1G05100	up-regulation	MAPKKK18	AT1G12040	down-regulation	LRX1
AT1G05562	up-regulation	None	AT1G13420	down-regulation	SOT8
AT1G06690	up-regulation	AT1G06690	AT1G14185	down-regulation	AT1G14185
AT1G07160	up-regulation	AT1G07160	AT1G14240	down-regulation	APY3
AT1G07720	up-regulation	KCS3	AT1G14380	down-regulation	IQD28
AT1G07985	up-regulation	AT1G07985	AT1G14550	down-regulation	PER5
AT1G09080	up-regulation	MED37B	AT1G14920	down-regulation	GAI
AT1G09970	up-regulation	LRR XI-23	AT1G14960	down-regulation	AT1G14960

Gene ID	Direction	Symbol	Gene ID	Direction	Symbol
AT1G12090	up-regulation	ELP	AT1G15210	down-regulation	ABCG35
AT1G14520	up-regulation	MIOX1	AT1G15580	down-regulation	IAA5
AT1G17860	up-regulation	KTI2	AT1G17190	down-regulation	GSTU26
AT1G05347	up-regulation	None	AT1G19220	down-regulation	ARF19
AT1G21460	up-regulation	SWEET1	AT1G19840	down-regulation	AT1G19840
AT1G26210	up-regulation	ATSOFL1	AT1G20620	down-regulation	CAT3
AT1G26470	up-regulation	AT1G26470	AT1G21310	down-regulation	EXT3
AT1G27950	up-regulation	LTPG1	AT1G28290	down-regulation	AGP31
AT1G29640	up-regulation	AT1G29640	AT1G28410	down-regulation	None
AT1G30040	up-regulation	GA2OX2	AT1G29025	down-regulation	AT1G29025
AT1G30070	up-regulation	AT1G30070	AT1G29450	down-regulation	SAUR64
AT1G30320	up-regulation	AT1G30320	AT1G30510	down-regulation	RFNR2
AT1G32870	up-regulation	ANAC13	AT1G30750	down-regulation	AT1G30750
AT1G32960	up-regulation	SBT3.3	AT1G33700	down-regulation	AT1G33700
AT1G33600	up-regulation	AT1G33600	AT1G34330	down-regulation	None
AT1G48100	up-regulation	AT1G48100 *	AT1G34510	down-regulation	PER8
AT1G49660	up-regulation	CXE5	AT1G44970	down-regulation	PER9
AT1G51350	up-regulation	AT1G51350	AT1G48930	down-regulation	AtGH9C1
AT1G51790	up-regulation	AT1G51790	AT1G49032	down-regulation	None
AT1G51820	up-regulation	AT1G51820	AT1G49780	down-regulation	None
AT1G55210	up-regulation	DIR20	AT1G51402	down-regulation	AT1G51402
AT1G55500	up-regulation	ECT4	AT1G52060	down-regulation	JAL9
AT1G60080	up-regulation	AT1G60080	AT1G52070	down-regulation	JAL10
AT1G60590	up-regulation	AT1G60590	AT1G52190	down-regulation	NPF1.2
AT1G61120	up-regulation	GES	AT1G52750	down-regulation	None
AT1G61255	up-regulation	None	AT1G53830	down-regulation	PME2
AT1G63530	up-regulation	None	AT1G53990	down-regulation	None
AT1G63840	up-regulation	AT1G63840	AT1G54000	down-regulation	GLL22
AT1G64970	up-regulation	VTE4	AT1G54530	down-regulation	AT1G54530
AT1G65060	up-regulation	4CL3	AT1G54660	down-regulation	None
AT1G66390	up-regulation	MYB90	AT1G54970	down-regulation	PRP1
AT1G66580	up-regulation	RPL10C	AT1G56010	down-regulation	NAC021
AT1G67810	up-regulation	SUFE2	AT1G58320	down-regulation	None
AT1G68620	up-regulation	CXE6	AT1G58350	down-regulation	ZW18
AT1G69250	up-regulation	AT1G69250	AT1G59580	down-regulation	MPK2
AT1G69610	up-regulation	None	AT1G61480	down-regulation	AT1G61480
AT1G70140	up-regulation	FH8	AT1G61590	down-regulation	PBL15
AT1G70780	up-regulation	AT1G70780	AT1G61810	down-regulation	BGLU45
AT1G72755	up-regulation	None	AT1G62770	down-regulation	PMEI9
AT1G72800	up-regulation	AT1G72800	AT1G62980	down-regulation	EXPA18
AT1G73880	up-regulation	UGT89B1	AT1G64590	down-regulation	AT1G64590
AT1G76470	up-regulation	AT1G76470	AT1G66280	down-regulation	BGLU22
AT1G76520	up-regulation	PILS3	AT1G67148	down-regulation	None
AT1G76600	up-regulation	AT1G76600 *	AT1G67590	down-regulation	AT1G67590
AT1G76980	up-regulation	None	AT1G67865	down-regulation	AT1G67865

Gene ID	Direction	Symbol	Gene ID	Direction	Symbol
AT1G77670	up-regulation	AT1G77670	AT1G67870	down-regulation	None
AT1G79270	up-regulation	ECT8	AT1G70860	down-regulation	AT1G70860
AT1G79410	up-regulation	Oct-05	AT1G71970	down-regulation	None
AT1G79920	up-regulation	None	AT1G73330	down-regulation	ATDR4
AT1G80160	up-regulation	AT1G80160	AT1G73870	down-regulation	COL7
AT2G02010	up-regulation	GAD4	AT1G74770	down-regulation	AT1G74770
AT2G02130	up-regulation	PDF2.3	AT1G75780	down-regulation	TUBB1
AT2G03760	up-regulation	SOT12	AT1G75785	down-regulation	None
AT2G04050	up-regulation	DTX3	AT1G76560	down-regulation	CP12-3
AT2G04070	up-regulation	DTX4	AT1G77690	down-regulation	LAX3
AT2G04350	up-regulation	LACS8	AT1G78260	down-regulation	AT1G78260
AT2G05710	up-regulation	ACO3	AT1G80050	down-regulation	APT2
AT2G05940	up-regulation	RIPK	AT2G01830	down-regulation	AHK4
AT2G15480	up-regulation	UGT73B5	AT2G01880	down-regulation	PAP7
AT2G15780	up-regulation	None	AT2G03590	down-regulation	UPS1
AT2G16900	up-regulation	None	AT2G03890	down-regulation	PI4KG7
AT2G17250	up-regulation	EMB2762	AT2G15370	down-regulation	None
AT2G18950	up-regulation	HPT1	AT2G16005	down-regulation	ROSY1
AT2G22500	up-regulation	PUMP5	AT2G16970	down-regulation	MEE15
AT2G22880	up-regulation	AT2G22880	AT2G16980	down-regulation	AT2G16980
AT2G23150	up-regulation	NRAMP3	AT2G18440	down-regulation	None
AT2G29380	up-regulation	HAI3	AT2G18980	down-regulation	PER16
AT2G29420	up-regulation	GSTU7	AT2G19970	down-regulation	AT2G19970
AT2G08340	up-regulation	None	AT2G22970	down-regulation	SCPL11
AT2G29470	up-regulation	GSTU3	AT2G23270	down-regulation	AT2G23270
AT2G29485	up-regulation	None	AT2G24980	down-regulation	AT2G24980
AT2G30550	up-regulation	AT2G30550	AT2G25150	down-regulation	SCT
AT2G31751	up-regulation	None	AT2G25310	down-regulation	AT2G25310
AT2G32220	up-regulation	RPL27A	AT2G27370	down-regulation	CASP3
AT2G33590	up-regulation	AT2G33590	AT2G28671	down-regulation	AT2G28671
AT2G34660	up-regulation	ABCC2	AT2G28670	down-regulation	None
AT2G36780	up-regulation	UGT73C3	AT2G28950	down-regulation	EXPA6
AT2G36792	up-regulation	None	AT2G29400	down-regulation	TOPP1
AT2G36790	up-regulation	UGT73C6	AT2G31440	down-regulation	AT2G31440
AT2G37240	up-regulation	AT2G37240	AT2G32090	down-regulation	AT2G32090
AT2G37260	up-regulation	WRKY44	AT2G32300	down-regulation	UCC1
AT2G37710	up-regulation	LECRK41	AT2G32880	down-regulation	AT2G32880
AT2G38280	up-regulation	AMPD	AT2G35770	down-regulation	None
AT2G39050	up-regulation	EULS3	AT2G35820	down-regulation	AT2G35820
AT2G39200	up-regulation	MLO12	AT2G37130	down-regulation	PER21
AT2G39350	up-regulation	ABCG1	AT2G37170	down-regulation	PIP2B
AT2G39518	up-regulation	None	AT2G38120	down-regulation	AUX1
AT2G39520	up-regulation	None	AT2G39430	down-regulation	DIR9
AT2G40435	up-regulation	AT2G40435	AT2G40110	down-regulation	AT2G40110
AT2G41730	up-regulation	AT2G41730	AT2G40205	down-regulation	RPL41G
AT2G41905	up-regulation	None	AT2G42247	down-regulation	None

Gene ID	Direction	Symbol	Gene ID	Direction	Symbol
AT2G42540	up-regulation	COR15A	AT2G42380	down-regulation	BZIP34
AT2G44510	up-regulation	AT2G44510	AT2G43000	down-regulation	JUB1
AT2G46430	up-regulation	CNGC3	AT2G43060	down-regulation	IBH1
AT2G47730	up-regulation	GSTF8	AT2G44110	down-regulation	MLO15
AT2G47890	up-regulation	COL13	AT2G44450	down-regulation	BGLU15
AT3G03341	up-regulation	AT3G03341	AT2G44480	down-regulation	BGLU17
AT3G03770	up-regulation	AT3G03770	AT3G01260	down-regulation	AT3G01260
AT3G04000	up-regulation	ChlADR2	AT3G01513	down-regulation	AT3G01513
AT3G04010	up-regulation	AT3G04010	AT3G01940	down-regulation	None
AT3G04120	up-regulation	GAPC1	AT3G02020	down-regulation	AK3
AT3G01485	up-regulation	None	AT3G03040	down-regulation	AT3G03040
AT3G04710	up-regulation	TPR10	AT3G05155	down-regulation	AT3G05155
AT3G05180	up-regulation	AT3G05180	AT3G05890	down-regulation	RCI2B
AT3G01615	up-regulation	None	AT3G07010	down-regulation	AT3G07010
AT3G06520	up-regulation	None *	AT3G09925	down-regulation	AT3G09925
AT3G08590	up-regulation	AT3G08590	AT3G11550	down-regulation	CASP2
AT3G09440	up-regulation	HSP70-3	AT3G12320	down-regulation	LNK3 *
AT3G13080	up-regulation	ABCC3	AT3G12710	down-regulation	AT3G12710
AT3G14690	up-regulation	CYP72A15	AT3G12900	down-regulation	AT3G12900
AT3G03095	up-regulation	None	AT3G14530	down-regulation	GGPPS9
AT3G21500	up-regulation	DXPS1	AT3G15115	down-regulation	None
AT3G22370	up-regulation	AOX1A	AT3G16410	down-regulation	NSP4
AT3G22840	up-regulation	ELIP1	AT3G16430	down-regulation	PBP2
AT3G23620	up-regulation	AT3G23620	AT3G16460	down-regulation	JAL34
AT3G24170	up-regulation	ATGR1	AT3G18200	down-regulation	AT3G18200
AT3G04695	up-regulation	None	AT3G18560	down-regulation	None
AT3G25610	up-regulation	ALA10	AT3G21240	down-regulation	4CL2
AT3G25730	up-regulation	ARF14	AT3G21710	down-regulation	VUP1
AT3G26744	up-regulation	SCRM	AT3G22800	down-regulation	LRX6
AT3G27880	up-regulation	AT3G27880	AT3G23050	down-regulation	IAA7
AT3G28210	up-regulation	SAP12	AT3G23090	down-regulation	AT3G23090
AT3G28345	up-regulation	ABCB15	AT3G24020	down-regulation	DIR16
AT3G28740	up-regulation	CYP81D11	AT3G26610	down-regulation	AT3G26610
AT3G30180	up-regulation	CYP85A2	AT3G28550	down-regulation	AT3G28550
AT3G42180	up-regulation	None	AT3G28880	down-regulation	AT3G28880
AT3G46658	up-regulation	None	AT3G29250	down-regulation	SDR4
AT3G46660	up-regulation	UGT76E12	AT3G29410	down-regulation	TPS25
AT3G47080	up-regulation	AT3G47080	AT3G29670	down-regulation	PMAT2
AT3G48610	up-regulation	NPC6	AT3G32030	down-regulation	TPS30
AT3G48690	up-regulation	CXE12	AT3G43670	down-regulation	AT3G43670
AT3G49780	up-regulation	PSK3	AT3G44326	down-regulation	AT3G44326
AT3G52450	up-regulation	PUB22	AT3G44510	down-regulation	None
AT3G53230	up-regulation	CDC48D	AT3G45070	down-regulation	AT3G45070
AT3G54400	up-regulation	AT3G54400	AT3G45600	down-regulation	TET3
AT3G54430	up-regulation	SRS6	AT3G07205	down-regulation	None
AT3G55110	up-regulation	ABCG18	AT3G45700	down-regulation	NPF2.4

Gene ID	Direction	Symbol	Gene ID	Direction	Symbol
AT3G55500	up-regulation	EXPA16	AT3G45710	down-regulation	NPF2.5
AT3G56320	up-regulation	AT3G56320	AT3G46370	down-regulation	AT3G46370
AT3G59040	up-regulation	AT3G59040	AT3G46900	down-regulation	COPT2
AT3G59220	up-regulation	PRN1	AT3G47710	down-regulation	PRE4
AT3G59700	up-regulation	LECRK55	AT3G48340	down-regulation	CEP2
AT3G61220	up-regulation	AT3G61220	AT3G50640	down-regulation	AT3G50640
AT3G61490	up-regulation	AT3G61490	AT3G51350	down-regulation	None
AT4G00050	up-regulation	UNE10	AT3G53240	down-regulation	AtRLP45
AT4G03985	up-regulation	None	AT3G54040	down-regulation	AT3G54040
AT4G02280	up-regulation	SUS3	AT3G54260	down-regulation	TBL36
AT4G02990	up-regulation	MTERF4	AT3G08405	down-regulation	None
AT4G04490	up-regulation	CRK36	AT3G54720	down-regulation	AMP1
AT4G09500	up-regulation	UGT79B7	AT3G54770	down-regulation	ARP1
AT4G09750	up-regulation	AT4G09750	AT3G55230	down-regulation	DIR24
AT4G10430	up-regulation	AT4G10430	AT3G56240	down-regulation	CCH
AT4G12290	up-regulation	AT4G12290	AT3G58120	down-regulation	BZIP61
AT4G12580	up-regulation	None	AT3G59370	down-regulation	AT3G59370
AT4G12735	up-regulation	AT4G12735	AT3G59480	down-regulation	AT3G59480
AT4G15620	up-regulation	AT4G15620	AT3G62680	down-regulation	PRP3
AT4G15630	up-regulation	AT4G15630	AT3G09965	down-regulation	None
AT4G16760	up-regulation	ACX1	AT4G00820	down-regulation	iqd17
AT4G17650	up-regulation	AT4G17650	AT4G01120	down-regulation	GBF2
AT4G18210	up-regulation	None	AT4G02970	down-regulation	None
AT4G18215	up-regulation	None	AT4G11210	down-regulation	DIR14
AT4G18220	up-regulation	None	AT4G11320	down-regulation	RDL5
AT4G18940	up-regulation	AT4G18940	AT4G12510	down-regulation	AT4G12510
AT4G18950	up-regulation	AT4G18950	AT4G12520	down-regulation	AT4G12520
AT4G18980	up-regulation	AtS40-3	AT4G13580	down-regulation	DIR18
AT4G19960	up-regulation	KUP9 *	AT4G13840	down-regulation	CER26
AT4G22590	up-regulation	TPPG	AT4G15230	down-regulation	ABCG30
AT4G23250	up-regulation	EMB1290	AT4G15290	down-regulation	CSLB5
AT4G24972	up-regulation	TPD1	AT4G15340	down-regulation	PEN1
AT4G25130	up-regulation	MSR4	AT4G15390	down-regulation	AT4G15390
AT4G25200	up-regulation	HSP23.6	AT4G15393	down-regulation	CYP702A5
AT4G25810	up-regulation	XTH23	AT4G16780	down-regulation	HAT4
AT4G26080	up-regulation	ABI1	AT4G17790	down-regulation	AT4G17790
AT4G27520	up-regulation	ENODL2	AT4G17800	down-regulation	AHL23
AT4G27830	up-regulation	BGLU10	AT4G18203	down-regulation	None
AT4G30470	up-regulation	AT4G30470	AT4G18510	down-regulation	CLE2
AT4G32920	up-regulation	AT4G32920	AT4G19370	down-regulation	AT4G19370
AT4G33540	up-regulation	AT4G33540	AT4G19680	down-regulation	IRT2
AT4G33550	up-regulation	AT4G33550	AT4G20140	down-regulation	GSO1
AT4G33905	up-regulation	AT4G33905	AT4G22214	down-regulation	AT4G22214
AT4G33950	up-regulation	SRK2E	AT4G22540	down-regulation	ORP2A
AT4G34120	up-regulation	CBSX2	AT4G22666	down-regulation	AT4G22666
AT4G08935	up-regulation	None	AT4G22810	down-regulation	AHL24

Gene ID	Direction	Symbol	Gene ID	Direction	Symbol
AT4G34139	up-regulation	None	AT4G25410	down-regulation	BHLH126
AT4G34230	up-regulation	CAD5	AT4G26010	down-regulation	AT4G26010
AT4G34590	up-regulation	BZIP11	AT4G26320	down-regulation	AGP13
AT4G36010	up-regulation	AT4G36010 *	AT4G27310	down-regulation	AT4G27310
AT4G36880	up-regulation	None	AT4G29340	down-regulation	PRO3
AT4G37180	up-regulation	HHO5	AT4G29690	down-regulation	AT4G29690
AT5G01410	up-regulation	PDX13	AT4G30170	down-regulation	PER45
AT5G01520	up-regulation	AIRP2	AT4G31470	down-regulation	AT4G31470
AT5G01540	up-regulation	LECRK62	AT4G31940	down-regulation	CYP82C4
AT5G01542	up-regulation	None	AT4G36570	down-regulation	None
AT5G04830	up-regulation	None	AT4G37160	down-regulation	sks15
AT5G01005	up-regulation	None	AT4G38910	down-regulation	BPC5
AT5G06530	up-regulation	ABCG22	AT5G01330	down-regulation	PDC3
AT5G06760	up-regulation	LEA46	AT5G04960	down-regulation	PME46
AT5G06865	up-regulation	None	AT5G06645	down-regulation	None
AT5G09840	up-regulation	AT5G09840	AT5G07690	down-regulation	MYB29
AT5G11060	up-regulation	KNAT4	AT5G08330	down-regulation	TCP21
AT5G11520	up-regulation	ASP3	AT5G10430	down-regulation	AGP4
AT5G13370	up-regulation	AT5G13370	AT5G10435	down-regulation	None
AT5G15090	up-regulation	VDAC3	AT5G11420	down-regulation	AT5G11420
AT5G15450	up-regulation	CLPB3	AT5G13320	down-regulation	PBS3
AT5G15700	up-regulation	AT5G15700	AT5G13910	down-regulation	LEP
AT5G16010	up-regulation	AT5G16010	AT5G14020	down-regulation	AT5G14020
AT5G16960	up-regulation	AT5G16960	AT5G14060	down-regulation	AK2
AT5G17450	up-regulation	HIPP21	AT5G14330	down-regulation	AT5G14330
AT5G20225	up-regulation	None	AT5G15130	down-regulation	WRKY72*
AT5G20280	up-regulation	SPS1	AT5G17330	down-regulation	GAD1
AT5G22860	up-regulation	AT5G22860	AT5G17820	down-regulation	AT5G17820
AT5G24080	up-regulation	AT5G24080	AT5G19600	down-regulation	SULTR3;5
AT5G24640	up-regulation	AT5G24640	AT5G19740	down-regulation	LAMP1
AT5G24850	up-regulation	CRYD	AT5G22390	down-regulation	AT5G22390
AT5G25120	up-regulation	CYP71B11	AT5G23020	down-regulation	MAM3
AT5G25930	up-regulation	AT5G25930	AT5G23280	down-regulation	TCP7
AT5G04175	up-regulation	None	AT5G23980	down-regulation	FRO4
AT5G27420	up-regulation	ATL31	AT5G23990	down-regulation	ATFRO5
AT5G27600	up-regulation	LACS7	AT5G24580	down-regulation	HIPP09
AT5G33290	up-regulation	XGD1	AT5G03985	down-regulation	None
AT5G36925	up-regulation	None	AT5G25460	down-regulation	AT5G25460
AT5G37300	up-regulation	WSD1	AT5G26260	down-regulation	AT5G26260
AT5G41900	up-regulation	BDG2	AT5G26290	down-regulation	AT5G26290
AT5G42050	up-regulation	AT5G42050	AT5G28020	down-regulation	CYSD2
AT5G42760	up-regulation	AT5G42760 *	AT5G35190	down-regulation	AT5G35190
AT5G06385	up-regulation	None	AT5G35940	down-regulation	JAL41
AT5G48430	up-regulation	AT5G48430	AT5G36140	down-regulation	None
AT5G48530	up-regulation	AT5G48530	AT5G36150	down-regulation	PEN3

Gene ID	Direction	Symbol	Gene ID	Direction	Symbol
AT5G48540	up-regulation	CRRSP55	AT5G37740	down-regulation	AT5G37740
AT5G48570	up-regulation	FKBP65	AT5G38150	down-regulation	PMI15
AT5G49330	up-regulation	MYB111 *	AT5G38540	down-regulation	None
AT5G49520	up-regulation	WRKY48 *	AT5G38700	down-regulation	AT5G38700
AT5G50360	up-regulation	AT5G50360 *	AT5G39120	down-regulation	None
AT5G51040	up-regulation	AT5G51040	AT5G40590	down-regulation	AT5G40590
AT5G52390	up-regulation	AT5G52390	AT5G41130	down-regulation	AT5G41130
AT5G52450	up-regulation	DTX16	AT5G42180	down-regulation	PER64
AT5G53970	up-regulation	AT5G53970	AT5G42590	down-regulation	CYP71A16
AT5G55070	up-regulation	AT5G55070	AT5G42600	down-regulation	MRN1
AT5G55200	up-regulation	Mge1	AT5G43520	down-regulation	AT5G43520
AT5G56010	up-regulation	HSP90-3	AT5G44480	down-regulation	DUR
AT5G56090	up-regulation	COX15	AT5G45210	down-regulation	AT5G45210
AT5G56350	up-regulation	AT5G56350	AT5G47980	down-regulation	BAHD1
AT5G57050	up-regulation	ABI2	AT5G47990	down-regulation	CYP705A5
AT5G57800	up-regulation	CER3	AT5G48000	down-regulation	CYP708A2
AT5G57990	up-regulation	UBP23	AT5G51780	down-regulation	AT5G51780
AT5G59820	up-regulation	ZAT12	AT5G51970	down-regulation	SDH
AT5G60990	up-regulation	RH10	AT5G52900	down-regulation	MAKR6
AT5G61560	up-regulation	None	AT5G53250	down-regulation	AGP22
AT5G61810	up-regulation	AT5G61810	AT5G53900	down-regulation	None
AT5G62470	up-regulation	MYB96	AT5G56320	down-regulation	ATEXPA14
AT5G65990	up-regulation	AVT3A	AT5G56540	down-regulation	AGP14
AT1G01110	down-regulation	IQD18	AT5G57620	down-regulation	MYB36
AT1G01580	down-regulation	FRO2	AT5G57625	down-regulation	AT5G57625
AT1G02810	down-regulation	PME7	AT5G58010	down-regulation	BHLH82
AT1G02900	down-regulation	RALF1	AT5G60200	down-regulation	DOF5.3
AT1G03520	down-regulation	None	AT5G61250	down-regulation	AtGUS1
AT1G03620	down-regulation	None	AT5G63180	down-regulation	AT5G63180
AT1G03740	down-regulation	AT1G03740	AT5G63800	down-regulation	BGAL6
AT1G04610	down-regulation	YUC3	AT5G65530	down-regulation	AT5G65530
AT1G05260	down-regulation	PER3	AT5G65690	down-regulation	PCK2
AT1G05790	down-regulation	AT1G05790	AT5G66390	down-regulation	PER72
AT1G08592	down-regulation	None	AT5G67390	down-regulation	AT5G67390
AT1G08900	down-regulation	SUGTL3	AT5G67400	down-regulation	PER73
AT1G09540	down-regulation	MYB61	ATCG00490	down-regulation	RBCL
AT1G09910	down-regulation	AT1G09910	ATMG00020	down-regulation	None

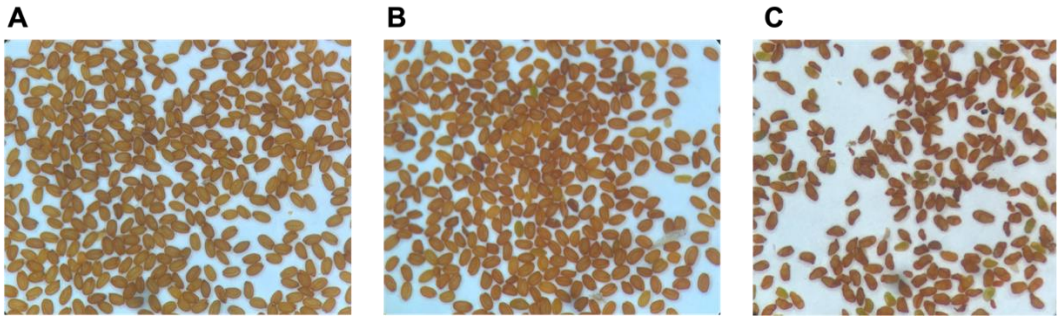

Appendix figure 7.1 Seed shape observed under light microscope from WT (A), amiRNA-ice1 (B) and *ice1-2* (C)

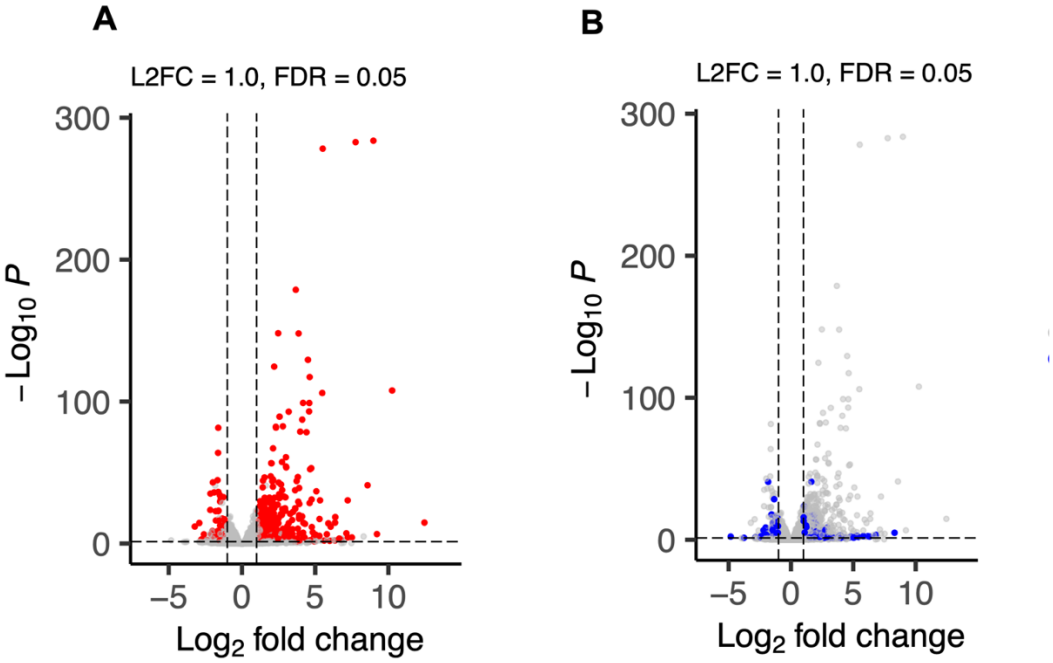

Appendix figure 7.2 Volcano plot from DEGs of cold-regulated genes in WT (WT 22ºC vs WT 4ºC). The common cold-regulated DEGs are highlighted in red (A) a cold-regulated DEGs specific to WT are highlighted in blue (B)

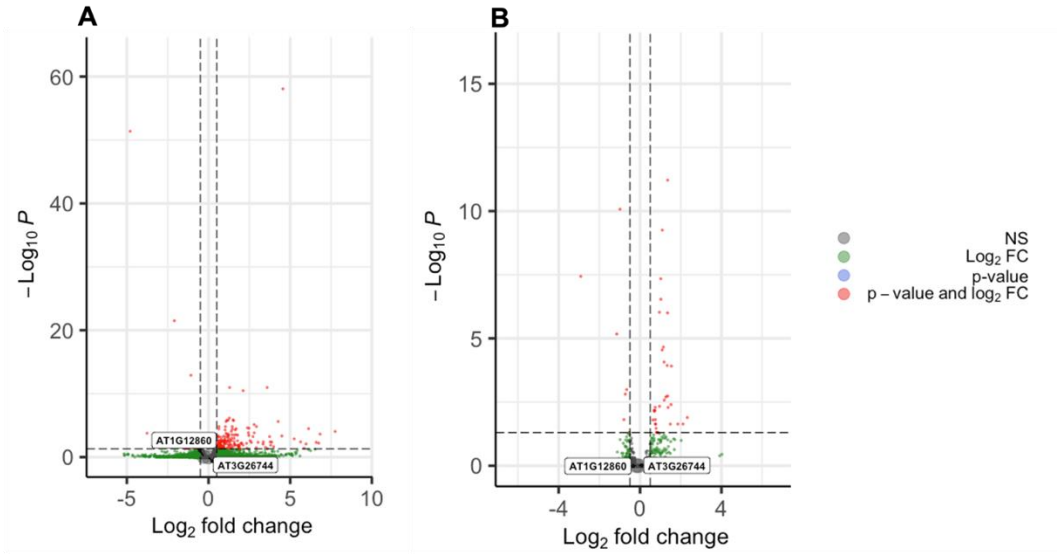

Appendix figure 7.3 Volcano plot representing the DEGs from comparison between untreated WT and untreated indICE1 (A) and DEGs from comparison between untreated WT and untreated indICE1^{S278D} (B) *ICE1* (AT3G26744) and *ICE2* (AT1G12860) are highlighted with grey boxes.

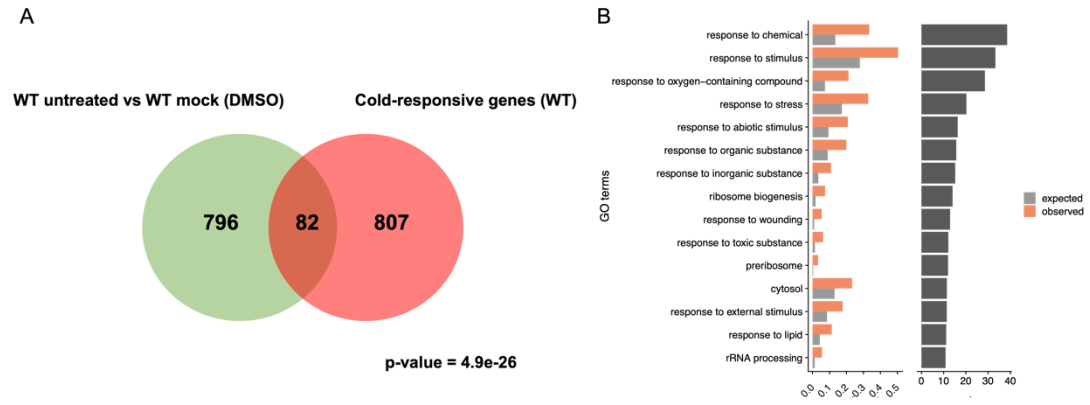

Appendix figure 7.4 Overlapping genes between comparisons testing effects of mock (DMSO) treatment (table 3.6, comparison 3) and cold-responsive genes in WT (table 3.2, comparison 1) (A). GO terms enrichment analysis from comparison between untreated WT and WT treated with mock (DMSO) (B).

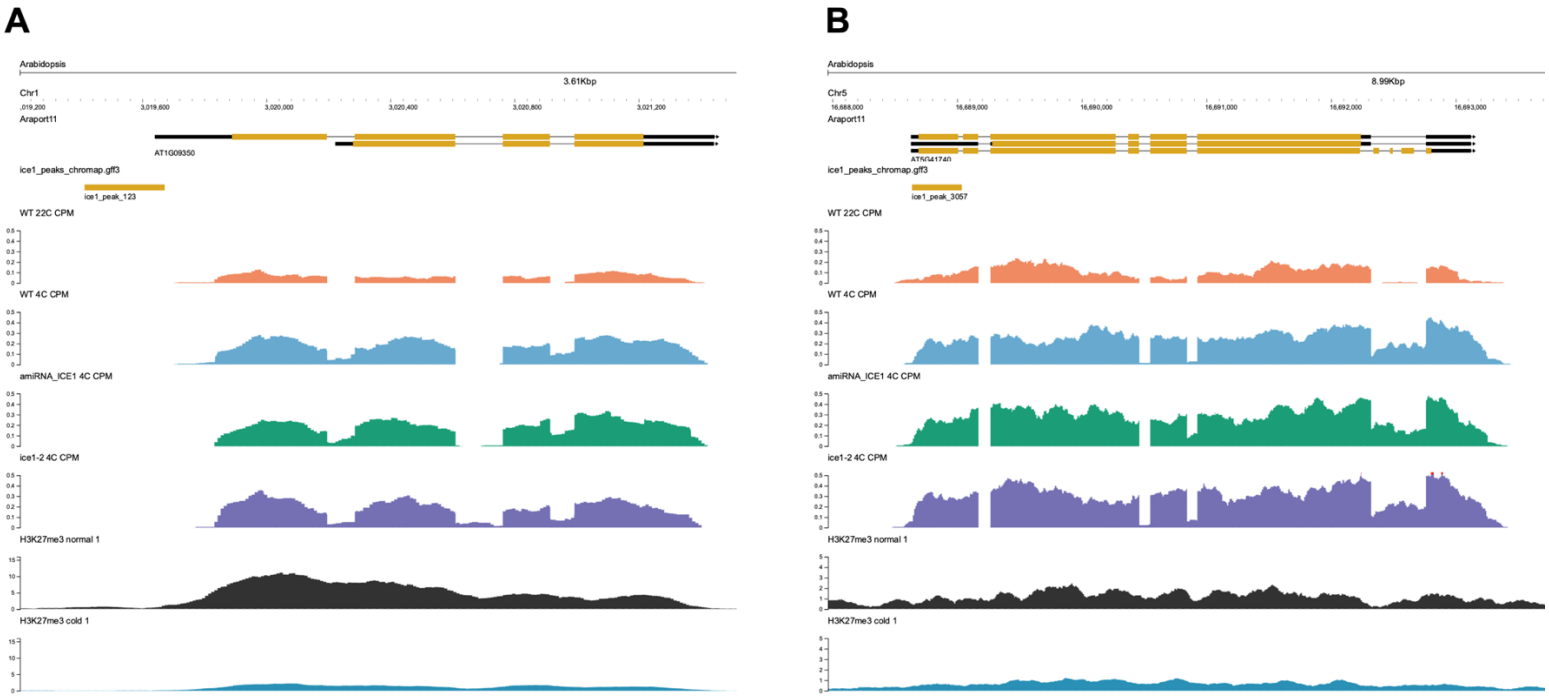

Appendix figure 7.5 Genome browser of *GolS3* (A) and AT5G41740 (B). Top panel indicate gene structures from Araport11. Second panel shows ICE1 binding site. Mapped reads were scaled to counts per million (CPM) units. The third to sixth panels show the structure of the mapped reads from plants grown at 22^{o}C and 4^{o}C. Seventh panel indicate H3K27me3 ChIP-seq signal before long cold treatment. The bottom panel represent the H3K27me3 ChIP-seq signal after long cold treatment.

Appendix 8

Appendix Table 8.1 DEGs and values from the pair-wise comparison of Leaf-origin cold memory (LCM) genes

Gene ID	baseMean	log2FoldChange	lfcSE	padj	Symbol	Gene ID	baseMean	log2FoldChange	lfcSE	padj	Symbol
AT2G16680	11.985	-8.119	1.340	0.000	None	AT2G20724	125.883	-1.022	0.370	0.049	None
AT5G35935	52.777	-6.957	1.183	0.000	None	AT1G41830	453.130	-1.022	0.365	0.045	SKS6
AT4G02960	7.959	-6.341	1.803	0.008	None	AT1G75840	645.570	-1.022	0.333	0.025	ARAC5
AT2G16676	6.004	-6.123	1.459	0.001	None	AT2G47160	587.528	-1.020	0.231	0.001	BOR1
AT3G42820	51.558	-5.557	1.227	0.000	None	AT5G39320	66.305	-1.020	0.343	0.032	UGD4
AT3G54590	6.046	-5.393	1.636	0.015	EXT2	AT1G02350	62.558	-1.018	0.337	0.029	None
AT5G19110	5.991	-5.072	1.664	0.027	AT5G19110	AT4G30996	287.876	-1.017	0.176	0.000	AT4G30996
AT3G13403	6.134	-4.693	1.487	0.021	None	AT3G51150	269.869	-1.016	0.288	0.008	KIN7G
AT1G06080	10.836	-4.369	1.383	0.021	ADS1	AT2G16440	53.183	-1.015	0.366	0.048	MCM4
AT4G11290	27.995	-4.315	1.035	0.001	PER39	AT3G27160	1784.608	-1.012	0.118	0.000	GHS1
AT1G75590	14.332	-4.150	1.032	0.002	AT1G75590	AT1G45207	66.472	-1.012	0.291	0.009	AT1G45207
AT4G08040	7.173	-4.128	1.438	0.039	ACS11	AT1G05810	176.019	-1.011	0.329	0.025	ARA
AT1G11070	8.022	-4.062	1.149	0.008	AT1G11070	AT3G12920	444.558	-1.010	0.319	0.020	BRG3
AT2G38240	70.882	-4.059	0.695	0.000	ANS	AT3G06150	627.235	-1.005	0.234	0.001	None
AT5G28335	25.134	-4.017	1.195	0.013	None	AT3G28945	88.024	-1.003	0.234	0.001	None
AT4G04420	4.925	-3.988	1.365	0.035	None	AT5G43060	268.662	-1.002	0.212	0.000	RD21B
AT3G49620	85.042	-3.622	0.672	0.000	DIN11	AT4G15730	96.130	1.003	0.225	0.000	AT4G15730
AT5G24240	24.923	-3.604	1.172	0.025	PI4KG3	AT4G13100	177.497	1.004	0.180	0.000	AT4G13100
AT3G16670	239.352	-3.599	0.605	0.000	AT3G16670	AT4G11360	909.055	1.006	0.207	0.000	RHA1B
AT1G72620	5.334	-3.575	1.164	0.025	None	AT1G54100	2242.582	1.006	0.305	0.015	ALDH7B4
AT2G42260	4.595	-3.543	1.218	0.036	PYM	AT3G03470	1704.677	1.008	0.224	0.000	CYP89A9
AT4G16807	4.874	-3.378	1.225	0.049	None	AT3G59140	442.966	1.009	0.331	0.027	ABCC10
AT3G45960	8.413	-3.363	0.972	0.010	EXLA3	AT1G29030	187.829	1.011	0.288	0.009	AT1G29030
AT4G36850	205.627	-3.281	0.427	0.000	AT4G36850	AT2G18230	357.770	1.013	0.251	0.002	PPA2
AT4G28720	18.113	-3.279	0.877	0.005	YUC8	AT3G62700	2593.743	1.014	0.231	0.001	ABCC14
AT5G44430	386.978	-3.266	0.982	0.014	PDF1.2C	AT3G50840	1243.490	1.018	0.316	0.018	AT3G50840
AT4G15680	47.691	-3.224	0.762	0.001	GRXS4	AT1G80270	188.021	1.020	0.265	0.004	PPR596
AT1G11925	7.491	-3.209	1.080	0.032	None	AT5G22290	431.864	1.021	0.228	0.000	NAC089
AT3G46880	22.746	-3.074	0.556	0.000	None	AT3G57940	212.968	1.021	0.253	0.002	AT3G57940
AT4G22620	8.251	-3.056	0.985	0.024	AT4G22620	AT1G30160	59.465	1.024	0.257	0.002	None

Gene ID	baseMean	log2FoldChange	lfcSE	padj	Symbol	Gene ID	baseMean	log2FoldChange	lfcSE	padj	Symbol
AT5G50915	24.381	-3.048	0.559	0.000	BHLH137	AT1G21000	2252.693	1.028	0.281	0.006	AT1G21000
AT3G02410	32.543	-3.023	0.942	0.019	ICMEL2	AT4G30960	4839.614	1.029	0.228	0.000	CIPK6
AT3G49110	36.231	-3.015	0.570	0.000	PER33	AT3G15150	42.975	1.033	0.356	0.037	MMS21
AT4G24275	30.108	-3.002	0.795	0.004	None	AT4G23880	327.911	1.034	0.324	0.019	AT4G23880
AT3G48160	6.853	-2.997	0.930	0.018	E2FE	AT5G03190	196.800	1.037	0.289	0.007	CPUORF47
AT2G05440	240.073	-2.975	0.516	0.000	ATGRP9	AT1G77920	461.343	1.041	0.288	0.007	TGA7
AT3G13404	13.593	-2.972	0.689	0.001	None	AT1G69310	233.360	1.042	0.264	0.002	WRKY57
AT4G33810	15.071	-2.960	0.785	0.004	None	AT5G10300	163.223	1.042	0.360	0.037	HNL
AT1G34440	9.880	-2.933	0.758	0.003	None	AT4G16870	581.437	1.043	0.370	0.044	None
AT5G24580	25.414	-2.928	0.808	0.006	HIPP09	AT2G29320	530.220	1.046	0.351	0.031	AT2G29320
AT2G26020	168.361	-2.908	0.599	0.000	PDF1.2B	AT1G24095	86.522	1.048	0.264	0.002	None
AT5G48490	64.065	-2.889	0.810	0.007	AT5G48490	AT4G30870	67.213	1.049	0.287	0.006	MUS81
AT5G46871	22.692	-2.803	0.555	0.000	AT5G46871	AT5G25755	35.705	1.052	0.349	0.029	None
AT3G03830	6.899	-2.800	0.831	0.012	SAUR28	AT3G63010	328.373	1.055	0.256	0.001	GID1B
AT3G55646	88.453	-2.798	0.654	0.001	AT3G55646	AT2G25140	498.286	1.055	0.211	0.000	CLPB4
AT3G12710	67.975	-2.747	0.815	0.012	AT3G12710	AT1G78670	1152.904	1.056	0.169	0.000	GGH3
AT5G62920	190.867	-2.708	0.437	0.000	ARR6	AT3G52310	98.592	1.057	0.293	0.007	None
AT2G31010	367.706	-2.706	0.555	0.000	AT2G31010	AT2G17710	355.117	1.057	0.298	0.008	AT2G17710
AT1G62440	18.124	-2.706	0.936	0.037	LRX2	AT3G11670	1375.788	1.058	0.248	0.001	DGD1
AT3G05620	9.331	-2.688	0.778	0.010	PME22	AT1G25277	52.358	1.062	0.324	0.016	None
AT4G34810	6.489	-2.680	0.932	0.039	AT4G34810	AT5G59350	98.073	1.062	0.327	0.017	AT5G59350
AT4G34770	45.512	-2.654	0.513	0.000	AT4G34770	AT5G49190	41.602	1.063	0.348	0.026	SUS2
AT2G43590	21.810	-2.642	0.696	0.004	AT2G43590	AT1G05310	158.294	1.066	0.334	0.019	PME8
AT1G09460	13.130	-2.631	0.583	0.000	None	AT3G11080	224.067	1.069	0.249	0.001	AtRLP35
AT3G16240	3533.755	-2.621	0.654	0.002	TIP2-1	AT1G67360	698.050	1.070	0.269	0.002	AT1G67360
AT5G44420	672.297	-2.567	0.723	0.008	PDF1.2A	AT2G47270	54.465	1.074	0.347	0.024	UPB1
AT4G15670	118.190	-2.560	0.592	0.001	GRXS7	AT2G01505	35.533	1.079	0.366	0.033	CLE16
AT1G76160	835.897	-2.557	0.445	0.000	sks5	AT2G31585	253.994	1.081	0.283	0.004	None
AT2G26010	81.011	-2.548	0.716	0.008	PDF1.3	AT3G13810	612.337	1.083	0.180	0.000	AtIDD11
AT1G19050	397.004	-2.535	0.541	0.000	ARR7	AT4G18220	48.400	1.083	0.344	0.021	None
AT3G17050	195.803	-2.531	0.544	0.000	None	AT5G52640	170.539	1.087	0.379	0.039	HSP90-1
AT1G18400	141.498	-2.522	0.441	0.000	BEE1	AT3G48830	39.091	1.088	0.357	0.027	AT3G48830
AT4G34790	67.038	-2.518	0.472	0.000	None	AT2G04110	224.707	1.088	0.349	0.023	None

Gene ID	baseMean	log2FoldChange	lfcSE	padj	Symbol	Gene ID	baseMean	log2FoldChange	lfcSE	padj	Symbol
AT3G27970	10.065	-2.505	0.673	0.005	AT3G27970	AT2G35550	53.100	1.089	0.359	0.027	BPC7
AT3G09780	6.841	-2.491	0.846	0.034	CCR1	AT5G21100	241.383	1.091	0.276	0.002	AT5G21100
AT4G12730	316.150	-2.486	0.675	0.006	FLA2	AT1G23040	191.269	1.093	0.296	0.005	AT1G23040
AT5G40020	13.366	-2.467	0.652	0.004	AT5G40020	AT1G46768	128.122	1.098	0.239	0.000	RAP2-1
AT4G28190	44.462	-2.423	0.763	0.020	ULT1	AT5G18130	3716.188	1.099	0.208	0.000	AT5G18130
AT3G05730	307.657	-2.394	0.525	0.000	AT3G05730	AT2G15480	238.087	1.100	0.183	0.000	UGT73B5
AT2G37025	72.370	-2.378	0.646	0.006	TRFL8	AT1G27360	118.211	1.103	0.208	0.000	SPL11
AT2G32590	8.370	-2.374	0.800	0.032	CAPH	AT1G59640	48.784	1.103	0.341	0.017	BPE
AT2G41170	46.695	-2.373	0.452	0.000	AT2G41170	AT3G14067	5483.151	1.104	0.163	0.000	SBT1.4
AT1G63295	11.487	-2.369	0.749	0.021	None	AT2G34655	244.624	1.104	0.256	0.001	AT2G34655
AT1G72760	8.500	-2.365	0.818	0.037	None	AT5G13750	180.327	1.105	0.396	0.046	ZIFL1
AT3G54400	184.459	-2.356	0.733	0.018	AT3G54400	AT3G05690	327.649	1.106	0.288	0.004	UNE8
AT3G25100	10.105	-2.356	0.814	0.037	CDC45	AT2G24280	1082.872	1.107	0.218	0.000	AT2G24280
AT4G15700	218.601	-2.344	0.461	0.000	GRXS3	AT2G39705	131.486	1.108	0.269	0.001	RTFL8
AT3G43190	18.520	-2.329	0.673	0.010	SUS4	AT3G28130	230.861	1.112	0.348	0.019	None
AT3G03820	40.316	-2.325	0.578	0.002	AT3G03820	AT3G57540	100.971	1.114	0.356	0.022	REM4.1
AT1G02700	11.138	-2.324	0.728	0.019	AT1G02700	AT3G63210	650.123	1.122	0.146	0.000	MARD1
AT2G44790	22.905	-2.313	0.516	0.000	UCC2	AT5G14640	613.331	1.122	0.305	0.006	ASK5
AT1G58370	51.367	-2.307	0.503	0.000	RXF12	AT4G16857	31.779	1.134	0.408	0.047	None
AT5G18010	12.040	-2.304	0.663	0.010	SAUR19	AT1G74430	53.386	1.136	0.371	0.026	MYB95
AT1G36060	27.312	-2.301	0.509	0.000	ERF055	AT5G57050	232.839	1.141	0.315	0.006	ABI2
AT4G34760	231.215	-2.289	0.582	0.003	SAUR50	AT4G00050	151.594	1.144	0.310	0.005	UNE10
AT3G58120	441.606	-2.289	0.690	0.014	BZIP61	AT5G06510	141.581	1.151	0.286	0.002	NFYA10
AT1G47840	11.492	-2.288	0.774	0.033	HXK3	AT2G20800	55.808	1.152	0.400	0.038	NDB4
AT5G46730	180.690	-2.263	0.327	0.000	AT5G46730	AT1G28570	108.236	1.153	0.322	0.007	AT1G28570
AT4G31000	219.842	-2.237	0.456	0.000	None	AT4G22980	117.166	1.158	0.314	0.005	AT4G22980
AT2G01818	14.022	-2.218	0.711	0.023	None	AT3G03060	69.803	1.160	0.307	0.004	AT3G03060
AT3G28915	18.742	-2.215	0.683	0.017	None	AT1G72770	649.131	1.160	0.298	0.003	HAB1
AT1G10460	15.306	-2.192	0.769	0.041	GLP7	AT1G80130	936.113	1.162	0.300	0.003	AT1G80130
AT4G04410	289.226	-2.192	0.394	0.000	None	AT4G38530	61.951	1.163	0.343	0.012	PLC3
AT1G43790	55.866	-2.184	0.475	0.000	TED6	AT1G22370	570.748	1.164	0.226	0.000	UGT85A5
AT3G12110	42.716	-2.173	0.643	0.012	ACT11	AT3G52170	74.510	1.166	0.423	0.049	AT3G52170
AT1G26820	24.665	-2.165	0.774	0.046	RNS3	AT1G31900	29.818	1.167	0.400	0.036	None

Gene ID	baseMean	log2FoldChange	lfcSE	padj	Symbol	Gene ID	baseMean	log2FoldChange	lfcSE	padj	Symbol
AT1G76090	368.139	-2.156	0.632	0.011	SMT3	AT1G55110	888.267	1.168	0.157	0.000	IDD7
AT4G28500	9.124	-2.155	0.684	0.021	NAC073	AT2G30100	309.369	1.169	0.349	0.013	AT2G30100
AT2G46630	121.297	-2.141	0.490	0.001	None	AT3G26840	584.196	1.171	0.319	0.006	AT3G26840
AT3G23670	9.174	-2.135	0.708	0.029	KIN12B	AT5G13820	136.516	1.172	0.313	0.005	TRP4
AT1G13670	18.045	-2.129	0.613	0.009	None	AT4G01910	44.182	1.174	0.324	0.006	AT4G01910
AT3G23730	67.853	-2.114	0.706	0.030	XTH16	AT2G32290	103.695	1.181	0.406	0.036	BAM6
AT1G65240	14.811	-2.113	0.589	0.007	AT1G65240	AT5G17860	257.719	1.183	0.299	0.002	CCX1
AT1G02640	411.036	-2.106	0.354	0.000	BXL2	AT3G57380	25.909	1.183	0.429	0.049	AT3G57380
AT4G34750	226.495	-2.088	0.310	0.000	AT4G34750	AT1G70000	116.547	1.187	0.428	0.048	AT1G70000
AT3G11700	1224.333	-2.085	0.387	0.000	FLA18	AT4G29110	255.378	1.189	0.346	0.010	None
AT3G06770	242.935	-2.077	0.620	0.013	AT3G06770	AT1G49450	69.192	1.191	0.430	0.048	AT1G49450
AT4G35350	58.304	-2.076	0.601	0.010	XCP1	AT1G78930	68.243	1.197	0.374	0.019	AT1G78930
AT4G27970	18.460	-2.070	0.518	0.002	SLAH2	AT3G57680	109.923	1.199	0.380	0.021	CTPA3
AT2G42380	137.776	-2.070	0.568	0.006	BZIP34	AT3G21250	564.526	1.202	0.286	0.001	MRP6
AT1G09750	1049.789	-2.070	0.542	0.004	AED3	AT5G01320	36.039	1.204	0.342	0.008	PDC4
AT1G20190	293.661	-2.069	0.539	0.004	EXPA11	AT1G06270	38.241	1.209	0.370	0.016	AT1G06270
AT1G69530	3802.239	-2.067	0.481	0.001	ATEXPA1	AT4G16680	632.474	1.212	0.271	0.000	None
AT1G33790	59.920	-2.055	0.390	0.000	None	AT1G32870	507.139	1.215	0.309	0.003	ANAC13
AT1G19380	346.649	-2.054	0.497	0.001	AT1G19380	AT2G31230	107.863	1.219	0.320	0.004	ERF15
AT1G63260	184.027	-2.053	0.577	0.008	TET10	AT5G58760	74.406	1.220	0.380	0.018	DDB2
AT5G39860	40.615	-2.036	0.561	0.006	PRE1	AT5G47220	1008.108	1.224	0.227	0.000	ERF2
AT5G55820	16.752	-2.020	0.555	0.006	AT5G55820	AT1G36680	45.329	1.227	0.388	0.021	None
AT1G02335	50.783	-2.019	0.622	0.017	GL22	AT4G34560	120.796	1.227	0.367	0.013	None
AT1G17700	23.956	-2.001	0.583	0.011	PRA1F1	AT3G29035	943.087	1.229	0.349	0.008	NAC59
AT1G60060	84.670	-2.001	0.332	0.000	None	AT1G19960	738.378	1.230	0.364	0.012	AT1G19960
AT2G34060	18.171	-1.996	0.600	0.014	PER19	AT5G42370	50.323	1.232	0.291	0.001	AT5G42370
AT4G23820	1240.493	-1.987	0.478	0.001	AT4G23820	AT4G32920	368.283	1.233	0.320	0.003	AT4G32920
AT4G34260	631.913	-1.981	0.306	0.000	FUC95A	AT4G38380	162.972	1.240	0.364	0.011	DTX45
AT5G02540	55.297	-1.977	0.661	0.030	AT5G02540	AT3G47430	218.554	1.242	0.295	0.001	PEX11B
AT1G75750	3608.132	-1.968	0.607	0.017	GASA1	AT4G22200	661.854	1.244	0.397	0.022	AKT2
AT1G19640	41.545	-1.967	0.393	0.000	JMT	AT3G21690	1091.915	1.251	0.285	0.001	DTX40
AT3G03265	77.257	-1.952	0.552	0.008	None	AT5G14580	112.885	1.253	0.402	0.023	PNP2
AT3G03840	16.671	-1.952	0.665	0.034	AT3G03840	AT5G05250	303.500	1.253	0.349	0.007	AT5G05250

Gene ID	baseMean	log2FoldChange	lfcSE	padj	Symbol	Gene ID	baseMean	log2FoldChange	lfcSE	padj	Symbol
AT2G13820	19.911	-1.942	0.619	0.022	AT2G13820	AT5G66400	288.828	1.255	0.395	0.020	RAB18
AT3G63110	182.224	-1.932	0.593	0.016	IPT3	AT2G20560	62.114	1.255	0.374	0.013	AT2G20560
AT4G14750	43.132	-1.931	0.536	0.007	IQD19	AT5G09785	17.853	1.257	0.450	0.046	None
AT4G22010	163.450	-1.930	0.321	0.000	sks4	AT3G28070	410.759	1.258	0.274	0.000	AT3G28070
AT5G48450	56.956	-1.927	0.475	0.002	sks3	AT3G22370	2905.467	1.260	0.432	0.036	AOX1A
AT1G19940	13.037	-1.923	0.653	0.033	AtGH9B5	AT5G23750	146.291	1.261	0.300	0.001	AT5G23750
AT4G05170	25.380	-1.900	0.501	0.004	AT4G05170	AT5G37500	251.786	1.262	0.412	0.026	GORK
AT5G62550	17.397	-1.898	0.554	0.011	AT5G62550	AT1G09180	59.605	1.263	0.387	0.016	ATSAR1
AT1G08340	11.754	-1.894	0.625	0.028	ROPGAP5	AT1G73040	46.695	1.272	0.405	0.021	None
AT1G03457	39.724	-1.891	0.539	0.009	AT1G03457	AT5G01250	17.911	1.273	0.456	0.046	None
AT4G25810	52.190	-1.885	0.612	0.025	XTH23	AT1G69440	157.633	1.274	0.317	0.002	AGO7
AT5G60720	17.892	-1.884	0.506	0.005	AT5G60720	AT5G02950	40.024	1.274	0.332	0.004	None
AT1G02630	11.739	-1.873	0.636	0.033	ETN8	AT2G03590	168.915	1.277	0.343	0.005	UPS1
AT4G34950	5005.850	-1.868	0.317	0.000	AT4G34950	AT5G45310	178.370	1.281	0.460	0.047	None
AT5G60860	194.650	-1.867	0.313	0.000	RABA1F	AT2G16720	59.989	1.283	0.443	0.037	MYB7
AT1G14290	464.387	-1.862	0.396	0.000	SBH2	AT5G44410	85.390	1.283	0.396	0.017	AT5G44410
AT2G38310	340.619	-1.856	0.436	0.001	PYL4	AT5G59700	169.871	1.287	0.229	0.000	AT5G59700
AT3G48100	165.630	-1.853	0.401	0.000	ARR5	AT1G31820	356.336	1.288	0.330	0.003	AT1G31820
AT4G32800	176.305	-1.832	0.440	0.001	ERF043	AT4G32940	21851.695	1.291	0.184	0.000	GAMMA-VPE
AT5G52882	487.825	-1.826	0.613	0.031	AT5G52882	AT3G61990	87.968	1.291	0.447	0.038	OMTF3
AT3G28420	16.834	-1.824	0.529	0.010	None	AT5G52320	198.904	1.292	0.366	0.008	CYP96A4
AT3G21050	20.493	-1.819	0.482	0.004	None	AT4G23250	431.258	1.292	0.244	0.000	EMB1290
AT1G22400	308.447	-1.806	0.301	0.000	UGT85A1	AT1G53170	297.120	1.293	0.278	0.000	ERF8
AT4G38850	49.990	-1.801	0.600	0.030	SAUR15	AT1G76955	99.500	1.294	0.397	0.016	None
AT1G73370	34.181	-1.796	0.325	0.000	SUS6	AT3G13080	12098.898	1.294	0.377	0.011	ABCC3
AT3G25500	690.970	-1.795	0.492	0.006	FH1	AT5G19740	171.834	1.298	0.251	0.000	LAMP1
AT3G23450	444.800	-1.793	0.494	0.006	AT3G23450	AT3G55290	20.823	1.300	0.455	0.040	AT3G55290
AT4G08160	36.910	-1.781	0.584	0.027	XYN3	AT2G34720	435.057	1.301	0.359	0.006	NFYA4
AT4G15660	117.420	-1.779	0.300	0.000	GRXS8	AT1G14600	90.593	1.301	0.255	0.000	AT1G14600
AT1G27460	370.340	-1.777	0.536	0.014	NPGR1	AT1G30820	921.442	1.308	0.283	0.000	AT1G30820
AT3G62020	38.982	-1.771	0.540	0.016	GLP10	AT2G04040	164.843	1.320	0.441	0.030	DTX1
AT1G80050	66.839	-1.769	0.392	0.000	APT2	AT4G24450	608.369	1.321	0.327	0.002	GWD2
AT2G42580	1401.727	-1.764	0.539	0.016	TTL3	AT2G21180	99.332	1.322	0.320	0.001	AT2G21180

Gene ID	baseMean	log2FoldChange	lfcSE	padj	Symbol	Gene ID	baseMean	log2FoldChange	lfcSE	padj	Symbol
AT5G07080	39.741	-1.764	0.457	0.003	None	AT5G59050	230.476	1.324	0.392	0.012	None
AT4G12420	1210.595	-1.761	0.475	0.005	SKU5	AT5G48400	109.312	1.335	0.469	0.041	GLR1.2
AT2G41830	171.632	-1.758	0.329	0.000	AT2G41830	AT5G03640	59.933	1.335	0.365	0.006	AT5G03640
AT4G38860	464.408	-1.757	0.427	0.001	AT4G38860	AT5G13210	741.768	1.338	0.407	0.015	AT5G13210
AT4G15690	217.362	-1.755	0.488	0.007	GRXS5	AT5G50800	224.670	1.346	0.382	0.008	SWEET13
AT5G25370	10.276	-1.754	0.580	0.028	PLDALPHA3	AT1G24265	51.086	1.352	0.402	0.013	AT1G24265
AT4G33420	26.719	-1.750	0.454	0.003	AT4G33420	AT5G24380	249.017	1.356	0.438	0.024	YSL2
AT3G13520	226.350	-1.738	0.556	0.022	AGP12	AT3G18610	135.321	1.357	0.260	0.000	NUCL2
AT4G30610	13.152	-1.726	0.573	0.029	SCPL24	AT1G52890	431.731	1.359	0.357	0.004	NAC019
AT1G33340	60.912	-1.723	0.430	0.002	AT1G33340	AT2G04050	3867.999	1.364	0.476	0.040	DTX3
AT5G59870	153.632	-1.722	0.350	0.000	HTA6	AT2G37830	25.026	1.367	0.491	0.047	None
AT5G61000	28.984	-1.719	0.482	0.007	RPA1D	AT1G27200	1017.692	1.368	0.349	0.003	None
AT1G62520	22.117	-1.710	0.479	0.007	None	AT1G79520	342.020	1.370	0.432	0.020	AT1G79520
AT3G60130	893.559	-1.704	0.426	0.002	BGLU16	AT1G10070	563.985	1.384	0.429	0.018	BCAT2
AT1G12080	41.561	-1.700	0.374	0.000	AT1G12080	AT3G63450	31.793	1.388	0.420	0.015	AT3G63450
AT5G46220	16.968	-1.698	0.493	0.010	AT5G46220	AT1G64600	93.134	1.390	0.371	0.005	AT1G64600
AT2G16660	6943.944	-1.696	0.516	0.015	AT2G16660	AT2G08865	20.009	1.396	0.473	0.033	None
AT5G02760	565.987	-1.695	0.511	0.014	AT5G02760	AT1G78070	1985.643	1.397	0.312	0.000	AT1G78070
AT2G36200	26.857	-1.692	0.393	0.001	AT2G36200	AT1G52570	50.311	1.405	0.430	0.016	PLDALPHA2
AT1G60390	14.115	-1.688	0.606	0.047	PGL2	AT4G27940	196.992	1.410	0.395	0.008	MTM1
AT2G33570	125.409	-1.683	0.558	0.029	GALS1	AT3G54600	1044.929	1.410	0.508	0.048	DJ1F
AT3G28180	1818.871	-1.681	0.410	0.002	CSLC4	AT1G55760	116.367	1.412	0.387	0.006	AT1G55760
AT3G26960	91.803	-1.681	0.421	0.002	None	AT5G61820	1085.951	1.416	0.354	0.002	AT5G61820
AT1G10682	292.365	-1.678	0.260	0.000	None	AT1G30530	186.236	1.432	0.311	0.000	UGT78D1
AT5G48900	135.790	-1.678	0.576	0.036	AT5G48900	AT4G03320	140.651	1.439	0.271	0.000	TIC20-IV
AT1G53730	548.982	-1.673	0.300	0.000	SRF6	AT3G15500	201.341	1.447	0.431	0.013	NAC055
AT5G15350	361.842	-1.673	0.515	0.017	ENODL17	AT3G58200	30.494	1.452	0.524	0.048	None
AT1G63300	44.781	-1.672	0.571	0.035	AT1G63300	AT2G43800	72.077	1.453	0.359	0.002	FH2
AT5G14920	2335.737	-1.668	0.521	0.019	GASA14	AT3G56080	439.122	1.453	0.377	0.003	AT3G56080
AT4G14310	27.427	-1.665	0.397	0.001	AT4G14310	AT5G43450	2230.609	1.456	0.485	0.030	AT5G43450
AT4G37450	56.274	-1.663	0.439	0.004	AGP18	AT1G30500	258.322	1.470	0.270	0.000	NFYA7
AT1G67750	35.984	-1.660	0.523	0.020	AT1G67750	AT4G21550	51.993	1.482	0.348	0.001	None
AT2G19620	97.607	-1.656	0.278	0.000	NDL3	AT5G52450	483.255	1.484	0.328	0.000	DTX16

Gene ID	baseMean	log2FoldChange	lfcSE	padj	Symbol	Gene ID	baseMean	log2FoldChange	lfcSE	padj	Symbol
AT5G20250	9319.144	-1.649	0.531	0.023	DIN10	AT2G43500	309.929	1.497	0.327	0.000	AT2G43500
AT1G02950	14.721	-1.643	0.489	0.013	ATGSTF4	AT2G41730	419.709	1.497	0.527	0.042	AT2G41730
AT3G17360	13.709	-1.638	0.524	0.023	POK1	AT1G78020	1506.533	1.498	0.302	0.000	None
AT1G76410	111.530	-1.632	0.281	0.000	ATL8	AT1G02520	41.678	1.499	0.435	0.010	ABCB11
AT5G51670	50.641	-1.630	0.493	0.014	None	AT1G06993	18.225	1.501	0.499	0.029	None
AT3G54920	950.076	-1.626	0.403	0.002	PMR6	AT1G13830	33.866	1.501	0.499	0.029	AT1G13830
AT1G63310	34.494	-1.623	0.385	0.001	AT1G63310	AT1G73390	468.879	1.504	0.460	0.016	AT1G73390
AT2G17880	153.577	-1.622	0.268	0.000	AT2G17880	AT1G19490	66.739	1.511	0.360	0.001	AT1G19490
AT2G36885	33.207	-1.622	0.492	0.015	AT2G36885	AT4G16750	42.534	1.513	0.432	0.009	ERF039
AT2G36050	282.361	-1.620	0.485	0.014	OFP15	AT5G24770	341.208	1.517	0.526	0.038	VSP2
AT3G16180	305.276	-1.614	0.470	0.010	NPF1.1	AT4G21910	1027.722	1.518	0.240	0.000	AT4G21910
AT1G72790	255.740	-1.610	0.410	0.003	AT1G72790	AT5G54250	654.040	1.522	0.296	0.000	CNGC4
AT3G25880	10.849	-1.609	0.580	0.048	AT3G25880	AT2G41380	61.602	1.524	0.411	0.005	AT2G41380
AT4G02330	122.269	-1.608	0.520	0.024	PME41	AT5G19580	65.812	1.525	0.455	0.013	AT5G19580
AT5G01730	21.289	-1.607	0.415	0.003	SCAR4	AT4G29700	63.101	1.526	0.505	0.028	AT4G29700
AT2G28130	134.286	-1.606	0.212	0.000	None	AT3G14280	243.953	1.529	0.371	0.001	AT3G14280
AT2G44740	110.218	-1.599	0.472	0.012	CYCU4-1	AT1G17745	728.531	1.529	0.419	0.006	PGDH
AT3G49940	441.673	-1.597	0.439	0.006	LBD38	AT1G28230	514.220	1.544	0.373	0.001	PUP1
AT4G37800	240.018	-1.593	0.550	0.037	XTH7	AT1G52040	1376.869	1.546	0.424	0.006	MBP1
AT4G30850	82.458	-1.587	0.378	0.001	HHP2	AT1G05680	233.547	1.547	0.543	0.041	UGT74E2
AT1G05135	793.945	-1.577	0.260	0.000	None	AT1G69540	16.908	1.548	0.450	0.010	AGL94
AT4G30640	16.829	-1.576	0.565	0.046	FBL19	AT2G47000	3831.650	1.551	0.513	0.028	ABCB4
AT5G09710	27.216	-1.575	0.463	0.011	None	AT5G20150	212.394	1.552	0.500	0.024	SPX1
AT1G04680	340.992	-1.571	0.335	0.000	AT1G04680	AT1G29860	20.017	1.556	0.492	0.021	WRKY71
AT5G10400	85.119	-1.569	0.361	0.001	HTR2	AT2G35950	40.638	1.562	0.377	0.001	None
AT3G07320	72.661	-1.566	0.413	0.004	AT3G07320	AT1G01250	23.287	1.563	0.381	0.002	ERF023
AT1G20610	14.715	-1.552	0.504	0.025	CYCB2-3	AT3G27250	77.465	1.563	0.484	0.018	AT3G27250
AT1G74670	1703.352	-1.549	0.408	0.004	GASA6	AT1G52410	1242.331	1.566	0.369	0.001	TSA1
AT5G44020	3104.266	-1.547	0.501	0.024	AT5G44020	AT5G10930	246.065	1.566	0.421	0.005	CIPK5
AT1G19440	181.138	-1.546	0.312	0.000	KCS4	AT1G07430	160.425	1.567	0.295	0.000	AIP1
AT1G09575	79.819	-1.545	0.423	0.006	AT1G09575	AT2G35070	110.136	1.571	0.358	0.001	None
AT2G21540	64.478	-1.542	0.514	0.030	SFH3	AT1G36675	41.103	1.574	0.463	0.012	None
AT3G10660	26.532	-1.539	0.418	0.005	CPK2	AT2G44880	17.229	1.580	0.450	0.009	AT2G44880

Gene ID	baseMean	log2FoldChange	lfcSE	padj	Symbol	Gene ID	baseMean	log2FoldChange	lfcSE	padj	Symbol
AT5G07030	49.105	-1.539	0.505	0.027	AT5G07030	AT1G02770	18.349	1.582	0.531	0.031	None
AT3G25900	20.594	-1.534	0.554	0.048	HMT-1	AT2G01175	14.437	1.588	0.572	0.048	AT2G01175
AT4G31620	85.160	-1.532	0.322	0.000	None	AT1G04570	22.452	1.589	0.544	0.035	None
AT4G03190	236.606	-1.529	0.329	0.000	GRH1	AT4G34990	60.045	1.602	0.342	0.000	MYB32
AT2G22860	80.898	-1.523	0.429	0.008	PSK2	AT1G29050	480.283	1.617	0.299	0.000	TBL38
AT3G61640	172.258	-1.520	0.339	0.000	AGP20	AT4G23990	96.463	1.621	0.475	0.011	CSLG3
AT4G21870	58.303	-1.519	0.313	0.000	HSP15.4	AT1G79270	1000.190	1.626	0.476	0.011	ECT8
AT1G59740	33.650	-1.516	0.411	0.005	NPF4.3	AT2G18193	2026.230	1.626	0.542	0.030	AT2G18193
AT1G15830	186.502	-1.510	0.432	0.009	AT1G15830	AT2G04070	2283.063	1.631	0.503	0.017	DTX4
AT1G17620	446.650	-1.507	0.380	0.002	AT1G17620	AT1G68600	1055.855	1.639	0.287	0.000	ALMT5
AT1G09200	193.631	-1.507	0.310	0.000	HTR2	AT1G01590	25.694	1.646	0.463	0.008	FRO1
AT3G61580	4514.494	-1.505	0.384	0.003	SLD1	AT3G28220	761.458	1.664	0.597	0.047	AT3G28220
AT3G10720	592.159	-1.504	0.389	0.003	PME25	AT4G21990	1741.522	1.673	0.572	0.035	37712.000
AT2G16060	32.917	-1.497	0.384	0.003	AHB1	AT1G62570	163.790	1.682	0.391	0.001	FMOGS-OX4
AT3G47380	38.663	-1.492	0.466	0.019	PMEI11	AT3G02020	3825.247	1.683	0.544	0.024	AK3
AT5G40230	25.391	-1.490	0.441	0.012	None	AT1G58270	106.399	1.688	0.587	0.039	ZW9
AT1G20850	199.142	-1.490	0.440	0.012	XCP2	AT3G13260	11.468	1.698	0.617	0.050	None
AT5G54510	206.236	-1.488	0.454	0.015	GH3.6	AT3G61060	1287.293	1.701	0.565	0.029	AtPP2-A13
AT3G07010	689.273	-1.488	0.477	0.023	AT3G07010	AT5G53420	731.024	1.703	0.419	0.002	AT5G53420
AT5G65730	1379.610	-1.488	0.538	0.049	XTH6	AT2G28110	125.879	1.705	0.494	0.010	IRX7
AT5G47130	14.797	-1.487	0.524	0.042	AT5G47130	AT1G51140	224.111	1.708	0.399	0.001	BHLH122
AT2G35190	30.622	-1.486	0.479	0.024	NPSN11	AT5G60910	122.686	1.714	0.358	0.000	AGL8
AT5G62360	801.736	-1.486	0.322	0.000	AT5G62360	AT2G36270	32.461	1.716	0.600	0.040	ABI5
AT2G17780	97.283	-1.486	0.373	0.002	MCA2	AT3G12580	97.585	1.729	0.568	0.027	MED37C
AT1G68230	24.492	-1.482	0.475	0.023	RTNLB14	AT4G16670	41.719	1.732	0.406	0.001	AT4G16670
AT3G43430	28.691	-1.475	0.505	0.035	AT3G43430	AT2G47190	72.807	1.734	0.410	0.001	ATMYB2
AT1G23030	629.776	-1.473	0.498	0.033	PUB11	AT3G14360	29.271	1.738	0.365	0.000	AT3G14360
AT1G04020	21.641	-1.467	0.439	0.013	None	AT4G39110	26.450	1.741	0.527	0.015	AT4G39110
AT4G35970	18.946	-1.466	0.514	0.040	APX5	AT1G69490	1281.556	1.762	0.361	0.000	NAC029
AT3G23805	62.262	-1.465	0.408	0.007	RALFL24	AT4G15550	165.580	1.764	0.353	0.000	UGT75D1
AT1G22690	174.095	-1.464	0.454	0.018	GASA9	AT2G25625	299.018	1.768	0.470	0.004	None
AT3G02210	19.540	-1.461	0.429	0.011	COBL1	AT3G18950	104.777	1.771	0.462	0.004	AT3G18950
AT5G36910	45.189	-1.461	0.422	0.010	THI2.2	AT5G47610	39.660	1.790	0.477	0.005	ATL79

Gene ID	baseMean	log2FoldChange	lfcSE	padj	Symbol	Gene ID	baseMean	log2FoldChange	lfcSE	padj	Symbol
AT1G07610	121.107	-1.456	0.480	0.028	MT1C	AT3G47420	479.678	1.791	0.473	0.004	ATPS3
AT3G01500	10628.434	-1.456	0.272	0.000	BCA1	AT4G18980	20.328	1.792	0.587	0.026	AtS40-3
AT2G16750	83.429	-1.452	0.296	0.000	AT2G16750	AT1G02850	461.318	1.794	0.303	0.000	BGLU11
AT1G47380	141.343	-1.450	0.268	0.000	AT1G47380	AT1G08230	215.350	1.801	0.421	0.001	GAT1
AT5G12050	217.030	-1.449	0.423	0.011	AT5G12050	AT1G15870	10.312	1.803	0.642	0.045	AT1G15870
AT2G39900	192.425	-1.448	0.354	0.002	WLIN2A	AT1G74870	55.036	1.804	0.630	0.040	AT1G74870
AT2G40330	25.273	-1.448	0.430	0.012	PYL6	AT5G06230	25.955	1.807	0.535	0.012	None
AT1G12845	63.018	-1.446	0.441	0.016	None	AT5G62480	427.114	1.810	0.463	0.003	GSTU9
AT1G29520	76.552	-1.445	0.309	0.000	AT1G29520	AT4G33070	28.133	1.812	0.560	0.017	PDC1
AT1G54217	74.169	-1.443	0.308	0.000	AT1G54217	AT1G75390	23.847	1.817	0.489	0.005	BZIP44
AT1G10470	2027.929	-1.443	0.342	0.001	ARR4	AT1G52030	40.240	1.822	0.650	0.045	F-ATMBP
AT1G15175	59.454	-1.442	0.364	0.002	None	AT1G62710	114.660	1.833	0.654	0.045	bVPE
AT3G54560	42.081	-1.441	0.444	0.017	H2AV	AT1G22160	328.669	1.840	0.292	0.000	FLZ5
AT2G30600	2932.667	-1.436	0.332	0.001	AT2G30600	AT1G54120	14.292	1.841	0.533	0.010	None
AT4G19050	30.315	-1.433	0.514	0.047	AT4G19050	AT5G51440	216.916	1.842	0.376	0.000	HSP23.5
AT5G02400	34.091	-1.427	0.400	0.007	PLL2	AT5G37260	99.358	1.844	0.622	0.032	RVE2
AT3G58620	350.303	-1.425	0.439	0.017	TTL4	AT3G19270	50.185	1.845	0.526	0.009	CYP707A4
AT3G45060	36.919	-1.423	0.512	0.047	NRT2.6	AT4G11910	144.894	1.875	0.426	0.001	SGR2
AT3G53650	26.363	-1.420	0.394	0.007	AT3G53650	AT1G52400	4221.970	1.882	0.430	0.001	BGLU18
AT4G21070	26.567	-1.414	0.464	0.027	BRCA1	AT5G55970	1042.646	1.894	0.410	0.000	AT5G55970
AT1G57820	55.529	-1.412	0.323	0.001	ORTH2	AT4G12030	1073.134	1.898	0.611	0.023	BASS5
AT5G05440	253.683	-1.408	0.472	0.031	PYL5	AT1G02470	158.456	1.900	0.403	0.000	AT1G02470
AT1G23480	289.084	-1.403	0.398	0.008	CSLA3	AT3G22550	118.343	1.901	0.435	0.001	FLZ8
AT4G26690	1670.019	-1.402	0.456	0.025	GDPDL3	AT2G04135	30.528	1.902	0.530	0.007	None
AT3G62930	21.509	-1.401	0.482	0.036	GRXS6	AT3G25290	52.398	1.920	0.619	0.024	AT3G25290
AT4G38840	276.844	-1.400	0.287	0.000	AT4G38840	AT4G03060	304.244	1.925	0.682	0.043	None
AT3G14170	29.232	-1.400	0.483	0.037	AT3G14170	AT5G15190	47.046	1.933	0.491	0.003	AT5G15190
AT2G33350	54.501	-1.395	0.332	0.001	AT2G33350	AT5G52930	22.972	1.937	0.657	0.033	None
AT4G02060	49.436	-1.390	0.440	0.021	MCM7	AT2G35570	37.706	1.939	0.547	0.008	None
AT3G03850	22.772	-1.382	0.446	0.024	AT3G03850	AT1G06160	213.440	1.944	0.511	0.004	ERF094
AT2G30540	57.406	-1.378	0.458	0.029	GRXS9	AT4G01080	67.287	1.956	0.484	0.002	TBL26
AT1G29660	931.229	-1.375	0.384	0.007	AT1G29660	AT1G50400	22.571	1.969	0.419	0.000	TOM40-2
AT1G33440	29.898	-1.373	0.481	0.041	NPF4.4	AT4G20320	141.787	1.985	0.614	0.017	AT4G20320

Gene ID	baseMean	log2FoldChange	lfcSE	padj	Symbol	Gene ID	baseMean	log2FoldChange	lfcSE	padj	Symbol
AT1G04430	1962.343	-1.373	0.327	0.001	AT1G04430	AT1G65480	23.796	1.986	0.643	0.024	FT
AT5G04890	31.223	-1.373	0.431	0.020	RTM2	AT1G62560	553.609	2.007	0.689	0.036	FMOGS-OX3
AT3G23530	476.920	-1.370	0.178	0.000	AT3G23530	AT4G22940	21.344	2.014	0.726	0.048	AT4G22940
AT5G11420	1385.891	-1.370	0.380	0.007	AT5G11420	AT3G61890	280.626	2.018	0.305	0.000	ATHB-12
AT1G26208	39.998	-1.365	0.495	0.049	None	AT2G46680	619.399	2.026	0.502	0.002	ATHB-7
AT5G09730	35.558	-1.365	0.359	0.004	BXL3	AT1G79900	39.499	2.048	0.731	0.046	BAC2
AT1G50240	26.610	-1.364	0.375	0.006	TIO	AT3G23240	28.685	2.066	0.487	0.001	ERF1B
AT3G15540	86.435	-1.364	0.463	0.033	IAA19	AT2G36800	312.740	2.067	0.564	0.006	UGT73C5
AT1G14890	160.545	-1.362	0.275	0.000	None	AT5G56840	47.657	2.078	0.684	0.027	AT5G56840
AT2G32690	1346.740	-1.361	0.304	0.000	GRP23	AT5G02020	1480.103	2.079	0.553	0.004	SIS
AT5G65660	729.492	-1.361	0.309	0.001	AT5G65660	AT4G34860	72.579	2.079	0.441	0.000	INVB
AT5G22580	430.983	-1.358	0.458	0.032	AT5G22580	AT5G64550	254.355	2.089	0.371	0.000	None
AT1G07150	42.547	-1.357	0.394	0.010	MAPKKK13	AT1G30220	57.278	2.094	0.506	0.001	INT2
AT3G28200	341.556	-1.340	0.462	0.037	PER31	AT2G42065	76.331	2.096	0.733	0.040	None
AT3G14240	709.096	-1.339	0.317	0.001	SBT1.5	AT1G16400	95.328	2.121	0.729	0.036	CYP79F2
AT4G18670	479.379	-1.335	0.400	0.014	LRX5	AT1G11700	108.216	2.123	0.572	0.005	None
AT3G23430	239.394	-1.324	0.312	0.001	PHO1	AT4G21440	24.344	2.147	0.455	0.000	ATMYB102
AT5G02170	35.592	-1.324	0.418	0.020	AVT1E	AT3G61900	37.060	2.183	0.595	0.006	AT3G61900
AT1G45130	171.769	-1.322	0.426	0.024	BGAL5	AT3G23630	15.026	2.189	0.531	0.001	IPT7
AT2G48030	388.478	-1.319	0.389	0.012	None	AT1G24070	54.608	2.195	0.562	0.003	CSLA10
AT5G65470	374.117	-1.319	0.447	0.033	OFUT39	AT3G28500	14.404	2.212	0.756	0.035	RPP2C
AT1G06490	37.289	-1.318	0.470	0.045	CALS7	AT4G24010	12.024	2.216	0.805	0.049	CSLG1
AT5G48460	249.138	-1.316	0.428	0.025	FIM2	AT1G18710	279.563	2.220	0.324	0.000	AtMYB47
AT2G05790	479.648	-1.313	0.397	0.015	AT2G05790	AT5G16980	49.254	2.226	0.542	0.002	AT5G16980
AT2G01830	110.329	-1.311	0.350	0.005	AHK4	AT1G64780	43.414	2.244	0.552	0.002	AMT1-2
AT2G28740	180.964	-1.309	0.299	0.001	HIS4	AT2G28755	9.723	2.258	0.648	0.009	AT2G28755
AT5G18500	813.364	-1.303	0.328	0.002	AT5G18500	AT5G54095	13.546	2.280	0.613	0.005	AT5G54095
AT1G78970	335.784	-1.302	0.423	0.025	LUP1	AT3G48020	56.587	2.316	0.385	0.000	None
AT4G33220	1070.328	-1.301	0.386	0.012	PME44	AT1G56600	1167.314	2.331	0.382	0.000	GOLS2
AT5G26000	20125.636	-1.300	0.399	0.016	TGG1	AT4G04610	2049.461	2.344	0.645	0.006	36982.000
AT1G52827	41.818	-1.299	0.447	0.036	None	AT2G41190	187.963	2.346	0.612	0.004	AVT1A
AT5G66920	89.681	-1.296	0.462	0.045	sks17	AT2G39820	10.713	2.363	0.684	0.010	EIF6-1
AT5G49100	174.451	-1.296	0.355	0.006	AT5G49100	AT4G12735	328.354	2.367	0.604	0.003	AT4G12735

Gene ID	baseMean	log2FoldChange	lfcSE	padj	Symbol	Gene ID	baseMean	log2FoldChange	lfcSE	padj	Symbol
AT2G34430	86252.411	-1.294	0.342	0.004	LHB1B1	AT1G24020	20.793	2.371	0.765	0.024	MLP423
AT2G37585	82.710	-1.293	0.324	0.002	GLCAT14C	AT1G52000	2242.662	2.375	0.455	0.000	JAL5
AT3G20570	96.061	-1.286	0.378	0.011	ENODL9	AT5G50360	13.421	2.393	0.677	0.008	AT5G50360
AT1G49210	36.507	-1.285	0.414	0.024	ATL76	AT2G40435	88.348	2.395	0.496	0.000	AT2G40435
AT2G35650	230.282	-1.281	0.232	0.000	CSLA7	AT5G06760	11.373	2.396	0.778	0.025	LEA46
AT5G07440	572.277	-1.281	0.218	0.000	GDH2	AT3G17790	535.484	2.402	0.531	0.000	PAP17
AT1G23460	86.884	-1.280	0.270	0.000	AT1G23460	AT4G15440	174.823	2.403	0.466	0.000	CYP74B2
AT3G16370	1981.919	-1.278	0.432	0.033	APG	AT1G05857	4.968	2.461	0.873	0.044	None
AT2G34510	1007.843	-1.273	0.448	0.042	AT2G34510	AT5G66670	6.642	2.494	0.801	0.023	AT5G66670
AT4G09420	52.434	-1.273	0.383	0.014	AT4G09420	AT5G49120	4.954	2.553	0.915	0.046	FLZ15
AT5G60840	323.639	-1.270	0.292	0.001	None	AT5G04150	36.935	2.596	0.523	0.000	None
AT1G49730	325.219	-1.269	0.356	0.008	None	AT1G34060	350.441	2.642	0.484	0.000	TAR4
AT2G34770	545.597	-1.269	0.451	0.044	FAH1	AT4G28040	49.450	2.670	0.861	0.024	AT4G28040
AT3G18730	26.846	-1.268	0.393	0.018	TSK	AT4G24000	92.109	2.670	0.625	0.001	CSLG2
AT4G16500	242.399	-1.267	0.276	0.000	CYS4	AT5G25390	10.369	2.677	0.942	0.042	SHN3
AT3G16920	50.678	-1.263	0.443	0.041	CTL2	AT4G28790	22.504	2.686	0.568	0.000	BHLH23
AT1G69700	99.633	-1.261	0.290	0.001	HVA22C	AT5G52300	40.465	2.725	0.958	0.041	LTI65
AT5G04680	26.258	-1.261	0.400	0.021	AT5G04680	AT1G70640	32.652	2.728	0.495	0.000	None
AT1G05000	59.786	-1.260	0.349	0.007	AT1G05000	AT3G49570	119.414	2.782	0.921	0.028	LSU3
AT1G26770	29.636	-1.259	0.397	0.020	ATEXPA10	AT5G14380	13.800	2.841	0.749	0.004	AGP6
AT4G13330	55.364	-1.258	0.456	0.049	None	AT3G26460	8.297	2.869	0.714	0.002	AT3G26460
AT5G62180	36.410	-1.258	0.300	0.001	CXE20	AT2G04066	19.060	2.895	0.912	0.020	None
AT5G23870	459.815	-1.258	0.338	0.005	PAE9	AT4G33040	110.691	2.964	0.494	0.000	GRXC6
AT1G32100	56.667	-1.257	0.430	0.035	PRR1	AT1G48000	93.382	2.964	0.592	0.000	MYB112
AT3G54750	75.173	-1.257	0.269	0.000	AT3G54750	AT1G11785	9.004	2.969	0.757	0.003	None
AT4G02130	649.890	-1.254	0.393	0.019	GATL6	AT2G04460	28.672	2.999	0.978	0.025	None
AT1G28290	53.827	-1.254	0.382	0.015	AGP31	AT2G18050	1455.256	3.000	0.469	0.000	HIS1-3
AT5G03720	33.803	-1.251	0.454	0.049	HSFA3	AT1G14080	13.302	3.079	0.926	0.014	FUT6
AT3G07460	1428.433	-1.248	0.369	0.012	None	AT1G12940	38.924	3.084	1.030	0.030	NRT2.5
AT3G57780	96.001	-1.244	0.269	0.000	None	AT4G38340	57.509	3.161	0.775	0.002	NLP3
AT5G65440	666.278	-1.240	0.239	0.000	None	AT3G17980	8.250	3.367	1.063	0.021	CAR4
AT1G67040	21.976	-1.239	0.434	0.040	None	AT3G49540	12.115	3.395	1.115	0.027	None
AT4G16120	120.811	-1.237	0.323	0.004	COBL7	AT4G26950	20.222	3.395	1.103	0.025	None

Gene ID	baseMean	log2FoldChange	lfcSE	padj	Symbol	Gene ID	baseMean	log2FoldChange	lfcSE	padj	Symbol
AT4G00020	36.789	-1.236	0.359	0.010	MEE43	AT3G28270	127.159	3.399	0.701	0.000	AT3G28270
AT4G02660	49.419	-1.236	0.391	0.021	AT4G02660	AT4G18360	10.342	3.423	1.184	0.038	GLO5
AT3G15356	2260.353	-1.235	0.199	0.000	LEC	AT5G04180	8.018	3.433	0.857	0.002	ACA3
AT1G69040	594.721	-1.234	0.338	0.006	ACR4	AT5G62165	49.088	3.456	0.896	0.003	AGL42
AT1G45688	539.176	-1.234	0.268	0.000	AT1G45688	AT1G16060	12.537	3.468	1.214	0.040	ADAP
AT1G56720	164.805	-1.232	0.436	0.043	AT1G56720	AT4G25330	5.390	3.495	1.030	0.012	AT4G25330
AT1G75960	145.077	-1.230	0.444	0.048	AAE8	AT5G25110	35.475	3.602	0.864	0.001	CIPK25
AT4G23550	34.702	-1.227	0.382	0.019	None	AT1G69480	67.164	3.672	0.878	0.001	PHO1-H10
AT1G60140	2977.369	-1.226	0.353	0.010	TPS10	AT1G14420	7.441	3.730	1.148	0.017	AT59
AT2G36120	1331.319	-1.224	0.304	0.002	DOT1	AT5G39520	210.841	3.844	1.122	0.011	AT5G39520
AT4G37530	177.346	-1.222	0.200	0.000	PER51	AT3G13400	41.323	3.891	0.693	0.000	sks13
AT1G26200	24.242	-1.221	0.433	0.043	AT1G26200	AT2G16367	33.489	3.954	1.013	0.003	None
AT1G01620	4468.635	-1.218	0.387	0.021	PIP1-3	AT1G64110	91.726	3.968	0.619	0.000	AT1G64110
AT5G38410	21755.745	-1.215	0.248	0.000	AT5G38410	AT1G18860	27.242	3.995	0.769	0.000	None
AT2G34300	188.436	-1.207	0.277	0.001	AT2G34300	AT4G34550	6.384	4.026	1.460	0.049	AT4G34550
AT3G05490	195.304	-1.207	0.432	0.046	RALFL22	AT4G24150	9.263	4.070	0.995	0.002	GRF8
AT3G06140	31.895	-1.204	0.365	0.015	LUL4	AT2G47770	9.118	4.070	1.091	0.005	TSPO
AT2G28950	483.608	-1.204	0.341	0.008	EXPA6	AT1G43640	4.317	4.162	1.399	0.031	TULP5
AT3G29810	55.413	-1.199	0.375	0.019	COBL3	AT3G48240	5.530	4.172	1.369	0.027	None
AT3G07340	198.192	-1.198	0.302	0.002	BHLH62	AT5G15500	178.876	4.219	0.853	0.000	AT5G15500
AT2G26690	1000.720	-1.196	0.271	0.001	NPF6.2	AT5G43840	20.848	4.250	1.001	0.001	HSFA6A
AT1G25530	42.115	-1.194	0.357	0.013	AT1G25530	AT5G42800	22.183	4.311	1.498	0.039	DFRA
AT5G60950	193.106	-1.194	0.413	0.037	COBL5	AT3G28830	21.723	4.349	0.744	0.000	AT3G28830
AT4G23400	3005.604	-1.194	0.345	0.010	PIP1-5	AT1G60740	4.342	4.396	1.400	0.022	PRXIID
AT3G42660	56.070	-1.193	0.363	0.015	AT3G42660	AT4G35010	14.726	4.458	1.074	0.001	BGAL11
AT3G60320	2509.911	-1.189	0.342	0.009	NRG2	AT1G24520	4.888	4.476	1.417	0.021	BCP1
AT1G20330	1071.017	-1.189	0.341	0.009	SMT2	AT3G01240	10.603	4.564	1.017	0.000	AT3G01240
AT4G25835	120.870	-1.187	0.371	0.019	AT4G25835	AT3G28750	24.226	4.689	0.732	0.000	None
AT1G16170	263.361	-1.185	0.207	0.000	None	AT4G22880	15.703	4.693	1.479	0.020	LDOX
AT4G36540	842.912	-1.180	0.261	0.000	BEE2	AT5G45880	12.748	4.829	1.240	0.003	AT5G45880
AT3G61380	115.179	-1.178	0.195	0.000	AT3G61380	AT5G53660	6.664	4.832	1.354	0.007	GRF7
AT3G01670	390.510	-1.176	0.280	0.001	AT3G01670	AT1G56650	44.494	4.841	0.990	0.000	MYB75
AT3G15520	276.246	-1.174	0.207	0.000	CYP37	AT2G26450	6.301	4.844	1.213	0.002	PME13

Gene ID	baseMean	log2FoldChange	lfcSE	padj	Symbol	Gene ID	baseMean	log2FoldChange	lfcSE	padj	Symbol
AT1G29670	2928.598	-1.172	0.352	0.014	AT1G29670	AT3G05610	10.174	4.912	1.148	0.001	PME21
AT5G62865	162.411	-1.167	0.389	0.029	None	AT2G07040	6.384	4.954	1.305	0.004	PRK2
AT2G45180	18962.638	-1.167	0.285	0.002	AT2G45180	AT4G16590	7.559	5.081	1.805	0.044	None
AT4G27720	399.467	-1.166	0.313	0.005	AT4G27720	AT5G47350	37.528	5.159	1.502	0.010	AT5G47350
AT4G03390	708.707	-1.165	0.291	0.002	SRF3	AT3G54800	3.669	5.164	1.846	0.046	AT3G54800
AT3G01450	77.743	-1.163	0.228	0.000	AT3G01450	AT3G57690	4.190	5.209	1.673	0.023	AGP23
AT2G38080	102.010	-1.163	0.394	0.033	IRX12	AT4G03290	3.922	5.249	1.745	0.029	CML6
AT1G66180	769.691	-1.162	0.373	0.023	AT1G66180	AT1G55560	7.791	5.297	1.342	0.002	sks14
AT5G25190	318.842	-1.160	0.419	0.048	ERF003	AT4G24640	4.168	5.319	1.705	0.023	APPB1
AT1G62380	1675.931	-1.157	0.280	0.001	ACO2	AT3G28790	8.537	5.352	1.321	0.002	AT3G28790
AT4G19120	1060.377	-1.157	0.403	0.039	ERD3	AT1G70260	40.812	5.486	1.006	0.000	AT1G70260
AT3G57800	917.468	-1.157	0.404	0.040	BHLH60	AT1G03050	5.052	5.505	1.620	0.012	AT1G03050
AT5G10390	51.655	-1.157	0.395	0.035	HTR2	AT5G49920	2.227	5.548	1.885	0.034	AT5G49920
AT3G23820	3047.567	-1.152	0.257	0.000	GAE6	AT1G08733	2.853	5.587	1.810	0.024	None
AT5G52970	479.320	-1.151	0.175	0.000	AT5G52970	AT2G47030	17.184	5.624	1.139	0.000	PME4
AT3G08030	943.342	-1.146	0.329	0.009	AT3G08030	AT5G28680	2.345	5.624	1.832	0.025	ANX2
AT3G16570	706.877	-1.140	0.332	0.010	RALF23	AT2G47040	41.554	5.642	1.017	0.000	PME5
AT5G11070	764.928	-1.140	0.274	0.001	None	AT5G47000	5.042	5.689	1.697	0.013	PER65
AT3G54690	287.776	-1.136	0.291	0.003	SETH3	AT3G62170	12.581	5.809	1.245	0.000	VGDH2
AT1G20970	1893.168	-1.135	0.214	0.000	AT1G20970	AT1G61563	2.282	5.817	2.087	0.047	RALFL8
AT1G62790	217.302	-1.134	0.249	0.000	AT1G62790	AT3G60900	7.514	5.878	2.034	0.038	FLA10
AT3G60290	186.675	-1.131	0.295	0.004	AT3G60290	AT3G01270	25.395	5.933	0.988	0.000	AT3G01270
AT3G50560	73.096	-1.131	0.343	0.015	AT3G50560	AT3G62710	7.249	5.981	1.690	0.008	AT3G62710
AT5G64120	309.564	-1.126	0.261	0.001	PER71	AT1G29140	2.910	5.992	1.898	0.021	AT1G29140
AT5G48560	84.272	-1.124	0.325	0.010	BHLH78	AT1G58120	7.178	6.026	1.589	0.004	AT1G58120
AT3G01680	363.040	-1.122	0.255	0.001	SEOB	AT3G07820	21.457	6.038	1.263	0.000	AT3G07820
AT3G27770	1093.869	-1.121	0.240	0.000	None	AT2G26850	2.766	6.065	1.838	0.015	AT2G26850
AT4G00300	1075.093	-1.119	0.254	0.001	None	AT2G05850	3.590	6.076	1.860	0.016	SCPL38
AT2G36570	83.272	-1.114	0.274	0.002	PXC1	AT3G18810	2.576	6.224	1.962	0.020	PERK6
AT2G42220	2226.614	-1.113	0.248	0.000	STR9	AT3G43860	8.070	6.230	1.761	0.008	AtGH9A4
AT3G05910	1089.990	-1.109	0.352	0.021	PAE12	AT3G62230	8.021	6.246	1.655	0.004	AT3G62230
AT2G01910	1051.294	-1.108	0.260	0.001	MAP65-6	AT3G28980	8.498	6.262	1.711	0.006	AT3G28980
AT5G13710	1591.324	-1.107	0.392	0.043	SMT1	AT3G17060	2.820	6.271	1.910	0.015	PME67

Gene ID	baseMean	log2FoldChange	lfcSE	padj	Symbol	Gene ID	baseMean	log2FoldChange	lfcSE	padj	Symbol
AT1G75680	570.252	-1.107	0.298	0.005	AtGH9B7	AT2G26410	3.660	6.276	1.685	0.005	Iqd4
AT3G62660	1076.294	-1.106	0.351	0.021	GATL7	AT5G39880	8.819	6.297	1.720	0.006	AT5G39880
AT1G29070	1424.230	-1.105	0.160	0.000	RPL34	AT3G13390	8.804	6.307	1.761	0.007	sks11
AT1G59710	425.519	-1.104	0.294	0.004	AT1G59710	AT3G20580	3.455	6.317	1.889	0.013	COBL10
AT1G47210	63.065	-1.101	0.316	0.009	CYCA3-2	AT1G66390	4.280	6.328	2.168	0.035	MYB90
AT1G19950	50.252	-1.100	0.341	0.018	HVA22H	AT2G47050	9.692	6.361	1.598	0.002	AT2G47050
AT5G18970	32.404	-1.099	0.362	0.028	AT5G18970	AT1G04470	3.395	6.378	1.887	0.012	None
AT4G18740	315.378	-1.099	0.297	0.005	AT4G18740	AT2G23900	3.218	6.410	1.749	0.006	AT2G23900
AT1G17430	153.952	-1.096	0.327	0.013	None	AT1G67290	4.108	6.509	1.709	0.004	GLOX1
AT3G23750	883.718	-1.096	0.318	0.010	TMK4	AT5G27870	3.607	6.516	1.903	0.011	PME28
AT1G70370	577.454	-1.093	0.286	0.004	PGL3	AT1G72260	23.351	6.615	1.801	0.006	THI2.1
AT5G46700	31.953	-1.092	0.343	0.020	TRN2	AT4G12890	3.949	6.641	2.280	0.036	AT4G12890
AT3G43270	313.314	-1.089	0.162	0.000	PME32	AT4G02250	4.665	6.654	1.862	0.007	AT4G02250
AT3G04630	102.461	-1.088	0.273	0.002	WDL1	AT5G48140	4.805	6.729	2.324	0.037	AT5G48140
AT3G48720	556.955	-1.083	0.285	0.004	AT3G48720	AT1G01980	4.298	6.754	1.728	0.003	SEC1A
AT5G38420	10861.274	-1.081	0.211	0.000	RBCS-2B	AT1G35490	4.465	6.761	1.671	0.002	AT1G35490
AT1G21310	1140.454	-1.081	0.338	0.019	EXT3	AT3G14040	12.591	6.836	1.622	0.001	AT3G14040
AT5G06700	2055.075	-1.076	0.236	0.000	TBR	AT1G55570	4.476	6.843	1.806	0.004	sks12
AT1G19835	1737.965	-1.071	0.232	0.000	FPP4	AT3G49270	5.176	6.870	2.357	0.036	None
AT5G35750	723.000	-1.068	0.293	0.006	AHK2	AT1G69940	4.732	6.894	1.675	0.001	PPME1
AT2G01918	38.537	-1.067	0.357	0.030	PQL3	AT2G32660	11.516	6.915	1.872	0.005	AtRLP22
AT2G32880	763.385	-1.067	0.165	0.000	AT2G32880	AT5G07410	14.995	6.948	1.652	0.001	PME48
AT1G50460	363.795	-1.065	0.269	0.002	HKL1	AT5G07430	13.144	6.966	1.623	0.001	PME50
AT5G18600	1089.677	-1.057	0.227	0.000	GRXS2	AT3G07850	15.245	7.170	1.610	0.001	AT3G07850
AT5G18690	37.031	-1.055	0.335	0.021	AGP25	AT1G05580	6.162	7.229	1.634	0.001	CHX23
AT5G65360	240.805	-1.054	0.299	0.008	HTR2	AT3G01700	7.313	7.262	1.690	0.001	AGP11
AT2G41110	158.706	-1.051	0.278	0.004	CAM2	AT4G21630	6.541	7.274	2.621	0.048	SBT3.14
AT2G37180	143.578	-1.050	0.304	0.010	PIP2-3	AT2G38900	7.032	7.354	2.161	0.011	AT2G38900
AT3G54720	510.096	-1.046	0.191	0.000	AMP1	AT4G15750	41.147	7.515	2.395	0.022	None
AT4G00400	304.678	-1.044	0.372	0.045	GPAT8	AT5G61720	7.398	7.636	1.605	0.000	AT5G61720
AT5G19770	2148.968	-1.043	0.301	0.010	TUBA3	AT5G17220	15.619	7.858	2.121	0.005	GSTF12
AT5G21930	1952.601	-1.043	0.293	0.008	PAA2	AT5G49180	10.364	7.926	2.470	0.019	PME58
AT1G69030	129.316	-1.037	0.272	0.004	None	AT1G02790	29.241	8.005	1.726	0.000	PGA3

Gene ID	baseMean	log2FoldChange	lfcSE	padj	Symbol	Gene ID	baseMean	log2FoldChange	lfcSE	padj	Symbol
AT1G52190	1735.868	-1.035	0.311	0.014	NPF1.2	AT4G12960	70.732	8.076	2.264	0.007	GILT
AT1G24530	284.259	-1.032	0.327	0.021	AT1G24530	AT1G61720	14.382	8.306	2.168	0.004	BAN
AT5G60800	322.837	-1.029	0.325	0.021	AT5G60800	AT1G56100	16.037	8.480	2.172	0.003	AT1G56100
AT3G62030	3138.496	-1.028	0.151	0.000	ROC4	AT3G08770	103.324	11.138	2.400	0.000	LTP6
AT1G23750	56.361	-1.025	0.359	0.041	AT1G23750						

Appendix Table 8.2 DEGs and values from the pair-wise comparison of Root-origin cold memory (LCM) genes

Gene ID	baseMean	log2FoldChange	lfcSE	padj	Symbol	Gene ID	baseMean	log2FoldChange	lfcSE	padj	Symbol
AT1G75590	14.332	-5.550	1.523	0.018	AT1G75590	AT1G17620	446.650	-1.370	0.383	0.020	AT1G17620
AT3G59900	9.156	-5.461	1.436	0.012	ARGOS	AT2G15830	175.824	-1.367	0.242	0.000	None
AT5G59360	8.076	-4.775	1.488	0.040	None	AT5G44400	210.564	-1.340	0.328	0.006	AT5G44400
AT4G30280	39.825	-4.461	1.225	0.018	XTH18	AT1G14520	107.577	-1.333	0.428	0.048	MIOX1
AT1G06080	10.836	-4.272	1.339	0.041	ADS1	AT4G23800	33.855	-1.325	0.390	0.028	HMGB6
AT4G08950	690.135	-4.065	1.245	0.036	EXO	AT2G14560	3080.490	-1.325	0.338	0.009	LURP1
AT3G49570	119.414	-3.825	0.939	0.006	LSU3	AT3G56400	1714.330	-1.323	0.381	0.024	WRKY70
AT4G11290	27.995	-3.420	0.971	0.022	PER39	AT3G20570	96.061	-1.316	0.394	0.032	ENODL9
AT1G53070	12.690	-3.256	0.917	0.021	AT1G53070	AT5G40230	25.391	-1.313	0.412	0.041	None
AT4G24010	12.024	-3.229	1.005	0.040	CSLG1	AT3G14570	96.327	-1.306	0.330	0.008	CALS8
AT1G53700	18.477	-2.978	0.867	0.026	WAG1	AT3G22235	1230.637	-1.300	0.404	0.039	None
AT4G35320	88.939	-2.972	0.655	0.001	None	AT1G18360	219.132	-1.299	0.375	0.024	AT1G18360
AT5G24660	305.743	-2.942	0.643	0.001	LSU2	AT2G17880	153.577	-1.288	0.276	0.001	AT2G17880
AT5G26220	252.522	-2.932	0.622	0.001	GGCT2;1	AT1G66180	769.691	-1.284	0.374	0.026	AT1G66180
AT2G28315	12.789	-2.845	0.862	0.033	UXT1	AT1G19960	738.378	-1.281	0.366	0.023	AT1G19960
AT3G44220	9.220	-2.833	0.861	0.034	AT3G44220	AT2G40820	58.668	-1.279	0.387	0.032	AT2G40820
AT2G25060	11.524	-2.805	0.880	0.041	ENODL14	AT1G69490	1281.556	-1.268	0.362	0.023	NAC029
AT2G26750	10.804	-2.742	0.841	0.036	AT2G26750	AT1G61795	60.782	-1.262	0.349	0.019	RIC9
AT5G50335	76.604	-2.734	0.723	0.013	None	AT1G24470	51.222	-1.254	0.395	0.042	KCR2
AT5G49800	10.288	-2.715	0.780	0.024	None	AT1G80050	66.839	-1.243	0.394	0.044	APT2
AT2G20750	24.632	-2.600	0.639	0.006	EXPB1	AT5G25350	2900.338	-1.234	0.344	0.020	EBF2
AT1G33760	63.980	-2.567	0.665	0.011	ERF022	AT1G23060	55.116	-1.231	0.367	0.031	AT1G23060

Gene ID	baseMean	log2FoldChange	lfcSE	padj	Symbol	Gene ID	baseMean	log2FoldChange	lfcSE	padj	Symbol
AT5G45830	15.070	-2.566	0.758	0.028	DOG1	AT3G01670	390.510	-1.229	0.285	0.003	AT3G01670
AT1G67750	35.984	-2.555	0.562	0.001	AT1G67750	AT1G73500	1002.623	-1.228	0.193	0.000	MKK9
AT2G44080	348.623	-2.497	0.264	0.000	ARL	AT4G38950	115.800	-1.220	0.369	0.033	KIN7F
AT1G78090	18.293	-2.493	0.637	0.009	TPPB	AT1G14350	116.589	-1.218	0.364	0.031	MYB124
ATCG00350	139.082	-2.460	0.780	0.044	PSAA	AT5G46700	31.953	-1.215	0.363	0.031	TRN2
AT4G01950	114.162	-2.459	0.708	0.024	ATGPAT3	AT5G41140	284.416	-1.186	0.315	0.013	AT5G41140
AT4G17030	57.356	-2.445	0.670	0.018	EXLB1	AT3G21510	66.963	-1.184	0.257	0.001	AHP1
AT4G36230	10.849	-2.419	0.760	0.042	AT4G36230	AT1G62380	1675.931	-1.179	0.281	0.004	ACO2
AT3G50060	404.279	-2.372	0.735	0.039	MYB77	AT1G45201	616.430	-1.179	0.283	0.005	ATTLL1
AT1G02630	11.739	-2.340	0.748	0.046	ETN8	AT5G62220	152.747	-1.158	0.339	0.027	XLT2
AT1G73600	3657.254	-2.297	0.612	0.014	AT1G73600	AT1G29520	76.552	-1.154	0.325	0.021	AT1G29520
AT5G01790	20.041	-2.291	0.584	0.009	None	AT5G22310	246.999	-1.153	0.221	0.000	AT5G22310
AT2G12190	48.644	-2.262	0.371	0.000	AT2G12190	AT2G28190	1106.296	-1.150	0.219	0.000	CSD2
AT5G07030	49.105	-2.240	0.526	0.003	AT5G07030	AT4G14680	687.412	-1.149	0.240	0.001	APS3
AT1G28290	53.827	-2.236	0.427	0.000	AGP31	AT1G73370	34.181	-1.145	0.368	0.048	SUS6
AT5G22580	430.983	-2.202	0.462	0.001	AT5G22580	AT1G49750	2245.207	-1.141	0.231	0.000	AT1G49750
AT1G73830	205.147	-2.172	0.447	0.001	BEE3	AT1G33170	72.026	-1.140	0.362	0.045	AT1G33170
AT5G62280	316.856	-2.169	0.402	0.000	AT5G62280	AT1G45207	66.472	-1.137	0.314	0.018	AT1G45207
AT5G55950	15.362	-2.164	0.680	0.042	AT5G55950	AT2G47500	121.924	-1.132	0.264	0.003	KIN14I
AT1G21140	32.994	-2.156	0.571	0.013	AT1G21140	AT1G41830	453.130	-1.132	0.366	0.049	SKS6
AT1G11670	14.481	-2.134	0.663	0.039	None	AT5G23870	459.815	-1.131	0.340	0.032	PAE9
AT3G24450	22.311	-2.121	0.618	0.026	AT3G24450	AT1G07570	66.074	-1.129	0.259	0.003	APK1A
AT5G25190	318.842	-2.098	0.420	0.000	ERF003	AT3G15356	2260.353	-1.125	0.201	0.000	LEC
AT3G16670	239.352	-2.095	0.600	0.023	AT3G16670	AT1G19350	1455.973	-1.121	0.193	0.000	BES1
AT4G21760	13.972	-2.093	0.666	0.045	BGLU47	AT4G39730	808.219	-1.120	0.321	0.023	PLAT1
AT2G36870	38.627	-2.082	0.641	0.037	XTH32	AT2G36570	83.272	-1.115	0.283	0.009	PXC1
AT2G26020	168.361	-2.079	0.624	0.032	PDF1.2B	AT4G14930	767.964	-1.099	0.314	0.023	AT4G14930
AT3G23170	143.725	-2.074	0.489	0.004	AT3G23170	AT5G59350	98.073	-1.099	0.343	0.040	AT5G59350
AT4G39510	31.969	-2.067	0.582	0.021	CYP96A12	AT1G23080	1427.913	-1.095	0.350	0.047	PIN7
AT1G03010	52.254	-2.065	0.393	0.000	None	AT1G10682	292.365	-1.092	0.260	0.004	None
AT3G23150	131.872	-2.051	0.334	0.000	ETR2	AT3G43800	562.099	-1.090	0.328	0.032	GSTU27
AT3G26200	114.621	-2.043	0.599	0.027	CYP71B22	AT4G20840	143.648	-1.084	0.333	0.036	AT4G20840
AT5G62550	17.397	-2.032	0.625	0.037	AT5G62550	AT2G32690	1346.740	-1.056	0.305	0.024	GRP23

Gene ID	baseMean	log2FoldChange	lfcSE	padj	Symbol	Gene ID	baseMean	log2FoldChange	lfcSE	padj	Symbol
AT3G03850	22.772	-2.017	0.499	0.006	AT3G03850	AT1G03310	486.622	-1.048	0.309	0.028	ISA2
AT1G25530	42.115	-2.008	0.396	0.000	AT1G25530	AT1G12990	528.660	-1.042	0.337	0.050	AT1G12990
AT2G16060	32.917	-1.952	0.429	0.001	AHB1	AT3G59010	162.998	-1.041	0.243	0.003	PME35
AT1G62180	1082.451	-1.940	0.565	0.026	37347.000	AT1G52290	393.431	-1.034	0.295	0.023	PERK15
AT3G26960	91.803	-1.936	0.425	0.001	None	AT3G24480	739.710	-1.030	0.304	0.028	LRX4
AT2G41170	46.695	-1.910	0.469	0.006	AT2G41170	AT4G35880	78.186	-1.026	0.294	0.023	None
AT1G04310	109.946	-1.869	0.357	0.000	ERS2	AT2G41090	5062.880	-1.025	0.210	0.000	CML10
AT4G21990	1741.522	-1.820	0.573	0.042	37712.000	AT3G16530	932.648	-1.020	0.211	0.001	AT3G16530
AT4G34770	45.512	-1.818	0.492	0.016	AT4G34770	AT3G57780	96.001	-1.007	0.280	0.020	None
ATCG00420	25.225	-1.810	0.555	0.036	NDHJ	AT3G52360	67.774	-1.005	0.293	0.027	None
AT4G10955	18.589	-1.808	0.579	0.047	AT4G10955	AT2G42610	256.267	-1.003	0.278	0.019	LSH10
AT3G22760	21.047	-1.794	0.540	0.032	TCX3	AT1G29418	82.380	1.005	0.258	0.010	None
AT5G02760	565.987	-1.792	0.512	0.023	AT5G02760	AT5G27120	930.304	1.011	0.265	0.012	NOP5-1
AT5G55620	252.149	-1.779	0.498	0.020	AT5G55620	AT5G08610	590.592	1.028	0.277	0.016	RH26
AT4G19050	30.315	-1.772	0.569	0.048	AT4G19050	AT1G30250	1037.769	1.037	0.316	0.034	None
AT2G24762	163.803	-1.772	0.393	0.002	GDU4	AT4G37900	159.839	1.044	0.286	0.018	GRDP2
AT2G30040	79.169	-1.758	0.521	0.029	MAPKKK14	AT1G08070	43.280	1.052	0.292	0.019	PCMP-H12
AT3G57240	660.671	-1.731	0.548	0.044	BG3	AT5G52070	204.582	1.055	0.224	0.001	AT5G52070
AT5G15950	691.826	-1.730	0.491	0.022	SAMDC2	AT3G07750	103.391	1.059	0.322	0.034	AT3G07750
AT4G15550	165.580	-1.727	0.354	0.000	UGT75D1	AT1G29280	45.613	1.103	0.316	0.023	WRKY65
AT5G18290	61.084	-1.720	0.396	0.003	SIP1-2	AT5G09950	34.240	1.128	0.356	0.043	PCMP-H35
AT4G37800	240.018	-1.707	0.551	0.049	XTH7	AT1G69210	47.591	1.135	0.347	0.036	AT1G69210
AT5G42720	67.556	-1.704	0.374	0.001	None	AT3G52310	98.592	1.152	0.310	0.015	None
AT1G49660	220.205	-1.687	0.251	0.000	CXE5	AT1G52450	51.249	1.166	0.318	0.017	None
AT1G49210	36.507	-1.682	0.420	0.007	ATL76	AT2G35070	110.136	1.172	0.366	0.041	None
AT4G21650	321.510	-1.679	0.365	0.001	SBT3.13	AT3G52670	62.004	1.193	0.333	0.020	None
AT5G21100	241.383	-1.672	0.285	0.000	AT5G21100	AT4G38380	162.972	1.202	0.369	0.037	DTX45
AT5G05960	69.894	-1.670	0.529	0.044	AT5G05960	AT2G36730	46.384	1.223	0.299	0.006	None
AT1G45010	37.752	-1.663	0.456	0.018	AT1G45010	AT5G63625	42.272	1.237	0.362	0.027	None
AT1G02360	68.051	-1.660	0.358	0.001	AT1G02360	AT3G53220	22.417	1.274	0.413	0.050	AT3G53220
AT3G51750	29.350	-1.657	0.489	0.028	None	AT2G15810	119.407	1.279	0.366	0.023	None
AT5G65640	41.034	-1.656	0.428	0.010	BHLH93	AT4G35770	5138.735	1.282	0.372	0.026	STR15
AT2G28630	1341.363	-1.639	0.494	0.032	KCS12	AT5G49110	100.853	1.286	0.388	0.032	AT5G49110

Gene ID	baseMean	log2FoldChange	lfcSE	padj	Symbol	Gene ID	baseMean	log2FoldChange	lfcSE	padj	Symbol
AT1G69900	80.647	-1.620	0.444	0.018	AT1G69900	AT4G16680	632.474	1.376	0.272	0.000	None
AT1G25560	1893.132	-1.611	0.375	0.003	TEM1	AT1G16500	168.837	1.414	0.433	0.036	None
AT1G10657	90.725	-1.610	0.395	0.006	None	AT2G27775	45.687	1.475	0.397	0.016	AT2G27775
AT5G04890	31.223	-1.610	0.491	0.035	RTM2	AT2G04040	164.843	1.476	0.443	0.032	DTX1
AT1G32450	246.695	-1.589	0.433	0.017	NPF7.3	AT5G57640	37.528	1.477	0.388	0.012	None
AT5G58390	61.824	-1.584	0.475	0.032	PER67	AT1G03580	225.607	1.482	0.406	0.017	None
AT2G30230	174.872	-1.581	0.315	0.000	AT2G30230	AT5G09570	38.829	1.504	0.416	0.019	AT5G09570
AT5G24655	49.191	-1.568	0.484	0.037	LSU4	AT5G60250	92.928	1.510	0.292	0.000	AT5G60250
ATCG00120	96.806	-1.565	0.462	0.029	ATPA	AT1G70640	32.652	1.537	0.458	0.031	None
AT2G43150	2345.476	-1.551	0.346	0.002	AT2G43150	AT5G49190	41.602	1.560	0.364	0.003	SUS2
AT5G39610	899.453	-1.541	0.299	0.000	NAC92	AT5G66052	509.580	1.608	0.288	0.000	None
AT1G12090	9525.179	-1.535	0.469	0.035	ELP	AT1G51380	40.460	1.617	0.483	0.031	RH34
AT4G25830	40.651	-1.526	0.474	0.039	AT4G25830	AT2G18196	53.862	1.637	0.512	0.041	HIPP30
AT4G37450	56.274	-1.510	0.453	0.032	AGP18	AT2G18050	1455.256	1.671	0.469	0.021	HIS1-3
AT4G24350	504.599	-1.484	0.457	0.037	AT4G24350	AT1G02620	130.765	1.688	0.528	0.041	AT1G02620
AT3G15540	86.435	-1.482	0.475	0.047	IAA19	AT2G22470	59.242	1.748	0.396	0.002	AGP2
AT3G62780	33.836	-1.480	0.465	0.041	None	AT4G33980	823.707	1.800	0.530	0.028	AT4G33980
AT2G42200	33.559	-1.480	0.469	0.044	SPL9	AT4G18170	69.872	1.849	0.403	0.001	WRKY28
AT5G18970	32.404	-1.469	0.399	0.016	AT5G18970	AT2G46310	87.340	1.896	0.380	0.000	CRF5
AT1G18400	141.498	-1.464	0.441	0.032	BEE1	AT5G37260	99.358	1.957	0.628	0.048	RVE2
AT1G76800	178.961	-1.463	0.306	0.001	AT1G76800	AT4G15990	53.224	1.962	0.600	0.035	None
AT4G11211	59.145	-1.460	0.385	0.013	None	AT1G17665	209.115	2.146	0.649	0.033	AT1G17665
AT5G50800	224.670	-1.454	0.393	0.016	SWEET13	AT3G50770	252.093	2.154	0.585	0.016	CML41
AT4G30020	561.292	-1.452	0.336	0.003	SBT2.6	AT5G06760	11.373	2.182	0.672	0.037	LEA46
AT3G50340	115.376	-1.446	0.332	0.003	AT3G50340	AT3G55970	128.699	2.491	0.696	0.020	JRG21
AT5G37660	48.645	-1.443	0.329	0.002	CRRSP60	AT1G43590	18.034	2.501	0.728	0.026	None
AT5G42860	37.348	-1.443	0.457	0.044	None	AT2G38240	70.882	2.865	0.654	0.003	ANS
AT1G12845	63.018	-1.441	0.454	0.042	None	AT2G06002	29.310	2.889	0.856	0.029	None
AT1G08160	45.400	-1.422	0.442	0.040	AT1G08160	AT2G02990	27.360	3.660	0.999	0.017	RNS1
AT4G39330	255.259	-1.420	0.416	0.027	CAD9	AT3G01270	25.395	3.820	1.100	0.024	AT3G01270
AT5G18690	37.031	-1.418	0.370	0.011	AGP25	AT2G47040	41.554	4.018	1.008	0.008	PME5
AT5G03760	264.561	-1.416	0.347	0.006	CSLA9	AT3G01240	10.603	4.494	1.414	0.042	AT3G01240
AT3G52340	370.042	-1.416	0.305	0.001	SPP2	AT5G07410	14.995	4.517	1.316	0.026	PME48

Gene ID	baseMean	log2FoldChange	lfcSE	padj	Symbol	Gene ID	baseMean	log2FoldChange	lfcSE	padj	Symbol
AT5G42530	20102.038	-1.414	0.153	0.000	AT5G42530	AT3G05610	10.174	4.532	1.450	0.047	PME21
AT1G76955	99.500	-1.406	0.414	0.028	None	AT2G47030	17.184	4.545	1.280	0.021	PME4
AT2G40100	431.283	-1.405	0.208	0.000	LHCB4.3	AT3G13400	41.323	4.693	0.961	0.000	sks13
AT1G63310	34.494	-1.403	0.423	0.032	AT1G63310	AT2G47050	9.692	4.706	1.412	0.032	AT2G47050
AT1G70210	62.370	-1.380	0.431	0.041	CYCD1-1	AT5G35935	52.777	4.888	1.103	0.002	None
AT1G80760	290.158	-1.377	0.440	0.047	NIP6-1						

Table 8.3 Number of DMRs identified in Regenerated Plants primed with Cold.

Number	**Type of DMGs**	**CG contexts**		**CHG contexts**		**CHH contexts**	
		Gain	**Loss**	**Gain**	**Loss**	**Gain**	**Loss**
1	Cold-LO	847	47	20	3	72	23
2	Cold-RO	3	25	0	0	162	35

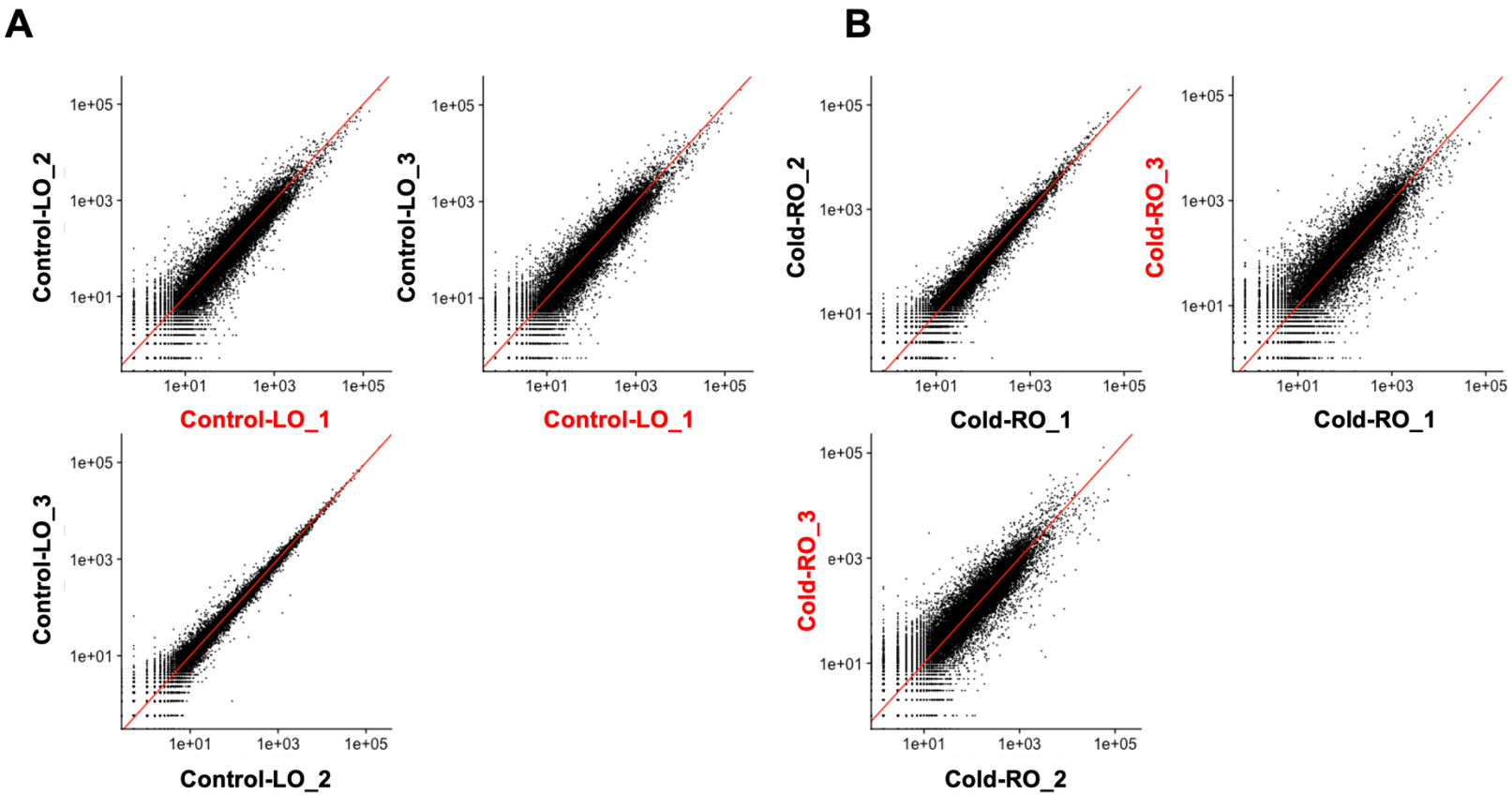

Appendix figure 8.1 Scatter Plot from three replicates from Control-LO (A) and Cold-RO (B). The text highlighted with red indicated the replicates that have been removed from the analysis.

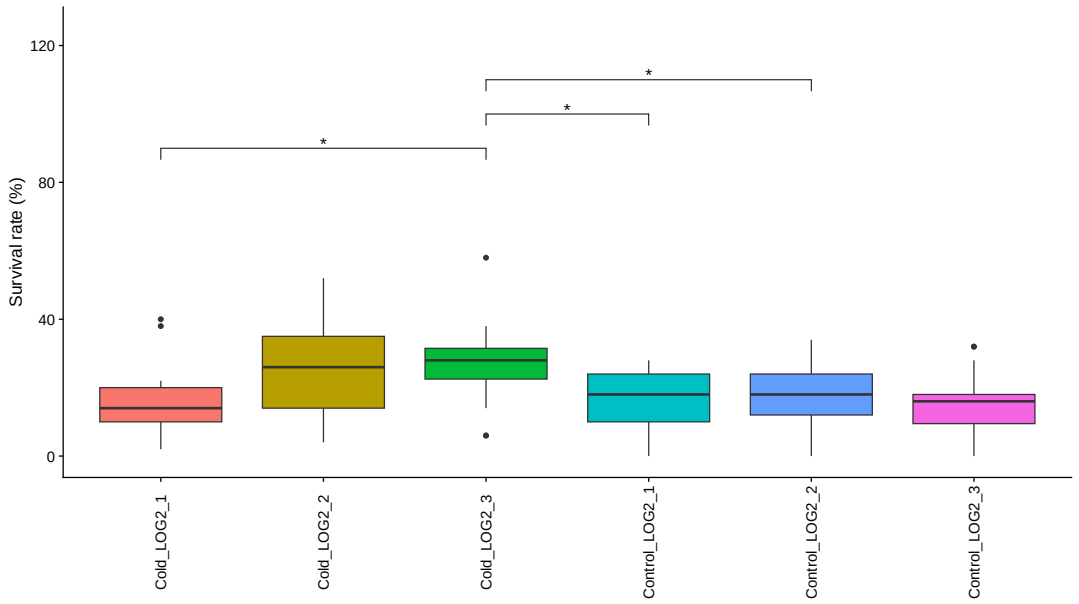

Appendix figure 8.2 Freezing tolerance assay comparing between leaf-origin (LO) clones from different treatment. Survival rates were calculated from recovered plants after being exposed to -5ºC. Each data point was calculated from 50 seedlings. Seven replicates were used in the statical analysis. Asterisk indicates the significant difference between comparisons (Tukey's HSD test, *** $p < 0.001$, ** $p < 0.01$, * $p < 0.05$, ns $p > 0.05$)

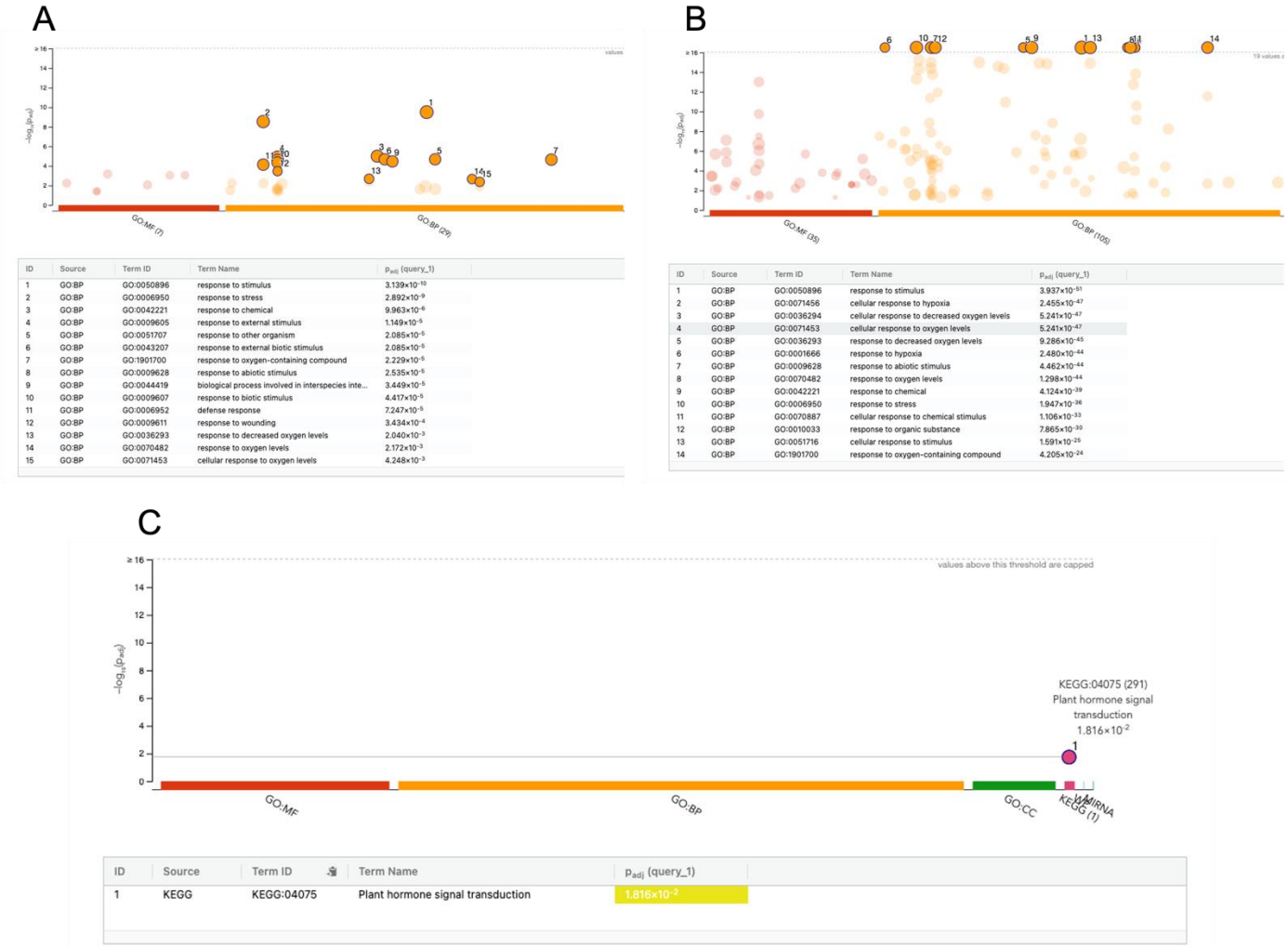

Appendix figure 8.3 GO analysis of Specific 22LCR genes (A) Shared-cold responsive genes (B), and Specific 4LCR genes (C)

Appendix 9

Appendix Table 9.1 DEGs and values from the pair-wise comparison of Leaf-origin cold memory (LCM) genes from indRKD4 aprent

Gene ID	baseMean	log2FoldChange	lfcSE	padj	Symbol	Gene ID	baseMean	log2FoldChange	lfcSE	padj	Symbol
AT2G45570	16.584	-6.858	1.847	0.006	CYP76C2	AT5G56870	796.026	-1.140	0.278	0.002	BGAL4
AT5G63225	12.802	-5.986	1.929	0.033	None	AT1G14520	253.391	-1.129	0.303	0.006	MIOX1
AT1G56060	22.003	-5.707	1.293	0.000	None	AT5G66200	2233.916	-1.129	0.128	0.000	ARO2
AT5G05340	19.636	-5.292	1.534	0.013	PER52	AT3G59580	149.223	-1.128	0.355	0.028	NLP9
AT3G53150	15.976	-4.368	1.466	0.045	None	AT5G03120	1212.525	-1.126	0.187	0.000	None
AT1G44130	22.075	-4.245	1.420	0.044	AT1G44130	AT1G69890	596.403	-1.124	0.242	0.000	AT1G69890
AT5G42900	14.970	-4.158	1.125	0.006	COR27	AT5G45750	653.991	-1.120	0.194	0.000	RABA1C
AT1G13670	31.777	-4.150	1.104	0.005	None	AT1G66090	231.998	-1.117	0.344	0.023	AT1G66090
AT4G39070	21.958	-4.051	1.024	0.003	BBX20	AT4G28190	208.946	-1.117	0.302	0.006	ULT1
AT2G44910	63.075	-3.951	0.713	0.000	ATHB-4	AT4G01950	960.932	-1.115	0.222	0.000	ATGPAT3
AT3G45410	19.208	-3.951	1.075	0.007	LECRK13	AT3G58570	467.234	-1.104	0.233	0.000	RH52
AT2G33560	24.528	-3.900	1.032	0.005	BUBR1	AT4G31000	523.268	-1.098	0.250	0.001	None
AT1G35140	2110.670	-3.700	0.478	0.000	EXL1	AT1G14920	1264.886	-1.079	0.174	0.000	GAI
AT3G48360	4085.714	-3.687	0.168	0.000	BT2	AT4G18760	285.881	-1.079	0.301	0.009	RLP51
AT1G33760	41.004	-3.683	1.029	0.009	ERF022	AT4G37260	2222.635	-1.079	0.150	0.000	MYB73
AT3G44350	29.789	-3.431	1.066	0.025	None	AT1G78850	3843.405	-1.076	0.177	0.000	AT1G78850
AT4G25810	169.798	-3.398	0.471	0.000	XTH23	AT3G54920	1469.766	-1.071	0.138	0.000	PMR6
AT4G07195	23.948	-3.342	0.843	0.003	None	AT1G23030	2382.643	-1.067	0.126	0.000	PUB11
AT4G16563	841.885	-3.337	0.169	0.000	AT4G16563	AT5G66080	191.459	-1.066	0.324	0.021	AT5G66080
AT5G25910	31.011	-3.307	0.991	0.018	AtRLP52	AT2G23290	740.848	-1.062	0.220	0.000	AtMYB70
AT5G39865	28.531	-3.170	0.922	0.013	AT5G39865	AT3G06770	948.018	-1.059	0.215	0.000	AT3G06770
AT5G28145	26.318	-3.148	0.943	0.018	None	AT2G37025	201.216	-1.059	0.333	0.027	TRFL8
AT4G08950	2148.759	-3.077	0.210	0.000	EXO	AT3G12110	439.882	-1.054	0.276	0.004	ACT11
AT5G65390	166.227	-3.028	0.398	0.000	None	AT5G64260	1033.040	-1.054	0.201	0.000	EXL2
AT3G49930	68.173	-2.998	0.779	0.004	AT3G49930	AT2G34090	291.838	-1.053	0.270	0.003	MEE18
AT5G57560	7946.766	-2.848	0.191	0.000	XTH22	AT4G34950	8406.471	-1.049	0.096	0.000	AT4G34950
AT4G37220	50.626	-2.782	0.846	0.021	AT4G37220	AT3G13750	31843.736	-1.048	0.137	0.000	BGAL1
AT4G38400	188.043	-2.720	0.424	0.000	EXLA2	AT3G13520	1695.786	-1.044	0.216	0.000	AGP12
AT4G28720	84.961	-2.698	0.542	0.000	YUC8	AT1G10120	263.572	-1.039	0.305	0.015	BHLH74
AT1G50040	825.480	-2.640	0.198	0.000	AT1G50040	AT1G69900	162.065	-1.038	0.338	0.036	AT1G69900

Gene ID	baseMean	log2FoldChange	lfcSE	padj	Symbol	Gene ID	baseMean	log2FoldChange	lfcSE	padj	Symbol
AT3G01795	75.568	-2.625	0.683	0.004	None	AT3G55430	1250.221	-1.038	0.143	0.000	AT3G55430
AT2G35980	36.011	-2.599	0.679	0.004	NHL10	AT4G30270	2569.622	-1.036	0.307	0.016	XTH24
AT1G21910	1156.885	-2.590	0.490	0.000	ERF012	AT1G22882	822.154	-1.034	0.181	0.000	SUN3
AT4G31620	41.154	-2.547	0.814	0.031	None	AT4G10890	110.109	-1.031	0.330	0.031	AT4G10890
AT1G72620	36.029	-2.536	0.827	0.036	None	AT5G44130	1536.295	-1.031	0.214	0.000	FLA13
AT4G36410	72.081	-2.527	0.700	0.008	UBC17	AT1G76160	2209.434	-1.030	0.163	0.000	sks5
AT1G10550	149.296	-2.524	0.834	0.040	XTH33	AT1G80190	152.930	-1.027	0.312	0.021	PSF1
AT5G23400	51.928	-2.499	0.739	0.016	AT5G23400	AT3G27960	477.610	-1.022	0.185	0.000	KLCR2
AT3G54160	34.160	-2.439	0.760	0.025	AT3G54160	AT4G05330	361.032	-1.022	0.243	0.001	AGD13
AT5G17850	59.822	-2.422	0.631	0.004	CCX2	AT3G07540	385.671	-1.020	0.270	0.005	FH10
AT3G02800	47.548	-2.376	0.801	0.047	DSP3	AT1G08890	496.461	-1.019	0.196	0.000	SUGTL4
AT4G10860	53.804	-2.373	0.749	0.028	AT4G10860	AT2G33580	206.017	-1.006	0.275	0.007	LYK5
AT3G59350	863.544	-2.339	0.265	0.000	AT3G59350	AT3G28910	549.775	-1.006	0.228	0.000	MYB30
AT5G50915	421.293	-2.310	0.538	0.001	BHLH137	AT2G27200	208.987	-1.005	0.295	0.015	LSG1-1
AT5G25240	351.712	-2.276	0.302	0.000	None	AT3G16240	11188.784	-1.004	0.175	0.000	TIP2-1
AT3G45970	2287.721	-2.254	0.211	0.000	EXLA1	AT3G13450	441.770	-1.001	0.239	0.001	DIN4
AT3G50800	44.225	-2.222	0.747	0.046	AT3G50800	AT1G12730	264.744	-1.001	0.236	0.001	AT1G12730
AT1G29980	70.825	-2.214	0.513	0.001	None	AT4G26850	9075.555	1.003	0.131	0.000	VTC2
AT2G30770	43.725	-2.180	0.705	0.034	CYP71A13	AT1G73870	2037.619	1.006	0.152	0.000	COL7
AT2G35710	150.259	-2.174	0.508	0.001	PGSIP8	AT4G15430	384.396	1.012	0.248	0.002	AT4G15430
AT4G36850	546.986	-2.172	0.320	0.000	AT4G36850	AT4G15550	322.347	1.014	0.259	0.003	UGT75D1
AT5G20250	12905.398	-2.096	0.181	0.000	DIN10	AT2G15050	1287.867	1.015	0.191	0.000	LTP7
AT3G19680	5647.296	-2.074	0.165	0.000	AT3G19680	AT2G26170	216.905	1.015	0.289	0.011	CYP711A1
AT4G30860	43.299	-2.008	0.634	0.028	ASHR3	AT1G79160	122.882	1.028	0.347	0.047	None
AT1G02640	796.427	-1.982	0.216	0.000	BXL2	AT3G13080	10833.860	1.030	0.176	0.000	ABCC3
AT3G23730	251.146	-1.970	0.359	0.000	XTH16	AT1G32900	2226.108	1.034	0.167	0.000	GBSS1
AT1G32170	354.259	-1.905	0.237	0.000	XTH30	AT5G14760	320.832	1.042	0.290	0.008	AO
AT4G28900	118.919	-1.900	0.605	0.030	None	AT2G40130	388.760	1.054	0.239	0.000	SMXL8
AT5G67480	2787.881	-1.876	0.165	0.000	BT4	AT2G03760	936.121	1.056	0.182	0.000	SOT12
AT1G02660	955.426	-1.871	0.217	0.000	PLIP2	AT2G27840	356.093	1.061	0.292	0.007	HDT4
AT3G47340	2694.355	-1.830	0.401	0.000	ASN1	AT5G15950	1611.755	1.064	0.154	0.000	SAMDC2
AT5G38900	90.710	-1.830	0.503	0.007	AT5G38900	AT5G18270	327.858	1.066	0.303	0.011	ANAC087
AT1G11260	13702.112	-1.812	0.174	0.000	STP1	AT5G23730	109.839	1.069	0.346	0.034	RUP2

Gene ID	baseMean	log2FoldChange	lfcSE	padj	Symbol	Gene ID	baseMean	log2FoldChange	lfcSE	padj	Symbol
AT4G32480	435.764	-1.800	0.259	0.000	AT4G32480	AT5G51260	251.942	1.072	0.318	0.016	None
AT2G41330	120.896	-1.795	0.498	0.008	AT2G41330	AT1G55920	565.047	1.076	0.215	0.000	SAT1
AT1G10560	94.801	-1.775	0.434	0.002	PUB18	AT2G04070	1506.847	1.078	0.193	0.000	DTX4
AT1G22530	4741.898	-1.770	0.169	0.000	PATL2	AT4G27585	876.418	1.079	0.217	0.000	AT4G27585
AT5G61440	96.359	-1.757	0.509	0.013	ACHT5	ATCG00490	478.148	1.086	0.334	0.023	RBCL
AT2G06850	4100.910	-1.755	0.190	0.000	XTH4	AT5G55620	1148.486	1.091	0.172	0.000	AT5G55620
AT4G03210	842.296	-1.754	0.250	0.000	XTH9	AT3G29250	243.551	1.091	0.335	0.023	SDR4
AT3G30775	473.795	-1.750	0.270	0.000	POX1	AT5G41761	213.164	1.098	0.337	0.023	None
AT2G42870	310.755	-1.740	0.313	0.000	PAR1	AT1G62560	1608.676	1.101	0.200	0.000	FMOGS-OX3
AT5G57550	448.393	-1.724	0.333	0.000	XTH25	AT2G21320	402.889	1.103	0.244	0.000	BBX18
AT1G76410	124.496	-1.723	0.382	0.000	ATL8	AT1G64900	1765.184	1.116	0.114	0.000	CYP89A2
AT1G21525	110.969	-1.718	0.462	0.006	None	AT2G36800	203.831	1.117	0.338	0.020	UGT73C5
AT1G07135	440.204	-1.710	0.327	0.000	AT1G07135	AT1G69730	725.410	1.122	0.228	0.000	WAKL9
AT5G22500	89.188	-1.709	0.547	0.031	FAR1	AT3G23160	120.126	1.129	0.331	0.015	AT3G23160
AT5G04780	49.633	-1.681	0.570	0.049	None	AT2G31560	656.231	1.131	0.166	0.000	AT2G31560
AT2G31010	283.427	-1.678	0.321	0.000	AT2G31010	AT4G14400	4762.564	1.133	0.170	0.000	ACD6
AT2G27080	285.223	-1.676	0.417	0.002	NHL13	AT3G01600	213.160	1.134	0.362	0.031	anac044
AT4G01250	183.224	-1.676	0.366	0.000	WRKY22	AT2G46790	958.655	1.136	0.144	0.000	APRR9
AT5G07000	92.872	-1.661	0.438	0.005	SOT14	AT2G18900	591.297	1.142	0.250	0.000	AT2G18900
AT4G25260	193.230	-1.660	0.378	0.001	PMEI7	AT1G78170	142.816	1.145	0.374	0.036	AT1G78170
AT5G51550	4142.737	-1.649	0.150	0.000	EXL3	AT1G05170	270.861	1.151	0.291	0.003	B3GALT2
AT3G21550	141.849	-1.644	0.516	0.027	DMP2	AT3G58990	1907.696	1.155	0.225	0.000	IPMI1
AT1G07050	93.362	-1.643	0.508	0.024	AT1G07050	AT3G55130	853.477	1.170	0.182	0.000	ABCG19
AT3G54400	690.693	-1.640	0.241	0.000	AT3G54400	AT1G30530	557.792	1.173	0.236	0.000	UGT78D1
AT5G03355	374.260	-1.627	0.213	0.000	None	AT3G09440	2413.841	1.181	0.203	0.000	HSP70-3
AT1G76090	1583.265	-1.624	0.197	0.000	SMT3	AT5G54100	1293.877	1.184	0.213	0.000	AT5G54100
AT5G35777	465.211	-1.622	0.232	0.000	None	AT5G54130	871.537	1.184	0.255	0.000	AT5G54130
AT1G16520	88.494	-1.616	0.485	0.018	AT1G16520	AT5G41010	251.359	1.186	0.319	0.006	NRPB12
AT4G13340	7204.784	-1.605	0.115	0.000	LRX3	AT1G71780	157.114	1.189	0.321	0.006	None
AT1G14330	423.152	-1.597	0.294	0.000	AT1G14330	AT5G10930	361.006	1.189	0.242	0.000	CIPK5
AT4G04223	186.784	-1.584	0.427	0.006	None	AT2G38860	447.058	1.196	0.297	0.002	DJ1E
AT5G11070	2191.955	-1.580	0.141	0.000	None	AT5G52640	167.267	1.210	0.374	0.024	HSP90-1
AT3G59080	492.467	-1.580	0.269	0.000	AT3G59080	AT5G64550	285.265	1.210	0.356	0.015	None

Gene ID	baseMean	log2FoldChange	lfcSE	padj	Symbol	Gene ID	baseMean	log2FoldChange	lfcSE	padj	Symbol
AT2G34510	3143.793	-1.577	0.141	0.000	AT2G34510	AT1G23950	154.367	1.217	0.347	0.011	None
AT3G62720	914.405	-1.576	0.205	0.000	XXT1	AT2G21640	1518.175	1.226	0.230	0.000	AT2G21640
AT3G15450	10198.579	-1.567	0.182	0.000	AT3G15450	AT5G02890	176.322	1.227	0.414	0.047	AT5G02890
AT2G02100	286.430	-1.555	0.320	0.000	PDF2.2	AT1G45191	221.062	1.230	0.306	0.002	BGLU1
AT1G19380	208.136	-1.552	0.325	0.000	AT1G19380	AT2G46650	1394.548	1.233	0.228	0.000	CYTB5-C
AT2G23100	186.199	-1.529	0.307	0.000	None	AT5G41900	174.194	1.233	0.345	0.009	BDG2
AT2G33830	4066.675	-1.522	0.185	0.000	DRMH1	AT3G27060	1195.992	1.251	0.233	0.000	TSO2
AT2G36400	161.067	-1.521	0.451	0.016	GRF3	AT5G58770	504.385	1.252	0.277	0.000	AT5G58770
AT2G30930	2958.135	-1.520	0.125	0.000	AT2G30930	AT4G19130	79.653	1.255	0.384	0.022	AT4G19130
AT5G23660	526.108	-1.519	0.186	0.000	SWEET12	AT2G36970	178.272	1.260	0.321	0.003	UGT86A1
AT1G57990	2362.830	-1.518	0.195	0.000	PUP18	AT1G12020	232.212	1.264	0.271	0.000	None
AT2G15880	1408.190	-1.518	0.167	0.000	PEX3	AT5G67280	480.083	1.264	0.206	0.000	RLK
AT4G16780	1526.245	-1.518	0.180	0.000	HAT4	AT1G07090	220.237	1.267	0.365	0.012	LSH6
AT1G13700	441.367	-1.505	0.297	0.000	PGL1	AT2G40475	253.811	1.275	0.299	0.001	AT2G40475
AT5G65660	1400.569	-1.501	0.172	0.000	AT5G65660	AT2G04050	3030.224	1.276	0.365	0.011	DTX3
AT3G57930	471.021	-1.499	0.245	0.000	None	AT1G08230	119.708	1.283	0.416	0.035	GAT1
AT2G28120	651.506	-1.499	0.234	0.000	AT2G28120	AT1G04945	149.803	1.294	0.332	0.003	AT1G04945
AT1G22740	732.010	-1.498	0.219	0.000	RABG3B	AT1G05680	286.662	1.297	0.341	0.004	UGT74E2
AT4G39830	151.936	-1.485	0.387	0.004	AT4G39830	AT2G47000	1485.597	1.300	0.235	0.000	ABCB4
AT5G49360	14008.979	-1.475	0.160	0.000	BXL1	AT1G76620	118.296	1.300	0.432	0.041	AT1G76620
AT1G11380	506.620	-1.470	0.204	0.000	None	AT1G76240	480.171	1.304	0.256	0.000	AT1G76240
AT1G61667	103.640	-1.459	0.361	0.002	AT1G61667	AT1G09180	188.103	1.306	0.309	0.001	ATSAR1
AT2G17230	2370.426	-1.459	0.143	0.000	EXL5	AT2G44940	212.887	1.309	0.245	0.000	ERF034
AT5G54380	2281.359	-1.450	0.162	0.000	THE1	AT2G32290	184.164	1.330	0.293	0.000	BAM6
AT1G15520	277.172	-1.436	0.330	0.001	ABCG40	AT5G54470	188.303	1.335	0.284	0.000	AT5G54470
AT4G26550	150.813	-1.430	0.446	0.026	AT4G26550	AT5G02950	96.301	1.349	0.384	0.011	None
AT2G15890	7548.173	-1.423	0.134	0.000	MEE14	AT1G04930	79.222	1.352	0.415	0.023	AT1G04930
AT3G57520	1643.314	-1.420	0.244	0.000	RFS2	AT4G01080	340.020	1.355	0.405	0.017	TBL26
AT4G02330	288.210	-1.413	0.339	0.001	PME41	AT3G04140	419.021	1.367	0.252	0.000	AT3G04140
AT1G15125	456.695	-1.403	0.278	0.000	AT1G15125	AT5G22300	98.884	1.378	0.390	0.010	NIT4
AT3G28007	59.676	-1.402	0.414	0.016	SWEET4	AT4G36240	88.543	1.411	0.425	0.019	GATA7
AT2G47440	4515.073	-1.398	0.145	0.000	AT2G47440	AT1G18590	786.665	1.418	0.237	0.000	SOT17
AT1G03870	2370.357	-1.387	0.143	0.000	FLA9	AT5G24155	119.449	1.421	0.459	0.033	AT5G24155

Gene ID	baseMean	log2FoldChange	lfcSE	padj	Symbol	Gene ID	baseMean	log2FoldChange	lfcSE	padj	Symbol
AT3G50140	55.547	-1.385	0.469	0.048	None	AT1G64500	1153.188	1.435	0.175	0.000	AT1G64500
AT2G42580	2052.102	-1.378	0.185	0.000	TTL3	AT4G38620	124.100	1.437	0.411	0.011	MYB4
AT5G22920	2674.481	-1.374	0.179	0.000	RZPF34	AT4G24700	107.364	1.445	0.333	0.001	AT4G24700
AT1G22190	1274.570	-1.373	0.233	0.000	RAP2-13	AT2G36590	120.445	1.460	0.421	0.013	PROT3
AT4G31800	499.594	-1.371	0.322	0.001	WRKY18	AT3G24460	427.444	1.463	0.384	0.004	AT3G24460
AT1G11070	242.995	-1.370	0.426	0.025	AT1G11070	AT4G03060	1084.455	1.472	0.248	0.000	None
AT4G17460	1896.317	-1.368	0.149	0.000	HAT1	AT5G03100	71.909	1.473	0.418	0.010	AT5G03100
AT1G50490	76.675	-1.367	0.446	0.036	UBC20	AT4G21490	140.185	1.477	0.403	0.007	NDB3
AT4G34760	1056.566	-1.364	0.222	0.000	SAUR50	AT1G77280	177.206	1.481	0.366	0.002	AT1G77280
AT1G75750	3114.261	-1.364	0.193	0.000	GASA1	AT4G27940	213.818	1.498	0.307	0.000	MTM1
AT2G30600	4196.195	-1.353	0.157	0.000	AT2G30600	AT1G56600	326.871	1.502	0.392	0.004	GOLS2
AT5G44010	109.463	-1.346	0.345	0.003	AT5G44010	AT3G47420	923.318	1.506	0.281	0.000	ATPS3
AT5G63810	1200.595	-1.345	0.199	0.000	BGAL10	AT5G47610	91.889	1.506	0.361	0.001	ATL79
AT2G21660	10142.857	-1.335	0.142	0.000	RBG7	AT5G52320	302.420	1.518	0.310	0.000	CYP96A4
AT4G29870	242.550	-1.329	0.331	0.002	AT4G29870	AT2G19650	259.392	1.520	0.260	0.000	AT2G19650
AT1G79700	317.173	-1.328	0.341	0.003	AT1G79700	AT2G18193	1835.912	1.523	0.361	0.001	AT2G18193
AT2G15090	961.615	-1.323	0.279	0.000	KCS8	AT1G27360	190.915	1.532	0.383	0.002	SPL11
AT1G70090	1078.944	-1.323	0.193	0.000	GATL9	AT1G64780	274.627	1.533	0.327	0.000	AMT1-2
AT5G20230	1467.026	-1.319	0.403	0.022	BCB	AT5G43450	2269.079	1.548	0.188	0.000	AT5G43450
AT3G05880	1517.713	-1.316	0.201	0.000	RCI2A	AT3G09230	110.641	1.558	0.435	0.009	MYB1
AT5G23210	1107.226	-1.314	0.160	0.000	SCPL34	AT5G38120	68.848	1.558	0.490	0.027	4CLL8
AT1G12710	922.228	-1.312	0.163	0.000	AtPP2-A12	AT3G21750	497.022	1.558	0.228	0.000	UGT71B1
AT1G28330	908.518	-1.311	0.214	0.000	DRM1	AT5G37500	183.853	1.561	0.370	0.001	GORK
AT3G54810	1350.506	-1.305	0.149	0.000	GATA8	AT3G15990	81.533	1.571	0.452	0.012	SULTR3;4
AT5G20960	182.831	-1.305	0.276	0.000	AAO1	AT5G39840	161.438	1.581	0.423	0.005	AT5G39840
AT4G37240	417.499	-1.304	0.345	0.005	AT4G37240	AT3G45210	239.127	1.592	0.311	0.000	None
AT5G08150	107.547	-1.304	0.381	0.014	SOB5	AT5G42760	117.838	1.604	0.417	0.004	AT5G42760
AT1G78000	335.431	-1.303	0.312	0.001	SULTR1;2	AT5G66740	119.175	1.617	0.518	0.032	AT5G66740
AT3G22600	203.916	-1.303	0.390	0.018	AT3G22600	AT1G19670	2290.938	1.637	0.364	0.000	CLH1
AT1G77640	131.207	-1.295	0.415	0.032	ERF013	AT3G44990	256.734	1.653	0.414	0.002	XTH31
AT2G33570	352.323	-1.285	0.256	0.000	GALS1	AT3G44450	376.144	1.657	0.231	0.000	BIC2
AT3G04060	135.952	-1.285	0.422	0.038	anac046	AT2G41730	215.844	1.671	0.364	0.000	AT2G41730
AT1G03850	194.005	-1.279	0.364	0.011	AT1G03850	AT1G51440	229.831	1.685	0.346	0.000	AT1G51440

Gene ID	baseMean	log2FoldChange	lfcSE	padj	Symbol	Gene ID	baseMean	log2FoldChange	lfcSE	padj	Symbol
AT2G41640	513.861	-1.278	0.289	0.000	AT2G41640	AT4G29700	127.853	1.689	0.520	0.023	AT4G29700
AT3G07650	109.709	-1.276	0.379	0.017	COL9	AT1G22340	44.564	1.696	0.553	0.036	UGT85A7
AT2G39870	1917.088	-1.271	0.155	0.000	None	AT4G25480	148.138	1.703	0.386	0.000	DREB1A
AT2G36885	204.127	-1.270	0.364	0.012	AT2G36885	AT5G53200	61.612	1.704	0.484	0.011	TRY
AT3G53310	146.142	-1.266	0.400	0.028	REM20	AT4G39780	136.886	1.708	0.357	0.000	ERF060
AT2G20680	170.817	-1.266	0.316	0.002	MAN2	AT5G14730	88.608	1.715	0.519	0.020	AT5G14730
AT1G60140	2301.107	-1.260	0.149	0.000	TPS10	AT5G61350	49.933	1.753	0.546	0.025	AT5G61350
AT1G61100	3793.312	-1.259	0.134	0.000	AT1G61100	AT3G49660	75.547	1.794	0.544	0.020	WDR5A
AT5G23050	515.064	-1.252	0.257	0.000	AAE17	AT5G01790	149.924	1.826	0.393	0.000	None
AT5G14920	872.654	-1.251	0.174	0.000	GASA14	AT5G51440	294.898	1.867	0.293	0.000	HSP23.5
AT1G36940	114.938	-1.249	0.326	0.004	None	AT4G05010	86.000	1.875	0.636	0.049	None
AT3G04640	255.254	-1.240	0.392	0.028	AT3G04640	AT5G45080	54.728	2.004	0.596	0.017	PP2A6
AT2G16660	12972.092	-1.240	0.138	0.000	AT2G16660	AT5G24110	47.622	2.025	0.677	0.044	WRKY30
AT2G44500	1455.801	-1.237	0.155	0.000	OFUT20	AT2G28815	65.847	2.033	0.491	0.001	None
AT1G03457	99.436	-1.236	0.375	0.020	AT1G03457	AT5G62480	354.588	2.048	0.287	0.000	GSTU9
AT5G51670	169.216	-1.230	0.315	0.003	None	AT1G11700	154.717	2.074	0.429	0.000	None
AT1G28050	194.059	-1.229	0.344	0.009	COL15	AT1G57590	135.058	2.090	0.487	0.001	PAE2
AT3G47800	2185.427	-1.222	0.181	0.000	AT3G47800	AT1G07290	41.366	2.115	0.602	0.011	None
AT3G05490	700.989	-1.221	0.206	0.000	RALFL22	AT4G15500	72.358	2.158	0.645	0.018	UGT84A4
AT2G28200	116.665	-1.217	0.402	0.040	ZAT5	AT5G04950	282.602	2.218	0.616	0.008	NAS1
AT1G77630	233.415	-1.216	0.349	0.012	LYM3	AT5G49480	712.427	2.240	0.289	0.000	ATCP1
AT2G36410	1261.705	-1.215	0.218	0.000	AT2G36410	AT1G77870	39.174	2.250	0.720	0.031	MUB5
AT1G22330	600.840	-1.215	0.197	0.000	AT1G22330	AT2G04885	43.394	2.353	0.733	0.025	None
AT5G25190	1456.511	-1.213	0.196	0.000	ERF003	AT2G34650	61.889	2.360	0.648	0.007	PID
AT2G36080	223.091	-1.210	0.332	0.007	ARF31	AT5G54450	100.452	2.542	0.526	0.000	None
AT4G16146	203.439	-1.203	0.299	0.002	AT4G16146	AT5G52940	26.409	2.866	0.959	0.044	None
AT5G52882	1037.711	-1.199	0.245	0.000	AT5G52882	AT2G15020	938.578	2.934	0.504	0.000	AT2G15020
AT5G66920	182.045	-1.198	0.348	0.013	sks17	AT3G21890	29.156	2.934	0.926	0.028	MIP1B
AT4G34750	352.426	-1.194	0.206	0.000	AT4G34750	AT2G18190	57.061	3.127	0.525	0.000	AT2G18190
AT5G45340	240.141	-1.185	0.327	0.007	CYP707A3	AT3G27630	25.273	3.198	0.972	0.021	SMR7
AT5G65920	140.897	-1.181	0.356	0.019	PUB31	AT4G34550	30.259	3.224	0.911	0.010	AT4G34550
AT4G22010	724.414	-1.179	0.190	0.000	sks4	AT1G15870	27.115	3.276	0.911	0.008	AT1G15870
AT1G76600	306.144	-1.178	0.280	0.001	AT1G76600	ATCG00710	14.242	3.421	1.133	0.041	PSBH

Gene ID	baseMean	log2FoldChange	lfcSE	padj	Symbol	Gene ID	baseMean	log2FoldChange	lfcSE	padj	Symbol
AT4G02540	1037.681	-1.167	0.204	0.000	AT4G02540	AT5G37490	27.407	3.616	1.205	0.043	PUB21
AT1G72790	556.981	-1.167	0.233	0.000	AT1G72790	AT1G73325	73.136	3.667	0.790	0.000	None
AT1G75770	156.002	-1.165	0.385	0.040	None	AT3G09450	69.111	3.771	0.797	0.000	None
AT5G05440	299.736	-1.164	0.385	0.041	PYL5	AT5G56840	29.005	3.840	0.905	0.001	AT5G56840
AT4G32800	254.172	-1.159	0.219	0.000	ERF043	AT1G09217	13.038	4.111	1.291	0.027	None
AT5G44260	295.492	-1.154	0.221	0.000	TZF5	AT1G26790	16.548	4.234	1.242	0.015	None
AT2G18700	7109.821	-1.150	0.131	0.000	TPS11	AT2G36750	19.980	5.291	1.352	0.003	UGT73C1
AT1G09575	152.174	-1.149	0.308	0.005	AT1G09575	AT2G05695	15.379	5.914	1.562	0.005	None
AT1G24170	1051.118	-1.144	0.202	0.000	GATL8	AT1G05990	12.172	7.759	1.643	0.000	CML7

Appendix Table 9.2 DEGs and values from the pair-wise comparison of Leaf-origin cold memory (L*CM) genes from ami-cbfs parent

Gene ID	baseMean	log2FoldChange	lfcSE	padj	Symbol	Gene ID	baseMean	log2FoldChange	lfcSE	padj	Symbol
AT1G78170	142.816	-2.355	0.393	0.000	AT1G78170	AT1G69900	162.065	1.186	0.334	0.019	AT1G69900
AT5G51440	294.898	-1.770	0.297	0.000	HSP23.5	AT3G62720	914.405	1.190	0.203	0.000	XXT1
AT4G25480	148.138	-1.570	0.380	0.003	DREB1A	AT1G03870	2370.357	1.193	0.142	0.000	FLA9
AT2G40475	253.811	-1.540	0.301	0.000	AT2G40475	AT1G57990	2362.830	1.199	0.194	0.000	PUP18
AT5G62480	354.588	-1.524	0.289	0.000	GSTU9	AT2G16660	12972.092	1.207	0.138	0.000	AT2G16660
AT5G02890	176.322	-1.493	0.415	0.016	AT5G02890	AT2G26560	1049.420	1.208	0.247	0.000	PLP2
AT5G49480	712.427	-1.451	0.288	0.000	ATCP1	AT1G22530	4741.898	1.213	0.168	0.000	PATL2
AT3G30720	256.146	-1.324	0.335	0.005	QQS	AT4G30270	2569.622	1.214	0.307	0.005	XTH24
AT3G29250	243.551	-1.323	0.340	0.006	SDR4	AT5G65660	1400.569	1.218	0.169	0.000	AT5G65660
AT1G64390	1170.567	-1.284	0.232	0.000	AtGH9C2	AT2G44500	1455.801	1.223	0.154	0.000	OFUT20
AT5G01790	149.924	-1.240	0.386	0.049	None	AT5G37710	299.804	1.233	0.328	0.010	AT5G37710
AT3G61890	227.342	-1.165	0.322	0.015	ATHB-12	AT3G57520	1643.314	1.243	0.243	0.000	RFS2
AT2G39700	403.346	-1.121	0.274	0.003	EXPA4	AT4G34760	1056.566	1.243	0.221	0.000	SAUR50
AT5G10930	361.006	-1.113	0.241	0.000	CIPK5	AT5G49360	14008.979	1.248	0.160	0.000	BXL1
AT4G30410	200.976	-1.097	0.289	0.009	IBL1	AT5G54380	2281.359	1.259	0.161	0.000	THE1
AT2G40610	2399.220	-1.082	0.161	0.000	EXPA8	AT5G03355	374.260	1.271	0.211	0.000	None
AT4G24780	2498.192	-1.049	0.109	0.000	AT4G24780	AT2G41640	513.861	1.281	0.286	0.001	AT2G41640
AT1G69530	10520.508	-1.038	0.170	0.000	ATEXPA1	AT5G57550	448.393	1.294	0.331	0.006	XTH25
AT5G06270	180.323	-1.037	0.291	0.018	AT5G06270	AT3G50060	817.412	1.314	0.184	0.000	MYB77

Gene ID	baseMean	log2FoldChange	lfcSE	padj	Symbol	Gene ID	baseMean	log2FoldChange	lfcSE	padj	Symbol
AT1G55920	565.047	-1.031	0.213	0.000	SAT1	AT2G30930	2958.135	1.327	0.125	0.000	AT2G30930
AT1G45010	182.599	-1.021	0.314	0.044	AT1G45010	AT2G17230	2370.426	1.327	0.142	0.000	EXL5
AT1G18590	786.665	-1.011	0.236	0.001	SOT17	AT4G38400	188.043	1.353	0.412	0.041	EXLA2
AT5G54100	1293.877	-1.010	0.214	0.000	AT5G54100	AT3G54810	1350.506	1.355	0.148	0.000	GATA8
AT2G06850	4100.910	1.011	0.190	0.000	XTH4	AT1G02660	955.426	1.356	0.214	0.000	PLIP2
AT5G23050	515.064	1.014	0.256	0.005	AAE17	AT2G47440	4515.073	1.369	0.144	0.000	AT2G47440
AT5G44130	1536.295	1.018	0.214	0.000	FLA13	AT5G51550	4142.737	1.374	0.149	0.000	EXL3
AT1G22882	822.154	1.018	0.180	0.000	SUN3	AT4G02540	1037.681	1.380	0.204	0.000	AT4G02540
AT3G01290	2037.021	1.018	0.181	0.000	HIR3	AT1G11260	13702.112	1.405	0.174	0.000	STP1
AT2G23290	740.848	1.022	0.218	0.000	AtMYB70	AT1G77640	131.207	1.492	0.407	0.013	ERF013
AT1G78100	738.756	1.038	0.147	0.000	AT1G78100	AT4G25810	169.798	1.492	0.443	0.032	XTH23
AT4G34750	352.426	1.040	0.201	0.000	AT4G34750	AT5G67480	2787.881	1.499	0.164	0.000	BT4
AT2G15880	1408.190	1.058	0.166	0.000	PEX3	AT4G13340	7204.784	1.504	0.114	0.000	LRX3
AT5G35777	465.211	1.064	0.231	0.000	None	AT5G25240	351.712	1.539	0.294	0.000	None
AT2G33830	4066.675	1.065	0.185	0.000	DRMH1	AT1G32170	354.259	1.546	0.235	0.000	XTH30
AT5G56870	796.026	1.066	0.277	0.007	BGAL4	AT5G20250	12905.398	1.581	0.181	0.000	DIN10
AT4G03210	842.296	1.070	0.250	0.001	XTH9	AT1G11380	506.620	1.602	0.203	0.000	None
AT1G76600	306.144	1.092	0.275	0.005	AT1G76600	AT5G44260	295.492	1.611	0.222	0.000	TZF5
AT2G38310	523.235	1.099	0.237	0.000	PYL4	AT2G23100	186.199	1.641	0.303	0.000	None
AT5G51670	169.216	1.103	0.313	0.020	None	AT1G21910	1156.885	1.672	0.487	0.026	ERF012
AT1G02380	275.821	1.112	0.250	0.001	None	AT5G24030	871.713	1.710	0.413	0.003	SLAH3
AT2G23130	2112.360	1.113	0.122	0.000	AGP17	AT4G04223	186.784	1.712	0.426	0.004	None
AT1G12710	922.228	1.114	0.161	0.000	AtPP2-A12	AT3G45970	2287.721	1.729	0.210	0.000	EXLA1
AT4G03400	3026.020	1.120	0.122	0.000	DFL2	AT3G19680	5647.296	1.797	0.164	0.000	AT3G19680
AT1G04240	711.566	1.126	0.234	0.000	SHY2	AT3G59350	863.544	1.814	0.264	0.000	AT3G59350
AT1G72790	556.981	1.128	0.232	0.000	AT1G72790	AT3G48360	4085.714	1.833	0.166	0.000	BT2
AT2G39870	1917.088	1.133	0.154	0.000	None	AT5G57560	7946.766	1.947	0.190	0.000	XTH22
AT3G50650	205.658	1.139	0.307	0.011	SCL7	AT4G08950	2148.759	1.999	0.207	0.000	EXO
AT2G34510	3143.793	1.155	0.141	0.000	AT2G34510	AT1G50040	825.480	2.106	0.195	0.000	AT1G50040
AT2G28120	651.506	1.163	0.232	0.000	AT2G28120	AT1G35140	2110.670	2.215	0.476	0.000	EXL1
AT4G17460	1896.317	1.182	0.149	0.000	HAT1	AT4G16563	841.885	2.338	0.160	0.000	AT4G16563

Appendix Table 9.3 Shared Genes between LCM and L*CM with *CBFs*-regulated Genes

Gene ID	Symbols	Category	Gene ID	Symbols	Category
AT1G07135	NA	specific to LCM	AT5G14760	AO	specific to LCM
AT1G08890	SUGTL4	specific to LCM	AT5G17850	CCX2	specific to LCM
AT1G22330	NA	specific to LCM	AT5G24110	WRKY30	specific to LCM
AT1G28330	DRM1	specific to LCM	AT5G37500	GORK	specific to LCM
AT1G56600	GOLS2	specific to LCM	AT5G42900	COR27	specific to LCM
AT1G60140	TPS10	specific to LCM	AT5G52320	CYP96A4	specific to LCM
AT1G73325	None	specific to LCM	AT5G64260	EXL2	specific to LCM
AT2G04070	DTX4	specific to LCM	AT1G02660	PLIP2	shared LCM and L*CM
AT2G31010	NA	specific to LCM	AT1G03870	FLA9	shared LCM and L*CM
AT2G45570	CYP76C2	specific to LCM	AT1G11260	STP1	shared LCM and L*CM
AT2G46650	CYTB5-C	specific to LCM	AT1G18590	SOT17	shared LCM and L*CM
AT3G05880	RCI2A	specific to LCM	AT1G32170	XTH30	shared LCM and L*CM
AT3G06770	NA	specific to LCM	AT2G33830	DRMH1	shared LCM and L*CM
AT3G15450	NA	specific to LCM	AT3G19680	NA	shared LCM and L*CM
AT3G44990	XTH31	specific to LCM	AT3G45970	EXLA1	shared LCM and L*CM
AT3G54400	NA	specific to LCM	AT4G25480	DREB1A	shared LCM and L*CM
AT3G58990	IPMI1	specific to LCM	AT4G38400	EXLA2	shared LCM and L*CM
AT4G03060	None	specific to LCM	AT5G44260	TZF5	shared LCM and L*CM
AT4G14400	ACD6	specific to LCM	AT5G56870	BGAL4	shared LCM and L*CM
AT4G36410	UBC17	specific to LCM	AT1G69530	ATEXPA1	Specific L*CM
AT4G39070	BBX20	specific to LCM	AT3G30720	QQS	Specific L*CM
AT5G08150	SOB5	specific to LCM	AT4G24780	NA	Specific L*CM

Appendix Table 9.4 Shared Genes between Cold-induced memory genes and CBF3-induced memory genes

Gene ID	Symbol	Direction
AT1G10490	AT1G10490	Up regulation
AT3G10050	OMR1	Up regulation
AT4G07825	None	Up regulation
AT5G19120	AT5G19120	Up regulation
AT5G27120	NOP5-1	Up regulation
AT1G09070	SRC2	Down regulation
AT1G75040	PR5	Down regulation
AT3G09390	MT2A	Down regulation
AT5G07830	AtGUS2	Down regulation
AT5G10380	ATL55	Down regulation
AT5G20230	BCB	Down regulation
AT5G37600	GLN1-1	Down regulation
AT5G45800	MEE62	Down regulation

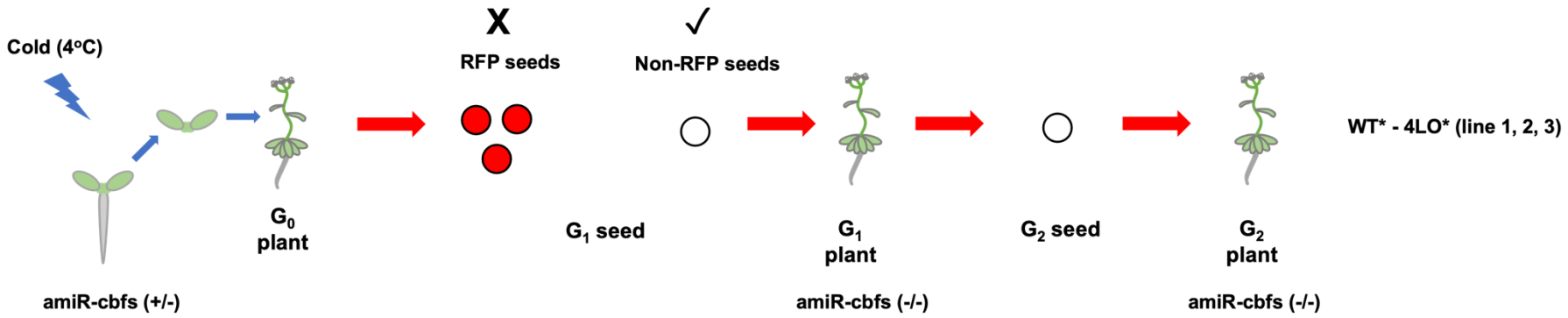

Appendix Figure 9.1 Schematic diagram representing the strategy to screen out amiRNA-cbfs construct. Blue arrows indicate somatic embryogenesis. Red arrows indicate seed propagation. G_0 plants propagate G_1 seeds containing RFP and non-RFP seeds. Only non-RFP seeds were selected for further propagation.

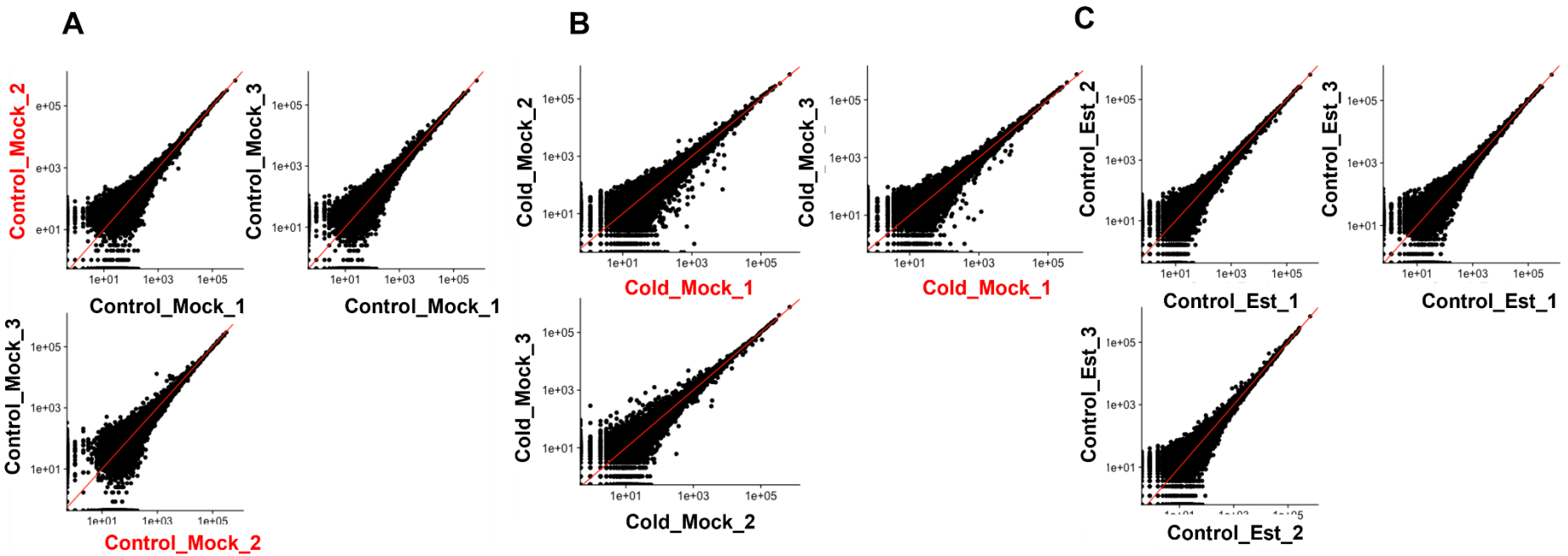

Appendix Figure 9.2 Scatter plot from 22LOM (Control-Mock) plant lines (A), 4LOM (Cold-Mock) plant lines (B), and 22LOE (Control-Est) plant lines (C). Highlighted texts indicate the excluded replicates.